

8.2.14 Multi-Dimensional Flow Testing

8.2.14.1 Introduction

Flow blockage tests (References 8.2-59 and 8.2-60) were performed using simulated pressurized water reactor (PWR) fuel assemblies. These tests provided data on single-phase flow redistribution for nonuniform inlet and outlet conditions. S-RELAP5 has a two-dimensional component used to model multidimensional flows. These flow blockage tests have been used as a basis for evaluating the two-dimensional component in S-RELAP5. The comparisons to the measured data and to other codes that have been approved for flow distribution calculations show that the two-dimensional component in S-RELAP5 can be used to model multidimensional flow problems. Section 8.2.14.3 describes the test facility. Sections 8.2.14.4 through 8.2.14.6 describe the modeling and comparison to the tests. The two-dimensional model is used in both SBLOCA and RLBLOCA applications. The purpose of the assessment is to show that the two-dimensional component functions acceptably. No bias or uncertainty is derived from this assessment.

8.2.14.2 Summary and Conclusions

The flow split radial distributions of axial velocities calculated by S-RELAP5 show good agreement with data from References 8.2-59 and 8.2-60 for all three tests considered. The comparison of S-RELAP5 with flow blockage data shows that the two-dimensional model in S-RELAP5 is sufficient to describe flow redistribution in multidimensional problems in predicting the flows for these blockage tests.

8.2.14.3 Facility Description

The test configuration for both sets of tests (References 8.2-59 and 8.2-60) is shown in Figure 8.2-564. The test assembly consists of two simulated PWR assemblies with a pin array representative of a 15 x 15 fuel assembly. The simulated assemblies are about 38 inch long and are enclosed in a rectangular canister. For the bulk of the testing, the gap between the two simulated fuel assemblies was left open (Figure 8.2-565). For the Reference 8.2-60 testing, a perforated plate was inserted between the two simulated fuel assemblies (Figure 8.2-566). The tests consisted of introducing asymmetric flows in the inlet region and measuring flow recovery in the bundle. The test reported in Reference 8.2-60 also had the outlet of one assembly blocked along with some minor modifications to the test assembly. Because of the detail of the measurements and the nearly prototypic geometry (in the radial, or x-y, direction), the test results from Reference 8.2-59 have become a standard benchmark test for flow redistribution codes.

8.2.14.4 Test Description

The tests consisted of introducing asymmetric flow in the inlet region and measuring flow recovery in the bundle with a series of pitot tube arrays (see Figure 8.2-564). The Pitot tubes measure flow velocities at many points in each plane. The first array is 2.5 inch above the inlet. The remainders are located at 5-in intervals, with the last one at 32.5 inch (Level 7 in the discussion in Section 8.2.14.5). For the test series without the perforated plate between the assemblies, two different test configurations were evaluated. The first configuration (Test 1) has a nominal 1100 gpm entering one fuel assembly and 550 gpm in the other. The second configuration (Test 2) has one inlet blocked and a nominal 1500 gpm entering the other. In both cases, the exits are open. The case with the perforated plate inserted between the two assemblies (Test 3) has the inlet and outlet blocked on one assembly and has a nominal inlet flow of 1300 gpm.

8.2.14.5 S-RELAP5 Model Description

[

] This, in effect, collapses the test

assembly in the direction perpendicular to the asymmetric flows. [

] Figure 8.2-567 shows the model

used for the analysis.

Cross flow form losses were calculated for each case from the measured flows based on Jakob's expression for the pressure drop across banks of tubes (Reference 8.2-61).

[

]

[

]

[] and the dynamic viscosity for water at 70°F is 1.06×10^{-5} ft²/sec. This expression was evaluated for each row using the Reynolds number based on the gap size and on the difference between the measured mass flows at two different elevations (to determine the velocity of the cross flow). The horizontal velocity was then adjusted, assuming that each volume contributes, or receives, the same mass during cross flow. The form loss for cross flow then displayed a radial dependence (see Figure 8.2-568), which varied somewhat for each test and each elevation.

For the case with a perforated plate separating the two test assemblies, an additional loss term was added. The loss coefficient, ζ , was based on an expression in Reference 8.2-62 for a plate with sharp-edged, circular holes.

$$\zeta = \left(\frac{0.707 \cdot \sqrt{(1-f)} + 1-f}{f} \right)^2$$

where f is the fraction of the area open to flow.

The inlet flows were then set to the appropriate values for each case and the velocities and flows calculated.

8.2.14.6 Calculated Results

8.2.14.6.1 Comparison to Data

A review of the data for Test 1 indicates that the real flows were probably 1138 gpm and 512 gpm for Bundle A (Bundle 1) and Bundle B (Bundle 2), respectively. Figure 8.2-569 through Figure 8.2-574 compare the reported axial fluid velocities for the Test 1, to those calculated by S-RELAP5 with inlet flows of 1138 and 512 gpm. [

] The remaining axial measurements show far less deviation from conservation of mass and the agreement for these cases is excellent.

Figure 8.2-575 compares the reported mass flow fraction in Bundle A with that calculated by S-RELAP5. The agreement is excellent, with only minor deviations occurring at Levels 6 and 7.

A review of the data for Test 2 indicates that the real inlet flow was probably 1281 gpm, rather than the nominal 1500 gpm for the test. This value was used in the S-RELAP5 model. Figure 8.2-576 through Figure 8.2-581 compare the S-RELAP5 velocity distributions with the reported axial fluid velocities. In general, the agreement is excellent. The largest discrepancy occurs on the side of the blocked bundle next to the wall. Here, S-RELAP5 calculates more of a tendency to back flow. The measurement velocities, which are based on Pitot tube readings, show that the flow stops near the wall.

Figure 8.2-582 compares the fractional flow in Bundle A. The agreement is good over most of the axial height of the bundle, with only minor deviations occurring at levels 2, 6, and 7. The overall agreement is good.

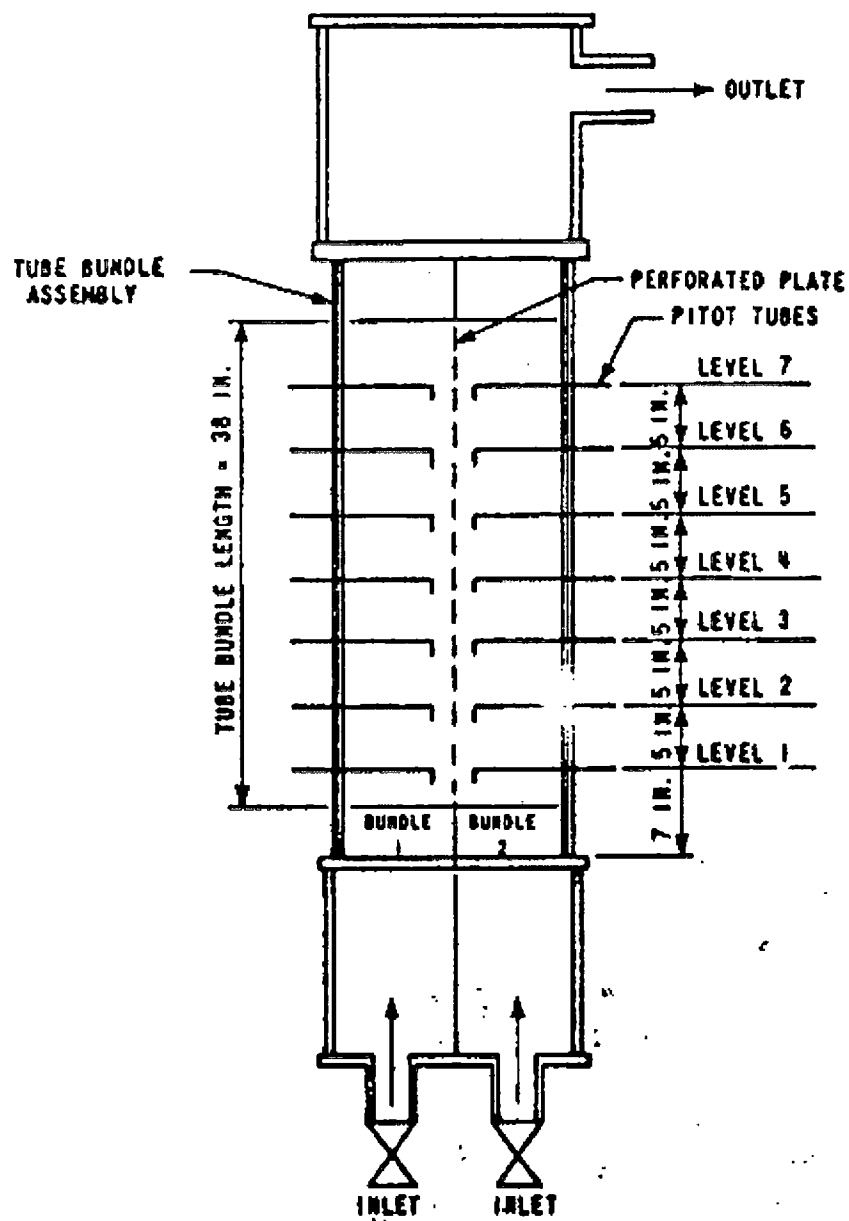
Figure 8.2-583 through Figure 8.2-588 compare the reported axial fluid velocities for Test 3 to those calculated by S-RELAP5. The agreement for these data is excellent for all levels. [

]

8.2.14.7 Discussion of Results

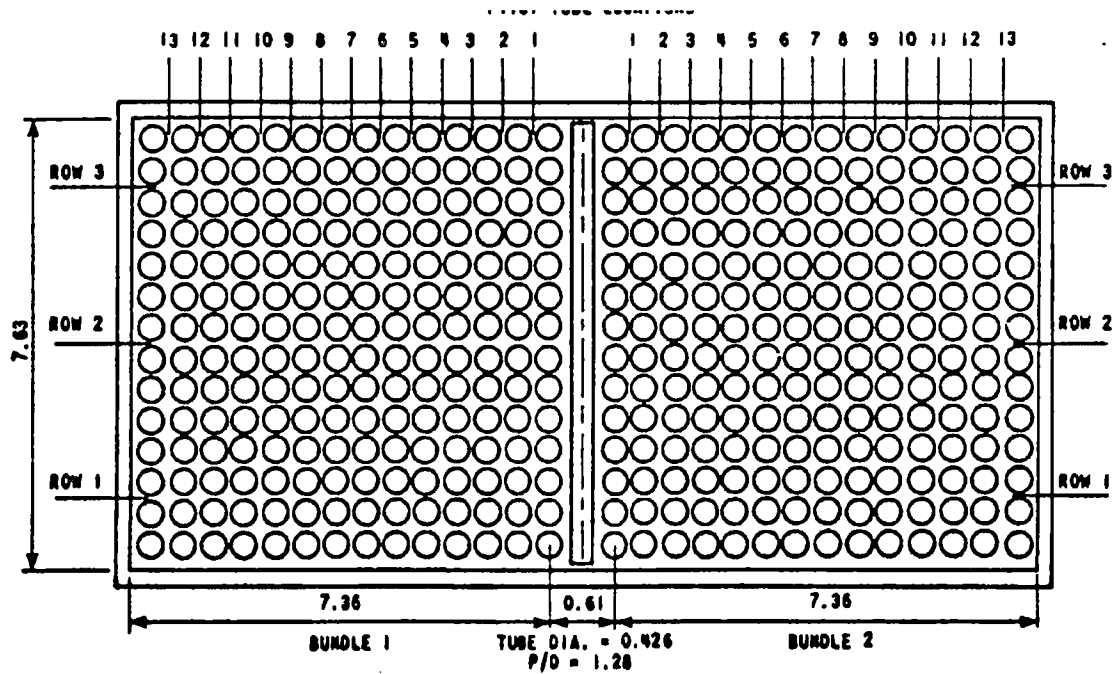
A series of flow blockage tests was analyzed using the two-dimensional component in S-RELAP5. The code was able to calculate the axial flow redistribution within the two test assemblies. Overall, S-RELAP5 does as well as, or better than, core flow distribution codes used for core flow and subchannel analysis of PWR cores. Calculated results were generally in reasonable agreement with the data.

Figure 8.2-564 Schematic of Test Assembly Showing Both Inlets and Levels for Pitot Tubes



The diagram shows a 13x13 grid of circles representing pitot tube locations. The columns are labeled at the top with numbers 1 through 13. The rows are labeled on the left with numbers 1 through 13. The grid is divided into three horizontal sections labeled ROW 1, ROW 2, and ROW 3. The vertical distance between the centerlines of ROW 1 and ROW 2 is 7.36, and the vertical distance between the centerlines of ROW 2 and ROW 3 is 7.63. The horizontal distance between the centerlines of the first and second columns is 0.61. The horizontal distance between the centerlines of the first and second columns is 7.36. The tube diameter is 0.425 and the pitch-to-diameter ratio is 1.28.

**Figure 8.2-566 Cross Sectional View of Test Assemblies with
Perforated Plate Between Test Assemblies**



**Figure 8.2-567 Nodalization Diagram for S-RELAP5 Modeling of Flow
Blockage Tests**

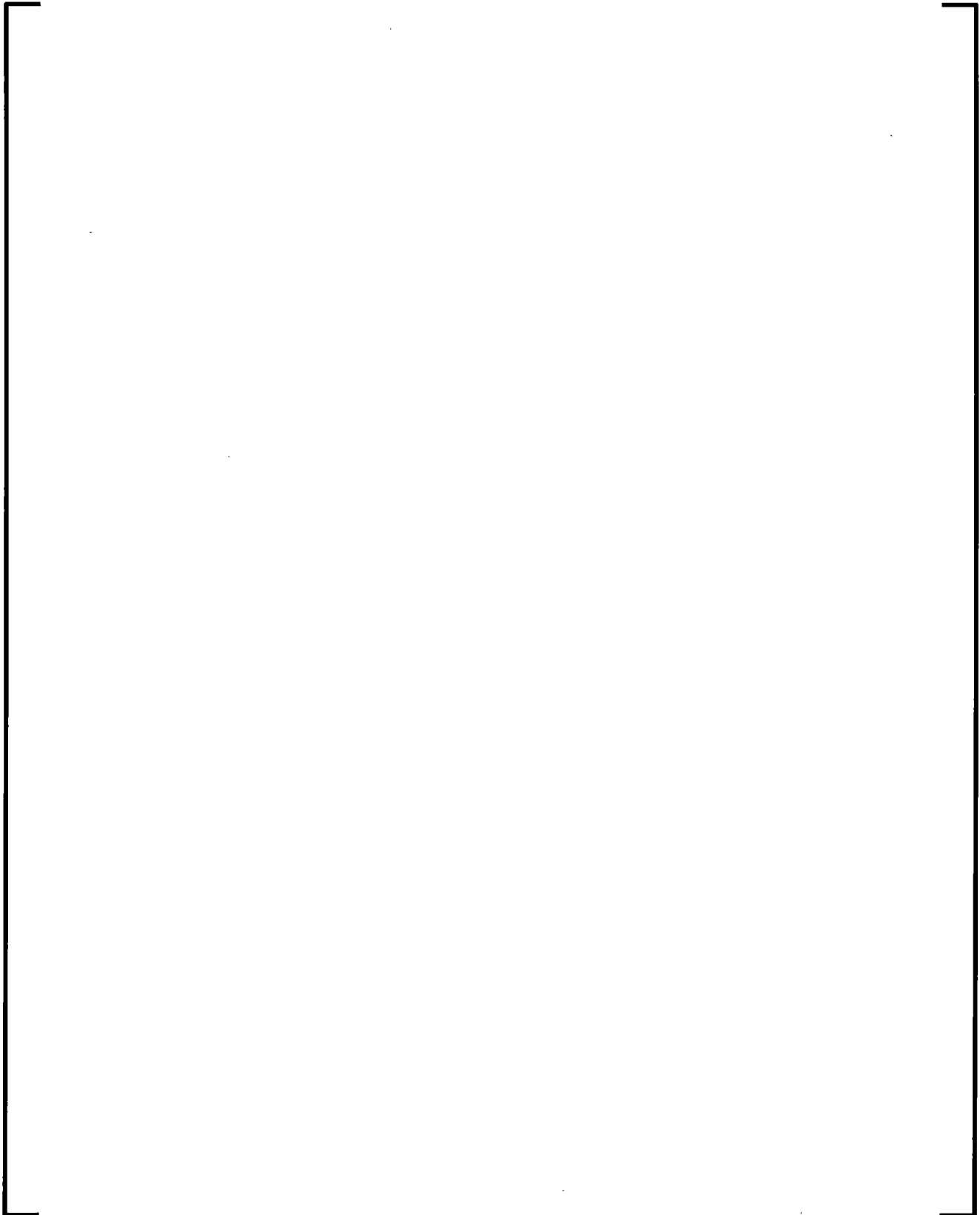


**Figure 8.2-568 Dependence of Form Loss Coefficient on Distance
from Gap Between the Bundles**

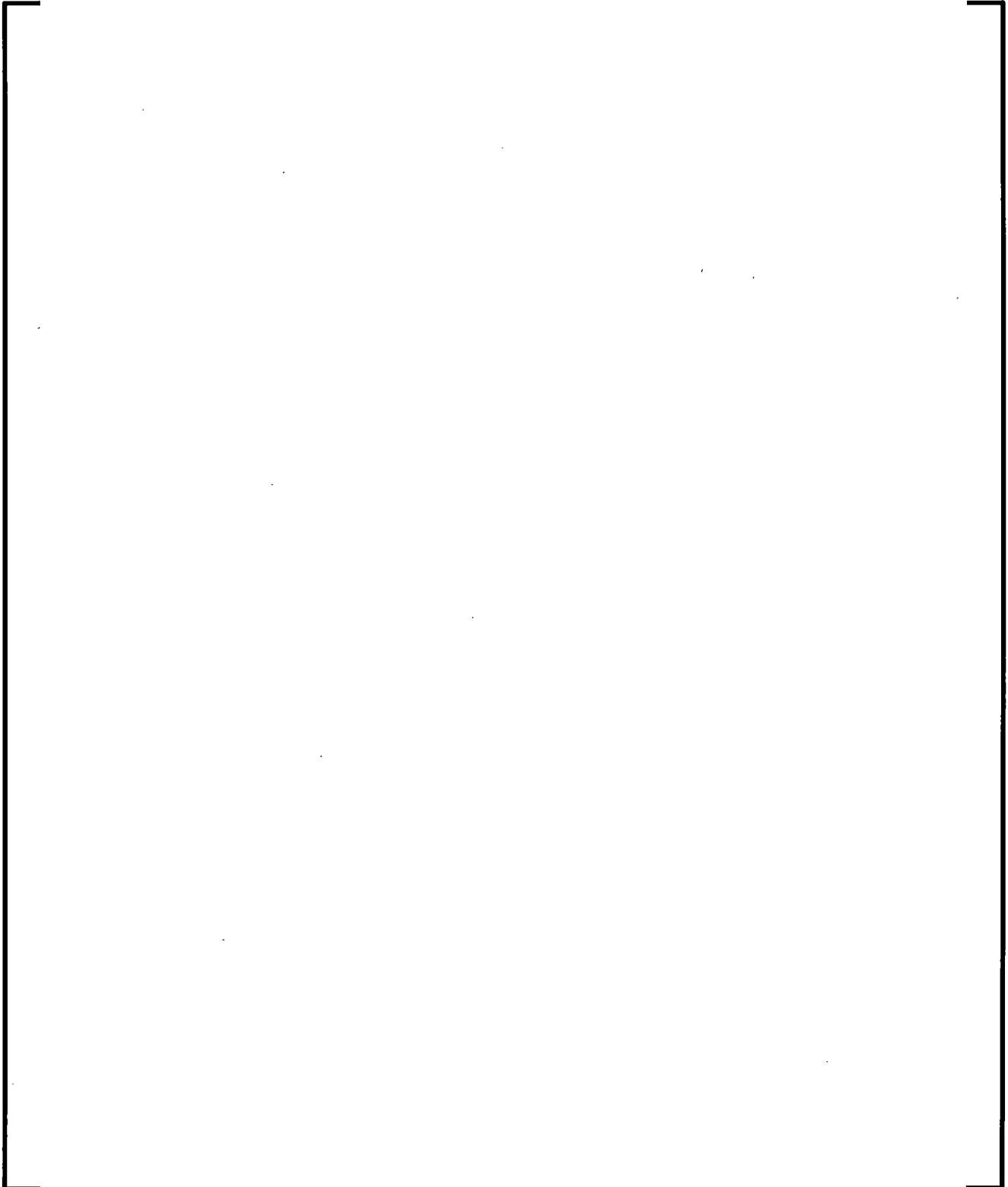


**Figure 8.2-569 Axial Velocities for at 7.5 Inches, Asymmetric Flow -
Test 1**

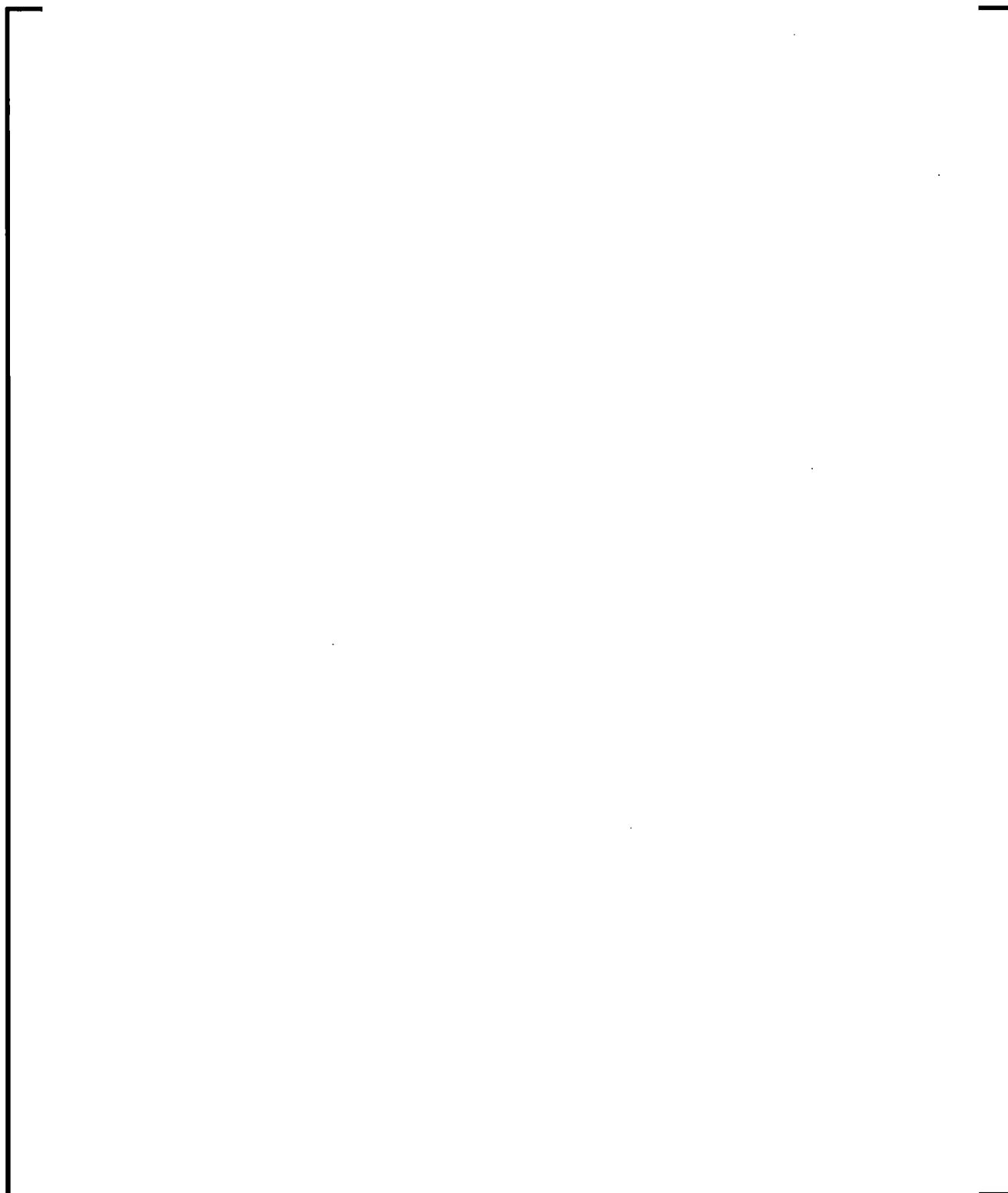


**Figure 8.2-570 Axial Velocities for at 12.5 Inches, Asymmetric Flow -
Test 1**

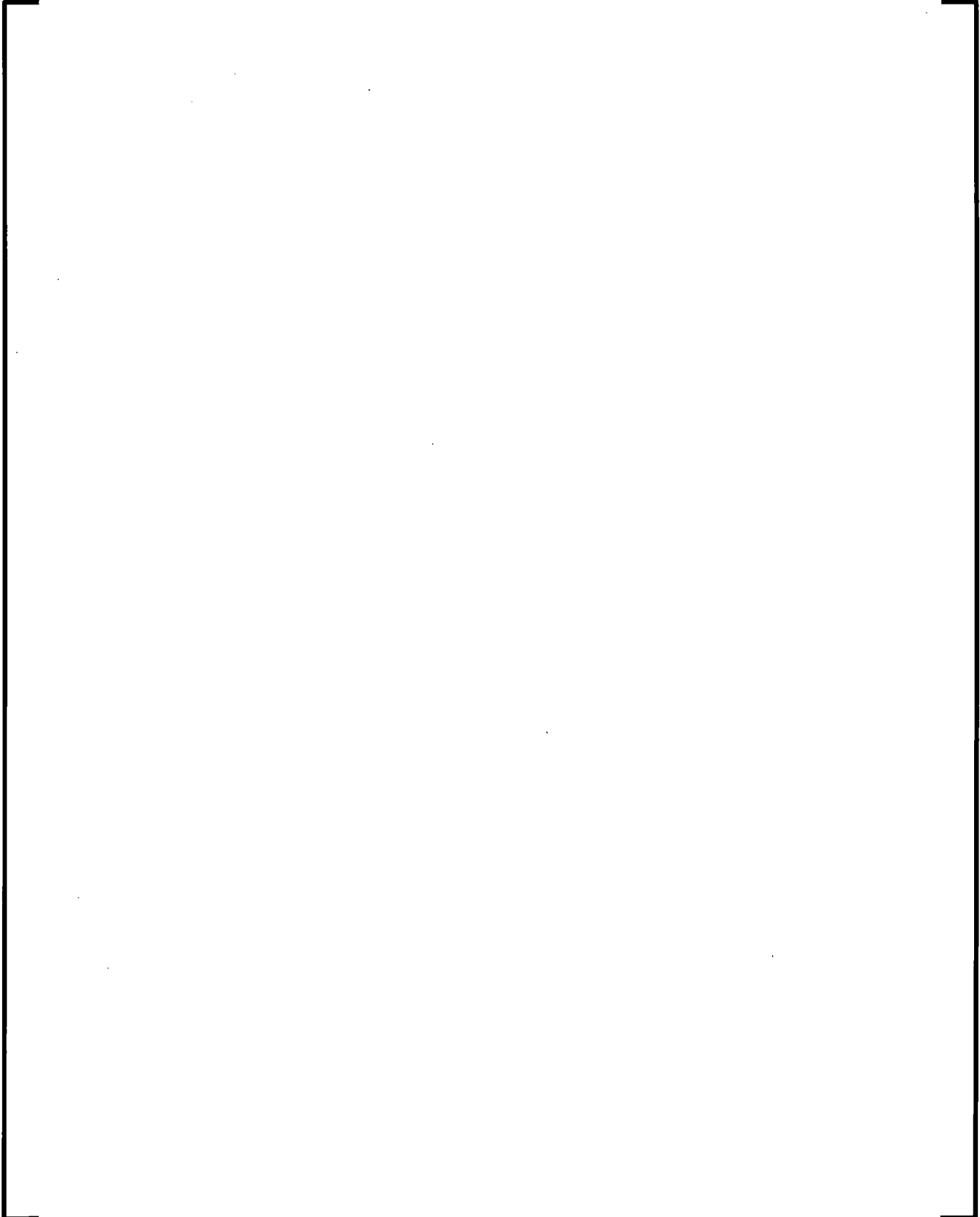


**Figure 8.2-571 Axial Velocities for at 17.5 Inches, Asymmetric Flow -
Test 1**

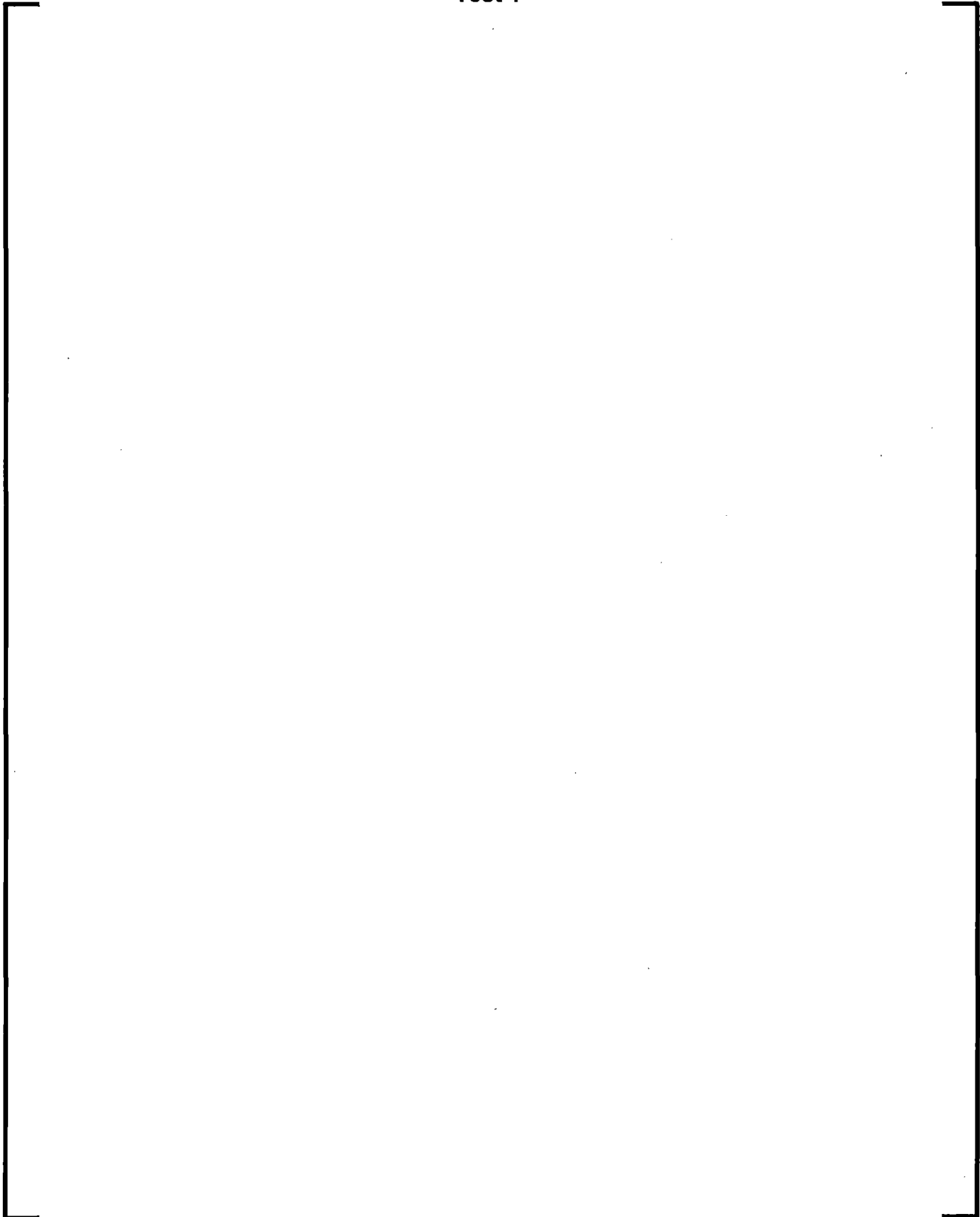


**Figure 8.2-572 Axial Velocities for at 22.5 Inches, Asymmetric Flow -
Test 1**

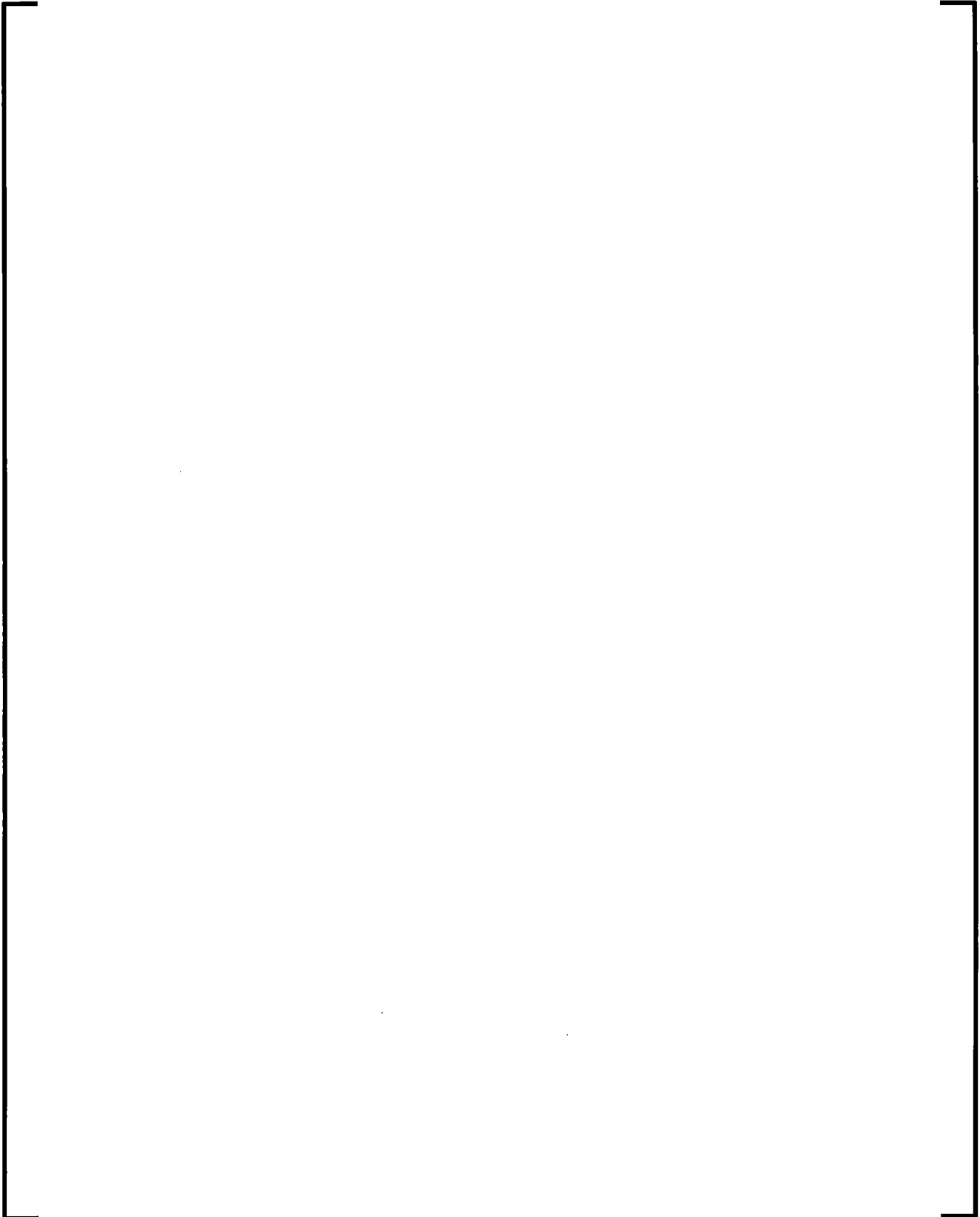


**Figure 8.2-573 Axial Velocities for at 27.5 Inches, Asymmetric Flow -
Test 1**

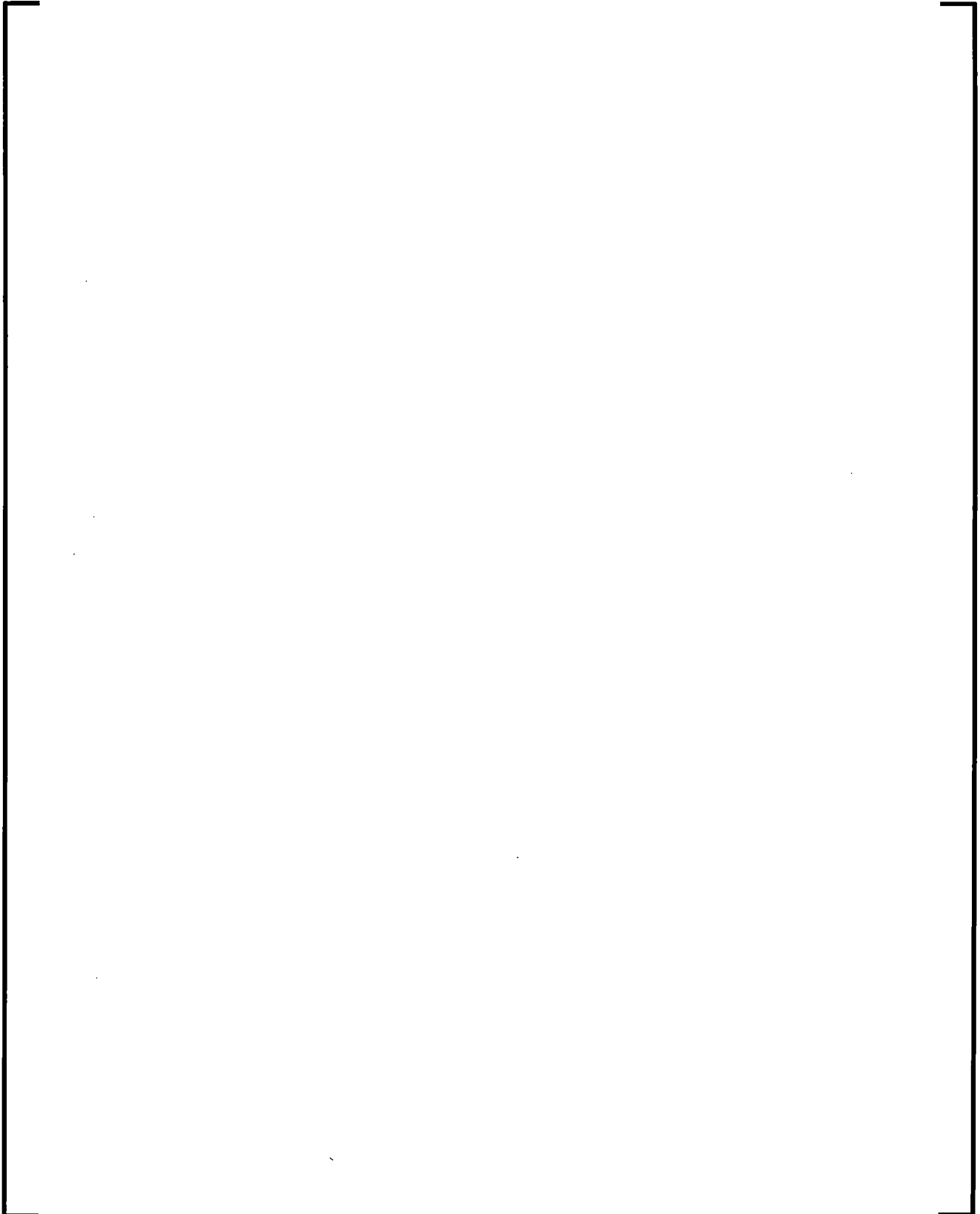


**Figure 8.2-574 Axial Velocities for at 32.5 Inches, Asymmetric Flow -
Test 1**



Figure 8.2-575 Axial Flow Fractions for Asymmetric Flow - Test 1



**Figure 8.2-576 Axial Velocities at 7.5 Inches, for Asymmetric Flow -
Test 2**



**Figure 8.2-577 Axial Velocities at 12.5 Inches, for Asymmetric Flow -
Test 2**



**Figure 8.2-578 Axial Velocities at 17.5 Inches, for Asymmetric Flow -
Test 2**



**Figure 8.2-579 Axial Velocities at 22.5 Inches, for Asymmetric Flow -
Test 2**



**Figure 8.2-580 Axial Velocities at 27.5 Inches, for Asymmetric Flow -
Test 2**



**Figure 8.2-581 Axial Velocities at 32.5 Inches, for Asymmetric Flow -
Test 2**



Figure 8.2-582 Axial Flow Fractions for Asymmetric Flow - Test 2



**Figure 8.2-583 Axial Velocities at 7.5 Inches, for Asymmetric Flow -
Test 3**



**Figure 8.2-584 Axial Velocities at 12.5 Inches, for Asymmetric Flow -
Test 3**



**Figure 8.2-585 Axial Velocities at 17.5 Inches, for Asymmetric Flow -
Test 3**



**Figure 8.2-586 Axial Velocities at 22.5 Inches, for Asymmetric Flow -
Test 3**



**Figure 8.2-587 Axial Velocities at 27.5 Inches, for Asymmetric Flow -
Test 3**



**Figure 8.2-588 Axial Velocities at 32.5 Inches, for Asymmetric Flow -
Test 3**



8.2.15 ACHILLES ISP 25

8.2.15.1 Introduction

International Standard Problem Number 25 (ISP 25) (Reference 8.2-63) is based on a test in the ACHILLES facility that simulated the latter phase of accumulator injection. ISP 25 tests the ability of system codes, to evaluate the impact of the nitrogen cover gas in the accumulator on the large-break loss-of-coolant accident (LBLOCA). The accumulator in a pressurized water reactor (PWR) is pressurized with nitrogen. When the system pressure falls below the nitrogen pressure, the borated water from the accumulator empties into the primary system. The cover gas then enters the upper part of the downcomer where it causes the pressure to increase. The increased pressure depresses the level in the downcomer, resulting in a surge of water into the core. The gas bypasses the core and flows out through the break; and in a few seconds the pressure drops, the downcomer level recovers, and the nitrogen has no further effect on the transient.

The difference between a pressurization surge caused by steam and one caused by nitrogen is that the nitrogen does not condense the way steam does. In effect, the nitrogen can act like a large piston pushing the fluid into the core. In this case, the code could over-predict the surge into the core and the transient cooling caused by this in-surge, thereby under predicting peak cladding temperature (PCT). The ability of S-RELAP5 to predict both system and temperature responses was confirmed by comparing the calculated values to the measurements.

8.2.15.2 Summary and Conclusions

ISP 25 was analyzed using S-RELAP5 and modeling consistent with the realistic LBLOCA methodology. S-RELAP5 was able to predict good values for liquid surge into the core, for liquid carryover to the upper plenum, and for rod thermocouple readings. In particular, the surge into the core when the nitrogen flow is initiated is under-predicted, resulting in the lower system pressure increase as compared to the test.

[

]

8.2.15.3 Test Facility

Figure 8.2-589 shows the schematic for the ACHILLES test facility. The facility can simulate the latter stages of accumulator injection in an LBLOCA. The simulated downcomer is connected to the bottom of the core, and valve V108 is closed before nitrogen injection begins, and is used to hold the water in the downcomer until injection occurs. Valve V109 is opened before injection begins and provides a flow path for the pumped water so that it does not enter the core. This valve closes on initiation of nitrogen injection. The simulated core has 69 simulated fuel rods with geometry similar to that of a Westinghouse 17 x 17 design. The simulated core has 8 spacer grids. The rods are housed in a piece of pipe. The exit region has a centrifugal separator to collect carryover water. The steam then joins the nitrogen bypass flow and exits.

The nitrogen tank is connected to the top of the simulated downcomer and valve V426, which is initially closed, opens to initiate the nitrogen flow. Nitrogen forces flow through the core by increasing the pressure in the downcomer. Nitrogen also flows through a bypass path to join the steam that has passed through the core, and then it exits. Flowmeter F106 measures the nitrogen flow from the tank and flowmeter F103 measures the bypass flow.

Figure 8.2-590 shows the cross section of the test assembly. The rods are identified by coordinates. The letters on the left are combined with the numbers across the bottom to identify the simulated fuel rods. Each rod has multiple thermocouples on the surface of the rod. The PCT level (2.13 m) is the most heavily instrumented, with 66 thermocouples.

8.2.15.4 Test Description

Before beginning the test, valves V108 and V426 are closed and the pumped water is flowing into the simulated lower reactor vessel internals through flowmeter F101 and out through valve V109. The core power is adjusted to maintain a temperature of about 963.4 K at the peak power location. Table 8.2-67 summarizes the general conditions before the nitrogen injection begins. Table 8.2-68 gives the axial power distribution.

Valve V109 is closed and valves V108 and V426 are opened to initiate the event. An immediate pressure transient occurs at the top of the downcomer, forcing flow into the core. Most of the flow bypasses through flowmeter F103. The amount of flow is controlled by Orifice #2 (see Figure 8.2-589). The initial pressurization of the downcomer causes a rapid surge into the simulated core. As the nitrogen leaves the system via the bypass (Orifice #2), the pressure drops at the top of the downcomer, the level recovers, and the core reflooding depends on the pumped water flow, which is entering both the downcomer and the core. The power ramps down (see Figure 8.2-591) and the core quenches.

8.2.15.5 S-RELAP5 Model Description

Figure 8.2-592 displays the base nodalization diagram for ISP 25. [

]

Figure 8.2-593 presents the range of variation in the thermocouple readings at the PCT elevation (2.13 m). This is not a consequence of power variation because the rods are all the same power. Three rods set the lower bound: B8, H2, and H8. Figure 8.2-590 shows that all three of these rods are located in the same environment in the test assembly. The early quench indicates that the flow field near the shroud is far different from that in the interior.

The remaining rods can be divided into one group that tracks the maximum fairly well and another group that falls well below the maximum, but not as dramatically as the three rods setting the lower limit. To get a reasonable prediction of core temperatures will require a multidimensional analysis.

The radial and azimuthal inhomogeneity is even greater than would be experienced in a core because the flow path on the periphery has hydraulic properties which are significantly different from the interior flow paths. While a reactor core is anisotropic and inhomogeneous, it does not have the range of variations this test assembly has. Thus, predicting the reflood behavior for this test assembly is significantly more challenging than for a PWR core. This test is International Standard Problem ISP-25 and the summary report 8.2-63 concluded that "none of the codes produced a completely satisfactory prediction," which further indicates the atypicality of the ACHILLES test.

[

] The comparisons to data were made by comparing the predictions for the central channel with the measured values for the same 21 rods. The

[

] are used for film boiling (FILMBL) and dispersed flow film boiling (DFFBHTC) heat transfer coefficients. Since a hot pin is not modeled separately, the rod-to-rod radiation heat transfer option is not used in the bundle region. Additionally, the maximum PCT does not exceed 1800 °F, which means the rod-to-rod radiation model would have minimal impact on the results. The [

] at the bundle exit since, in the test facility, there is a steam/water separator in the upper plenum which is also modeled in the S-RELAP5 input model.

8.2.15.6 Calculated Results

Figure 8.2-594 shows the nitrogen flow at the Venturi flowmeter, F106. The agreement is excellent until frost forms in the throat of the venturi at about 7.5 seconds (Reference 8.2-63). The time-to-empty agrees to within about 2.5 seconds. Figure 8.2-595 presents the nitrogen flow rate through the bypass (F103). [

]

Figure 8.2-596 compares the calculated liquid carryover at the core exit to the measured carryover. [

] Nothing in the thermocouple data distinguishes this time period.

Figure 8.2-597 compares the steaming rate at the core exit and shows a good agreement between the calculations and the measured data.

The downcomer level measurements are generally slightly higher than the calculated values (Figure 8.2-598), indicating that the pressure drop through the core and the two sets of separators is slightly higher than is modeled (See Figure 8.2-612 and Figure 8.2-613). Losses through the loop were added as specified in Reference 8.2-63 in order to bring the level to its current position. The core collapsed level (Figure 8.2-599), which is not very sensitive to pressure drop variations, matches quite well.

The downcomer ΔP measurements indicate an insurge of water in the core as soon as the nitrogen injection starts. The core ΔP measurements indicate an increase in the core level. The data indicate that most of the insurge of water was pushed out of the core within 5 seconds. This is not completely reflected in the downcomer ΔP measurements. Insufficient information is available to understand this difference. The calculated results (Figure 8.2-599) show less insurge into the core and as a result the downcomer level (Figure 8.2-598) increased during this early phase of the transient. Once the cover gas effect subsides, the calculated downcomer and core levels agreed reasonably well with the data. The results indicate that S-RELAP5 will underpredict the liquid insurge into the core, resulting in less core cooling after the accumulator tanks empty and the cover gas from the tanks enters the primary system.

Figure 8.2-600 through Figure 8.2-605 compare calculated temperatures for the central region to measured temperatures for the []

The maximum, minimum, and average temperatures are plotted along with the calculated temperature for elevations from 1.08 m to 3.18 m. The calculated values are generally in good agreement with the measured values. []

]

Just above the PCT elevation the behavior of the central region begins to become more complicated. [

]

Considering the observed atypicality in the bundle flow behavior, the differences in results are considered acceptable.

The impact of the nitrogen injection, which is the focus of this comparison, can be seen in the first 25 seconds of the transient. Figure 8.2-606 to Figure 8.2-611 are the same comparisons discussed in the previous paragraph, except the time and temperature scales have been adjusted to emphasize the nitrogen effects.

[

]

The smaller decrease in the calculated cladding temperature results in lower core steam production, resulting in a lower system pressure increase compared to the data as shown in Figure 8.2-612 and Figure 8.2-613. These results support the conclusions drawn earlier from the core and downcomer ΔP results.

8.2.15.7 Discussion of Results

The rod thermocouples all show a transient temperature reduction at the beginning of the event. This initial cool-down is caused by the nitrogen in-surge that initiates the event. S-RELAP5 calculates a conservatively small cool-down compared to the data.

The heat-up that follows is unaffected by the nitrogen, which has bled out of the system by this time. However, the test assembly has gaps around the outer edge that allow steam and liquid to bypass the core. This results in very different behavior between peripheral rods and central rods. At the higher elevations, the quench behavior of the rods, even in the central region begins to vary. More detailed modeling of the phenomena involved would be required to capture this inhomogeneity. The hydraulic behavior of the test assembly is far more inhomogeneous than a PWR core, and modeling this test assembly with increased complexity would not have any particular implications for realistic LBLOCA. [

]

Table 8.2-67 Initial Conditions for ACHILLES ISP 25

Parameter	Value
Power (kW)	0.0
Pumped Water Flow rate (kg/s)	0.291
Pumped Water Temperature (K)	396 (123 °C)
Peak Initial Cladding Temperature (K)	963.4 (690.25 °C)
System Pressure (bar)	3.01
Nitrogen Pressure (bar)	13.3
Nitrogen Temperature (K)	294.15 (21 °C)

**Table 8.2-68 Axial Power Shape for Simulated Fuel Rods, ACHILLES
ISP 25**

Lower End of Region (mm)	Upper End of Region (mm)	Relative Power
0	383	0.428
383	644	0.751
644	906	0.979
906	1167	1.168
1167	1429	1.309
1429	2213	1.408
2213	2475	1.316
2475	2736	1.178
2736	2998	0.992
2998	3259	0.765
3259	3658	0.436
3658	3782	0.000

Figure 8.2-589 Schematic of ACHILLES Test Rig

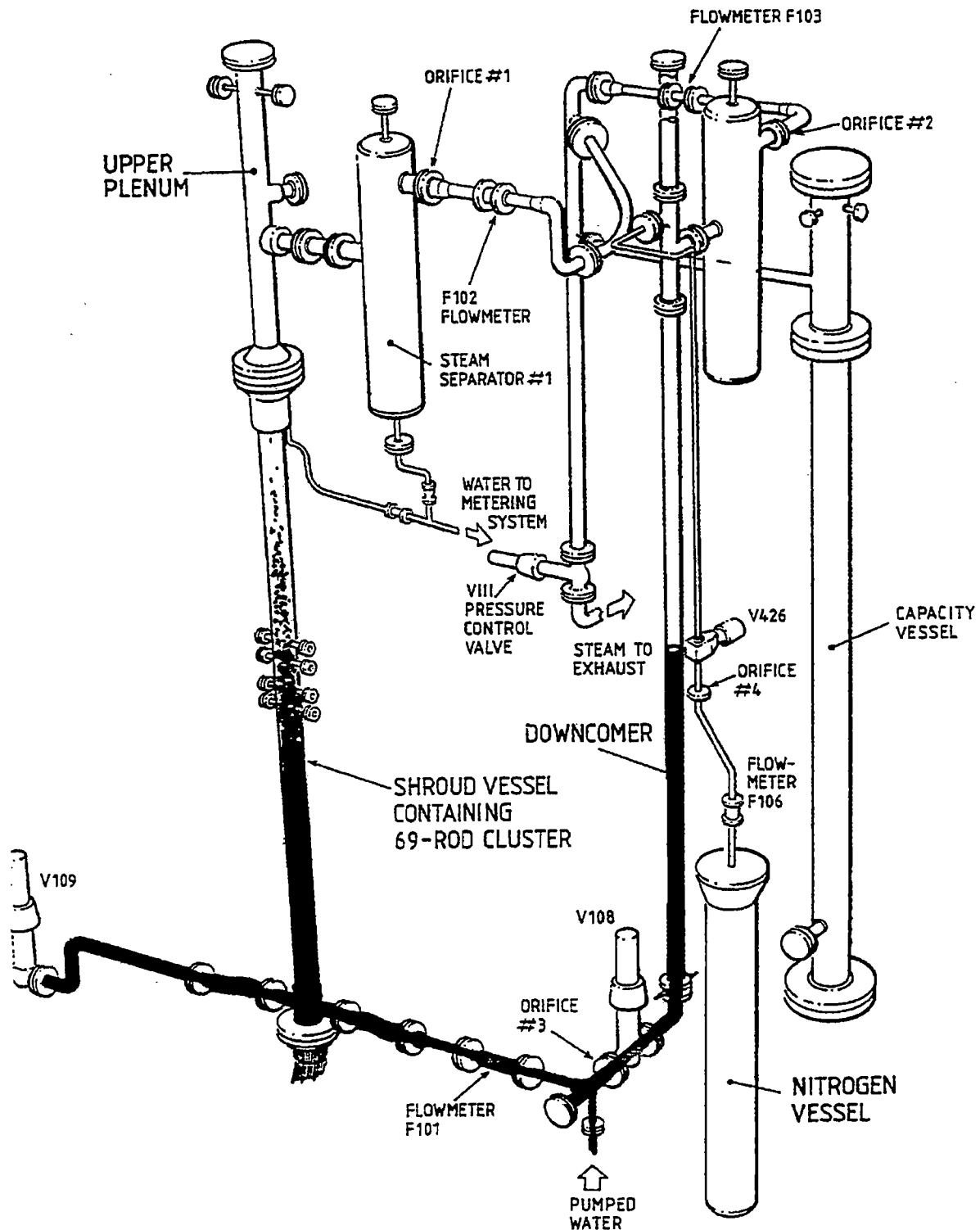


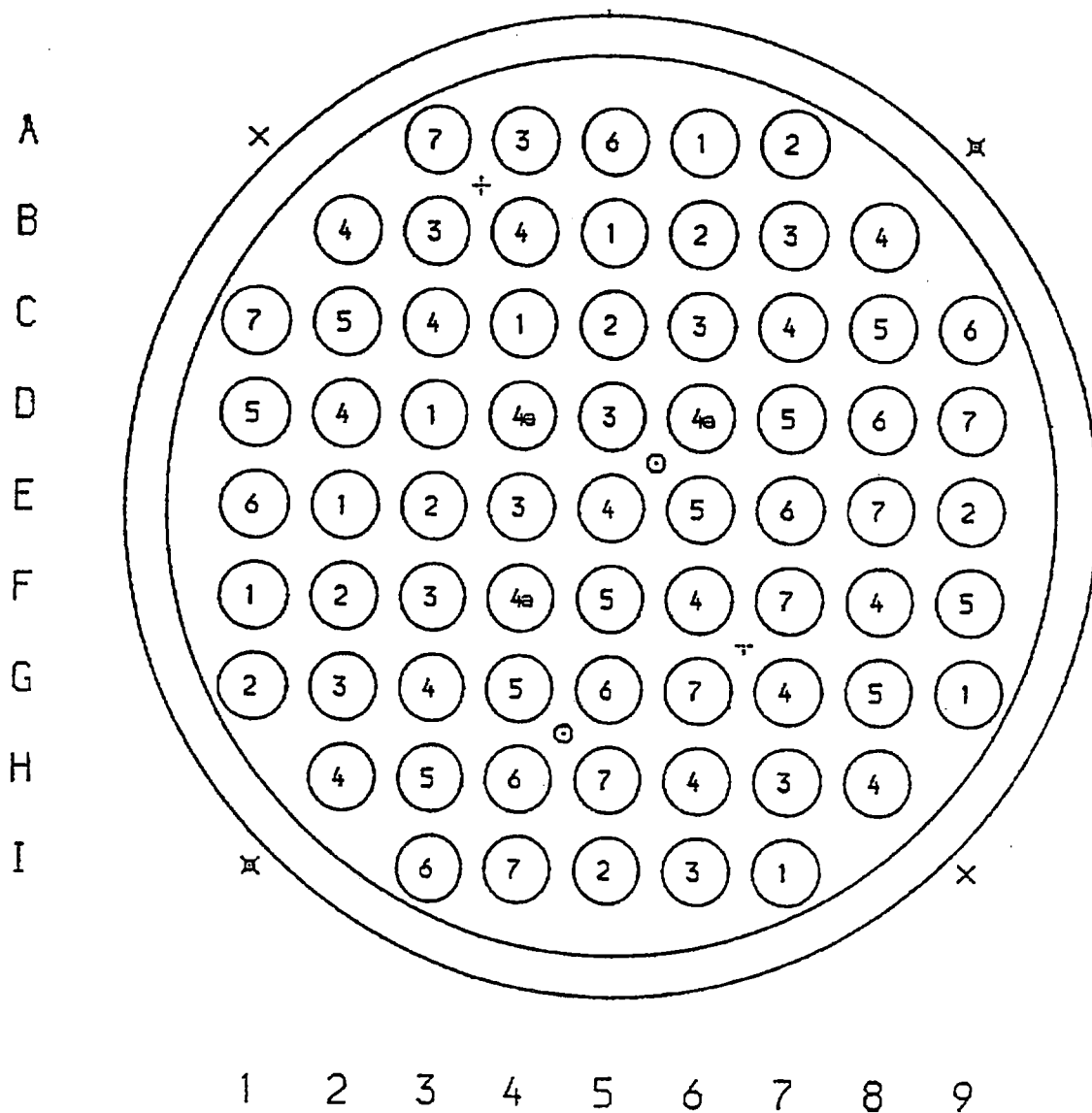
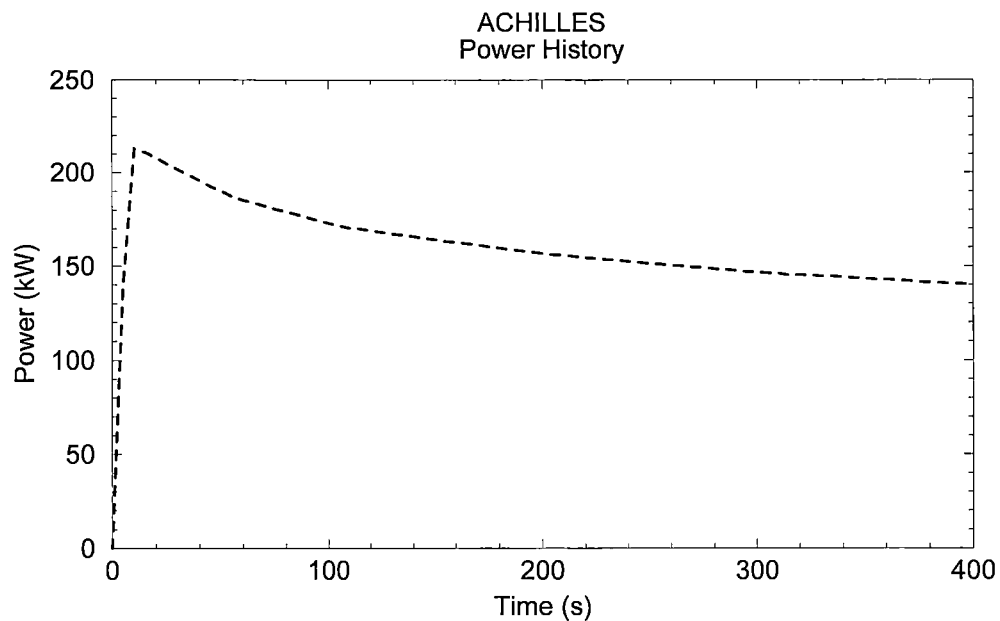
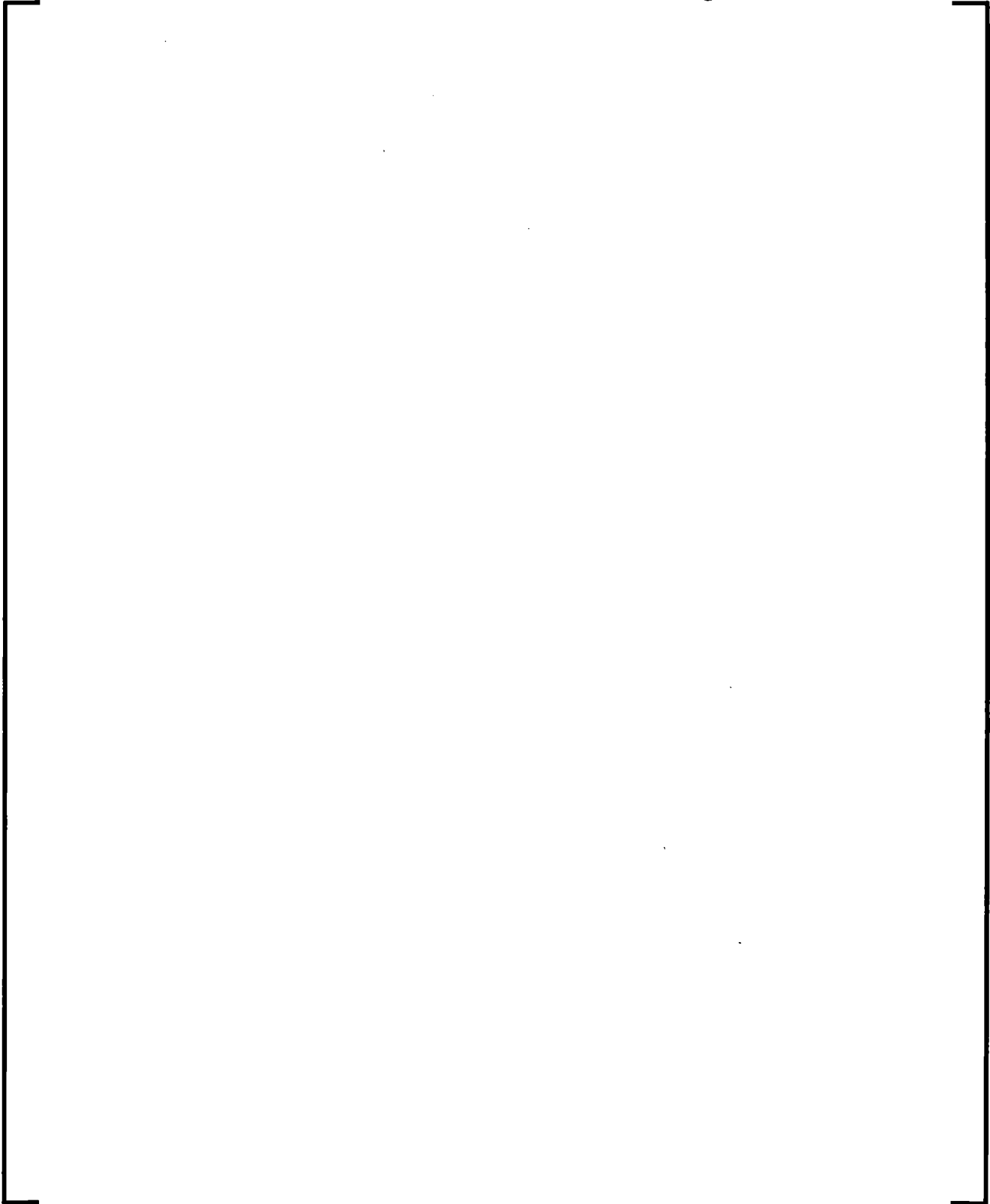
Figure 8.2-590 ACHILLES Test Assembly Cross Section

Figure 8.2-591 Power History, ACHILLES ISP 25

ID:25472 23Feb2010 09:30:06 meth.dmx

PLOT FILE NAME: power.eps, JOB ID: achilles_plots.sh.o57281, DATE: Wed Jun 16 15:15:31 PDT 2010

Figure 8.2-592 ACHILLES Nodalization Diagram



**Figure 8.2-593 Thermocouple Variation Range at the PCT Elevation,
ACHILLES ISP 25**



Figure 8.2-594 Total Nitrogen Flow, ACHILLES ISP 25



Figure 8.2-595 Nitrogen Bypass Flow, ACHILLES ISP 25



Figure 8.2-596 Liquid Carryover from Core, ACHILLES ISP 25



Figure 8.2-597 Steaming Rate at Core Exit, ACHILLES ISP 25



Figure 8.2-598 Downcomer Level, ACHILLES ISP 25



Figure 8.2-599 Core Collapsed Liquid Level, ACHILLES ISP 25



Figure 8.2-600 Rod Thermocouple at 1.08 m, ACHILLES ISP 25



Figure 8.2-601 Rod Thermocouple at 1.81 m, ACHILLES ISP 25



Figure 8.2-602 Rod Thermocouple at 2.13 m, ACHILLES ISP 25



Figure 8.2-603 Rod Thermocouple at 2.33 m, ACHILLES ISP 25



Figure 8.2-604 Rod Thermocouple at 2.65 m, ACHILLES ISP 25



Figure 8.2-605 Rod Thermocouple at 3.18 m, ACHILLES ISP 25



Figure 8.2-606 Nitrogen Insurge Impact at 1.08 m, ACHILLES ISP 25



Figure 8.2-607 Nitrogen Insurge Impact at 1.81 m, ACHILLES ISP 25



Figure 8.2-608 Nitrogen Insurge Impact at 2.13 m, ACHILLES ISP 25



Figure 8.2-609 Nitrogen Insurge Impact at 2.33 m, ACHILLES ISP 25



Figure 8.2-610 Nitrogen Insurge Impact at 2.65 m, ACHILLES ISP 25



Figure 8.2-611 Nitrogen Insurge Impact at 3.18 m, ACHILLES ISP 25



**Figure 8.2-612 Upper Plenum Pressure for S-RELAP5 and Test Data,
ACHILLES ISP 25**



**Figure 8.2-613 Downcomer Pressure for S-RELAP5 and Test Data,
ACHILLES ISP 25**



8.2.16 Ferrell-McGee Assessment Using S-RELAP5

8.2.16.1 Introduction

The Ferrell-McGee tests (Reference 8.2-64), were simple separate effects tests with adiabatic two phase flow through an expansion. The purpose of the assessment is to evaluate the capability of S-RELAP5 to calculate flow and pressure drop phenomena for flow through an abrupt expansion at low pressure. The test assessment demonstrates S-RELAP5 capability to calculate basic phenomena; thus, it is appropriate that this assessment be included in the S-RELAP5 assessment matrix.

8.2.16.2 Summary and Conclusions

The Ferrell-McGee test section was modeled by S-RELAP5 using the specified flow rate for the inflow boundary conditions, the test pressure for the outlet boundary condition, and the specified pipe dimensions where the area change included form losses. The calculated two-phase pressure drop from the Ferrell-McGee simulation was [

] of the measured data, and therefore in excellent agreement with the data. This agreement demonstrates that the two-phase wall friction is acceptable, especially at low pressures, and that using the single-phase loss coefficient for abrupt area changes under two-phase conditions is also acceptable. Therefore, S-RELAP5 is expected to accurately model the two-phase frictional pressure drop and the two-phase pressure drop form loss modeling in the RLBLOCA Revision 3 plant model during a LBLOCA analysis.

8.2.16.3 Facility Description

The Ferrell-McGee test loop is shown in Figure 8.2-614, and the adiabatic test section is shown in Figure 8.2-615. Figure 8.2-615 shows the pressure tap locations, the location of the abrupt area change, and lengths of the upper and lower pipes. The test was executed by first establishing the desired flow rate, pre-heat the fluid to desired subcooling, and apply power to the heated section (located upstream of the test section) to establish the desired test conditions. The test loop was allowed to come up to test conditions over a period of one hour before data was recorded.

8.2.16.4 S-RELAP5 Model Description

The Ferrell-McGee Test 2C-7 was simulated using S-RELAP5. The Revision 3 RLBLOCA input development guidelines (Section 9.0) were not followed since this assessment validates S-RELAP5 two-phase frictional flow in general. The test conditions were obtained from Reference 8.2-64 and are shown in Table 8.2-69. The test section geometry modeled is shown in Table 8.2-70.

For the inlet conditions, a time dependent volume was set to a pressure of 122.163 psia and quality of 0.0243 to approximate the station 1 pressure and void fraction from the measurements (Reference 8.2-64), the flow area was set to the lower test section flow area, and a time dependent junction was used to specify the inlet flow rates discussed above. The test section was represented by the pipe component which was initialized to saturated liquid at 118 psia. The outlet junction was set to the upper test section flow area, as was the outlet volume. The outlet volume was initialized to saturated steam at 117.97 psia, to represent the test section outlet pressure.

[

]

The loss terms are required to be specified by other means. For the Ferrell-McGee problem, the form losses were determined from Crane (Reference 8.2-65) and are computed (using diameters) as:

$$K_{\text{expansion}} = \left(1 - \frac{A_{\text{upstream}}}{A_{\text{downstream}}}\right)^2 = \left(1 - \frac{0.46^2}{0.59^2}\right)^2 = 0.154$$

$$K_{\text{contraction}} = 0.5 \cdot \left(1 - \frac{A_{\text{downstream}}}{A_{\text{upstream}}}\right)^2 = 0.5 \cdot \left(1 - \frac{0.46^2}{0.59^2}\right)^2 = 0.196$$

The S-RELAP5 nodalization diagram for the Ferrell-McGee experiment is shown in Figure 8.2-616.

8.2.16.5 Calculated Results

The problem was run to steady conditions with the above specified input. At the end of the calculation, the pressures were recorded and plotted as a function test section length, shown in Figure 8.2-617. The dashed line with hollow squares are the measured data at the specified measurement locations, while the S-RELAP5 results are the solid line with filled circles representing the cell centered pressures. Visual examination of the plot indicates that the overall pressure drop from the experiment is captured reasonably well with the S-RELAP5 model. S-RELAP5 captures the pressure rise from the expansion, which is emphasized by the form losses, and causes minor differences between measured and calculated results in the 24 to 48 inch elevation. That region is immediately downstream of the expansion, and the experimentalists (Reference 8.2-64) reported that it required several diameters for the flow and pressure gradient to stabilize. [

]

In summary, the Ferrell-McGee test section was modeled by S-RELAP5 using the specified flow rate for the inflow boundary conditions, the test pressure for the outlet boundary condition, and the specified pipe dimensions where the area change included form losses. Overall, the calculation is in very good agreement with the data. These results indicate that the overall two phase pressure drop in the RLBLOCA Revision 3 methodology will be well calculated, as well as using appropriate form losses for abrupt area change representation.

Table 8.2-69 Conditions for Test 2C-7, Ferrell-McGee

Pressure	120 psia
Flow Rate	1145 lb/hr
Quality	0.076

Table 8.2-70 Test Section Geometry for Test 2C-7, Ferrell-McGee

Lower	Length	24 inch
	Diameter	0.46 inch
	ϵ / D	0.00005 (Figure 4.6 on page 55 in Reference 8.2-65)
Upper	Length	48 inch
	Diameter	0.59 inch
	ϵ / D	0.00002 (page 56 in Reference 8.2-65)

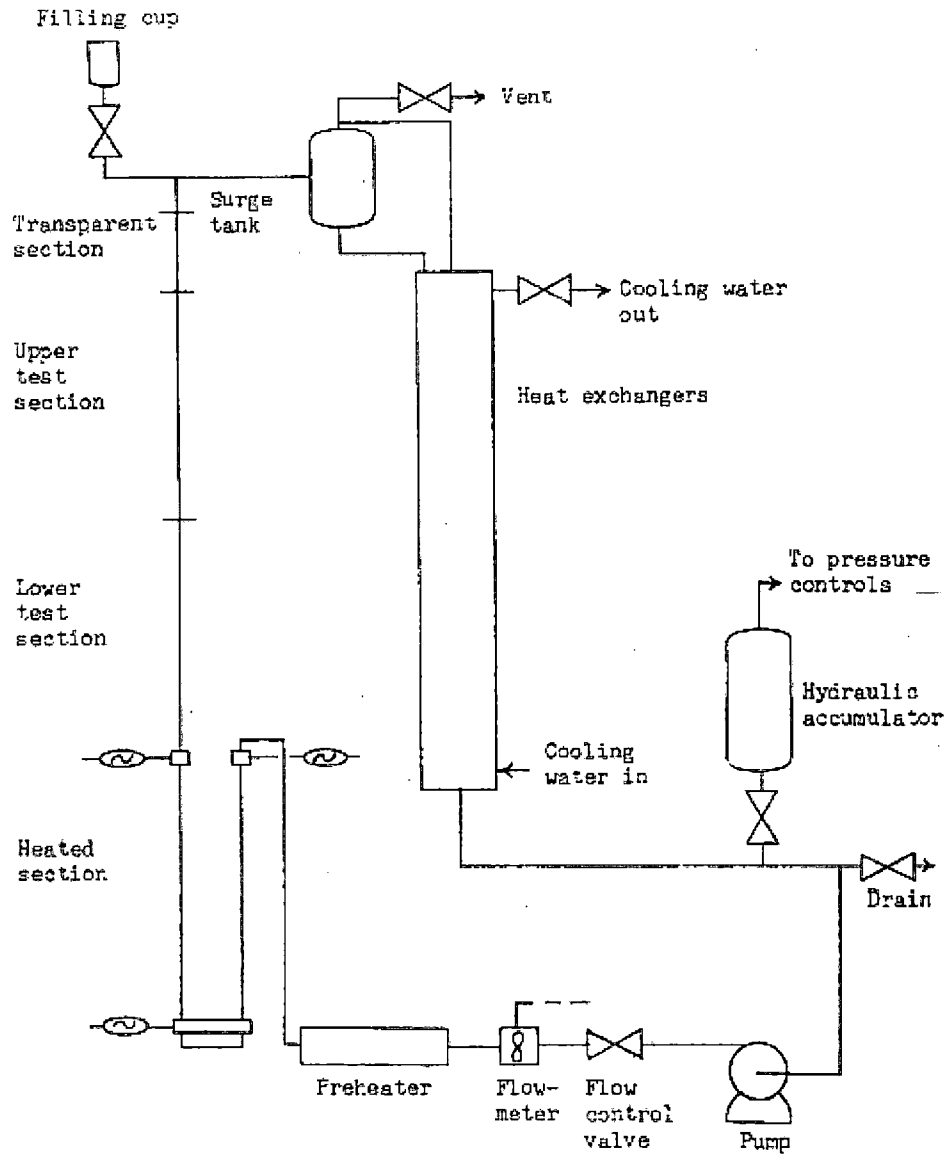
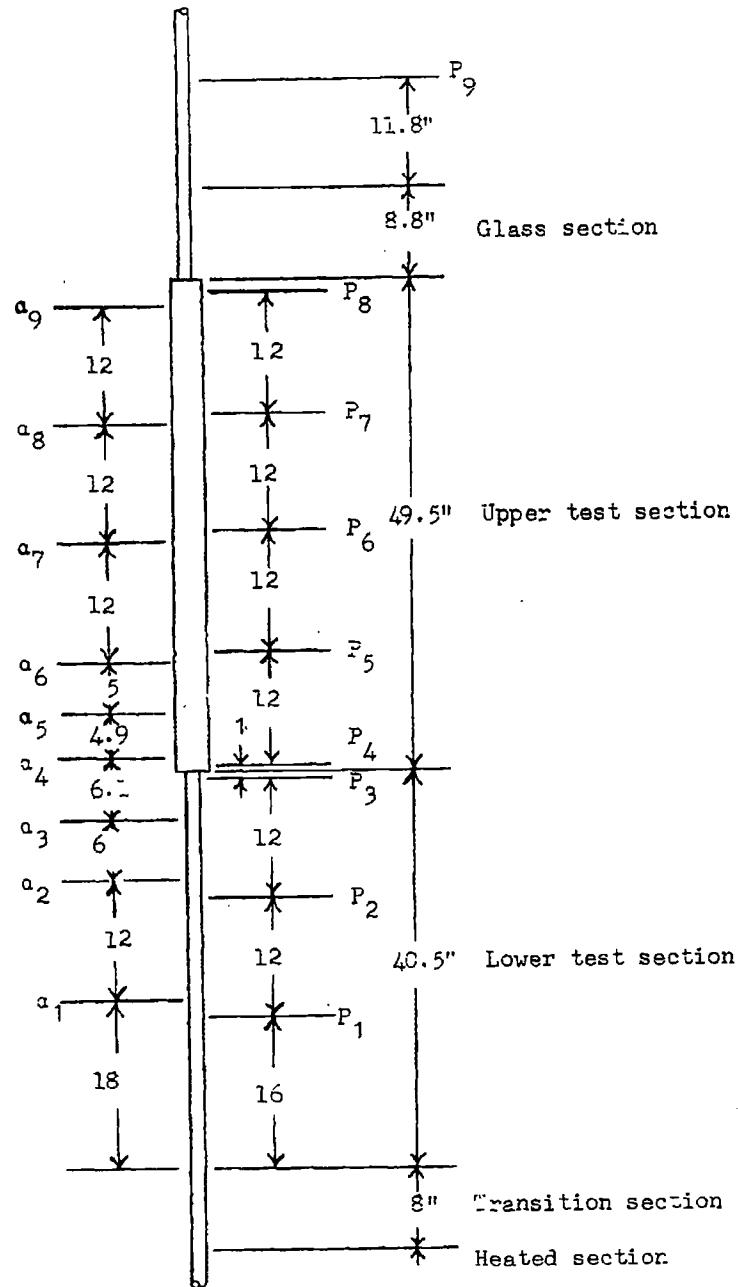
Figure 8.2-614 Schematic Of Ferrell-McGee Test Loop

Figure 8.2-615 Schematic of the Ferrell-McGee Test Section

**Figure 8.2-616 S-RELAP5 Nodalization for the Ferrell-McGee
Experiment**

**Figure 8.2-617 Comparison of Measured and Calculated Pressures
from the S-RELAP5 Simulation of the Ferrell-McGee Test 2C-7**

8.2.17 Moby Dick Test 3141 Assessment Using S-RELAP5

8.2.17.1 Introduction

The Moby Dick Flow Experiments were performed at the Centre d'Études Nucléaires de Grenoble in France, Reference 8.2-66 (Note that the TRACE Assessment Manual is referenced which includes all the relevant information about the experiment). The objective of this series of experiments was to study steady-state, two-phase, two component critical flow in a vertical, divergent nozzle at low pressure. During testing, a low quality water and nitrogen mixture flowed at high velocity through a vertical test section which included a divergent nozzle. Flashing was observed downstream of the divergent nozzle. Pressures and void fractions were measured at various points along the test section.

For this S-RELAP5 benchmark, the Moby Dick test 3141 is used as this test establishes choked flow for a two component (nitrogen/water) flow in a divergent nozzle, similar to the flow exiting the break during a postulated LBLOCA event. In support of the Revision 3 RLBLOCA methodology, this assessment is performed using the HEM option at the choke point. Otherwise, this assessment validates the code performance with respect to two component critical flow.

8.2.17.2 Summary and Conclusions

The critical flow model with non-condensables present in S-RELAP5 was examined and was determined to be performing as intended, and that model provides good agreement with test results. When the injected nitrogen gas causes a pressure increase, choking at the break becomes possible, depending both on the magnitude of the pressure rise and the flow area at the break. A benchmark of the S-RELAP5 critical flow calculation while nitrogen insurges the system and passes through the break, compares very well with test data obtained from the Moby Dick Critical Flow Experiments. Therefore, the critical flow model with non-condensables present is expected to capture the appropriate phenomena when the nitrogen cover gas surges into the RLBLOCA plant model as the accumulator empties.

8.2.17.3 Facility Description

The Moby Dick test facility's primary loop has five main components; a pump, a pre-heater, a nitrogen injection system, a test section, and a condenser. A simplified schematic of the facility as represented by the TRACE computer code is shown in Figure 8.2-618. Flow is directed vertically upward in the test section. The outlet of the vertical test section is located inside the condenser. Test flow conditions were obtained by maintaining constant inlet conditions to the test section and lowering the downstream pressure in the condenser to atmospheric pressure. Reference 8.2-66 describes the Moby Dick facility and provides the test data for the experiments. Figure 8.2-619 is a sketch of the actual Moby Dick facility, and Figure 8.2-620 depicts the vertical test tube, both are extracted from Reference 8.2-66.

Nitrogen is injected into the pipe at a location 0.985 meters upstream of the expansion. The gas is injected through four porous screens surrounding the flow pipe. Pressure measurements are taken at the various positions labeled with P1-P22, on Figure B.2-2 of Reference 8.2-66. Water temperature was measured at the inlet to the test section, and the temperature of the injected nitrogen was also measured. The accuracy of the temperature measurement is indicated to be ± 0.2 °C. The water mass flow rate was also measured.

Table B.2.1 of Reference 8.2-66 provides the dimensions of the test section. These are further shown here in Table 8.2-71.

8.2.17.4 S-RELAP5 Model Description

The S-RELAP5 model of the Moby-Dick test facility is based on the model used for the RELAP5/MOD2 Developmental Assessment, Reference 8.2-17 and is shown in Figure 8.2-621. [

] The boundary conditions are listed in Table 8.2-72. Time dependent volumes with the pressures listed in Table 8.2-72 were used at the inlet and outlet of the test section. The nitrogen was injected at a distance of 993 mm from the diffuser instead of the 985 mm specified as a result of node spacing that was used and is shown in Figure 8.2-621. This difference is considered insignificant.

The choked flow model was enabled at the entrance to the diffuser and disabled elsewhere.

8.2.17.5 Calculated Results

Summary results are presented in Table 8.2-73, showing the steady-state flow. Figure 8.2-622 compares the calculated axial pressures to the data obtained from the Moby Dick experiment. The data is read from the graph in Reference 8.2-66, page B-53, Fig. B.2-16.

The results show that S-RELAP5 predicted well the pressure gradient in the straight pipe, before and after the divergent nozzle. Flashing occurred at the diverging nozzle entrance and choked flow was calculated by S-RELAP5 using the HEM critical flow model. The calculated choked flow rate compares very well (within 5%) to the test steady-state flow rate.

Table 8.2-71 Moby Dick Facility Dimensions

Straight Inlet Section Length	2.668 m
Internal Diameter	0.014 m
Nitrogen Injection	0.985 m Upstream of Nozzle
Conical Convergent Nozzle Length:	0.2534 m
Straight Outlet Section Length	0.420 m
Internal Diameter	0.045 m
Divergent Angle	7°

Table 8.2-72 Boundary Conditions for the Moby Dick Test

Variable	Moby-Dick Test 3141	S-RELAP5
Upstream Liquid Temperature (°C)	35.5	35.5
Upstream Pressure (Pa)	561900	561900
Discharge Pressure (Pa)	103178	103180
Nitrogen Entrance Temperature (°C)	18	18
Nitrogen Flowrate (kg/sec)	6.101x10 ⁻³	6.101x10 ⁻³

Table 8.2-73 Steady-State Conditions for the Moby Dick Test

	Test	S-RELAP5
Choking at Divergent Nozzle	Yes	Yes
Liquid Flowrate (kg/sec)	1.222	1.2756
Pressure Upstream of Choking Plane (Pa)	-	261648
Pressure Downstream of Choking Plane (Pa)	-	103299

Pressure Sink

Straight Section

Divergent Section

Straight Section
0.27 m Length

Nitrogen Injection

2 3 4

Straight Section
2.393 m Length

Pressure Source

Figure 8.2-619 Moby Dick Test Loop

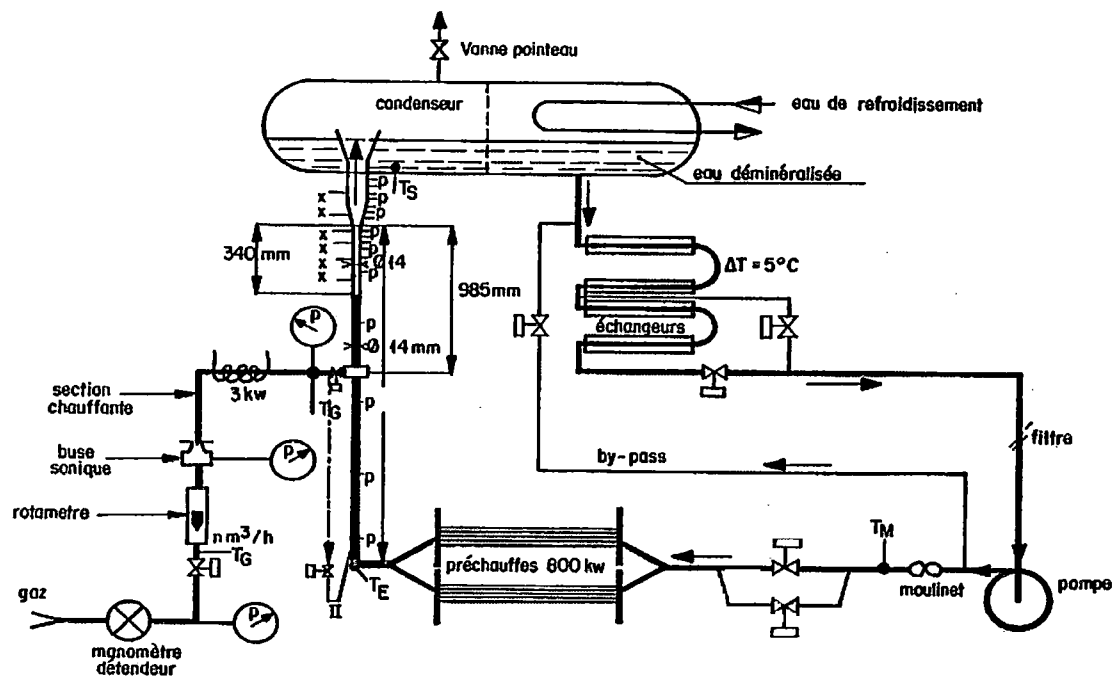


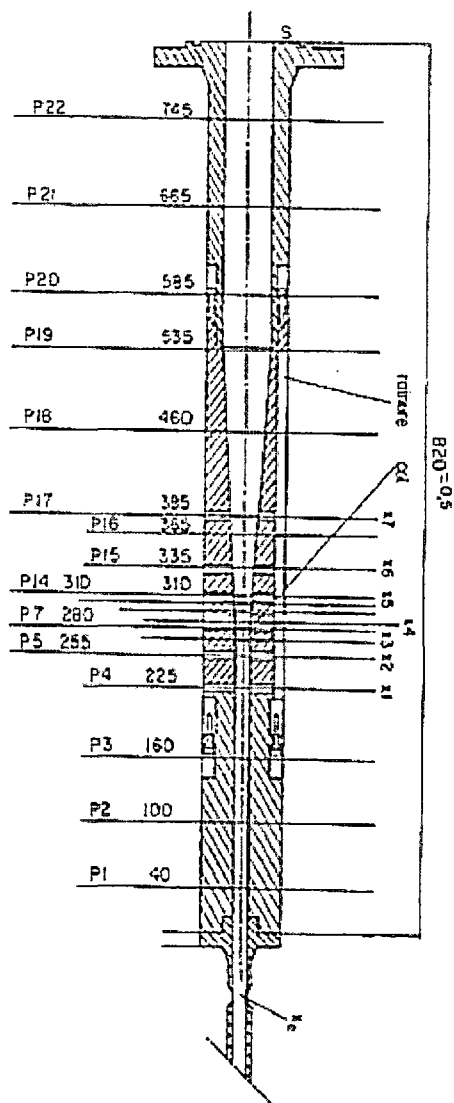
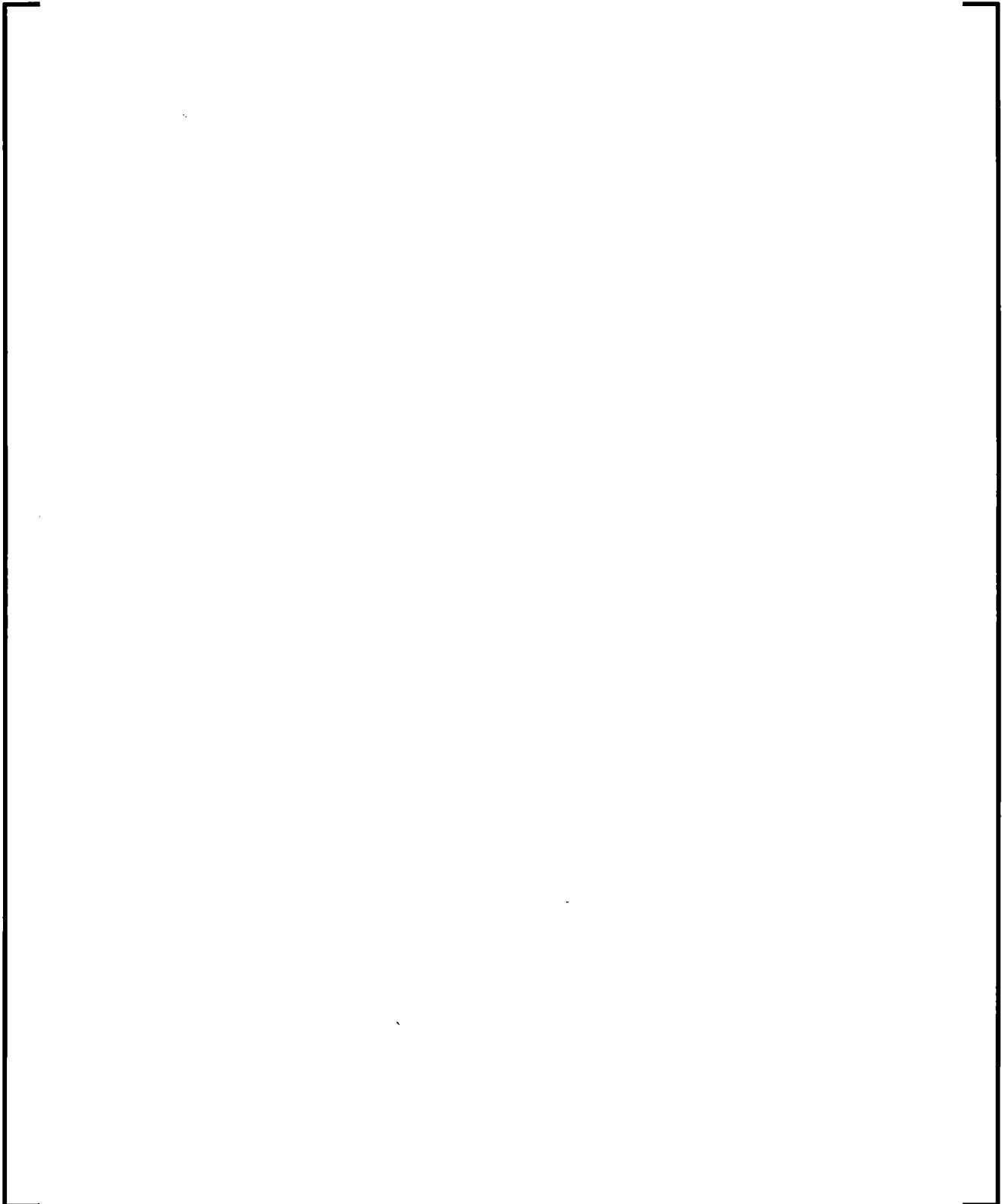
Figure 8.2-620 Moby Dick Test Section

Figure 8.2-621 S-RELAP5 Nodalization for Moby Dick Test



**Figure 8.2-622 Comparison of Moby Dick Data and S-RELAP5
Calculated Pressures**



8.2.18 Repetition of FLECHT-SEASET Benchmarks

A subset of the benchmarks documented in Sections 8.2.3, have been repeated with all EM modifications for this revision of the methodology. This subset consisted of the nine FLECHT experiments, which were chosen because these forced reflood separate-effect tests use injection or flooding rates that are very demanding for simulations with the realistic system codes, and because this test selection covers the whole range of pressure, sub-cooling and flooding rate, and includes cosine and skewed axial power profiles. The purpose of re-performing these benchmarks was to verify the impact of the EM changes described in Section 8.1.5 as well as to validate the model for heat transfer enhancement due to grid spacer reflood effects, described in Section 7.5.4.10.1. To perform this verification and validation, AREVA NP selected the FLECHT SEASET Tests 31504, 31701, 31302, 31203, 31805, 32013, and 34209, and FLECHT Skewed Tests 13609 and 13914.

The test conditions and descriptions remain the same as documented in Section 8.2.3.

8.2.18.1 Calculated Results

[

]

[

Figure 8.2-623 provides the peak cladding temperature versus elevation result for test 31504. This test had a flooding rate of 0.97 inches per second, a pressure of 40 psia, and a coolant temperature of 123 °F. As shown in Figure 8.2-623, below the mid-plane of the core, the changes to the EM have little impact, and the code predicts the experiment well. Above the grid spacer at the 81.24 inch elevation, the code predicts additional heat transfer and cooler maximum cladding temperatures. The trend of the data is well predicted and the heat transfer remains conservative, predicting higher than measure temperatures. Based upon comparison to the FLECHT SEASET Test 31504, the EM changes to support Revision 3 of the methodology, including the model to enhance heat transfer due to grid spacer reflood effects, have no adverse impact on the results, with the calculation trending closer to the measurements, but remaining conservative.

Figure 8.2-623 Maximum Cladding Temperature at All Measured Elevations, FLECHT SEASET Test 31504



8.2.19 References

- 8.2-1 NUREG/CR-2456, ORNL-5848, Experimental Investigations of Uncovered Bundle Heat Transfer and Two-Phase Mixture Level Swell Under High Pressure Low Heat Flux Conditions, ORNL, March 1982.
- 8.2-2 NUREG/CR-2469, ORNL/NUREG-85, An Analysis of Transient Film Boiling of High-Pressure Water in a Rod Bundle, ORNL, March 1982.
- 8.2-3 NUREG/CR-2114, ORNL/NUREG/TM-446, ORNL Small-Break LOCA Heat Transfer Test Series 1: High-Pressure Reflood Analysis, ORNL, August 1981.
- 8.2-4 NUREG/CR-2455, ORNL-5846, Experimental Investigations of Bundle Boil-off and Reflood under High-Pressure Low Heat Flux Conditions, ORNL, April 1982.
- 8.2-5 UKAEA Research Group, AERE-R 5373, Heat Transfer to Steam-Water Mixtures Flowing in Uniformly Heated Tubes in Which the Critical Heat Flux has been Exceeded, October 1967.
- 8.2-6 Biasi et al., Studies on Burnout Part 3 - A New Correlation for Round Ducts and Uniform Heating and Its Comparison with World Data, *Energia Nucleare*, 14:530–536, 1967.
- 8.2-7 AREVA NP, EMF-2100(P). *S-RELAP5 Models and Correlations Code Manual*, December 2009, Revision 14.
- 8.2-8 D. C. Groeneveld, S. C. Cheng, and T. Doan, 1986 *AECL-UO Critical Heat Flux Lookup Table*, *Heat Transfer Engineering*, 7:46–62, 1986.
- 8.2-9 AREVA NP (Framatome ANP), EMF-2057(P) Revision 0. H. B. Robinson Unit 2 Plant Realistic Large Break LOCA/ECCS Analysis, August 2001.
- 8.2-10 AREVA NP (Framatome ANP), EMF-2103(P)(A) Revision 0, Realistic Large Break LOCA ECCS Methodology for Pressurized Water Reactors, April 2003.

- 8.2-11 J. C. M. Leung, *Transient Critical Heat Flux and Blowdown Heat Transfer Studies*, PhD thesis, Northwestern University, June 1980.
- 8.2-12 P. Griffith, J. F. Pearson, and R. J. Lepkowski, *Critical Heat Flux During a Loss-of Coolant Accident*, Nuclear Safety, 18:298–309, 1977.
- 8.2-13 Electric Power Research Institute, EPRI NP-1459, NUREG/CR-1532, WCAP-9699 Volumes 1 and 2, *FLECHT SEASET Program, PWR FLECHT SEASET Unblocked Bundle, Forced and Gravity Reflood Task Data Report*, June 1980.
- 8.2-14 Pacific Northwest Laboratory, NUREG/CR-3046, PNL-4385, COBRA/TRAC-A Thermal-Hydraulics Code for Transient Analysis of Nuclear Reactor Vessels and Primary Coolant Systems, Volume 4: Developmental Assessment and Data Comparisons, March 1983.
- 8.2-15 Los Alamos National Laboratory, LA-9700-MS, NUREG/CR-3208, *TRAC-PD2 Developmental Assessment*, January 1985.
- 8.2-16 C. P. Booker, *Post-test TRAC-PD2/MOD1 Predictions for FLECHT SEASET Test 31504*, Proceedings of the Topical Meeting on Advances in Reactor Physics and Core Thermal Hydraulics, pages 1033–1043, 1982.
- 8.2-17 Idaho National Laboratory, EGG-TFM-7952, RELAP5/MOD2 Code Manual, Volume 3: Developmental Assessment Problems, December 1987.
- 8.2-18 Y. A. Hassan. Analysis of FLECHT and FLECHT SEASET Reflood Tests with RELAP5/MOD2, Nuclear Technology, 74:176–188, 1986.
- 8.2-19 G. T. Analytis, M. Richner, M. Andreani, and S. N. Aksan, Assessment and Uncertainty Identification for RELAP5/MOD2 and TRAC-BD1/MOD1 Codes Under Core Uncovery and Reflooding Conditions, Proceedings of the U.S. NRC 14th Water Reactor Safety Information Meeting, 5:329–369, 1986.

- 8.2-20 Idaho National Engineering Laboratory, EGG-2552, NUREG/CR-5249, Quantifying Reactor Safety Margins: Application of Code Scaling, Applicability, and Uncertainty Evaluation Methodology to a Large Break, Loss-of-Coolant Accident, December 1989.
- 8.2-21 Westinghouse Electric Company, WCAP-9108, FLECHT Low Flooding Rate Skewed Test Series Data Report, May 1977.
- 8.2-22 EPRI, NUREG/CR 1533, EPRI NP 1460, WCAP-9729, Analysis of the FLECHT-SEASET Unblocked Bundle Steam Cooling and Boiloff Tests, January 1981.
- 8.2-23 L. E. Hochreiter S. C. Yao and W. J. Leech, *Heat Transfer Augmentation in Rod Bundles Near Grid Spacers*, Transactions ASME, 104:76–81, February 1982.
- 8.2-24 J. H. Mahaffy J. Spring M. J. Meholic, L. E. Hochreiter, Increased Convective Heat Transfer Caused by Spacer Grids in Laminar High Void Fraction Flows, 2008 ANS Winter Meeting, 2008.
- 8.2-25 Electric Power Research Institute, EPRI NP-1459, NUREG/CR-1532, WCAP-9699 Volumes 1 and 2, FLECHT SEASET Program, PWR FLECHT SEASET Unblocked Bundle, Forced and Gravity Reflood Task Data Report, June 1980.
- 8.2-26 Electric Power Research Institute, EPRI NP-2013, NUREG/CR-2256, WCAP-9891, PWR FLECHT SEASET Unblocked Bundle, Forced and Gravity Reflood Task Data Evaluation and Analysis Report, February 1982.
- 8.2-27 Siemens Power Corporation, EMF-2148(P) Revision 0, High Thermal Performance Spacer Reflood Heat Transfer Verification Data Report, December 1998.
- 8.2-28 Siemens Power Corporation, EMF-P60,149(P), *HTP Reflood Test Characterization Report*, December, 1998.

- 8.2-29 Studsvik Eco & Safety AB, MXC-301, NUREG/CR-2671, *The Marviken Full-Scale Critical Flow Tests, Summary Report*, May 1982.
- 8.2-30 Los Alamos National Laboratory, LA-11208-MS, NUREG/CR-5069, *TRAC-PF1/MOD1 Correlations and Models*, December 1988.
- 8.2-31 Nuclear Regulatory Commission, NUREG-1230, *Compendium of ECCS Research for Realistic LOCA Analysis*, December 1988.
- 8.2-32 Electric Power Research Institute, NUREG/CR-1899, EPRI NP-1527, GEAP-24898, *BWR Refill-Reflood Program Task 4.8 - Model Qualification Task Plan*, August 1981.
- 8.2-33 Idaho National Laboratory, EGG-TFM-7952, RELAP5/MOD2 Code Manual, Volume 3: Developmental Assessment Problems, December 1987.
- 8.2-34 Siemens AG UB KWU, U9 316/89/2 Quick Look Report - UPTF - Test No. 6, Downcomer Countercurrent Flow Test, March 1989.
- 8.2-35 Siemens AG UB KWU, U9 316/88/18, Experimental Data Report - UPTF - Test No. 6, Downcomer Countercurrent Flow Test, March 1989.
- 8.2-36 Siemens AG KWU, E314/90/003, Quick Look Report - UPTF - Test No. 7, Downcomer Countercurrent Flow Test, March 1990.
- 8.2-37 Siemens AG UB KWU, U9 316/89/14, Experimental Data Report - UPTF - Test No. 7, Downcomer Countercurrent Flow Test, July 1989.
- 8.2-38 Ermittlung Zeta-Wert Spalt, 3DProject/UPTF, February 1987. KWU Letter Report 364, Braase.
- 8.2-39 Siemens AG, R 515/85/23, UPTF Test Instrumentation, September 1985.

- 8.2-40 MPR Associates, Inc., MPR-1163, Summary of Results from the UPTF Downcomer Separate Effects Tests, Comparison to Previous Scaled Tests, and Application to U. S. Pressurized Water Reactors, 2D/3D Program. July 1990.
- 8.2-41 Siemens AG, Erlangen Germany, U9 316/88/11, Upper Plenum Test Facility, Test No. 8 Cold/Hot Leg Flow Pattern Test Quick Look Report, September 1988.
- 8.2-42 MPR Associates, Inc., MPR-1208, Summary of Results from the UPTF Cold Leg Flow Regime Separate Effects Tests, Comparison to Previous Scaled Tests, and Application to U. S. Pressurized Water Reactors, October 1992.
- 8.2-43 Siemens AG KWU, E316/88/3, Quick Look Report - UPTF - Test No. 10, Tie Plate Countercurrent Flow Test, March 1988.
- 8.2-44 Siemens AG, Erlangen Germany, R 515/86/13, Upper Plenum Test Facility, Test No. 12 Tie Plate Countercurrent Flow Test, October 1986.
- 8.2-45 Siemens UG KWU, U9 314/90/05, Quick Look Report - UPTF - Test No. 29 Entrainment/Deentrainment Test, November 1990.
- 8.2-46 Siemens AG KWU, E316/88/3, Quick Look Report - UPTF - Test No. 10, Tie Plate Countercurrent Flow Test, March 1988.
- 8.2-47 Siemens AG UB KWU, U9 316/88/1, Experimental Data Report - UPTF - Test No. 10, Tie Plate Countercurrent Flow Test, February 1988.
- 8.2-48 Siemens AG UB KWU, U9 314/90/05, Experimental Data Report - UPTF - Test No. 29, Entrainment/Deentrainment Test, June 1990.
- 8.2-49 MPR-1213, Summary of Results from the UPTF Carryover /Steam binding Separate Effects Tests, Comparisons to Previous Scaled Tests, and Application to U.S. Pressurized Water Reactors, October 1990.

- 8.2-50 Electric Power Research Institute, EPRI-294-2. Mixing of ECC Water with Steam: 1/3 Scale Test and Summary, June 1975.
- 8.2-51 AREVA NP (Framatome ANP), EMF-2102(P), Revision 0, *S-RELAP5: Code Verification and Validation*, August 2001.
- 8.2-52 ASEA and AB Atomenergi, R4-447/RTL-1007, Hydrodynamic and Heat Transfer Measurements on a Full-Scale Simulated 36-Rod Marviken Fuel Element with Uniform Heat Flux Distribution, 1968.
- 8.2-53 MPR Associates, Inc., MPR-1115, Research Information Report of the Slab Core Test Facility (SCTF) Core II Test Series, July 1989.
- 8.2-54 Japan Atomic Energy Research Institute (JAERI), JAERI-M 91-001, Study on ECC Injection Modes in Reflood Tests with SCTF Core II: Comparison between Gravity and Forced Feed, February 1991.
- 8.2-55 Japan Atomic Energy Research Institute (JAERI), JAERI-memo 58-155, Data Report on Large Scale Reflood Test-43 - CCTF Core II Shakedown Test C2-SH2 (Run 54), May 1983.
- 8.2-56 Japan Atomic Energy Research Institute (JAERI), JAERI-memo 85-026, Evaluation Report on CCTF Core-II Reflood Test C2-4 (Run 62) - Investigation of Reproducibility, March 1985.
- 8.2-57 Japan Atomic Energy Research Institute (JAERI), JAERI-memo 87-001, Evaluation Report on CCTF Core-II Reflood Test C2-8 (Run 67) - Effect of System Pressure, January 1987.
- 8.2-58 Japan Atomic Energy Research Institute (JAERI), JAERI-memo 87-002, Evaluation Report on CCTF Core-II Reflood Test C2-9 (Run 68) - Effect of LPCI Flow Rate, February 1987.
- 8.2-59 Westinghouse Electric Corporation, WCAP 7956, THINC-IV - An Improved Program for Thermal-Hydraulic Analysis of Rod Bundle Cores, June 1973.

- 8.2-60 E. Weiss, R. A. Markley, and A. Battacharyya, *Open Duct Cooling-Concept for the Radial Blanket Region of a Fast Breeder Reactor*, Nuclear Engineering and Design, 16:175–386, 1971.
- 8.2-61 M. Jakob, Heat Transfer and Flow Resistance in Cross Flow of Gases over Tube Banks, Transactions ASME, 60:384–386, 1938.
- 8.2-62 I. E. I'Delchik et al., *Handbook of Hydraulic Resistance*, Hemisphere Publishing Corporation, Second Edition, Revised and Augmented, 1986.
- 8.2-63 Atomic Energy Authority Technology, NEA/CSNI/R(91)1, *AEA-TRS-104,. I25 Comparison Report*, February 1991.
- 8.2-64 US AEC, Two Phase Flow Through Abrupt Expansions and Contractions, 1966. TID-23394, Volume 3.
- 8.2-65 Crane Co., Flow of Fluids through Valves, Fittings, and Pipe, 1988, Technical Paper No. 410.
- 8.2-66 US NRC, TRACE V5.0 Assessment Manual; Appendix B: Separate Effects Tests, 2010.
- 8.2-67 AREVA NP, EMF-2102(P), Revision 1, S-RELAP5: Code Verification and Validation, November 2010.

8.3 *Validation Using Integral Effects Tests*

This section gives the details of the integral effects tests (IET). The test facilities chosen for this validation are the Loss-of-Fluid Test (LOFT) tests (Section 4.1) and the Semiscale tests (Section 4.2). The following sections describe the testing, facilities and experiments, and provides summaries, conclusions, analysis models, and descriptions of the input.

Note that these assessments, where applicable, will use the RLBLOCA plant model multipliers that were either previously determined or developed by appropriate methods. The RLBLOCA multipliers used in the assessments are:

[]

Use of other values will be justified in each assessment.

[]

8.3.1 LOFT

8.3.1.1 Introduction

The Loss-Of-Fluid Test Facility (LOFT) integral effects Tests L2-3, L2-5, LP-02-6, and LP-LB-1 are assessed to justify the use of AREVA NP's realistic LBLOCA methodology, and the S-RELAP5 code developed by AREVA NP for realistic analysis of LBLOCA.

The assessment results demonstrate the accuracy of the COPENIC and S-RELAP5 codes, the capability of simulating the LBLOCA phenomena observed during the LOFT tests, and assess the calculated results versus measured results.

The LOFT facility was designed to simulate a LOCA in a large 4-loop Westinghouse PWR, and to provide data with which to evaluate the adequacy, and to improve analytical methods for analyzing the LOCA transient response of a PWR. The LOFT results have been widely used to validate thermal-hydraulic codes that analyze PWR accident and transient phenomena. Key LOFT LBLOCA tests have been included in the Code Scaling, Applicability, and Uncertainty (CSAU) assessment matrix (Reference 8.3-24) and RELAP5/MOD3 developmental assessment matrix. LOFT assessments have also been performed to verify RELAP5/MOD2 or MOD3 by various members of the NRC-sponsored International Code Assessment Program (ICAP).

AREVA NP selected four LOFT large-break loss-of-coolant experiments (LBLOCE), L2-3, L2-5, LP-02-6, and LP-LB-1, for assessment. All of the selected LOFT tests simulate a guillotine break in the pump-discharge cold-leg piping. The major differences between these tests are that L2-3 and L2-5 were initiated from 75% power, whereas LP-02-6 and LP-LB-1 were initiated from near 100% full power, and the primary coolant pump (PCP) flywheels were not attached during the coastdown of L2-5 and LP-LB-1, but were attached when the pump speed was above 750 rpm (78.54 rad/s) in Tests L2-3 and LP-02-6. These LOFT tests have been used to validate the S-RELAP5 code for the blowdown, refill, and reflood phases of an LBLOCA. The tests were selected because:

- The test initial and boundary conditions closely simulate the “design basis accident” LOCA conditions for typical 4-loop Westinghouse PWRs.
- The LOCA phenomenology of Tests L2-5 and LP-LB-1 is similar to that calculated for a 3-Loop Westinghouse PWR, and the LOCA phenomenology for Test LP-02-6 is similar to that calculated for a 4-Loop Westinghouse PWR.
- Test L2-5 was designated as International Standard Problem 13 (Reference 8.3-1) for code assessment by the Organization of Economic Cooperation and Development (OECD).
- Other code assessment calculations of L2-3, L2-5, LP-02-6, and LP-LB-1 are available for comparison.

The LOFT assessment calculations were performed with an input model developed to be consistent with the nodalization used in other assessments, and the nodalization to be applied for PWR plant calculations. The philosophy of developing the S-RELAP5 consistent input models is to use a similar nodalization scheme in terms of number and distribution of volumes, junctions, heat structures, and input specifications to represent corresponding components in the LOFT and plant models. Exceptions are made only where significant geometry differences justify a different, but consistent scheme.

This document contains comparisons of the results of the LOFT L2-3, L2-5, LP-02-6, and LP-LB-1 tests with calculated results using the AREVA NP RLBLOCA Evaluation Model. Section 8.3.1.2 presents the summary and conclusions drawn from the LOFT assessments. Section 8.3.1.3 describes the LOFT facility and the tests. Section 8.3.1.4 describes the AREVA NP S-RELAP5 LOFT input model. Sections 8.3.1.5, 8.3.1.6, 8.3.1.7, and 8.3.1.8 describe the tests and the AREVA NP LOFT model input, and compare the assessment calculation results with measured data for each test.

8.3.1.2 Summary and Conclusions

The LOFT test simulations are some of the assessment calculations performed to justify the applicability of the AREVA NP RLBLOCA methodology, and the capability of the S-RELAP5 code to realistically evaluate postulated PWR LBLOCAs.

The LOFT test analytical results demonstrate the ability of S-RELAP5 to realistically simulate the important system phenomena relevant to an LBLOCA that were observed during the unique LOFT LBLOCA tests. These include: (1) system depressurization, (2) core flow reversal and core dry-out, or critical heat flux (CHF), (3) the fuel cladding temperature excursion and peak cladding temperature (PCT), (4) two-phase pump flow and critical flows at the breaks, (5) prevention of core bottom-up quench during the early blowdown period, (6) ECC downcomer penetration and bypass, and (7) core refill, reflood, and final quench.

As shown by the results presented in Sections 8.3.1.5, 8.3.1.6, 8.3.1.7, and 8.3.1.8, the RLBLOCA evaluation model produced results in good agreement with the observations for LOFT Tests L2-3, L2-5, LP-02-6, and LP-LB-1. The results are summarized as follows:

- The COPENIC-calculated fuel initial centerline fuel temperatures were within 10% of the measured data.

•The S-RELAP5 code calculated results show agreement with the hydraulic responses of LOFT tests. That is, the calculated results either were within measured data and uncertainties, followed the major trends of the data if not within measured uncertainties, or were conservative with respect to the data if the phenomenon was not well simulated. The intact-loop mass flow rates, break flow in the broken loop, and loop volume densities all were well calculated. Coolant temperatures also were well calculated. Draining of the pressurizer was overpredicted, but because the pressurizer liquid tended to flow to the broken loop and was removed from the system, and that trend produced conservative results. Calculated pump speeds were accurately predicted up to the time where a two-phase mixture appeared. After that time, the pump speeds were lower than measured and therefore conservative, since the pumps then pushed less fluid into the downcomer and core.

•The code accurately calculated the thermal response (fuel centerline temperature and cladding temperature). The centerline temperatures have reasonable agreement with the data, and the cladding temperatures have reasonable agreement with the measured data. The hot rod PCT is well calculated, and the cladding quench times are significantly delayed with respect to the measured data.

The early bottom-up core quenching found in Tests L2-3 and LP-02-6 were not simulated in the code calculations. The upper regions of the core showed delayed dry-out with respect to the test data. However, once the upper regions went through dry-out, the calculated rewet was much later than measured. Generally, the code predicted higher than measured temperatures in the middle core region, lower than measured temperatures in the upper core region, and approximately measured temperatures in the lower region. In all cases, the calculated PCT was either equal to or greater than the measured PCT with analytical uncertainties included.

•The calculated ECC injection rates for the low pressure injection system (LPIS) and accumulator tended to underpredict the measured data; and therefore, they are acceptable.

8.3.1.3 Facility and Test Description

This section describes the LOFT facility and summarizes the characteristics and parameters of the LOFT LB nuclear tests. It also describes the LOFT Tests L2-3, L2-5, LP-02-6, and LP-LB-1. The quick-look reports (QLR) (References 8.3-2, 8.3-3, 8.3-4, and 8.3-5) discuss the LOFT test results.

8.3.1.3.1 Facility Description

LOFT was an NRC-sponsored nuclear test facility designed to simulate the nuclear and thermal-hydraulic phenomena that take place in a PWR LBLOCA. The LOFT facility was a 50 MWt experimental PWR designed to simulate the system response of a 4-loop Westinghouse PWR during a hypothetical LBLOCA. The facility included five major subsystems, an intact loop, a broken loop, a reactor vessel, an emergency core cooling system, and a blowdown suppression system. The LOFT facility was instrumented so that system parameters could be measured during the tests. A complete detailed discussion of the LOFT facility and an instrumentation description are found in Reference 8.3-6. The major components and test instrument locations in the system are shown in Figure 8.3-1.

LOFT had a single active intact loop that simulated the combined three intact loops of a 4-loop Westinghouse PWR. The intact loops included an active steam generator, two primary coolant pumps (PCP) in parallel, a pressurizer, a loop seal, and the connecting piping.

The broken loop in the LOFT facility was an inactive flow loop during normal operation. It consisted of a hot leg, a steam generator simulator, a pump simulator, and a cold leg. It became an active flow loop and simulated the broken loop of a 4-loop PWR during LOCA tests. The broken loop cold leg (BLCL) was divided into two parts: a pump side that connected the pump simulator to the blowdown suppression system, and the vessel side that connected the vessel downcomer to the blowdown suppression system. The steam generator and pump simulators provided flow resistances representative of a PWR during a LOCA. Both sides of the broken cold legs contained a quick-opening blowdown valve (QOBV) that opened to initiate the transient.

The LOFT reactor vessel had an annular downcomer, a lower plenum, below-core hardware, a nuclear core, above-core hardware, and an upper plenum. The downcomer was connected to the intact and broken cold legs, and the upper plenum was connected to the hot legs. The core contained 1,300 fuel rods arranged in five square (15 x 15) and four triangular (corner) assemblies with an average linear heat generation rate (LHGR) of about 7.0 kW/ft at full power. The LOFT fuel rods and pitch were typical of a PWR 15 x 15 rod array, except that the active length was 1.68 m (5.5 ft), while that of a PWR typically is 3.66 m (12 ft). For Test L2-5 and LP-02-6, all the fuel rods in the central assembly, except the outside row, were pressurized with helium to 2.51 MPa (350 psig) and all fuel rods in the peripheral assemblies were unpressurized. In the remaining tests L2-3 and LP-LB-1, all of the fuel rods were unpressurized.

The LOFT intact loop had two separate ECCSs connected to the cold leg. Each system contained an accumulator, an HPIS, and an LPIS. Only one ECCS was used during a LOCA test; and the other was used as backup for plant protection in case of unplanned emergency situations that might occur during the test.

The ECCS was not connected to the broken loop. For the LBLOCA tests, ECC was injected into the intact loop cold leg (ILCL). The HPIS and LPIS were connected to the accumulator injection piping. The LOFT blowdown suppression system consisted of a header and a suppression tank that simulated the PWR containment pressure and temperature environment expected to occur during an LBLOCA.

LOFT was designed with a primary system volume-to-core power ratio similar to that of a PWR. The design objective for the LOFT facility was to produce, on a reduced scale, the significant thermal hydraulic phenomena with representative conditions and a representative sequence of events that could occur in a PWR during postulated LOCAs. Volumetric scaling was generally used for the design of LOFT components. Primary system components, e.g., lower plenum, core region, upper plenum, outlet piping, steam generator, and inlet piping, also were designed with relative volumes equivalent to those in a PWR. Reference 8.3-7 examines the LOFT scaling. LOFT is a reduced-scale facility that is not uniformly scaled by consistent scaling criteria. Scaling distortions exist that must be therefore considered when applying the results of the LOFT LB tests.

The accumulator gas volume is scaled so that the ratio of accumulator gas volume to accumulator liquid volume injected is equal to that of a typical 4-loop PWR by adjusting the standpipe height.

The LOFT HPIS flow rate for the LB tests is volume-ratio scaled using the ratio of the LOFT to PWR total primary system fluid volume, plus the single failure criterion, and the assumption that flow from one of four injection lines is lost out of the break. The LPIS flow rate is scaled based on the combined downcomer and core flow areas. The single-failure criterion and the assumption that flow from one of four injection lines is lost out of the break also are used for LPIS scaling. The LOFT accumulator liquid volume is scaled to represent three of the four accumulators of a typical 4-loop PWR assuming that the liquid in the fourth accumulator is lost out of the break.

The major differences between LOFT and a 4-loop PWR are summarized as follows:

- LOFT has one active operating (intact) loop and a passive blowdown (broken) loop with only a steam generator and pump simulator, while a 4-loop PWR has four operating loops.
- LOFT has two pumps connected in parallel in the operating loop, while a PWR has only a single pump in each loop.
- The LOFT core has 1.68 m (5.5 ft) of active fuel length, while PWR core lengths are at least 3.66 m (12 ft). The axial power distribution of the LOFT core is similar to a beginning-of-life, bottom-skewed power distribution in a PWR core.
- LOFT has a short steam generator relative to a PWR.
- The LOFT cold leg ECC injection location is very close to the vessel inlet while PWR ECC injection lines are located near the pump outlet.
- Axial lengths and elevations of hydraulic components are not preserved relative to a PWR.

The LOFT scaling philosophy was to reduce the component coolant volume and flow areas by the core power ratio. The volume and power scaling was not completely achieved, and vertical scaling was not preserved. Regardless of these component differences and scaling distortions, the LOFT components are functionally similar to those of a PWR and provide sufficient similarity to permit the LOCA data to be used to validate the S-RELAP5 code for evaluating the PWR LOCA/ECCS performance.

8.3.1.3.2 Test Description

Summary of LOFT Large Break Tests

Between 1976 and 1985, 50 LOFT tests were performed. The LOFT facility was designed primarily for performing LBLOCA tests; however, only five tests, L2-2, L2-3, L2-5, LP-02-6 (L2-6), and LP-LB-1 (LB-1), were LBLOCA tests with a heated nuclear core. The first three LBLOCA tests were sponsored by the NRC and the last two were conducted under the auspices of the OECD sponsored by an international consortium. LP-02-6 was conducted under OECD, but was totally funded and sponsored by the NRC. LP-LB-1 was the only LOFT LBLOCA test funded by the OECD consortium. The OECD Test LP-FP-01 is also an LBLOCA test simulating a German-type reactor accident scenario resulting in the fuel rod rupture, and gap fission product release. It was therefore categorized as a fission product test rather than an LBLOCA test.

The LOFT test program was completed in July 1985, and summarized in the NRC's report, LOFT Program Experiments (Reference 8.3-8) and also in LOFT Program Research Findings (Reference 8.3-9). The influence of LOFT research findings on the thermal-hydraulic aspects of commercial PWR safety was presented in Reference 8.3-10. Accounts of the OECD LOFT project are documented in References 8.3-11 and 8.3-13. Table 8.3-1 lists the characteristics and parameters of the LOFT nuclear LBLOCA Tests.

Selection of LOFT LB Tests

AREVA NP selected LOFT LBLOCEs L2-3, L2-5, LP-02-6, and LP-LB-1 for assessment with S-RELAP5. All of the selected LOFT tests simulate cold-leg guillotine breaks. The major differences between these tests are as follows:

- L2-3 and L2-5 were initiated from 75% power while LP-02-6 and LP-LB-1 were initiated from near 100% full power.

- The PCP flywheels were not attached during the coastdown of L2-5 and LP-LB-1, but were attached when the pump speed was above 750 rpm (78.54 rad/s) in Test LP-02-6 and left attached for Test L2-3, simulating pump coast-down.

These LOFT tests have been used to validate the S-RELAP5 code for the blowdown, refill, and reflood phases of an LBLOCA. The tests were selected for S-RELAP5 assessment for the following reasons:

- The test initial and boundary conditions most closely simulate the “design basis accident” LOCA conditions for typical 4-loop Westinghouse PWRs.
- Test L2-3 provides scaling data when compared to Semiscale Test-06-3.
- The LOCA phenomenology for Tests L2-5 and LP-LB-1 is similar to that calculated for a Westinghouse 3-Loop PWR, and the LOCA phenomenology for Test LP-02-6 is similar to that calculated for a Westinghouse 4-Loop PWR.
- Test L2-3 was designated as United States Standard Problem 10 for code assessment by the NRC.
- Test L2-5 was designated as International Standard Problem 13 (Reference 8.3-1) for code assessment by the OECD.
- Other code assessment calculations of L2-5, LP-02-6, and LP-LB-1 are available for comparison.

Description of LOFT Tests Selected for AREVA NP Assessment

- LOFT Test L2-3

Test L2-3 was the second LBLOCA test conducted with unpressurized nuclear fuel rods in the LOFT facility in which the reactor core power provided the primary heat source. The test represented a hypothetical cold-leg guillotine break that simulated a double-ended, offset, shear break in a commercial (1000 MWe) 4-loop PWR. The test was initiated at 75% thermal power (36 MWt) and a 11.9 kW/ft maximum linear heat generator rate (MLHGR).

The test was initiated by opening the QOBVs. Reactor scram commenced 0.1 second into the transient and was completed 1.6 seconds later, HPIS injection was initiated at 14 seconds, accumulator injection at 16 seconds at 4.18 MPa system pressure, and LPIS injection at 29 seconds. The core was reflooded at 55 seconds. During this test, the PCPs operated continuously throughout the transient.

The cladding temperature initially started rising as expected and, after 2 to 3 seconds into the transient, the ILCL mass flow exceeded the broken-loop mass flow causing flow diversion to the downcomer. That process eventually caused a bottom-up rewet of the core, and the cladding was quenched momentarily. The conditions for core upflow quickly ceased, and the core dry-out and heat-up resumed 10 seconds into the blowdown. The core heat-up continued until sufficient ECC injection caused quenching of the core at 55 seconds. The final rewet pattern was first the bottom, then the top, and, finally, the middle regions of the core.

The measured PCT was 914 K (1186 °F) and occurred at 5 seconds. From Reference 8.3-13, a bias of 11.4 ± 16.2 K (20.5 ± 29.2 °F) should be applied to the measured PCT to account for the fin cooling effects on the surface-mounted thermocouples. Therefore, the reportable PCT for LOFT L2-3 is 942 K (1235 °F).

- LOFT Test L2-5

Test L2-5 was the third LBLOCA test conducted with pressurized nuclear fuel rods in the LOFT facility in which the reactor core power provided the primary heat source. The test represented a hypothetical cold-leg guillotine break that simulated a double-ended, offset, shear break in a commercial (1000 MWe) 4-loop PWR. The test was initiated at 75% thermal power (36 MWt) and a 12.2 kW/ft MLHGR.

Operation of the LOFT PCPs differs from a typical PWR in that the LOFT pump rotors are electromagnetically coupled to their flywheel system. Leaving the flywheels coupled until pump speed falls below 750 rpm (78.54 rad/s) allows the pump operation to simulate conditions intended to represent the normal pump coastdown of commercial 4-loop Westinghouse PWRs. Disconnecting the flywheel systems provided a rapid pump coastdown that is more typical of a 3-loop PWR than a 4-loop PWR. During the L2-5 test, the two PCPs were tripped at 1 second and disconnected resulting in the rapid coast-down of the pumps, thereby reducing the flow into the vessel to less than the flow to the break and preventing an early bottom-up fuel rod rewet.

The L2-5 HPIS flow is 58% of L2-3 and 75% of LP-02-6 because an improper small break HPIS flow condition was inadvertently specified for L2-5. The injections of high- and low-pressure ECCSs were delayed to 23.9 and 37.32 seconds, respectively, to simulate the expected delay in starting up the emergency power diesel generator to run the ECCS.

Before starting the transient, the power level in the reactor core was steadily increased, and then held at $36 \text{ MW} \pm 1.2 \text{ MW}$ for about 28 hours. This ensured that an appropriate decay heat power level would be obtained once the control rods were inserted into the reactor core. Test conditions before the beginning of the L2-5 test were as follows: The primary intact-loop mass flow rate was set at $192.4 \text{ kg/s} \pm 7.8 \text{ kg/s}$. The hot-leg pressure was $14.94 \text{ MPa} \pm 0.06 \text{ MPa}$. The primary coolant system hot- and cold-leg temperatures were held at $589.7 \text{ K} \pm 1.6^\circ\text{K}$ and $556.0 \text{ K} \pm 4.0^\circ\text{K}$, respectively.

Test L2-5 was conducted to address conservatism in current licensing analyses. Several Westinghouse plants are limited by Appendix K LOCA analysis results in which the calculated PCTs are predicted to occur during the reflood portion of the transient. Previous LOFT LB Tests L2-2 and L2-3 revealed that Appendix K requirements may be overly conservative because Appendix K criteria preclude the return to nucleate boiling (rewetting) before the end of blowdown (paragraph I.C.4.e.). However, Tests L2-2 and L2-3 demonstrated that system hydraulic behavior can lead to an early rewet of the fuel cladding. This early rewet not only limits the PCT measured during blowdown (i.e., 789 K (961 °F) and 914 K (1186 °F) for L2-2 and L2-3, respectively), but also removes a significant amount of stored energy from the fuel rod, therefore reducing the reflood PCT. The cladding temperatures during reflood after blowdown rewet will be much lower than those occurring without rewet. Preventing the early rewet provides maximum core stored energy at the end of blowdown, and beginning of refill/reflood.

The test results showed that the early bottom-up core-wide rewet that occurred in L2-2 and L2-3 did not occur in Test L2-5 as planned. The measured PCT was 1078 K (1481 °F), and because no early rewet occurred and hot rod temperature was fairly constant over a long period, there was no clear demarcation of whether PCT occurred during blowdown or reflood. The cladding completely quenched at 65 seconds \pm 2 seconds. The test was complete after LPIS was terminated at 107 seconds.

From Reference 8.3-13, a bias of 11.4 ± 16.2 K (20.5 ± 29.2 °F) should be applied to the measured PCT to account for the fin cooling effects on the surface-mounted thermocouples. Therefore, the reportable PCT for LOFT L2-5 is 1106 K (1531 °F).

- LOFT Test LP-02-6

LOFT Test LP-02-6 was the fourth LOFT nuclear-powered core LBLOCA test conducted with pressurized nuclear fuel rods, and with specification of minimum U.S. ECC injection rates. The MLHGR of 14.9 kW/ft was the typical technical specifications currently used for licensing analyses of PWR fuel rods with the same approximate pellet diameter used in a 15 x 15 fuel pin array. LP-02-6 represented an NRC "design-basis accident" test and was supposed to run at 100% power of 50 MWt, but because of questions concerning the integrity of the pressurized fuel rods in the central hot assembly, the power level was reduced to mitigate possible safety problems. LP-02-6 is an important LBLOCA test for code assessment because it addresses the issues relating to safety margins associated with the response of a PWR to the NRC design-basis accident scenario, including delayed minimum ECC safeguards.

Test LP-02-6 simulated a cold-leg guillotine break coincident with a loss of offsite power. The test was conducted with a delayed and degraded high- and low-pressure ECC injection. During the test, the PCPs were tripped and coasted down with their flywheels attached. The result was an early partial core rewet from the bottom up. When PCP speed dropped below 750 rpm (78.54 rad/s), the flywheels were uncoupled from the pumps to increase the pump speed deceleration. The attached flywheels produced pump coastdown characteristics more typical of a commercial 4-loop Westinghouse PWR.

Before initiating blowdown, the power level in the reactor core was steadily increased, then held at $46 \text{ MWt} \pm 1.2 \text{ MWt}$ to ensure that an appropriate decay heat power level would be obtained once the control rods were inserted into the reactor core. Test conditions at the beginning of the LP-02-6 test were as follows: The primary intact-loop mass flow rate was $248.7 \text{ kg/s} \pm 2.6 \text{ kg/s}$, the hot-leg pressure was $15.09 \text{ MPa} \pm 0.08 \text{ MPa}$, and the primary coolant system hot- and cold-leg temperatures were $589.0 \text{ K} \pm 1.0 \text{ K}$ and $559.0 \text{ K} \pm 1.1 \text{ K}$, respectively.

Test LP-02-6 was conducted to address conservatism in the current licensing analyses. Several Westinghouse plants are limited by Appendix K LOCA analysis results in which the calculated PCTs are predicted to occur during the reflood portion of the transient. LOFT LB tests L2-2 and L2-3 revealed that the original Appendix K requirements may be overly conservative because the criteria preclude the return to nucleate boiling (rewetting) before the end of blowdown (paragraph I.C.4.e). However, Tests L2-2 and L2-3 demonstrated that system hydraulic behavior can lead to an early rewet of the fuel cladding. This early rewet not only limits the PCT measured during blowdown (i.e., 789 K (961 °F) and 914 K (1186 °F) for L2-2 and L2-3, respectively), but also removes a significant amount of stored energy from the fuel rod, therefore reducing the reflood PCT. The cladding temperatures during reflood, after blowdown rewet, will be much lower than those occurring without rewet. Preventing the early rewet provides maximum core stored energy at the end of blowdown, and the beginning of refill/reflood. The LOFT L2-5 and LP-LB-1 tests deliberately altered pump operation to preclude the early bottom-up rewet. The L2-5 and LP-LB-1 results showed that the early bottom-up rewet observed in L2-2 and L2-3 did not occur, and respectively the measured PCTs were 1078 K (1481 °F) and 1256 K (1801 °F). The L2-5 and LP-LB-1 hot rod temperatures were fairly constant over a long period and no large difference occurred between the maximum PCT in the blowdown and reflood portions of the tests because no early rewet occurred.

The LOFT LP-02-6 test results showed the early bottom-up rewet of the fuel rods because the PCPs were allowed to coast down normally and the pump flow exceeded vessel side-break flow during the early part of blowdown, causing the early rewet. The early quench of the fuel rods extended to two-thirds of the core. Following the blowdown, the core underwent a second heat-up caused by a second dry-out. The measured PCT of 1077 K (1479 °F) occurred early in the blowdown because of the large removal of the stored energy from the fuel rods during blowdown. The cladding completely quenched at 56 seconds \pm 0.2 seconds. The test was complete after core reflood was completed at 59 seconds \pm 1.0 second.

From Reference 8.3-13, a bias of 11.4 ± 16.2 K (20.5 ± 29.2 °F) should be applied to the measured PCT to account for the fin cooling effects on the surface-mounted thermocouples. Therefore, the reportable PCT for LOFT LP-02-6 is 1105 K (1530 °F).

- LOFT Test LP-LB-1

The fifth LOFT LOCE, LP-LB-1 with unpressurized nuclear fuel rods, simulated a hypothetical double-ended cold-leg guillotine break initiated from conditions representative of a PWR operating near its licensing limits. The initial core power was near the facility design limit of 50 MWt with MLHGR of 15.8 kW/ft. Included in the test's boundary conditions were loss of offsite power coincident with the LOCE, a rapid PCP coastdown, and a minimum safeguard ECCS injection assumption from a European PWR. To minimize possible fuel pin damage, all of the fuel rods in the core were initially unpressurized.

Similar to LOFT Test L2-5, the PCP flywheels were uncoupled from the pump rotors to effect a rapid pump coastdown and prevent an early bottom-up core rewet. In this test, the PCPs were tripped and uncoupled from their flywheels within 1 second after the start of the transient.

The ECC injection assumption for this test resulted in an accumulator liquid volume that was approximately 70%, and a pumped injection flow rate that was around 50% of that used in Test LP-02-6. The pumped injection was accomplished using the LPIS with a delay of nearly 32 seconds to simulate the delay in starting the emergency power diesel generator.

Before the start of the transient, the power level in the reactor core was steadily increased, then held at $49.3 \text{ MWt} \pm 1.2 \text{ MWt}$ to ensure that an appropriate decay heat power level would be obtained once the control rods were inserted into the reactor core. Test conditions at the beginning of the LP-LB-1 test are as follows: The primary intact-loop mass flow rate was $305.8 \text{ kg/s} \pm 2.6 \text{ kg/s}$. The hot-leg pressure was $14.77 \text{ MPa} \pm 0.06 \text{ MPa}$. The primary coolant system cold-leg temperature was $556 \text{ K} \pm 1.0 \text{ K}$, with a fluid temperature increase of $29.5 \text{ K} \pm 1.4 \text{ K}$.

Similarly to Test L2-5, Test LP-LB-1 was conducted to produce an LBLOCA with a maximum of core-stored energy at the end of blowdown by preventing an early bottom-up core rewet. Then, using the high-temperature conditions at the start of reflood, the test explored the reflood behavior of the system and provided information against which best estimate computer code simulations could be evaluated.

As desired, the early bottom-up core-wide rewet did not occur in Test LP-LB-1. By altering the PCP coastdown, an early bottom-up rewet was prevented. The test did have a partial top-down rewet that resulted in two peaks in the cladding temperature history. A measured PCT of 1256 K ($1801 \text{ }^{\circ}\text{F}$) occurred at about 13 seconds. The cladding temperature at the peak power location remained at an elevated temperature for a long time. The cladding was completely quenched at $72 \text{ seconds} \pm 1 \text{ second}$. The test was terminated at 132 seconds.

From Reference 8.3-13, a bias of $11.4 \pm 16.2 \text{ K}$ ($20.5 \pm 29.2 \text{ }^{\circ}\text{F}$) should be applied to the measured PCT to account for the fin cooling effects on the surface-mounted thermocouples. Therefore, the reportable PCT for LOFT LP-LB-1 is 1284 K ($1852 \text{ }^{\circ}\text{F}$).

8.3.1.4 S-RELAP5 Model Description

The computer codes used to perform the LOFT test assessment calculations were COPENIC and S-RELAP5. COPENIC is the AREVA NP realistic fuel rod thermal-mechanical behavior analysis code. S-RELAP5 is an AREVA NP-modified version of the Idaho National Laboratory (INL) RELAP5/MOD2 and MOD3 codes. Section 7.0 and Reference 8.3-14 present a more extensive description of the AREVA NP codes. The COPENIC code provides input to calculate the fuel conditions, and stored energy for all fuel types modeled by S-RELAP5 at the initiation of the realistic LBLOCA calculation. The COPENIC models have been integrated with S-RELAP5 to provide a consistent realistic calculation of the thermal-mechanical responses of the fuel rods during the LOCA.

The S-RELAP5 LOFT input model for AREVA NP assessments was developed at AREVA NP. The nodalization model used for the analysis of LOFT Tests is shown in Figure 8.3-2 and Figure 8.3-3. This model provides detailed thermal and hydraulic representations of all the major LOFT system components. It results from developing an LBLOCA analysis input model that is consistent with the nodalization scheme used in all assessment and PWR plant calculations (see Section 9.0). AREVA NP has developed an input model and nodalization prescription that is intended to maintain consistent nodalization, and input selection among all the realistic LBLOCA analyses. The AREVA NP input prescription defines the acceptable nodalization, a recommended numbering system, and parameter inputs for an S-RELAP5 PWR plant or experimental facility input model.

The AREVA NP LOFT input model described in this document was developed according to the AREVA NP LBLOCA input model and nodalization prescription and revised for this study to be consistent with the RLBLOCA Rev. 3 methodology guidelines (see Section 9.0). [

] These sensitivity results compare favorably with the calculated PCT results from the analysis reported in this document.

[

]

The S-RELAP5 code uses a nine-digit integer for designating hydrodynamic component volumes. One-dimensional components are used to represent all regions except the reactor vessel downcomer, core, and upper plenum. For one-dimensional components, the numbering system is CCCXX0000, where CCC is the component number and XX is the volume number within a component. Figure 8.3-3 shows the detailed two-dimensional representation of the core and reactor vessel downcomer. The two-dimensional component numbering system is CCCYYXX00, where CCC is the component number, YY refers to volume number in the azimuthal direction for a downcomer region, or in the radial direction for a reactor core region. XX refers to the volume number in the axial direction. Section 7.0 provides the detail of S-RELAP5 input nomenclature and the types of hydrodynamic components that may be selected. The S-RELAP5 input model for the LOFT facility consists of the following seven major parts.

- Intact loop and pressurizer components (100-160)
- ECC system components (170-195)
- Broken-loop and reflood-assisted bypass valve (RABV) components (400-465)
- Blowdown suppression tank components (462-466)
- Reactor vessel components (505-570)
- Secondary coolant system components (600-682)
- Heat structures representing the reactor vessel wall, vessel internal structures, primary coolant system (PCS) pipe walls, and steam-generator U-tubes.

8.3.1.4.1 Intact-Loop Components

The left-hand side of Figure 8.3-2 shows the nodalization of the intact loop, pressurizer surge line, and pressurizer. Intact-loop components include the hot leg, pressurizer, and surge line; steam generator primary; loop seal; PCPs; and cold leg. The intact loop component numbering starts at 100.

The noding in the intact loop is sufficiently detailed to allow prediction of LOCA thermal-hydraulics phenomena without including excessive nodalization that does not add to the accuracy of the analysis. [

] These components are removed in the transient calculation.

[] component 120 is used to model the steam generator U-tubes. The [

]

[

]

The required pump performance input includes rated head, flow, and hydraulic torque and the internal friction torque coefficients. Single-phase homologous curves that determine pump head and torque as a function of volumetric flow rate and speed are also needed. [

]

[

]

8.3.1.4.2 Broken-Loop Components

[

]

The noding in the broken loop is sufficiently detailed to predict LOCA thermal-hydraulics phenomena without including excessive nodalization that results in extremely small time step sizes caused by the Courant limit and does not add to the accuracy of the analysis. The thermal-hydraulic phenomena that may significantly dominate LOCA realistic analysis results include break flow, system depressurization, and ECC bypass phenomena.

[

]

[

]

[

]

[

]

8.3.1.4.3 *Reactor Vessel Components*

[

]

[

]

This nodalization provides sufficient detail to predict the behavior of the cold ECCS water that flows to the lower plenum during refill and reflood. [

]

[

]

[

] Section 8.3.1.4.6 discusses the reactor core and fuel rod heat structure input models.

[

]

[

] The flow

areas for the remaining volumes were based on upper plenum dimensions. [

]

8.3.1.4.4 ECCS Components

Figure 8.3-2 shows the nodalization of the HPIS, LPIS, accumulator, and injection lines as used in this analysis. [

]

[

]

8.3.1.4.5 Blowdown Suppression Tank Components

The blowdown suppression tank simulating the PWR containment is represented by time-dependent volumes 462 and 466. The pressure and temperature conditions measured at the blowdown suppression tank are specified for these volumes.

8.3.1.4.6 Reactor Core and Heat Structure Models

The core nodalization is explicitly shown in Figure 8.3-3. [

]

[

] The core heat structure

geometry nodalization in the S-RELAP5 core model is exactly the same as was used in the COPENIC nodalization.

8.3.1.4.7 COPENIC Fuel Models

The LOFT core components modeled by the COPENIC code [

]

Diagrams representing the COPENIC axial and radial nodalization of the fuel rods are depicted in Figure 8.3-4. [

]

[

]

[

]

8.3.1.5 LOFT Test L2-3 – Analysis and Results

8.3.1.5.1 Model Initialization and Steady State, Test L2-3

A steady-state initialization calculation was made to obtain the desired initial conditions for the transient simulation. The results of the steady-state calculation compared to the measured initial conditions, and event setpoints for the Test L2-3 simulation are presented and discussed in this section.

[

] The LOFT

analysis model has a set of steady-state controllers that allows the analyst to specify the desired conditions as setpoints for a steady-state calculation. [

]

A steady-state initialization calculation was performed to reach the desired steady-state conditions for initiating the LOCA calculation. Table 8.3-2 compares the calculated initial conditions with the test conditions measured before break initiation. The calculated and measured initial conditions agree quite well, and the calculated initial conditions are generally within the uncertainty band of the measured quantities. [

] Table 8.3-3 noticeably demonstrates that the desired steady-state conditions were successfully achieved and that the calculation accurately reached the L2-3 test initial conditions.

Event setpoints and boundary conditions that have an impact after the start of the transient portion of the Test L2-3 simulation are given in Table 8.3-3. Test initial and boundary conditions, as given in the experimental data report (EDR) for L2-3 (Reference 8.3-2), were the primary basis for the assessment calculation. [

]

8.3.1.5.2 *Transient Simulation, Test L2-3*

This section contains detailed comparisons of the results of the S-RELAP5 calculation with the measured results of LOFT Test L2-3. The controllers for the initial conditions are either disabled or removed at the start of the transient calculation. [

]

Comparisons of System Transient Thermal-Hydraulic Response, Test L2-3

Comparisons of calculated and measured data are shown in Figure 8.3-5 through Figure 8.3-34 and discussed throughout this section. In these figures, the legends distinguish between measured and calculated curves. [

] Those cases are readily apparent by inspecting the legend. Further, SI units are plotted on the left-hand y axis, and U.S. customary units are plotted on the right-hand y axis.

- System Pressure, Test L2-3

[

].

Nevertheless, the calculated pressures compared very well (good agreement) with the data and showed similar depressurization behavior at various loop locations.

[

]

[

]

- Liquid Level, Test L2-3

[

]

- Loop Densities, Test L2-3

[

]

[

]

[

]

- Mass Flow Rates, Test L2-3

[

]

- Pump Speeds, Test L2-3

[

]

- Fluid Temperatures, Test L2-3

Figure 8.3-18 compares the measured upper plenum fluid temperature and the calculated liquid and steam temperatures. [

]

[

]

- Comparisons of ECC Performance, Test L2-3

Figure 8.3-22 through Figure 8.3-24 show ECCS injection performance. Figure 8.3-22 compares calculated and measured accumulator liquid level. [

]

Figure 8.3-24 displays the LPIS flow rate. [

]

Comparisons of Fuel Thermal Responses, Test L2-3

[

]

- Fuel Cladding Surface Temperature, Test L2-3

[

] The figure

also shows the axial nodalization and its relationship to bottom of heated length (BOHL).

[

]

[

]

8.3.1.5.3 Discussion of Results, Test L2-3

This section evaluates the calculated results given in Section 8.3.1.5.2. Several analytical and test research programs have been conducted to understand the expected phenomena and the major events for LBLOCA (Reference 8.3-17). For assessment purposes, the LOCA phenomena of primary interest are as follows:

- Fuel initial stored energy

- System blowdown and depressurization
- Primary coolant pump (PCP) performance
- Departure from nucleate boiling (DNB), or CHF
- Bottom-up or top-down rewet
- Subcooled and two-phase critical flow through the break
- System refill and ECC bypass
- Core reflood and rod quench
- PCT.

In this section, the code-calculated phenomena relative to measured system hydraulics and core thermal response to an LBLOCA will be discussed. The next subsection provides an overview of the results of the Test L2-3 calculation with a discussion of the calculated sequence of major events compared to the observed phenomena relative to the PWR LBLOCA scenario. The subsection following the sequence of events presents a more detailed core thermal response by presenting the calculated and measured PCT values relative to core elevation.

Sequence of Events for PWR LOCA Scenario, Test L2-3

Table 8.3-4 compares the major events in the L2-3 test. The measured time of occurrence of the events are compared with those calculated by S-RELAP5.

- Initial Fuel Stored Energy, Test L2-3

The initial fuel-stored energy before a LOCA is a very important parameter because the initial energy contained in the fuel rods is the dominant source for clad heating during the early blowdown phase of the LOCA. The initial stored energy in the fuel must therefore be accurately calculated for a realistic LOCA analysis. As stated previously, the COPENIC code is coupled with S-RELAP5 to provide a realistic calculation of the initial fuel-stored energy, and to calculate the reasonable mechanical behavior of the rods during the LOCA transient. [

]

- Blowdown and Depressurization Rate, Test L2-3

The LOCA simulation was initiated by opening the QOBVs and is defined as time 0.0 for the transient. [

]

- PCP Performance, Test L2-3

The pump speed comparisons shown in Figure 8.3-17 [

]

- Departure from Nucleate Boiling (DNB) (or CHF) and Core Heat-up, Test L2-3

[

]

- Bottom-Up and Top-Down Rewet Phenomena, Test L2-3

[

]

[

]

- Critical Flow at the Break, Test L2-3

[

]

- Refill and ECC Bypass Phenomena, Test L2-3

[

]

[

]

Figure 8.3-33 shows both the calculated collapsed liquid level in the reactor vessel lower plenum, core, and upper plenum (vessel liquid level), and the collapsed liquid level in the core (core liquid level) from the bottom of the active core. [

]

[

]

- Core Reflood and Quench Phenomena, Test L2-3

[

]

PCT Comparison Relative to Core Elevation, Test L2-3

The differences between calculated and measured cladding temperature time histories were discussed in Section 8.3.1.5.2.

Figure 8.3-34 shows the comparison of the maximum calculated temperatures with the maximum measured temperatures versus core elevation, and is referred to as a PCT plot. [

]

8.3.1.6 LOFT Test L2-5 - Analysis and Results

8.3.1.6.1 Model Initialization and Steady State, Test L2-5

A steady-state initialization calculation was made to obtain the desired initial conditions for the transient simulation. This section covers the results of the steady-state calculation compared to the measured initial conditions and event setpoints for the Test L2-5 simulation.

Initial and Boundary Conditions, Test L2-5

[

]

A steady-state initialization calculation was performed to reach the desired steady-state conditions for initiating the LOCA calculation. Table 8.3-5 compares the calculated initial conditions with the test conditions measured before break initiation. The calculated and measured initial conditions agree within the measurement uncertainty. Table 8.3-5 shows that the desired steady-state conditions were achieved and that the calculation reached the L2-5 test initial conditions.

Event setpoints and boundary conditions that have an impact after the start of the transient portion of the Test L2-5 simulation are given in Table 8.3-6. [

- The L2-5 EDR (Reference 8.3-18) stated that the liquid volume in the accumulator tank is $2.92 \text{ m}^3 \pm 0.01 \text{ m}^3$. This ignores the presence of the accumulator standpipe that limits accumulator injection to a fraction of 2.92 m^3 . The effective accumulator liquid volume is the measured liquid volume excluding the liquid volume below the top of the standpipe. When the liquid level drops below the top of the standpipe, the tank is considered empty.

8.3.1.6.2 Transient Simulation, Test L2-5

This section contains detailed comparisons of the results of the S-RELAP5 calculation with the measured results of LOFT Test L2-5. [

]

Comparisons of System Transient Thermal-Hydraulic Response, Test L2-5

Figure 8.3-35 through Figure 8.3-71 compare calculated and measured data and are discussed throughout this section. In those figures, measured and calculated quantities are indicated in the legend where the data is referenced by its channel identifier and the calculation by its S-RELAP5 parameter name and number. Further, the SI unit is plotted on the left-hand y-axis and the U.S. customary unit is plotted on the right-hand y-axis.

- System Pressure, Test L2-5

[

]

[

]

- Liquid Level, Test L2-5

[

]

- Loop Densities, Test L2-5

[

- Mass Flow Rates, Test L2-5

[

]

[

]

- Pump Speeds, Test L2-5

Figure 8.3-49 and Figure 8.3-50 compare the calculated pump speeds for [

]

- Fluid Temperatures, Test L2-5

Figure 8.3-51 compares the measured upper plenum fluid temperature and the calculated liquid and steam temperatures. [

- Comparisons of ECC Performance, Test L2-5

[

]

[

]

Comparisons of Fuel Thermal Responses, Test L2-5

[

]

- Fuel Cladding Surface Temperature, Test L2-5

[

]

[

]

- Fuel Pellet Centerline and Shoulder Temperature, Test L2-5

The initial stored energy in the fuel rods is a major contributor to the calculated PCT for LOCA analyses. [

]

8.3.1.6.3 Discussion of Results, Test L2-5

The LOCA phenomena of primary interest are given in Section 8.3.1.5.3. The code-calculated phenomena from Section 8.3.1.6.2 will be discussed as they relate to measured system hydraulics and core thermal response to an LBLOCA. The following sub-section provides an overview of the results of the Test L2-5 calculation with a discussion of the calculated sequence of major events compared to the observed phenomena relative to the PWR LBLOCA scenario. The next sub-section after that presents a more detailed core thermal response by presenting the calculated and measured PCT values relative to elevation.

Sequence of Events for PWR LOCA Scenario, Test L2-5

Table 8.3-7 compares the major events in Test L2-5. The measured time of occurrence of the events are compared with those calculated by S-RELAP5.

- Initial Fuel Stored Energy, Test L2-5

The initial fuel-stored energy before a LOCA is a very important parameter because the initial energy contained in the fuel rods is the dominant source for clad heating during the early blowdown phase of the LOCA. [

]

- Blowdown and Depressurization Rate, Test L2-5

The LOCA simulation was initiated by opening the QOBVs and is defined as time 0.0 for the transient. [

]

- PCP Performance, Test L2-5

[

]

- DNB (or CHF) and Core Heat-up, Test L2-5

[

]

- Bottom-Up and Top-Down Rewet Phenomena, Test L2-5

[

]

- Critical Flow at the Break, Test L2-5

The rate of coolant loss from the primary system must be calculated to analyze any LOCA. The initial surge of coolant out of the break becomes choked and critical flow exists before saturation pressure is reached upstream of the break. [

]

- Refill and ECC Bypass Phenomena, Test L2-5

[

]

[

]

The calculated collapsed liquid level in the reactor vessel lower plenum, core, and upper plenum (vessel liquid level) and the collapsed liquid level in the core (core liquid level) from the bottom of the active core are both shown in Figure 8.3-70.

[

]

[

]

- Core Reflood and Quench Phenomena, Test L2-5

[

]

PCT Comparison Relative to Core Elevation, Test L2-5

The differences between calculated and measured cladding temperature time histories were discussed in Section 8.3.1.6.2.

Figure 8.3-71 compares the calculated and measured PCT versus core elevation. In this figure, the PCT is referred to as a maximum cladding surface temperature, either calculated or measured at the various locations, during the LOCA transient history.

[

]

8.3.1.7 LOFT Test LP-02-6 - Analysis and Results*8.3.1.7.1 Model Initialization and Steady State, Test LP-02-6*

A steady-state initialization calculation was made to obtain the desired initial conditions for the transient simulation. The results of the steady-state calculation compared to the measured initial conditions and event setpoints for Test LP-02-6 simulation are presented and discussed in this section.

Initial and Boundary Conditions, Test LP-02-6

[

]

A steady-state initialization calculation was performed to reach the desired steady-state conditions for initiating the LOCA calculation. Table 8.3-8 compares the calculated initial conditions with the test conditions measured before break initiation. [

]

- [

]

8.3.1.7.2 *Transient Simulation, Test LP-02-6*

This section contains detailed comparisons of the results of the S-RELAP5 calculation with the measured results of the LOFT Test LP-02-6. [

]

Comparisons of System Thermal Hydraulic Response, Test LP-02-6

Calculated and measured data are compared in Figure 8.3-72 through Figure 8.3-107 and discussed throughout this section. In those figures, measured and calculated quantities are indicated in the legend where the data is referenced by its channel identifier and the calculation is referenced by its S-RELAP5 parameter name and number. Further, the SI unit is plotted on the left-hand y-axis and the U.S. customary unit is plotted on the right-hand y-axis.

- System Pressures, Test LP-02-6

[

]

[

]

Figure 8.3-76 compares the calculated and measured primary (ILHL) and steam generator secondary pressure. [

]

- Liquid Level, Test LP-02-6

Figure 8.3-77 compares the calculated pressurizer collapsed liquid level (i.e., the sum of volume length multiplied by the liquid fraction). [

]

- Loop Densities, Test LP-02-6

[

]

- Mass Flow Rates, Test LP-02-6

[

]

- Pump Speeds, Test LP-02-6

Figure 8.3-87 and Figure 8.3-88, respectively, show the calculated pump speeds

[

]

- Fluid Temperatures, Test LP-02-6

Figure 8.3-89 compares the measured upper plenum fluid temperature, and the calculated liquid and steam temperatures. [

- Comparisons of ECC Performance, Test LP-02-6

Figure 8.3-93 through Figure 8.3-96 show ECCS injection performance. Figure 8.3-93 compares the calculated and measured accumulator liquid level. [

Comparison of Fuel Thermal Response, Test LP-02-6

[

]

- Fuel Cladding Surface Temperatures, Test LP-02-6

[

]

[

]

- Fuel Pellet Centerline and Shoulder Temperatures, Test LP-02-6

Figure 8.3-104 shows a comparison of the calculated and measured fuel centerline temperature. [

]

8.3.1.7.3 Discussion of Results, Test LP-02-6

The LOCA phenomena of primary interest are given in Section 8.3.1.5.3. The code-calculated phenomena from Section 8.3.1.7.2 will be discussed as they relate to observed system hydraulics and core thermal response to an LBLOCA. The next sub-section provides an overview of the results of the Test LP-02-6 calculation with a discussion of the calculated sequence of major events compared to the observed phenomena relative to the PWR LBLOCA scenario. The sub-section following the next presents a more detailed core thermal response by presenting the calculated and measured PCT values relative to elevation.

Sequence of Events for PWR LOCA Scenario, Test LP-02-6

Table 8.3-10 compares the major events in the LP-02-6 test. The measured times of occurrence of the events are compared with those calculated by S-RELAP5.

- Initial Fuel Stored Energy, Test LP-02-6

The initial fuel stored energy before LOCA is a very important parameter because the initial energy contained in the fuel rods is the dominant source for clad heating during the early blowdown phase of the LOCA. [

]

- Blowdown and Depressurization Rate, Test LP-02-6

The LOCA simulation was initiated by opening the QOBVs and is defined as time 0.0 for the transient. [

- PCP Performance, Test LP-02-6

Figure 8.3-87 and Figure 8.3-88 compare the pump speed and indicate that [

]

- DNB (or CHF) and Core Heat-up, Test LP-02-6

[

]

- Bottom-Up and Top-Down Rewet Phenomena, Test LP-02-6

[

]

- Critical Flow at the Break, Test LP-02-6

The rate of coolant loss from the primary system must be calculated to analyze any LOCA. The initial surge of coolant out of the break becomes choked and critical flow exists before saturation pressure is reached upstream of the break. [

]

[

]

- Refill and ECC Bypass Phenomena, Test LP-02-6

The ECC flows down the downcomer to the reactor vessel lower plenum, [

]

As depressurization proceeds, [

]

[

]

- Core Reflood and Quench Phenomena, Test LP-02-6

[

] with

respect to the value reported in the LP-02-6 QLR (Reference 8.3-4).

PCT Comparison Relative to Core Elevation, Test LP-02-6

The differences between calculated and measured cladding temperature time histories were discussed in Section 8.3.1.7.2.

Figure 8.3-107 compares the calculated and measured PCT versus core elevation. This figure refers to the PCT as a maximum cladding surface temperature, either calculated or measured at the various locations, during the LOCA transient history.

[

]

8.3.1.8 LOFT Test LP-LB-1 - Analysis and Results

8.3.1.8.1 Model Initialization and Steady State, Test LP-LB-1

A steady-state initialization calculation was made to obtain the desired initial conditions for the transient simulation.

Initial and Boundary Conditions, Test LP-LB-1

Unless otherwise specified, the measured test conditions just before blowdown, as given in the LP-LB-1 QLR (Reference 8.3-5), were used to establish the steady-state conditions for initiating the LP-LB-1 transient calculation. [

]

A steady-state initialization calculation was performed to reach the desired steady-state conditions for initiating the LOCA calculation. Table 8.3-11 compares the calculated initial conditions with the test conditions measured before break initiation. [

]

Table 8.3-12 gives event setpoints and boundary conditions that have an impact after the start of the transient portion of the Test LP-LB-1 simulation. [

]

- [

8.3.1.8.2 *Transient Simulation, Test LP-LB-1*

This section contains detailed comparisons of the results of the S-RELAP5 calculation with the measured results of LOFT Test LP-LB-1. [

]

Comparisons of System Thermal-Hydraulic Response, Test LP-LB-1

Comparisons of calculated and measured data are shown in Figure 8.3-108 through Figure 8.3-144 and discussed throughout this section. In these figures, measured and calculated quantities are indicated in the legend where the data is reference by its channel identifier, and the calculation is referenced by its S-RELAP5 parameter name and number. Additionally, the SI unit is plotted on the left-hand y-axis and the U.S. customary unit is plotted on the right-hand y-axis.

- System Pressures, Test LP-LB-1

[

]

Figure 8.3-112 shows the primary system pressure responses compared to the secondary system pressures. [

]

- Liquid Level, Test LP-LB-1

Figure 8.3-115 compares the calculated pressurizer collapsed liquid level (i.e., the sum of volume length multiplied by the liquid fraction). [

]

- Loop Densities, Test LP-LB-1

[

]

[

]

- Mass Flow Rates, Test LP-LB-1

[

]

[

]

- Pump Speeds, Test LP-LB-1

Figure 8.3-125 and Figure 8.3-126 compare the calculated pump [

]

- Fluid Temperatures, Test LP-LB-1

[

]

[

]

[

]

- Comparisons of ECC Performance, Test LP-LB-1

[

Comparison of Fuel Thermal Response, Test LP-LB-1

[

]

- Fuel Cladding Surface Temperatures, Test LP-LB-1

[

]

Figure 8.3-135 through Figure 8.3-141 depict a selection of the cladding temperature comparisons [

]

[

]

- Fuel Pellet Centerline Temperature Test LP-LB-1

The initial stored energy in the fuel rods is a major contributor to the calculated PCT for the LOCA analysis. [

]

[

]

8.3.1.8.3 Discussion of Results, Test LP-LB-1

The LOCA phenomena of primary interest are given in Section 8.3.1.5.3. The code-calculated phenomena from Section 8.3.1.8.2 will be discussed relative to observed system hydraulics and core thermal response to an LBLOCA. The following sub-section provides an overview of the results of the Test LP-LB-1 calculation with a discussion of the calculated sequence of major events compared to the observed phenomena relative to the PWR LBLOCA scenario. The sub-section following the next presents a more detailed core thermal response by presenting the calculated and measured PCT values relative to elevation.

Sequence of Events for PWR LOCA Scenario, Test LP-LB-1

Table 8.3-13 compares the major events in the LP-LB-1 test. The measured times of occurrence of the events are compared with those calculated by S-RELAP5.

- Initial Fuel Stored Energy, Test LP-LB-1

The initial fuel stored energy before LOCA is a very important parameter because the initial energy contained in the fuel rods is the dominant source for clad heating during the early blowdown phase of the LOCA. [

- Blowdown and Depressurization Rate, Test LP-LB-1

The LOFT LP-LB-1 LOCA simulation was initiated by opening the QOBVs and is defined as time 0.0 for the transient. [

]

- PCP Performance, Test LP-LB-1

Figure 8.3-125 and Figure 8.3-126 present the pump speed comparisons [

]

- DNB (or CHF) and Core Heat-up, Test LP-LB-1

[

]

- Bottom-Up and Top-Down Rewet Phenomena, Test LP-LB-1

[

]

[

]

- Critical Flow at the Break, Test LP-LB-1

Calculating the rate at which coolant exits the primary system is essential for the analysis of any LOCA. The initial surge of coolant out of the break becomes choked and critical flow exists until saturation pressure is reached upstream of the break.

[

]

- Refill and ECC Bypass Phenomena, Test LP-LB-1

[

]

[

]

Figure 8.3-143 presents both the calculated collapsed liquid level in the reactor vessel lower plenum, core, and upper plenum (vessel liquid level), and the collapsed liquid level in the core (core liquid level) from the bottom of the active core. [

]

[

]

- Core Reflood and Quench Phenomena, Test LP-LB-1

[

]

PCT Comparison Relative to Core Elevation, Test LP-LB-1

The differences between calculated and measured cladding temperature time histories are discussed in Section 8.3.1.8.2.

Figure 8.3-144 compares the calculated and measured PCT versus core elevation. In this figure, the PCT is referred to as a maximum cladding surface temperature, either calculated or measured at the various locations, during the LOCA transient history.

[

]

Table 8.3-1 LOFT Nuclear Large Break Test Parameters

Test	Power (MWt)	MLHGR (KW/ft)	Pump Operation	Fuel Pressurized	HPIS	ECC LIPS	Accum	PCT (K)
L2-3 - Similar to L2-2, with higher power and increased LHGR.	36	11.9	On	No	2/3	1/2	3/4	914
L2-5 - Similar to L2-3, with pumps turned off and decoupled from their external flywheels within 1 s, US Appendix K ECC with 58% L2-3 HPIS	36	12.2	Off ⁴	Yes	1/3	1/2	3/4	1078
LP-02-6 - Similar to L2-5, with pumps turned off but initial coastdown with external flywheels, US Appendix K ECC, increased core power and MLHGR.	46	14.9	Off ⁵	Yes	1/3	1/2	3/4	1077
LP-LB-1 - Similar to LP-02-6, with pump turned off and decoupled from their external flywheels within 1 s, UK minimum safeguards ECC, and slightly increased core power and MLHGR.	49.3	15.8	Off ⁴	No	0/3	1/2	2/4	1256

⁴ Atypical rapid pump coastdown⁵ Normal pump coastdown

Table 8.3-2 Initial Conditions for LOFT Test L2-3 and S-RELAP5 Model

Parameter	Test L2-3	S-RELAP5
Core Power (MWt)	36.00 ± 1.0	
Pressure (MPa)	15.06 ± 0.03	
Hot-Leg Temperature (K)	592.9 ± 1.8	
Cold-Leg Temperature (K)	560.7 ± 1.8	
Mass Flow Rate (kg/s)	199.0 ± 6.3	
Pressurizer Level (m)	1.19 ± 0.01	
Steam Generator Secondary Pressure (MPa)	6.18 ± 0.08	
Steam Generator Downcomer Level ⁶ (m)	3.11 ± 0.025	
Steam Flow Rate (kg/s)	19.5 ± 0.4	
Feedwater Flow Rate (kg/s)	not reported	
Feedwater Temperature (K)	not reported	
Broken-Loop Hot-Leg Temperature (K)	565.5 ± 1.8	
Broken-Loop Cold-Leg Temperature (K)	554.3 ± 1.8	

⁶ The level is defined from the top of the tube sheet. The measured level is 0.25 m that is referenced as 0.0 at 2.95 m above the top of the tube sheet.

Table 8.3-3 Event Setpoints and Boundary Conditions for Simulation of LOFT Test L2-3

Parameter	Value
Test Initiation (s)	0.00
Reactor Scram Signal (Hot Leg Pressure) (MPa)	14.19
Reactor Scram Signal (time) (s)	0.103
HPIS Initiation (s)	14
LPIS Initiation (s)	29
Accumulator Nitrogen Volume (m ³)	0.84
Effective Accumulator Liquid Volume (m ³)	1.32
Accumulator Liquid Level (m)	2.10
Accumulator Standpipe Position (m)	1.12
Accumulator Pressure (MPa)	4.18
Accumulator Temperature (K)	307.2

Table 8.3-4 Event Sequence for LOFT Test L2-3

Event	Measured Data Time (s)	S-RELAP5 Time (s)
Test Initiation	0.00]
Reactor Scram	0.103	
PCT Reached	5.0	
Pressurizer Empty	≈10.0	
HPIS Initiation	14.0	
Accumulator Injection Initiation	16.0	
Lower Plenum Refill Started	Not Reported	
Lower Plenum Refill Completed	Not Reported	
Core Reflood Initiated	Not Reported	
LPIS Initiation	29.0	
Accumulator Empty	45.0	
Core Reflood Completed	Not Reported	
Core Cladding Quench	>50.0	

Table 8.3-5 Initial Conditions for LOFT Test L2-5 and S-RELAP5 Model

Parameter	Test L2-5	S-RELAP5
Core Power (MW _t)	36.00 ± 1.2	
Core Temperature Rise (K)	33.10 ± 4.3	
Hot-Leg Pressure (MPa)	14.94 ± 0.06	
Hot-Leg Temperature (K)	589.7 ± 1.6	
Cold-Leg Temperature (K)	556.6 ± 4.0	
Mass Flow Rate (kg/s)	192.4 ± 7.8	
Pressurizer Level (m)	1.14 ± 0.03	
Steam Generator Secondary Pressure (MPa)	5.85 ± 0.06	
Steam Generator Downcomer Level ⁷ (m)	3.18 ± 0.06	
Steam Flow Rate (kg/s)	19.1 ± 0.4	
Feedwater Flow Rate (kg/s)	not reported	
Feedwater Temperature (K)	not reported	
Broken-Loop Hot-Leg Temperature (K)	561.9 ± 4.3	
Broken-Loop Cold-Leg Temperature (K)	554.3 ± 4.2	

⁷ The level is defined from the top of the tube sheet. The measured level is 0.25 m that is referenced as 0.0 at 2.95 m above the top of the tube sheet.

**Table 8.3-6 Event Setpoints and Boundary Conditions for Simulation
of LOFT Test L2-5**

Parameter	Value
Test Initiation (s)	0.00
Reactor Scram Signal (Hot Leg Pressure) (MPa)	14.19
Reactor Scram Signal (time) (s)	0.06
Primary Coolant Pump Trip (s)	1.75
HPIS Initiation (s)	23.90
LPIS Initiation (s)	37.32
Accumulator Nitrogen Volume (m ³)	0.84
Effective Accumulator Liquid Volume (m ³)	1.45
Accumulator Liquid Level (m)	2.10
Accumulator Standpipe Position (m)	0.92
Accumulator Pressure (MPa)	4.29
Accumulator Temperature (K)	303.0

Table 8.3-7 Event Sequence for LOFT Test L2-5

Event	Measured Data Time (s)	S-RELAP5 Time (s)
Test Initiation	0.00	
Reactor Scram	0.24 ± 0.01	
Primary Coolant Pump Trip	0.94 ± 0.01	
Pressurizer Empty	15.40 ± 1.0	
Accumulator Injection Initiation	16.80 ± 0.1	
Lower Plenum Refill Started	22.0	
HPIS Initiation	23.90 ± 0.02	
PCT Reached	28.47 ± 0.02	
Lower Plenum Refill Completed	31.0	
Core Reflood Initiated	37.0	
LPIS Initiation	37.32 ± 0.02	
Accumulator Empty	49.60 ± 0.1	
Core Reflood Completed	55.30 ± 1.5	
Core Cladding Quench	65.00 ± 2.0	

Table 8.3-8 Initial Conditions for LOFT Test LP-02-6 and S-RELAP5 Model

Parameter	Test LP-02-6	S-RELAP5
Core Power (MW_t)	46.00 ± 1.2	
Hot-Leg Pressure (MPa)	15.09 ± 0.08	
Hot-Leg Temperature (K)	589.0 ± 1.0	
Cold-Leg Temperature (K)	555.9 ± 1.1	
Core Temperature Rise (K)	33.10 ± 4.3	
Mass Flow Rate (kg/s)	248.7 ± 2.6	
Pressurizer Level (m)	1.04 ± 0.04	
Steam Generator Secondary Pressure (MPa)	5.63 ± 0.2	
Steam Generator Downcomer Level ⁸ (m)	3.28 ± 0.6	
Steam Flow Rate (kg/s)	24.3 ± 0.4	
Feedwater Flow Rate (kg/s)	not reported	
Feedwater Temperature (K)	not reported	
Broken-Loop Hot-Leg Temperature (K)	560.0 ± 6.0	
Broken-Loop Cold-Leg Temperature (K)	553.0 ± 6.0	

⁸ The level is defined from the top of the tube sheet. The measured level is 0.25 m that is referenced as 0.0 at 2.95 m above the top of the tube sheet.

**Table 8.3-9 Event Setpoints and Boundary Conditions for Simulation
of LOFT Test LP-02-6**

Parameter	Value
Test Initiation (s)	0.00
Reactor Scram Signal (Hot Leg Pressure) (MPa)	14.80
Reactor Scram Signal (Time) (s)	0.06
Primary Coolant Pump Trip (s)	1.28
High Pressure Injection System Initiation (s)	24.77
Low Pressure Injection System Initiation (s)	37.32
Accumulator Nitrogen Volume (m ³)	0.84
Effective Accumulator Liquid Volume (m ³)	1.32
Accumulator Liquid Level (m)	2.10
Accumulator Standpipe Position (m)	1.12
Accumulator Pressure (MPa)	4.11
Accumulator Temperature (K)	302.0

Table 8.3-10 Event Sequence for LOFT Test LP-02-6

Event	Measured Data Time (s)	S-RELAP5 Time (s)
Test Initiation	0.00	
Reactor Scram	0.06 ± 0.01	
Primary Coolant Pump Trip	1.28 ± 0.01	
PCT Reached	4.9 ± 0.2	
Pressurizer Empty	15.5 ± 0.5	
Accumulator Injection Initiation	17.5 ± 0.5	
Lower Plenum Refill Started	not reported	
HPIS Initiation	24.77 ± 0.01	
Lower Plenum Refill Completed	30.7	
Core Reflood Initiated	not reported	
LPIS Initiation	37.32 ± 0.02	
Accumulator Empty	45.0	
Core Quench Completed	56.0 ± 0.2	
Core Reflood Completed	59.0 ± 1.0	

Table 8.3-11 Initial Conditions for the LOFT Test LP-LB-1 and the S-RELAP5 Model

Parameter	Test LP-LB-1	S-RELAP5
Core Power (MWt)	49.30 ± 1.2	
Core Temperature Rise (K)	29.5 ± 1.4	
Hot-Leg Pressure (MPa)	14.90 ± 0.08	
Cold-Leg Temperature (K)	556.0 ± 1.0	
Mass Flow Rate (kg/s)	305.8 ± 2.6	
Pressurizer Level (m)	1.04 ± 0.04	
Steam Generator Secondary Pressure (MPa)	5.53 ± 0.02	
Steam Generator Downcomer Level ⁹ (m)	3.2	
Steam Flow Rate (kg/s)	25.4 ± 0.4	
Feedwater Flow Rate (kg/s)	not reported	
Feedwater Temperature (K)	not reported	
Broken-Loop Hot-Leg Temperature (K)	561.0 ± 6.0	
Broken-Loop Cold-Leg Temperature (K)	552.0 ± 6.0	

⁹ The level is defined from the top of the tube sheet. The measured level is 0.25 m that is referenced as 0.0 at 2.95 m above the top of the tube sheet.

**Table 8.3-12 Event Setpoints and Boundary Conditions for
Simulation of LOFT Test LP-LB-1**

Parameter	Value
Test Initiation (s)	0.00
Reactor Scram Signal (Hot Leg Pressure) (MPa)	14.50
Reactor Scram Signal (time) (s)	0.008
Primary Coolant Pump Trip (s)	1.2
HPIS Initiation (s)	N/A
LPIS Initiation (s)	31.0
Accumulator Nitrogen Volume (m ³)	0.66
Effective Accumulator Liquid Volume (m ³)	0.72
Accumulator Liquid Level (m)	2.36
Accumulator Standpipe Position (m)	1.74
Accumulator Pressure (MPa)	4.20
Accumulator Temperature (K)	305.0

Table 8.3-13 Event Sequence for LOFT Test LP-LB-1

Event	Measured Data Time(s)	S-RELAP5 Time(s)
Test Initiation	0.00	
Reactor Scram	0.13 ± 0.01	
Primary Coolant Pump Trip	0.24 ± 0.01	
Blowdown PCT Reached	12.9 ± 0.5	
Pressurizer Empty	15 ± 1.0	
Accumulator Injection Initiation	17.5 ± 0.05	
Refill/Reflood PCT Reached	26.8 ± 0.5	
LPIS Initiation	32.0 ± 1.0	
Lower Plenum Refill Completed	34.5 ± 0.5	
Accumulator Empty	40.0 ± 1.0	
Accumulator Injection Completed	46.0 ± 2.0	
Core Quench Completed	72.0 ± 1.0	

Figure 8.3-1 LOFT Major Components

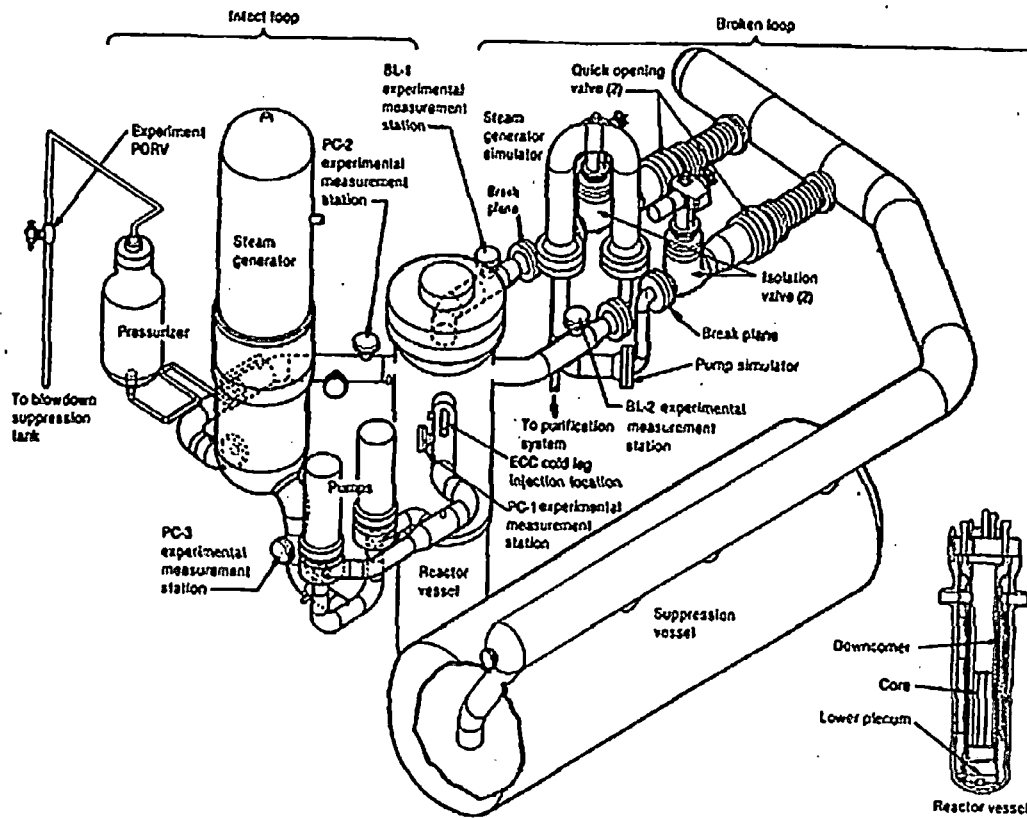


Figure 8.3-2 LOFT Large Break Model Nodalization



Figure 8.3-3 LOFT Downcomer and Core Nodalizations



Figure 8.3-4 COPENIC Fuel Model Nodalization



Figure 8.3-5 LOFT Test L2-3 Reactor Vessel Upper Plenum Pressure



Figure 8.3-6 LOFT Test L2-3 Pressurizer Pressure



Figure 8.3-7 LOFT Test L2-3 Primary and Secondary Pressures



Figure 8.3-8 LOFT Test L2-3 Pressurizer Collapsed Liquid Level



Figure 8.3-9 LOFT Test L2-3 ILHL Average Volume Fluid Density



Figure 8.3-10 LOFT Test L2-3 ILCL Average Volume Fluid Density



Figure 8.3-11 LOFT Test L2-3 BLHL Average Volume Fluid Density



Figure 8.3-12 LOFT Test L2-3 BLCL Average Volume Fluid Density



Figure 8.3-13 LOFT Test L2-3 BLHL Mass Flow Rate



Figure 8.3-14 LOFT Test L2-3 BLCL Mass Flow Rate



Figure 8.3-15 LOFT Test L2-3 ILHL Mass Flow Rate



Figure 8.3-16 LOFT Test L2-3 Pump Flow Minus Break Flow



Figure 8.3-17 LOFT Test L2-3 Pump Speed - Primary Coolant Pump 1



Figure 8.3-18 LOFT Test L2-3 Reactor Vessel Upper Plenum Fluid Temperature



**Figure 8.3-19 LOFT Test L2-3 Reactor Vessel Lower Plenum Fluid
Temperature**



Figure 8.3-20 LOFT Test L2-3 ILHL Fluid Temperature

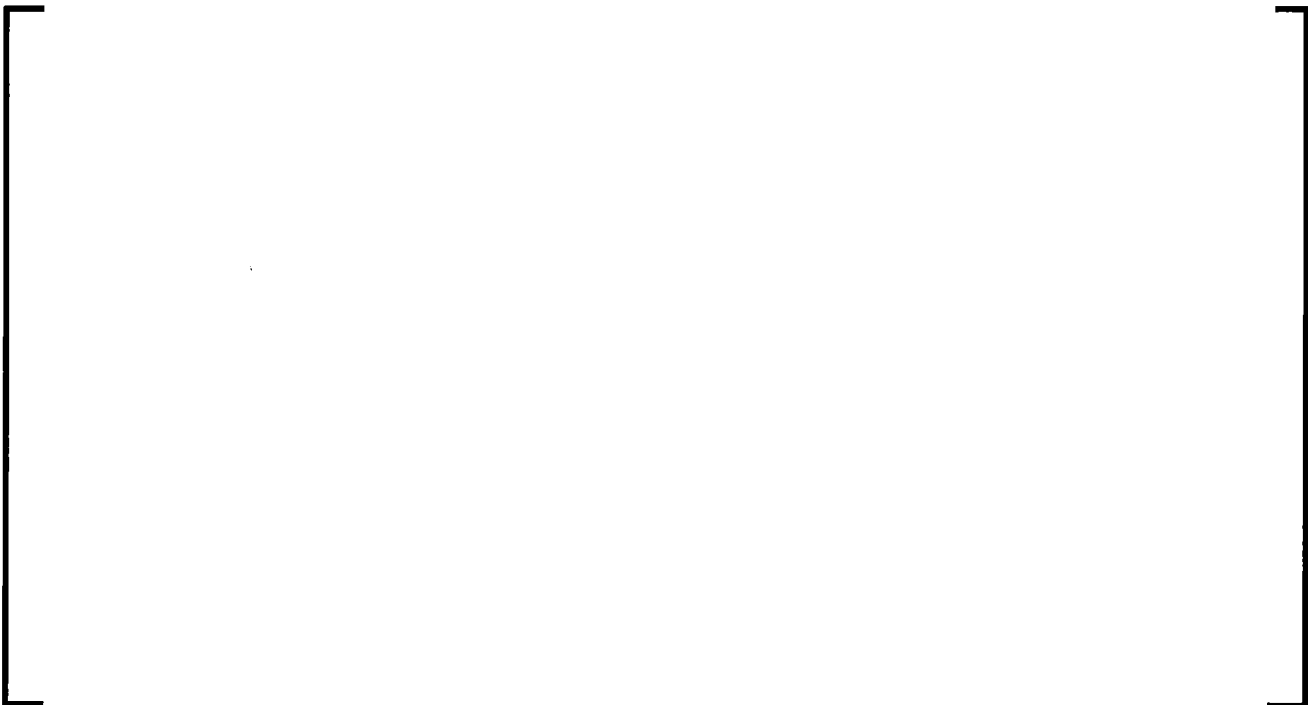


Figure 8.3-21 LOFT Test L2-3 ILCL Fluid Temperature



Figure 8.3-22 LOFT Test L2-3 Accumulator Liquid Level



Figure 8.3-23 LOFT Test L2-3 Accumulator Pressure



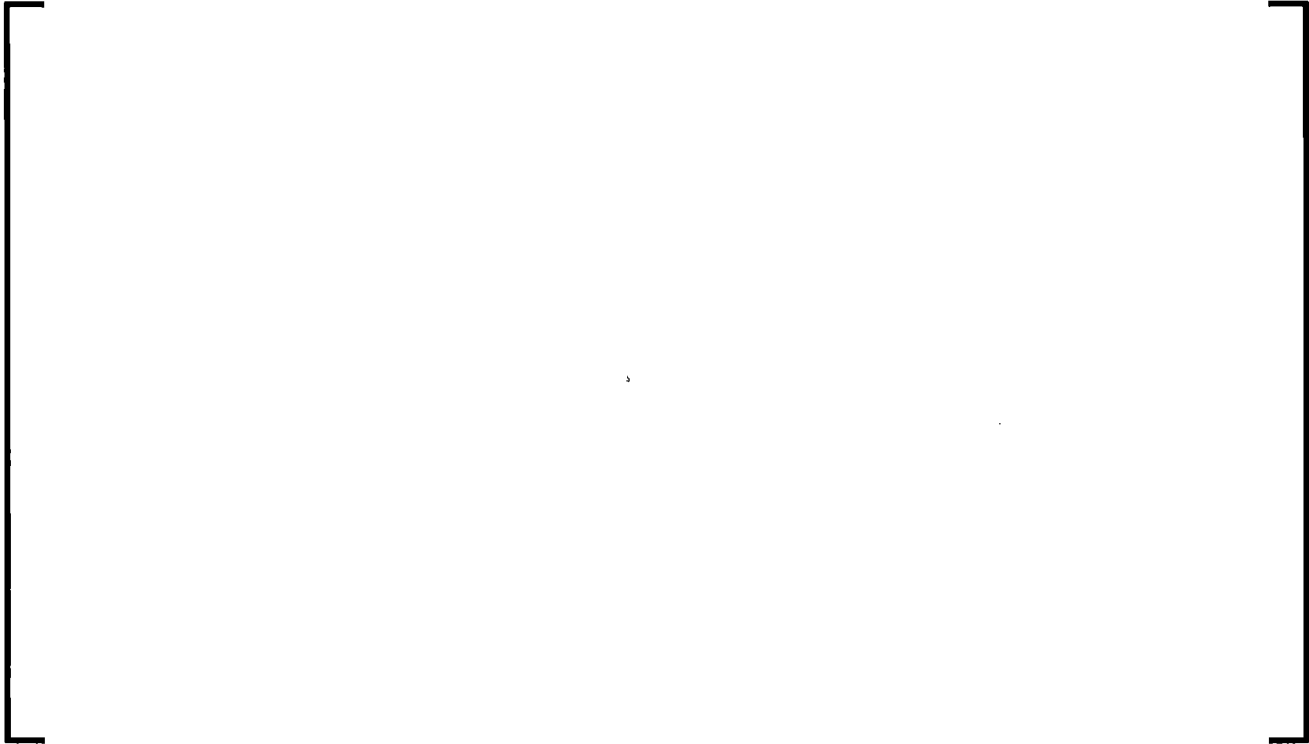
Figure 8.3-24 LOFT Test L2-3 Mass Flow Rate from LPIS



Figure 8.3-25 LOFT Test L2-3 Central Fuel Assembly Instrumented Fuel Rod Locations and S-RELAP5 Axial Fuel Rod Temperature Calculation Locations



**Figure 8.3-26 LOFT Test L2-3 Hot Rod Cladding Temperature at 5
Inches**



**Figure 8.3-27 LOFT Test L2-3 Hot Rod Cladding Temperature at 15
Inches**



**Figure 8.3-28 LOFT Test L2-3 Hot Rod Cladding Temperature at 21
Inches**



**Figure 8.3-29 LOFT Test L2-3 Hot Rod Cladding Temperature at 26
Inches**



**Figure 8.3-30 LOFT Test L2-3 Hot Rod Cladding Temperature at 39
Inches**



**Figure 8.3-31 LOFT Test L2-3 Hot Rod Cladding Temperature at 49
Inches**



**Figure 8.3-32 LOFT Test L2-3 Hot Rod Cladding Temperature at 58
Inches**



**Figure 8.3-33 LOFT Test L2-3 Calculated Collapsed Liquid Levels in
Reactor Vessel and Active Core**



Figure 8.3-34 LOFT Test L2-3 Comparison of PCTs Versus Core Elevations



Figure 8.3-35 LOFT Test L2-5 Reactor Vessel Upper Plenum Pressure



Figure 8.3-36 LOFT Test L2-5 ILHL Pressure



Figure 8.3-37 LOFT Test L2-5 ILCL Pressure



Figure 8.3-38 LOFT Test L2-5 Pressurizer Pressure



Figure 8.3-39 LOFT Test L2-5 Primary and Secondary Pressure



Figure 8.3-40 LOFT Test L2-5 Pressurizer Collapsed Liquid Level



Figure 8.3-41 LOFT Test L2-5 ILHL Average Volume Fluid Density



Figure 8.3-42 LOFT Test L2-5 ILCL Average Volume Fluid Density



Figure 8.3-43 LOFT Test L2-5 BLCL Average Volume Fluid Density



Figure 8.3-44 LOFT Test L2-5 BLHL Mass Flow Rate



Figure 8.3-45 LOFT Test L2-5 BLCL Mass Flow Rate



Figure 8.3-46 LOFT Test L2-5 ILHL Mass Flow Rate



Figure 8.3-47 LOFT Test L2-5 ILCL Mass Flow Rate



**Figure 8.3-48 LOFT Test L2-5 Difference Between Break Flow minus
Pump Flow**



Figure 8.3-49 LOFT Test L2-5 Pump Speed - Primary Coolant Pump 1



Figure 8.3-50 LOFT Test L2-5 Pump Speed - Primary Coolant Pump 2



Figure 8.3-51 LOFT Test L2-5 Reactor Vessel Upper Plenum Fluid Temperature



**Figure 8.3-52 LOFT Test L2-5 Reactor Vessel Lower Plenum Fluid
Temperature**



Figure 8.3-53 LOFT Test L2-5 ILHL Fluid Temperature



Figure 8.3-54 LOFT Test L2-5 ILCL Fluid Temperature



Figure 8.3-55 LOFT Test L2-5 Accumulator Liquid Level



Figure 8.3-56 LOFT Test L2-5 Accumulator Pressure



Figure 8.3-57 LOFT Test L2-5 Mass Flow Rate from HPIS



Figure 8.3-58 LOFT Test L2-5 Mass Flow Rate from LPIS



Figure 8.3-59 LOFT Test L2-5 Central Fuel Assembly Instrumented Fuel Rod Locations and S-RELAP5 Axial Fuel Rod Temperature Calculation Locations



**Figure 8.3-60 LOFT Test L2-5 Hot Rod Cladding Temperature at 5
Inches**



**Figure 8.3-61 LOFT Test L2-5 Hot Rod Cladding Temperature at 15
Inches**



**Figure 8.3-62 LOFT Test L2-5 Hot Rod Cladding Temperature at 21
Inches**



**Figure 8.3-63 LOFT Test L2-5 Hot Rod Cladding Temperature at 24
Inches**



**Figure 8.3-64 LOFT Test L2-5 Hot Rod Cladding Temperature at 26
Inches**



**Figure 8.3-65 LOFT Test L2-5 Hot Rod Cladding Temperature at 39
Inches**



**Figure 8.3-66 LOFT Test L2-5 Hot Rod Cladding Temperature at 49
Inches**



**Figure 8.3-67 LOFT Test L2-5 Hot Rod Cladding Temperature at 58
Inches**



Figure 8.3-68 LOFT Test L2-5 Fuel Centerline Temperature



**Figure 8.3-69 LOFT Test L2-5 Fuel Pellet Off-Center (Shoulder)
Temperature**



**Figure 8.3-70 LOFT Test L2-5 Calculated Collapsed Liquid Levels in
Reactor Vessel and Active Core**



Figure 8.3-71 LOFT Test L2-5 Comparison of PCTs Versus Core Elevations



Figure 8.3-72 LOFT Test LP-02-6 Reactor Vessel Upper Plenum Pressure



Figure 8.3-73 LOFT Test LP-02-6 ILHL Pressure



Figure 8.3-74 LOFT Test LP-02-6 ILCL Pressure



Figure 8.3-75 LOFT Test LP-02-6 Pressurizer Pressure



Figure 8.3-76 LOFT Test LP-02-6 Primary and Secondary Pressure



Figure 8.3-77 LOFT Test LP-02-6 Pressurizer Collapsed Liquid Level



Figure 8.3-78 LOFT Test LP-02-6 ILHL Average Volume Fluid Density



Figure 8.3-79 LOFT Test LP-02-6 ILCL Average Volume Fluid Density



Figure 8.3-80 LOFT Test LP-02-6 BLHL Average Volume Fluid Density



Figure 8.3-81 LOFT Test LP-02-6 BLCL Average Volume Fluid Density

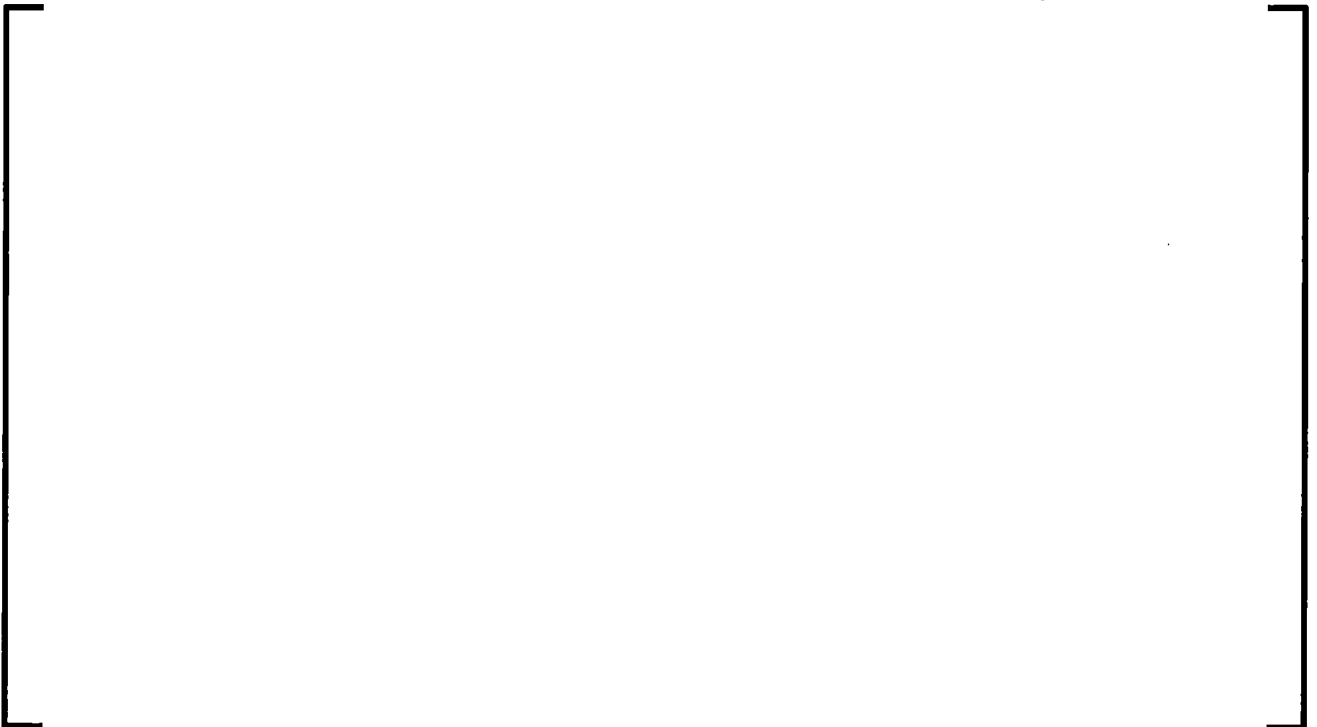


Figure 8.3-82 LOFT Test LP-02-6 BLHL Mass Flow Rate



Figure 8.3-83 LOFT Test LP-02-6 BLCL Mass Flow Rate



Figure 8.3-84 LOFT Test LP-02-6 ILHL Mass Flow Rate

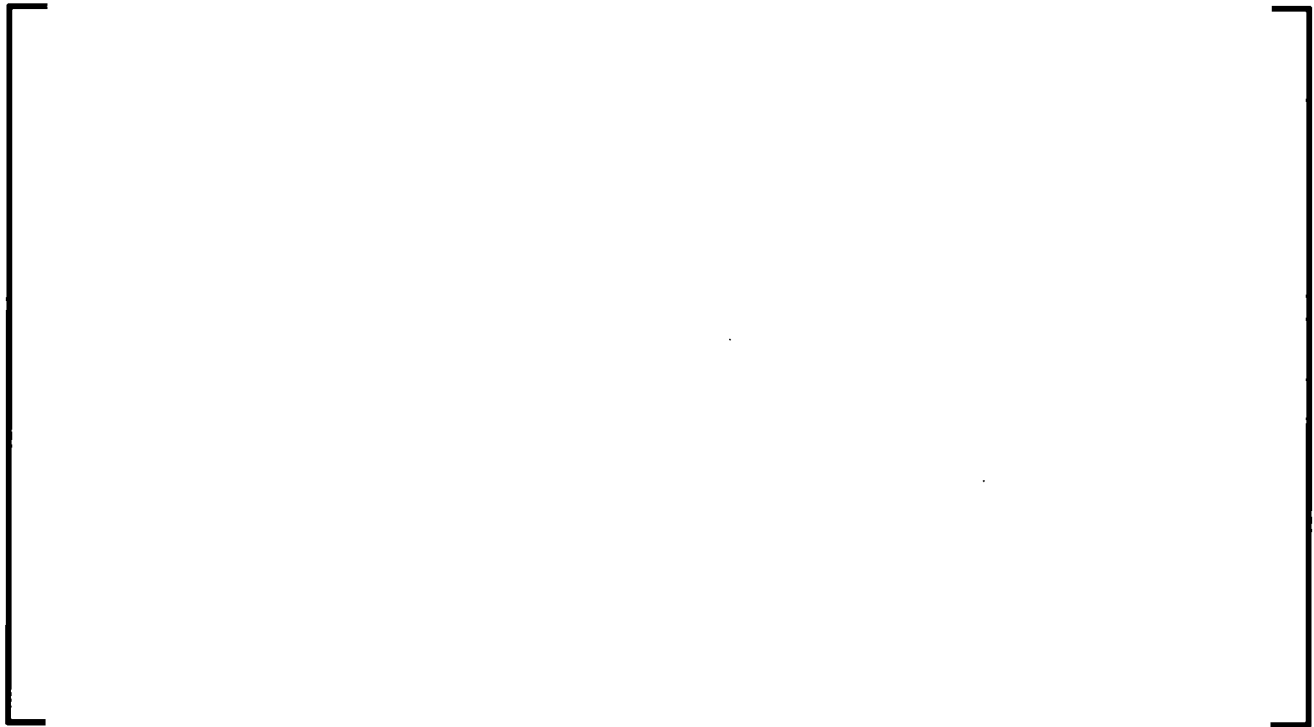


Figure 8.3-85 LOFT Test LP-02-6 ILCL Mass Flow Rate



**Figure 8.3-86 LOFT Test LP-02-6 Difference Between Pump Flow and
Break Flow**



**Figure 8.3-87 LOFT Test LP-02-6 Pump Speed - Primary Coolant
Pump 1**



**Figure 8.3-88 LOFT Test LP-02-6 Pump Speed - Primary Coolant
Pump 2**



**Figure 8.3-89 LOFT Test LP-02-6 Reactor Vessel Upper Plenum Fluid
Temperatures**



**Figure 8.3-90 LOFT Test LP-02-6 Reactor Vessel Lower Plenum Fluid
Temperatures**



Figure 8.3-91 LOFT Test LP-02-6 ILHL Fluid Temperatures



Figure 8.3-92 LOFT Test LP-02-6 ILCL Fluid Temperatures



Figure 8.3-93 LOFT Test LP-02-6 Accumulator Liquid Level



Figure 8.3-94 LOFT Test LP-02-6 Accumulator Pressure



Figure 8.3-95 LOFT Test LP-02-6 Mass Flow Rate from HPIS



Figure 8.3-96 LOFT Test LP-02-6 Mass Flow Rate from LPIS



**Figure 8.3-97 LOFT Test LP-02-6 Central Assembly Instrumented Fuel
Rod Locations and S-RELAP5 Axial Fuel Rod Temperature
Calculation Locations**



**Figure 8.3-98 LOFT Test LP-02-6 Hot Rod Cladding Temperatures at 5
Inches**



**Figure 8.3-99 LOFT Test LP-02-6 Hot Rod Cladding Temperatures at
15 Inches**



**Figure 8.3-100 LOFT Test LP-02-6 Hot Rod Cladding Temperatures
(Solid Pellet) at 26 Inches**



**Figure 8.3-101 LOFT Test LP-02-6 Hot Rod Cladding Temperatures at
39 Inches**



**Figure 8.3-102 LOFT Test LP-02-6 Hot Rod Cladding Temperatures at
49 Inches**



**Figure 8.3-103 LOFT Test LP-02-6 Hot Rod Cladding Temperatures at
54 Inches**



Figure 8.3-104 LOFT Test LP-02-6 Fuel Centerline Temperature



**Figure 8.3-105 LOFT Test LP-02-6 Instrument Rod Off Center
Temperatures at 26 Inches**



**Figure 8.3-106 LOFT Test LP-02-6 Calculated Collapsed Liquid Levels
in Reactor Vessel and Active Core**



Figure 8.3-107 LOFT Test LP-02-6 Comparison of PCTs Versus Core Elevations



**Figure 8.3-108 LOFT Test LP-LB-1 Reactor Vessel Upper Plenum
Pressure**



Figure 8.3-109 LOFT Test LP-LB-1 ILHL Pressure



**Figure 8.3-110 LOFT Test LP-LB-1 ILCL Pressure Between Steam
Generator and Pump**



Figure 8.3-111 LP-LB-1 Pressurizer Pressure



Figure 8.3-112 LP-LB-1 Primary and Secondary Side Pressures



Figure 8.3-113 LOFT Test LP-LB-1 Comparison of Upper Plenum Pressure and Accumulator Non-Condensable Quality



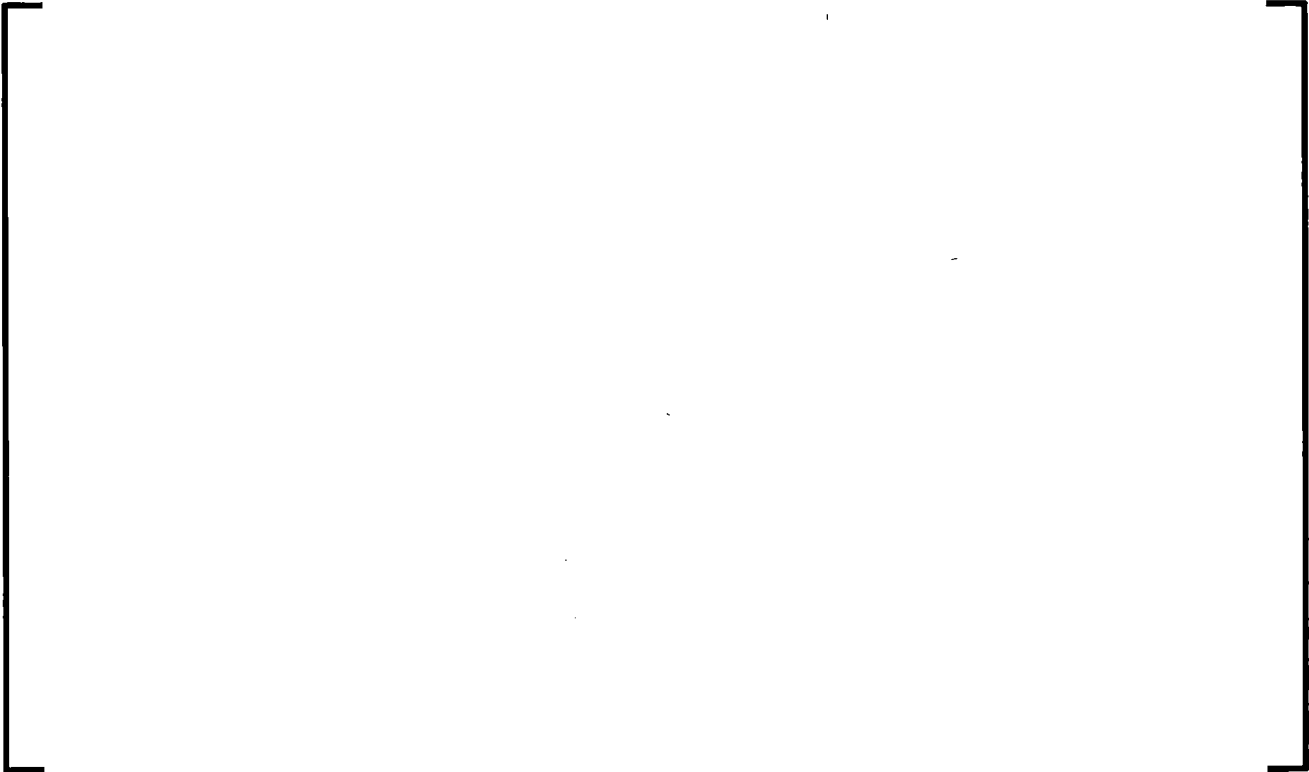
Figure 8.3-114 LOFT Test LP-LB-1 Comparison of Loop Pressure Difference (ILCL-ILHL)



Figure 8.3-115 LOFT Test LP-LB-1 Pressurizer Collapsed Liquid Level



**Figure 8.3-116 LOFT Test LP-LB-1 ILHL Average Volume Fluid
Density**



**Figure 8.3-117 LOFT Test LP-LB-1 ILCL Average Volume Fluid
Density**



**Figure 8.3-118 LOFT Test LP-LB-1 BLHL Average Volume Fluid
Density**



**Figure 8.3-119 LOFT Test LP-LB-1 BLCL Average Volume Fluid
Density**



Figure 8.3-120 LOFT Test LP-LB-1 BLHL Mass Flow Rate



Figure 8.3-121 LOFT Test LP-LB-1 BLCL Mass Flow Rate



Figure 8.3-122 LOFT Test LP-LB-1 ILHL Mass Flow Rate



Figure 8.3-123 LOFT Test LP-LB-1 ILCL Mass Flow Rate



Figure 8.3-124 LOFT Test LP-LB-1 Difference Between Pump Flow and Break Flow



**Figure 8.3-125 LOFT Test LP-LB-1 Pump Speed - Primary Coolant
Pump 1**



**Figure 8.3-126 LOFT Test LP-LB-1 Pump Speed - Primary Coolant
Pump 2**



**Figure 8.3-127 LOFT Test LP-LB-1 Reactor Vessel Upper Plenum
Fluid Temperatures**



**Figure 8.3-128 LOFT Test LP-LB-1 Reactor Vessel Lower Plenum
Fluid Temperatures**



Figure 8.3-129 LOFT Test LP-LB-1 ILHL Fluid Temperature



Figure 8.3-130 LOFT Test LP-LB-1 ILCL Fluid Temperature



Figure 8.3-131 LOFT Test LP-LB-1 Accumulator Liquid Level

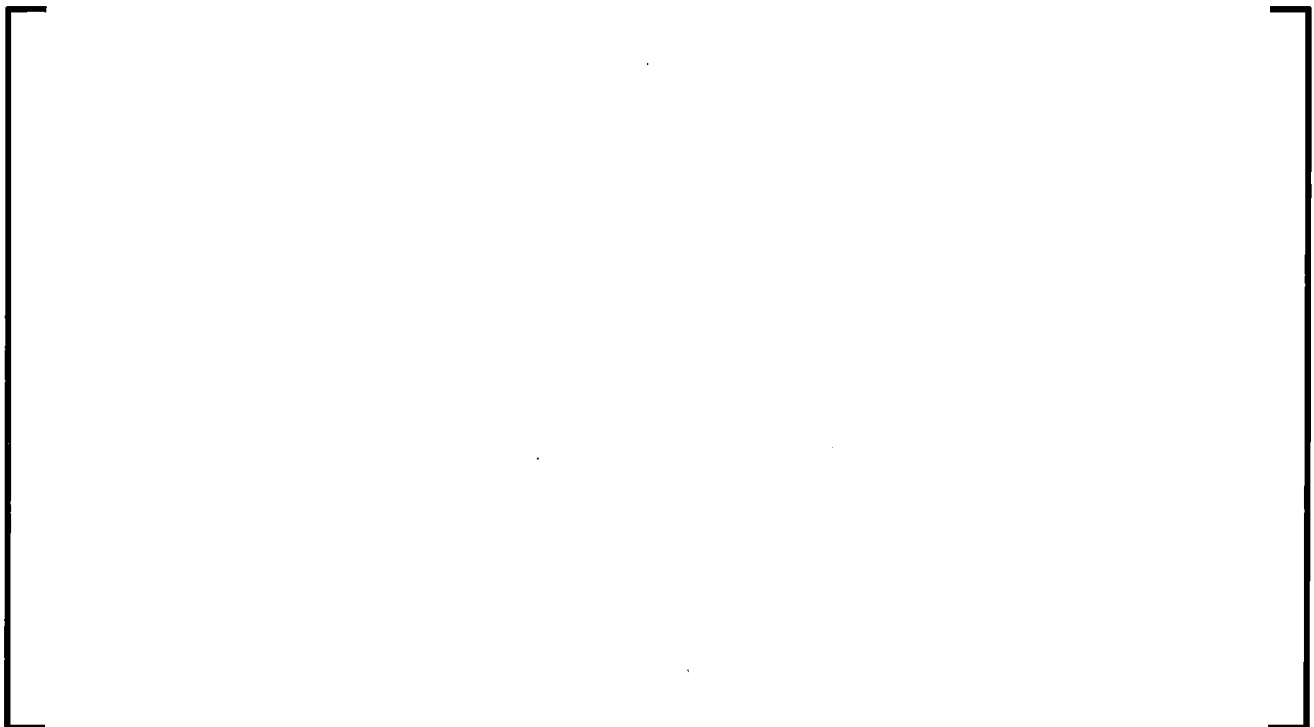


Figure 8.3-132 LOFT Test LP-LB-1 Accumulator Pressure



Figure 8.3-133 LOFT Test LP-LB-1 Mass Flow Rate from LPIS



**Figure 8.3-134 LOFT Test LP-LB-1 Central Assembly Instrumented
Fuel Rod Locations and S-RELAP5 Axial Fuel Rod Temperature
Calculation Locations**



**Figure 8.3-135 LOFT Test LP-LB-1 Hot Rod Cladding Temperatures at
11 Inches**



**Figure 8.3-136 LOFT Test LP-LB-1 Hot Rod Cladding Temperatures at
15 Inches**



**Figure 8.3-137 LOFT Test LP-LB-1 Hot Rod Cladding Temperatures at
24 Inches**



**Figure 8.3-138 LOFT Test LP-LB-1 Hot Rod Cladding Temperatures at
27 Inches**



**Figure 8.3-139 LOFT Test LP-LB-1 Hot Rod Cladding Temperatures at
39 Inches**



**Figure 8.3-140 LOFT Test LP-LB-1 Hot Rod Cladding Temperatures at
49 Inches**



**Figure 8.3-141 LOFT Test LP-LB-1 Hot Rod Cladding Temperatures at
54 Inches**

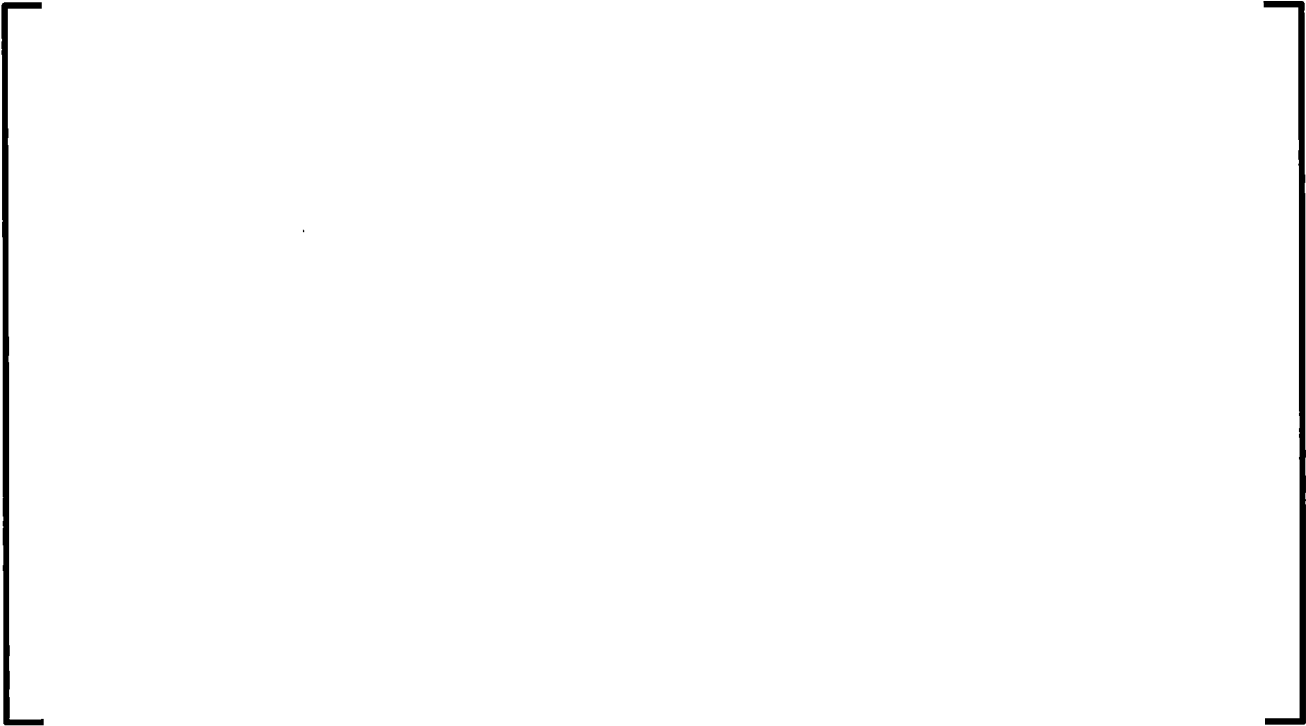


Figure 8.3-142 LOFT Test LP-LB-1 Fuel Centerline Temperature



**Figure 8.3-143 LOFT Test LP-LB-1 Calculated Collapsed Liquid
Levels in Reactor Vessel and Active Core**



Figure 8.3-144 LOFT Test LP-LB-1 Comparison of PCTs Versus Core Elevations



8.3.2 Semiscale

8.3.2.1 Introduction

This section documents the assessment results of S-RELAP5 against the Semiscale large-break loss-of-coolant accident (LBLOCA) tests S-06-3 and S-07-1. Test S-06-3 was performed in the Semiscale MOD-1 facility. The MOD-1 facility was scaled from the Loss of Fluid Test (LOFT) facility; the test was performed as a counterpart to LOFT Test L2-3. The results presented for this assessment are used to support the application of S-RELAP5 in pressurized water reactor (PWR) RLBLOCA analysis and to verify the capability of the S-RELAP5 code to calculate LOCA phenomena in facilities of different scale. Semiscale Test S-07-1 is a blowdown test performed in the Semiscale MOD-3 facility with cold leg emergency core coolant (ECC) injections. The results presented for this assessment are used to support the application of S-RELAP5 in PWR RLBLOCA analysis, and to verify the capability of the code to calculate blowdown film boiling heat transfer in the core. Test S-06-3 was performed as a counterpart to LOFT Test L2-3 and provides assessment for the blowdown, refill, and reflood phases of a LBLOCA.

8.3.2.2 Summary and Conclusions

S-RELAP5 was assessed against Semiscale Test S-06-3. The calculation results have been compared to test data for the three phases of the test (blowdown, refill, and reflood). While good agreement is obtained between code results and data for the major thermal-hydraulic variables, the MOD-1 Test S-06-3 experienced apparent ECC bypass that could not be captured thoroughly by the RLBLOCA methodology. This resulted in earlier refill being calculated and consequently earlier calculated reflood and quenching of the heater rods. [

]

S-RELAP5 was assessed against Semiscale Test S-07-1. The calculation results have been compared to test data. Good agreement is obtained between code results and data for the major thermal hydraulic variables including upper plenum pressure, break flow rates, coolant temperatures, and rod temperatures. The comparison demonstrates that S-RELAP5 is capable of simulating the blowdown film boiling heat transfer phenomena expected of a PWR LBLOCA transient. [

] The assessment of S-RELAP5 to predict bypass phenomena for NPPs is based primarily on full-scale UPTF Tests 6 and 7 as described in Section 8.2.9.3.

8.3.2.3 Facility Description, Semiscale MOD-1 Facility

The Semiscale MOD-1, $1\frac{1}{2}$ -loop facility was scaled to the LOFT facility, which in turn was scaled to a 4-loop PWR. It is designated a $1\frac{1}{2}$ -loop system because it is configured with one active loop and one passive blowdown loop. Subsequent Semiscale facilities have included components that have made the facility more typical of a PWR. All the Semiscale facilities were designed with 1/1600 to 1/2000 volume scaling, with full height, in reference to a 4-loop, 3400 MW_t PWR.

The MOD-1 system contains a reactor vessel with internals (Figure 8.3-145), including a 40-rod electrically heated core, an active intact loop scaled to represent three loops of a PWR, and a broken loop scaled to a single loop of a PWR. The intact loop contains an active steam generator and an active primary coolant pump, and is connected to the pressurizer. The broken loop contains hydraulic simulators for the steam generator and pump and break simulators or rupture assemblies connected to a blowdown suppression system. The blowdown suppression system simulates containment pressure.

The 40-rod electrically heated core has a PWR fuel pin pitch (0.563 inch), and the heated length (5.5 ft) and outside diameter (0.42 inch) are identical to the nuclear fuel rods of the LOFT core.

Semiscale Test Series 6 was performed to assist the LOFT program in planning the first nuclear test series. Test S-06-3 was performed as counterpart to LOFT Test L2-3. For this test, the four central heater rods were operated at approximately 39.4 kW/m, 32 rods were operated at approximately 24.9 kW/m, and four rods were unpowered to simulate passive rod locations. This configuration yielded a peaked power profile that simulates that of LOFT, and provides total core power of 1.004 MW. The layout of the heated rods in the core is shown in Figure 8.3-146.

The safety injection includes the high-pressure injection system (HPIS), low-pressure injection system (LPIS), and accumulators. For Test S-06-3, two HPIS pumps and two LPIS pumps delivered flow into the intact-loop cold leg along with the intact-loop accumulator. The primary coolant pump was powered for the entire transient.

8.3.2.4 S-RELAP5 Model Description for Semiscale MOD-1

The main features of the base input deck, as obtained from Reference 8.3-19, are as follows:

- The vessel, active loop, including pressurizer, and passive loop are modeled.
- [

]

- [

]

- [

]

- Nominal wall roughness was assigned for all components in the model based on the facility drawings.
- [

]

- [

]

Figure 8.3-148 and Figure 8.3-149 provide the S-RELAP5 vessel and loop nodalization for the MOD-1, Test S-06-03 simulation.

8.3.2.5 Test Conditions for Test S-06-3

[

]

8.3.2.6 Calculated Results for Semiscale Test S-06-3

The assessment results for Test S-06-3 are presented in this section. Figure 8.3-150 through Figure 8.3-171, and Table 8.3-14 and Table 8.3-15 show the major calculation results as well as the corresponding data.

Table 8.3-14 presents the code-calculated initial conditions as compared to the test data for Semiscale Test S-06-3. The S-RELAP5 results match reasonably well the Semiscale Test S-06-3 data as reported in References 8.3-19 and 8.3-20. Additionally, Figure 8.3-150 shows that the computed steady-state temperature distributions on the hot, and average rods are in good agreement with the measured data.

[

]

[

]

The downcomer flow phenomena, during the refill phase of an LBLOCA, observed in a full scale tests, like UPTF, are different from those observed in a small scale test facility like Semiscale. Under the 2D/3D program, UPTF Test 6 (Runs 131, 132, 133, 135 and 136) and Test 7 (Phase IV Run 203) were conducted specifically to investigate the ECC penetration and countercurrent flow phenomena in the downcomer of a PWR during the refill portion of LOCA. During the refill phase of a LBLOCA, ECC from the accumulators interacts with the loop steam in the cold legs, and with the steam flowing upwards in the downcomer. The resulting countercurrent flow in the downcomer is important since it affects how quickly the lower plenum refills and when core reflooding starts.

[

]

[

]

8.3.2.7 Facility Description, Semiscale MOD-3 Facility

The Semiscale MOD-3 facility is constructed with two fully active coolant loops. The intact loop, retained from the Semiscale MOD-1 system, was scaled to the LOFT facility, which in turn was scaled to a 4-loop PWR. Additionally, the broken loop was scaled directly to a 4-loop commercial PWR. All the Semiscale facilities were designed with 1/1600 to 1/2000 volume scaling, with full height, in reference to a 4-loop, 3400 MWt PWR.

The vessel in the MOD-3 system consists of the upper plenum with internals required to represent guide and support tubes, upper head, 25-rod electrically heated core, and an external single pipe downcomer. The active intact loop is scaled to represent three loops of a PWR, and the active broken loop is scaled to represent a single loop of a PWR. The intact loop contains a pump and the short Type I steam generator, and is connected to the pressurizer. The broken loop contains the taller Type II steam generator in addition to a pump and break simulators or rupture assemblies connected to a blowdown suppression system. The blowdown suppression system simulates containment pressure.

The 25-rod electrically heated core is characterized by fuel pin pitch (0.563 inch) and outside diameter (0.42 inch) typical of a PWR. The heated length (12 ft) of the MOD-3 core is identical to the 4-loop PWR core.

Test S-07-1 was performed to establish the baseline performance of the MOD-3 system during a blowdown with cold-leg ECC injections. It was conducted to obtain core heat transfer and departure from nucleate boiling (DNB) characteristics of the heater rods. The MOD-3 system was initialized in the experiment to a primary pressure of 15.9 MPa, total-loop flow of 9.4 kg/s and cold-leg temperatures of 559 K for the intact loop and 557 K for the broken loop at a core power level of 2.027 MW nominal (see Table 8.3-16 and Reference 8.3-21). The system was subjected to a double-ended cold-leg break through a rupture assembly and two non-communicative nozzles (Reference 8.3-22).

8.3.2.8 S-RELAP5 Model Description for Semiscale MOD-3

The Semiscale MOD-1 model described here was used as the starting point for the development of the MOD-3 input model. The features of the MOD-1 and MOD-3 facilities are compared in Table 8.3-17.

These features are further described below as follows:

- [

]

8.3.2.8.1 Core Nodalization for Semiscale Test S-07-1

[

]

[

]

8.3.2.9 Test Conditions for Test S-07-1

The specific test conditions simulated in the calculation are as follows:

- [

]

- [

- [

]

8.3.2.10 Calculated Results for Semiscale Test S-07-1

The assessment results for Test S-07-1 are presented in this section. The S-RELAP5 nodalization diagram of Test S-07-1 input model is shown in Figure 8.3-174 through Figure 8.3-176, Table 8.3-18 through Table 8.3-20, and Figure 8.3-177 through Figure 8.3-202 show the major calculation results as well as the corresponding data.

Table 8.3-16 shows the code calculated initial conditions compared to test data. The cold leg temperature in the broken loop was not matched because the code is not capable of predicting a loop-specific hot leg temperature. In this test, the measured hot leg temperature in the broken loop was 9 K lower than the hot leg temperature in the intact loop.

8.3.2.10.1 Technical Evaluation of Test S-07-1 Results

[

]

Based on this discussion, [

] This approach is reasonable.

8.3.2.10.2 General Thermal-Hydraulic Responses

The pressure response, break flow response, loop flow response, system temperatures, and other pertinent variables are discussed.

Upper Plenum Pressure

The upper plenum pressure response is illustrated in Figure 8.3-177, [

]

Secondary Steam Generator Pressures

Figure 8.3-178 and Figure 8.3-179 show the intact- and broken-loop steam generator pressure. Because the long-term data were used to develop the boundary pressure for the steam generator, the calculation should match the data. This is verified in the two figures.

Break Flow

Figure 8.3-180 and Figure 8.3-181 show the pump-side break flow rate response and the integrated pump side break flow, respectively. [

]

Figure 8.3-182 shows the vessel-side break flow response. [

]

Figure 8.3-183 shows the integrated vessel side break mass. [

]

Fluid Density

Figure 8.3-184 and Figure 8.3-185 respectively show the broken-loop volume average fluid density at the pump and vessel sides of the break. [

]

Loop Flow

Figure 8.3-186 and Figure 8.3-187 respectively show the intact-loop cold- and hot-leg flow rate. [

]

Inlet Core Flow

Figure 8.3-188 shows the flow rate at the core inlet. The maximum reversed core flow rate was predicted well. [

]

Coolant Temperature

Figure 8.3-189 through Figure 8.3-191 show coolant temperatures at various locations.

[

]

Upper Plenum Flow

Figure 8.3-192 shows the calculated flow through the support column. [

]

Figure 8.3-193 shows the calculated flow through the guide tubes. [

]

Figure 8.3-194 shows the bypass flow between upper head and downcomer. [

]

Rod Temperature Data

The heater rod assembly had 51 functioning thermocouples. Figure 8.3-195 shows the measured initial and maximum temperatures against elevation. Table 8.3-18 tabulates the measured initial and maximum temperature data in Figure 8.3-195.

[

]

Figure 8.3-196 through Figure 8.3-200 show the transient clad temperature responses in the vicinity of the peak node elevation. [

]

[

]

8.3.2.11 Conclusions

A summary of the benchmark results as to how the predictions compare with the data is presented here for the Tests S-06-3 and S-07-1.

8.3.2.11.1 Conclusions for Semiscale Test S-06-3

The S-RELAP5 code was assessed against Semiscale Test S-06-3. S-RELAP5 simulates the various observed LBLOCA major phenomena well (reasonable or acceptable agreement), including cladding temperature, break flow, fluid pressure, and temperature responses. The code calculated the LP refill much earlier than the data because of the small scale geometry of the Semiscale downcomer. It can be concluded, therefore, that the integral test S-06-3 results support the use of S-RELAP5 for PWR RLBLOCA analyses.

8.3.2.11.2 Conclusions for Semiscale Test S-07-1

An assessment against Semiscale Test S-07-1 has been performed, using S-RELAP5. The objective of this assessment was to study the adequacy of the S-RELAP5 heat transfer models during the blowdown phase of a postulated LBLOCA. Additionally, the capability of S-RELAP5 in simulating the major phenomena associated with the blowdown phase of an LBLOCA also can be assessed, though this is not the primary objective of this analysis. The code calculated the cladding thermal response and the system behavior reasonably well. It can be concluded that the S-RELAP5 heat transfer models are adequate in calculating the cladding thermal response during the blowdown phase of a postulated LBLOCA.

8.3.3 References

- 8.3-1 EG&G Idaho, Inc., EGG-NTAP-6276, International Standard Problem 13 (LOFT Experiment L2-5) Preliminary Comparison Report, April 1983.
- 8.3-2 Nuclear Regulatory Commission, NUGEG/CR-0792, Experimental Data Report for LOFT Power Ascension Experiment L2-3, July 1979.
- 8.3-3 EG&G Idaho, Inc., EGG-LOFT-5921, Quick-Look Report on LOFT Experiment L2-5, June 1982.
- 8.3-4 EG&G Idaho, Inc., OECD/LOFT-T-3404, Quick-Look Report on OECD LOFT Experiment LP-02-6, October 1983.

- 8.3-5 EG&G Idaho, Inc., OECD/LOFT-T-3504, Quick-Look Report on OECD LOFT Experiment LP-LB-1, February 1984.
- 8.3-6 Idaho National Engineering Laboratory, NUREG/CR-0247, TREE-1208, LOFT System and Test Description (5.5 ft Nuclear Core 1 LOCEs), July 1978.
- 8.3-7 ASME, 74-WA/HT-53, Examination of LOFT Scaling, 1974.
- 8.3-8 EG&G Idaho, Inc., NUREG/CR-3214, Summary of Nuclear Regulatory Commission's LOFT Program Experiments, July 1983.
- 8.3-9 EG&G Idaho, Inc., NUREG/CR-3005, Summary of Nuclear Regulatory Commission's LOFT Program Research Findings, June 1983.
- 8.3-10 J. P. Adams et al., Influence of LOFT PWR Transient Simulations on Thermal-Hydraulic Aspects of Commercial PWR Safety, Nuclear Safety, 27-2:179-192, April 1986.
- 8.3-11 EG&G Idaho Inc., OECD/LOFT-T-3907, An Account of the OECD LOFT Project, May 1990.
- 8.3-12 AIChE, Vol. 70 No. 138, A Correlation For The Minimum Film Boiling Temperature.
- 8.3-13 Nuclear Regulatory Commission, NUREG/CR-6061, Determination of the Bias in LOFT Fuel Peak Cladding Temperature Data from the Blowdown Phase of Large-Break LOCA Experiments, May 1993.
- 8.3-14 BAW-10231P-A, Revision 1, COPENIC Fuel Rod Design Computer Code, Framatome ANP, January 2004.
- 8.3-15 AREVA NP, 2A4-COPENIC, Fuel Rod Computer Code; User's Manual, November 2004.
- 8.3-16 Siemens Power Corporation, ECJ-83-87, Transmittal of Requested Input Decks. August 1987, Memo to H. Chow on August 6th, 1987.

- 8.3-17 Nuclear Regulatory Commission, NUREG-1230, Compendium of ECCS Research for Realistic LOCA Analysis, December 1988.
- 8.3-18 EG&G Idaho, Inc., NUREG/CR-2826, Experiment Data Report for LOFT Large Break Loss-of-Coolant Experiment L2-5, August 1982.
- 8.3-19 Institute of Nuclear Energy Research, NUREG/IA-0046, Assessment of RELAP5/MOD2 Using Semiscale Large Break Loss-of-Coolant Experiment S-06-3, April 1992.
- 8.3-20 Idaho National Engineering Lab, NUREG/CR-0251, TREE-1123, Experiment Data Report for Semiscale Mod-1 Test S-06-3 (LOFT Counterpart Test), July 1978.
- 8.3-21 Idaho National Engineering Lab, NUREG/CR-0281, TREE-1221, Experiment Data Report for Semiscale MOD-3 Blowdown Heat Transfer Test S-07-1 (Baseline Test Series), September 1978.
- 8.3-22 Idaho National Engineering Lab, NUREG/CR-0239, TREE-1212, Semiscale MOD-3 Test Program and System Description, July 1978.
- 8.3-23 EG&G Idaho, Inc., EGG-SEMI-5692, RELAP5 Standard Model Description for the Semiscale MOD-2A System, December 1981.
- 8.3-24 Idaho National Engineering Laboratory, EGG-2552, NUREG/CR-5249, Quantifying Reactor Safety Margins: Application of Code Scaling, Applicability, and Uncertainty Evaluation Methodology to a Large Break, Loss-of-Coolant Accident, December 1989.

Table 8.3-14 Comparison of Calculated and Measured Initial Conditions, Semiscale Test S-06-3

Parameter	Measured	S-RELAP5
Core power (MW)	1.004	
Fluid temperature (K), intact loop cold leg	563.000	
Fluid temperature (K), intact loop hot leg	598.000	
Fluid temperature (K), broken loop cold leg	562.000	
Fluid temperature (K), broken loop hot leg	591.000	
Intact loop cold leg flow (l/s)	6.680	
Pressurizer pressure (MPa)	15.769	
Pressurizer liquid mass (kg)	9.090	
Steam generator secondary side steam (MPa)	6.550	

Table 8.3-15 Sequence of Events Comparison for S-RELAP5 Simulation of Semiscale Test S-06-3

Event	Measured	S-RELAP5
Blowdown initiated	0.0	
High pressure injection started	0.0	
Pressurizer emptied	7.5	
Accumulator injection started	18.5	
PCT reached	20.5 ¹⁰	
Downcomer filled up	73.0 ¹²	
Accumulator injection stopped	90.0	

¹⁰ PCT of 1152 K measured for hot rod E-5 at an elevation 21 inch above the bottom of the heated core.¹¹ PCT of 1236 K calculated in hot rod region at an elevation 32.3 inch above the bottom of the heated core (mid-plane of heat structure 11)¹² Data from Reference 8.3-19

Table 8.3-16 Comparison of Calculated and Measured Initial Conditions, Semiscale Test S-07-1

Parameter	Measured¹³	S-RELAP5
Core power (MW)	2.027	
Upper plenum pressure (MPa)	15.95	
Intact loop steam generator secondary pressure in steam dome (MPa)	5.936	
Broken loop steam generator secondary pressure in steam dome (MPa)	5.965	
Intact loop cold leg temperature (K)	559	
Broken loop cold leg temperature (K)	557	
Broken loop hot leg to cold leg temperature differential (K)	30	
Intact loop hot leg to cold leg temperature differential (K)	37	
Intact loop cold leg flow (kg/s)	7.125	
Broken loop cold leg flow (kg/s)	2.283	

¹³ The measured hot leg temperature in the IL is 9 K hotter than in the BL. However, S-RELAP5 is capable of calculating only a single hot-leg temperature because it is a one-dimensional code.

Table 8.3-17 Comparison of Semiscale MOD-1, MOD-3 Test Geometries

Geometry	MOD-1	MOD-3
Scaled geometry	LOFT	4-Loop PWR
Active loop	1	2
Passive loops	1	0
Reactor vessel	LOFT Internal inlet downcomer annulus Internal downcomer annulus Lower plenum Core (see below) Upper plenum No upper head	PWR External inlet downcomer annulus External downcomer pipe (3-in Schedule 160) Lower plenum Core (see below) Upper plenum Upper head
Core	LOFT, short core (5.5 ft)	PWR, full length core (12 ft)
Intact loop	Active	Active
Steam generator	Type I	Same as MOD-1
Pump	Horizontal with flywheel to simulate LOFT pump	Same as MOD-1, but 10.98-in (27.9 cm) impeller installed such that nominal head-flow typical of PWR
Pressurizer	Yes	Same as MOD-1
Piping	3-in Schedule 160	Same as MOD-1 but length of vertical pump suction leg increased typical of PWR
Broken loop	Passive	Active
Steam generator	Steam generator simulator	Type II with 11 U-tube design (9 out of 11 plugged)
Pump	Pump simulator	Horizontal centrifugal pump
Piping	Spool pieces from 1.5-in to 5-in Schedule 160	1.5-in Schedule 160

**Table 8.3-18 Maximum and Initial Measured Cladding Temperatures
Semiscale Test S-07-1**

--

Table 8.3-19 Heat Structure Nodalization and Corresponding Thermocouples, Semiscale Test S-07-1

Table 8.3-20 Comparison of Initial and Maximum Clad Temperatures, Semiscale Test S-07-1

Figure 8.3-145 Schematic of Semiscale Test Facility

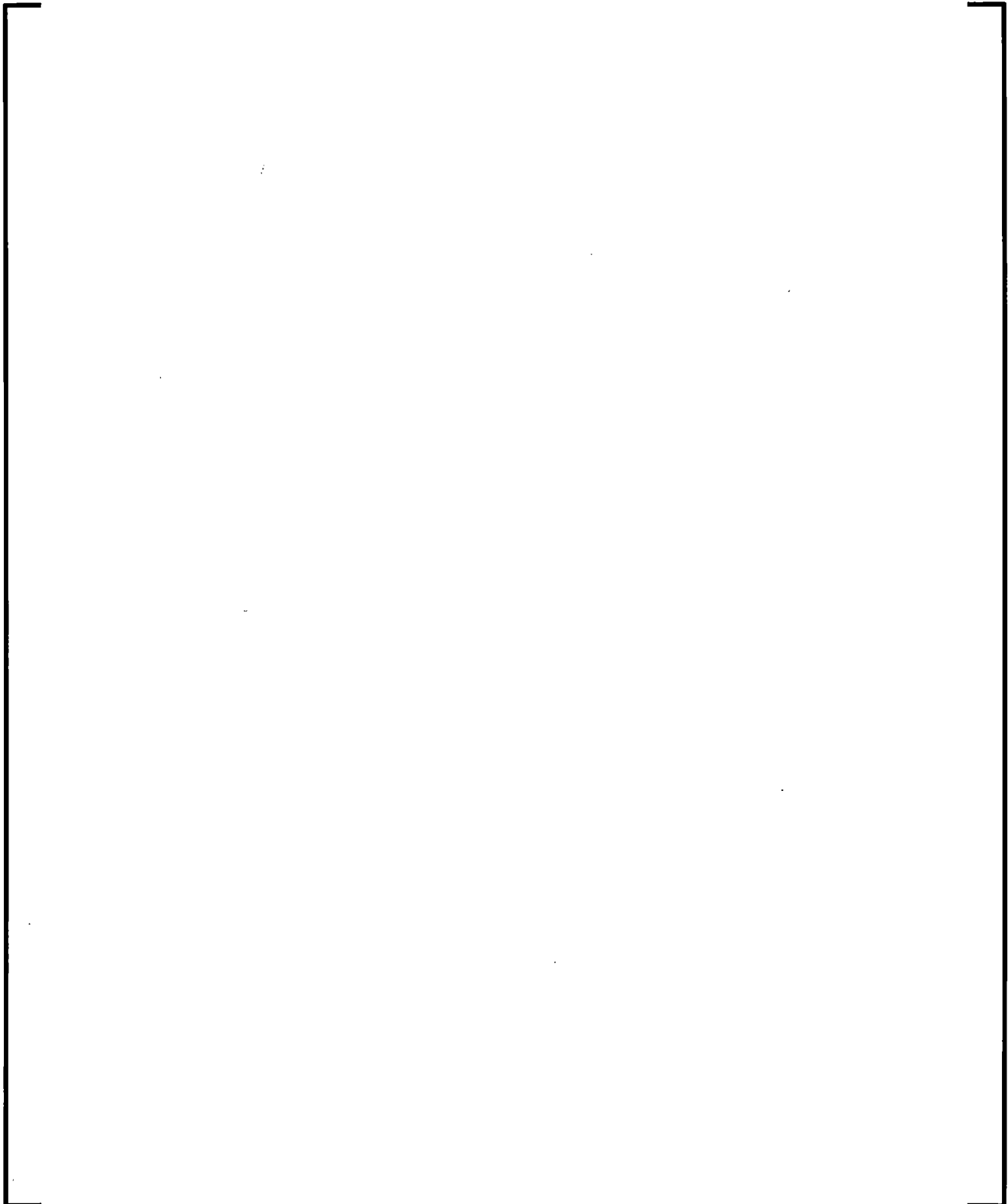
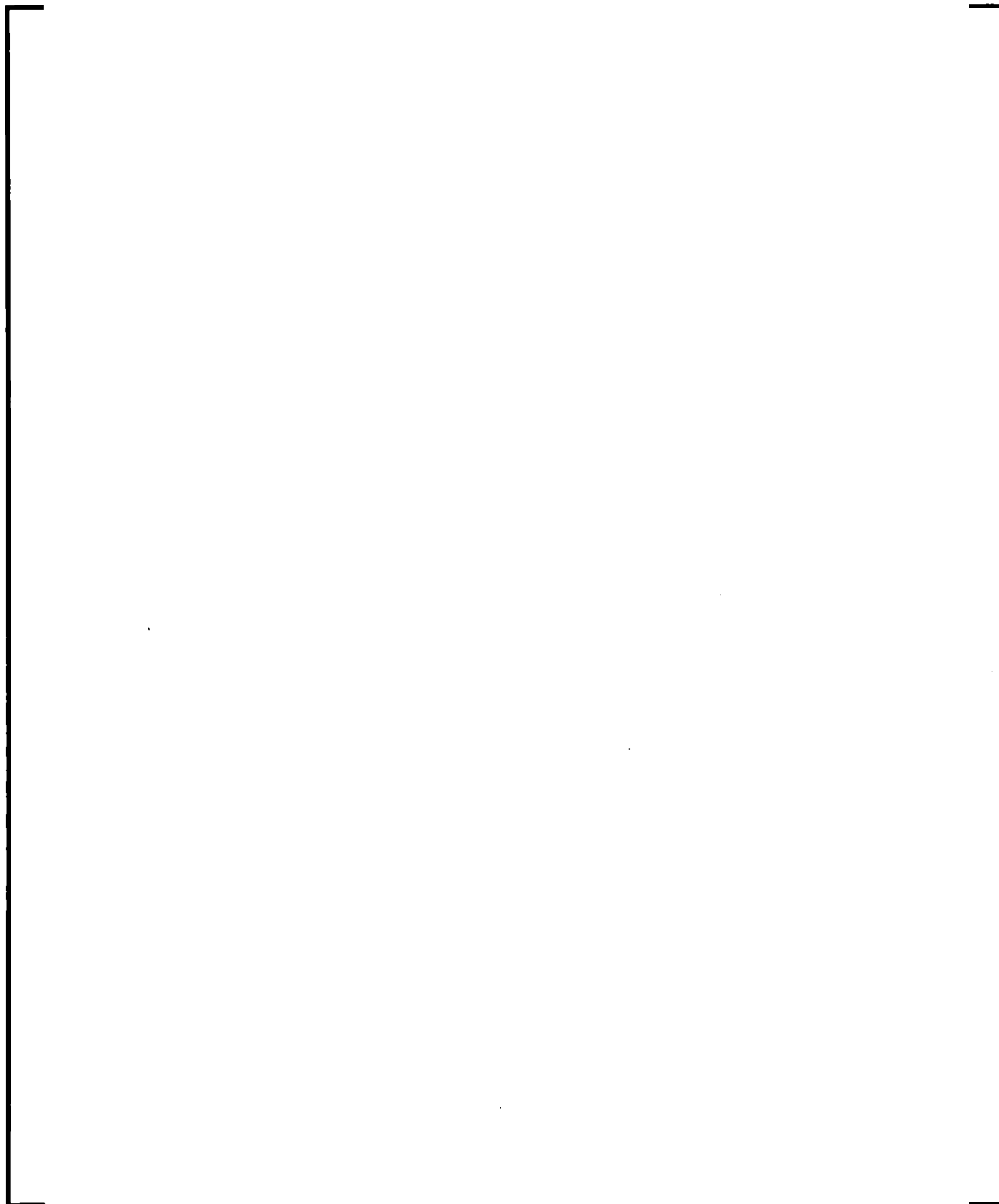
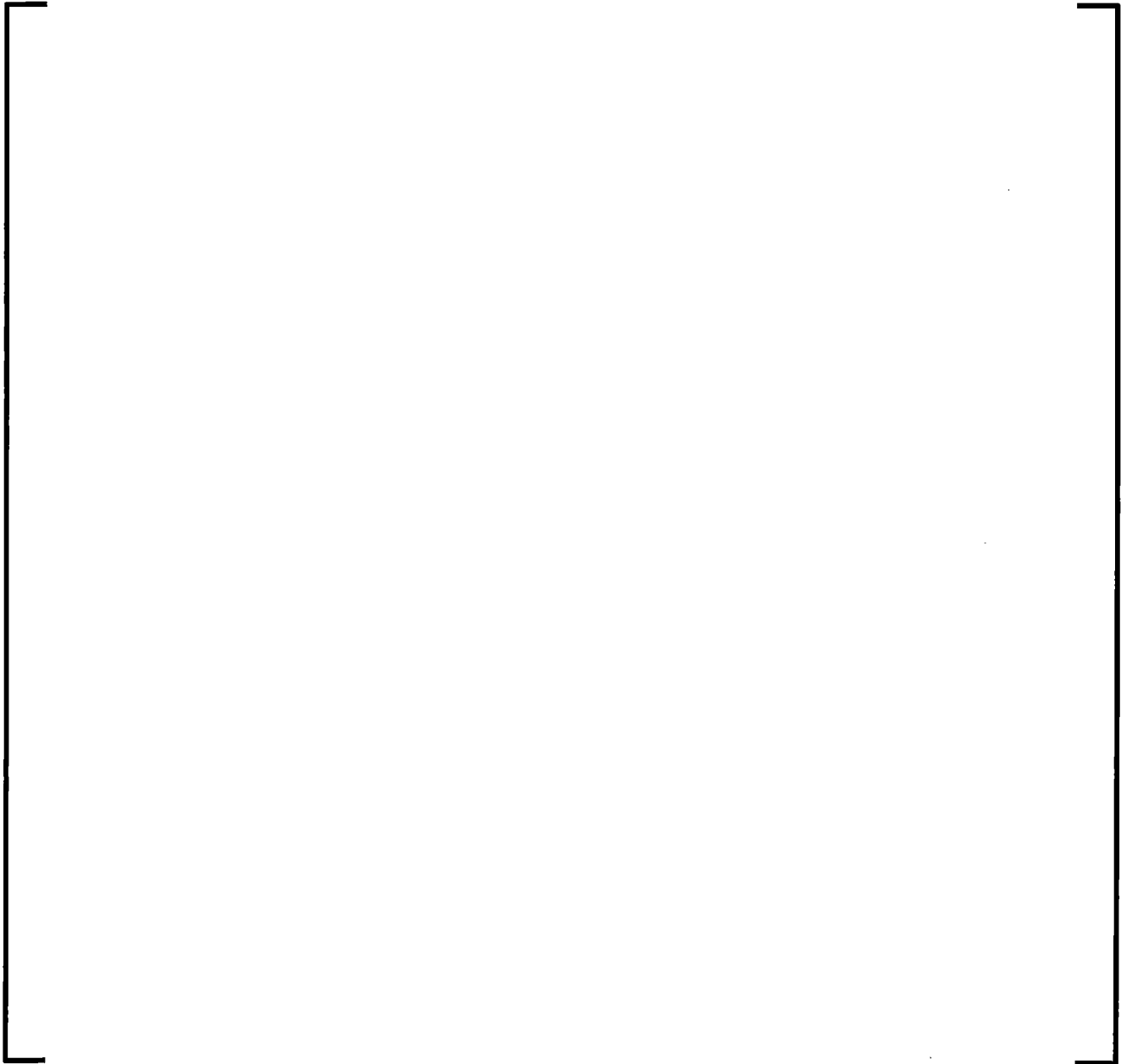


Figure 8.3-146 Heated Core Layout for Semiscale Test S-06-3



**Figure 8.3-147 Core Heat Structures and Grid Spacer Locations -
Semiscale Test S-06-03**



**Figure 8.3-148 S-RELAP5 Vessel Nodalization of Semiscale MOD-1
for Test S-06-3**

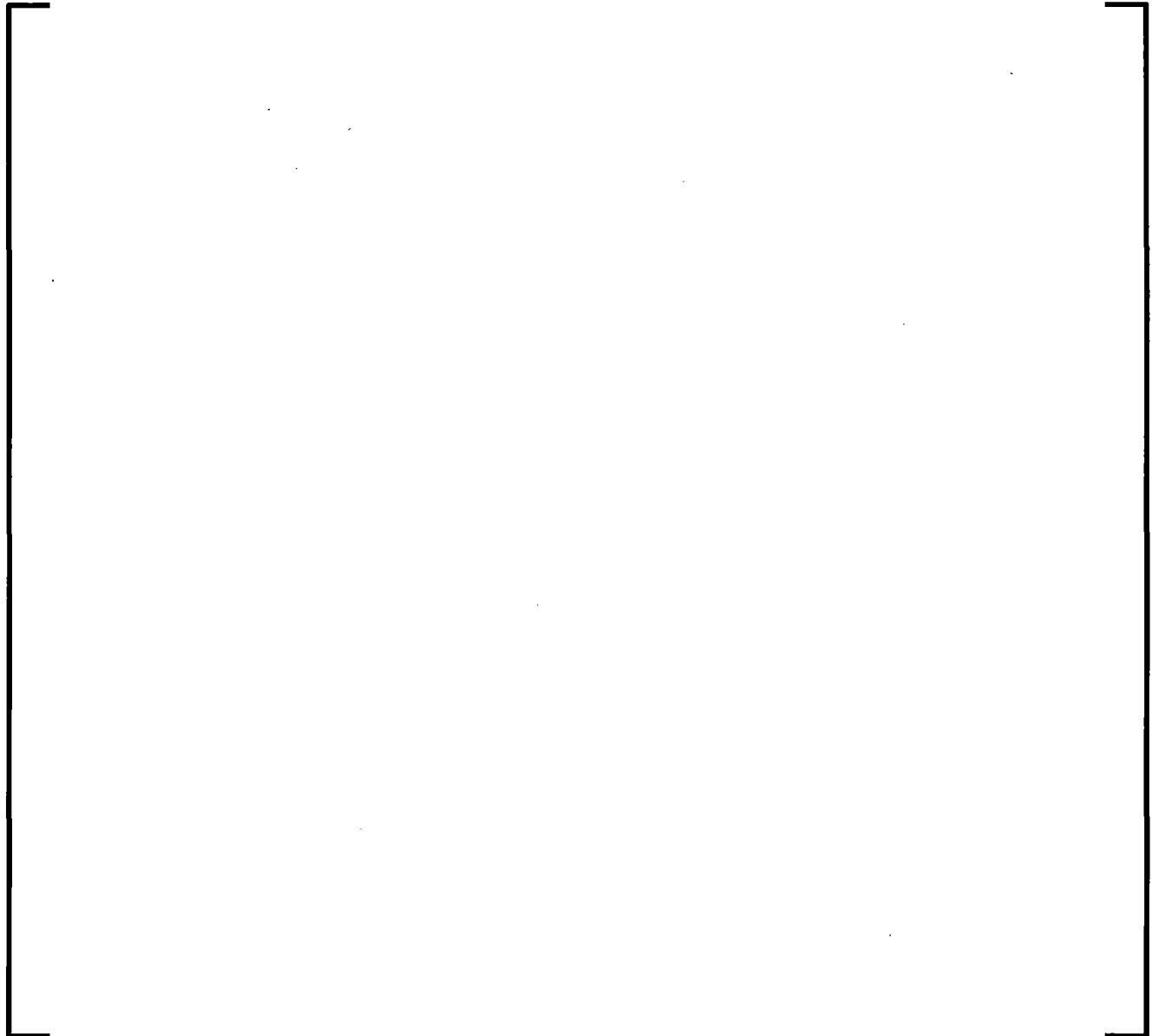


**Figure 8.3-149 S-RELAP5 Loop Nodalization of Semiscale MOD-1 for
Tests S-06-3**



Figure 8.3-150 Semiscale Test S-06-3: Initial Clad Temperatures



Figure 8.3-151 Semiscale Test S-06-3: Upper Plenum Pressure



Figure 8.3-152 Semiscale Test S-06-3: Break Flow Rate - Pump Side



Figure 8.3-153 Semiscale Test S-06-3: Break Flow Rate - Vessel Side



Figure 8.3-154 Semiscale Test S-06-3: Secondary Pressure



Figure 8.3-155 Semiscale Test S-06-3: Pressurizer Surge Flow



Figure 8.3-156 Semiscale Test S-06-3: Broken Loop Cold Leg Density



Figure 8.3-157 Semiscale Test S-06-3: Intact Loop Cold Leg Flow



Figure 8.3-158 Semiscale Test S-06-3: Intact Loop Hot Leg Flow



Figure 8.3-159 Semiscale Test S-06-3: Inlet Core Flow



**Figure 8.3-160 Semiscale Test S-06-3: Lower Plenum Coolant
Temperature**



**Figure 8.3-161 Semiscale Test S-06-3: Upper Plenum Coolant
Temperature**



**Figure 8.3-162 Semiscale Test S-06-3: Hot Rod - Hydrodynamic
Node 4**



**Figure 8.3-163 Semiscale Test S-06-3: Hot Rod - Hydrodynamic
Node 5**



**Figure 8.3-164 Semiscale Test S-06-3: Hot Rod - Hydrodynamic
Node 7**

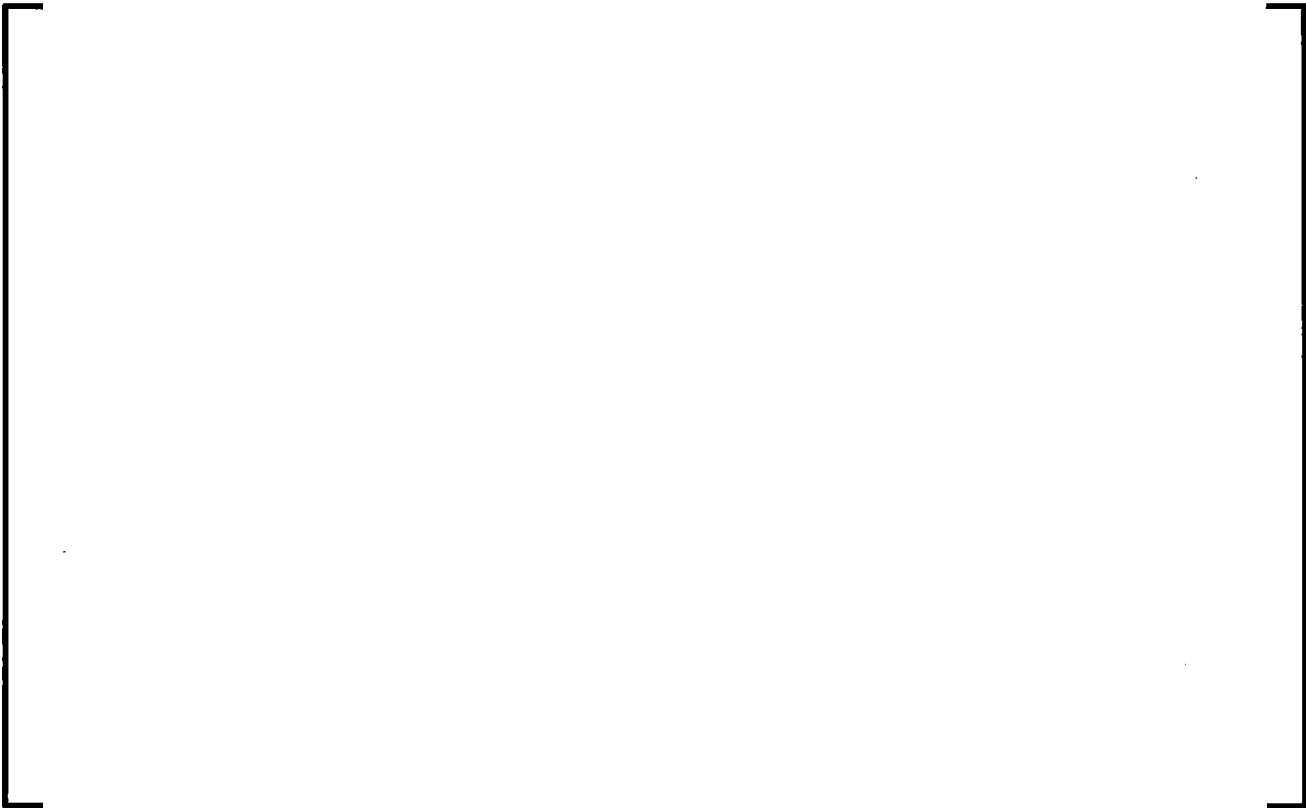


**Figure 8.3-165 Semiscale Test S-06-3: Average Rod - Hydrodynamic
Node 4**



**Figure 8.3-166 Semiscale Test S-06-3: Average Rod - Hydrodynamic
Node 5**



**Figure 8.3-167 Semiscale Test S-06-3: Average Rod - Hydrodynamic
Node 6**



**Figure 8.3-168 Semiscale Test S-06-3: Average Rod - Hydrodynamic
Node 7**



**Figure 8.3-169 Semiscale Test S-06-3: Average Rod - Hydrodynamic
Node 8**



Figure 8.3-170 Semiscale Test S-06-3: Peak Cladding Temperatures

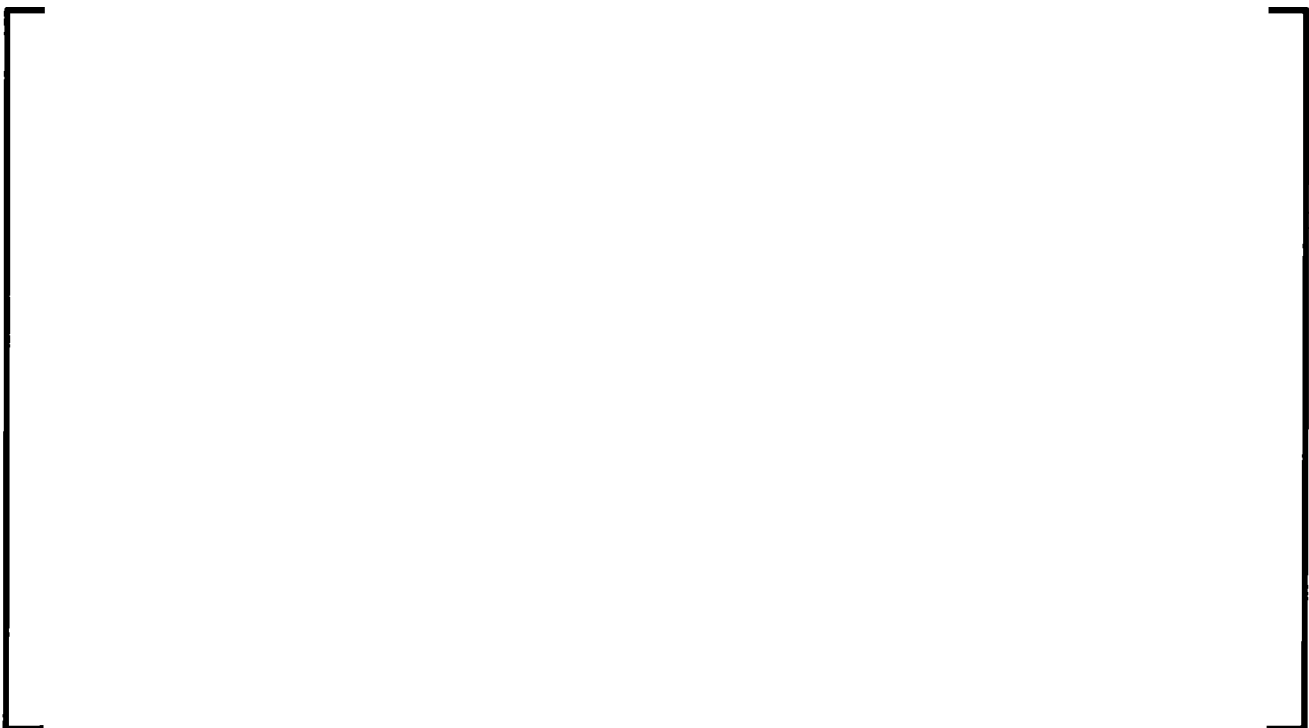
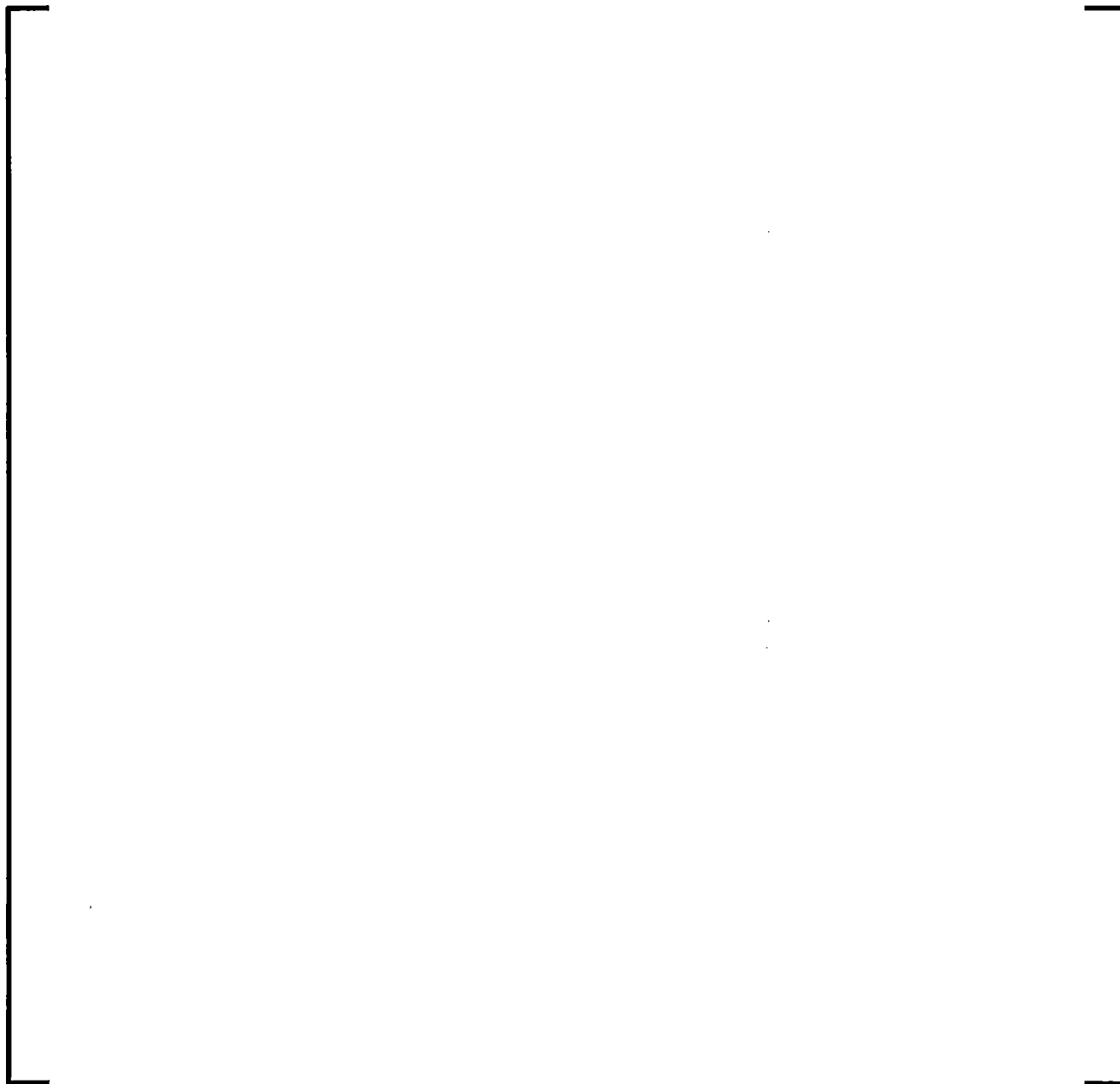


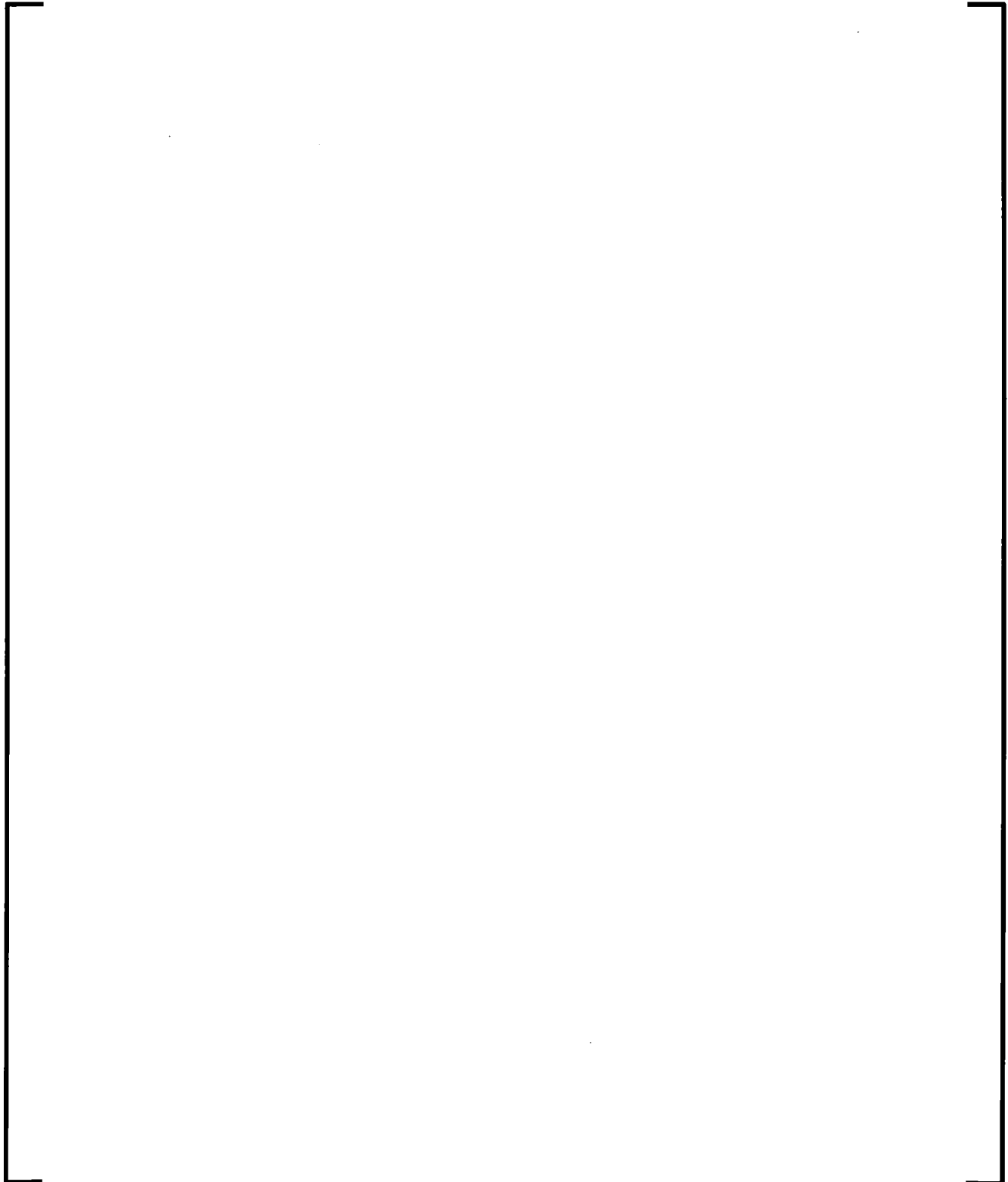
Figure 8.3-171 Semiscale Test S-06-03: Intact Loop Downcomer Level



Figure 8.3-172 Heated Core Layout for Semiscale Test S-07-1



**Figure 8.3-173 Core Heat Structures and Grid Spacer Locations –
Test S-07-1**



**Figure 8.3-174 S-RELAP5 Nodalization of Semiscale MOD-3 for Test
S-07-1**

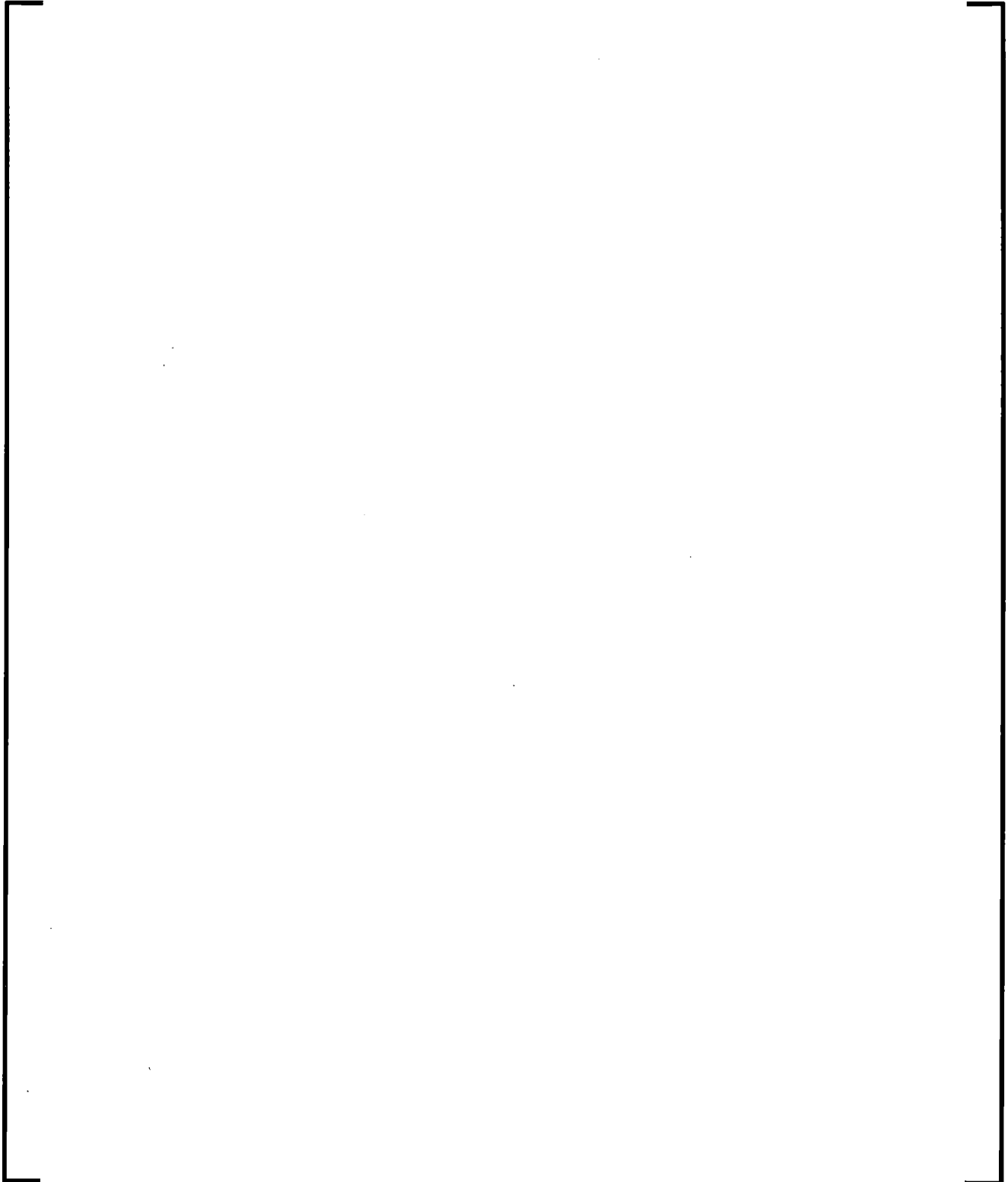


**Figure 8.3-175 S-RELAP5 Nodalization of Semiscale MOD-3 for Test
S-07-1**



**Figure 8.3-176 S- RELAP5 Nodalization of Semiscale MOD-3 for Test
S-07-1**



Figure 8.3-177 Semiscale Test S-07-1: Upper Plenum Pressure



Figure 8.3-178 Semiscale Test S-07-1: Intact Loop Secondary Pressure



**Figure 8.3-179 Semiscale Test S-07-1: Broken Loop Secondary
Pressure**



Figure 8.3-180 Semiscale Test S-07-1: Break Flow Rate - Pump Side



**Figure 8.3-181 Semiscale Test S-07-1: Integrated Break Mass - Pump
Side**



Figure 8.3-182 Semiscale Test S-07-1: Break Flow Rate - Vessel Side

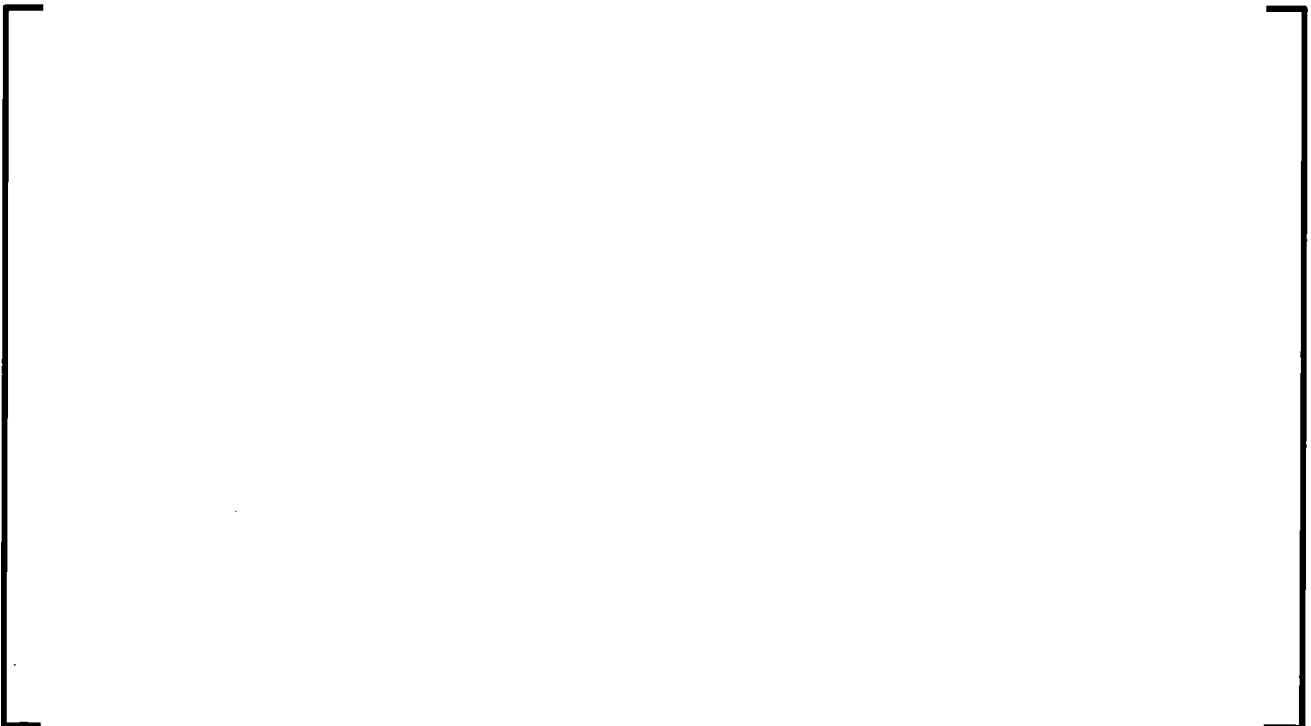


**Figure 8.3-183 Semiscale Test S-07-1: Integrated Break Mass - Vessel
Side**



**Figure 8.3-184 Semiscale Test S-07-1: Broken Loop Cold Leg Volume
Average Density - Pump Side**



**Figure 8.3-185 Semiscale Test S-07-1: Broken Loop Cold Leg Volume
Average Density - Vessel Side**



Figure 8.3-186 Semiscale Test S-07-1: Intact Loop Cold Leg Flow



Figure 8.3-187 Semiscale Test S-07-1: Intact Loop Hot Leg Flow



Figure 8.3-188 Semiscale Test S-07-1: Inlet Core Flow



**Figure 8.3-189 Semiscale Test S-07-1: Lower Plenum Coolant
Temperature**



**Figure 8.3-190 Semiscale Test S-07-1: Broken Loop Hot Leg Coolant
Temperature**



Figure 8.3-191 Semiscale Test S-07-1: Intact Loop Hot Leg Coolant Temperature



Figure 8.3-192 Semiscale Test S-07-1: Support Column Flow



Figure 8.3-193 Semiscale Test S-07-1: Guide Tube Flow



Figure 8.3-194 Semiscale Test S-07-1: Upper Head - Downcomer Bypass

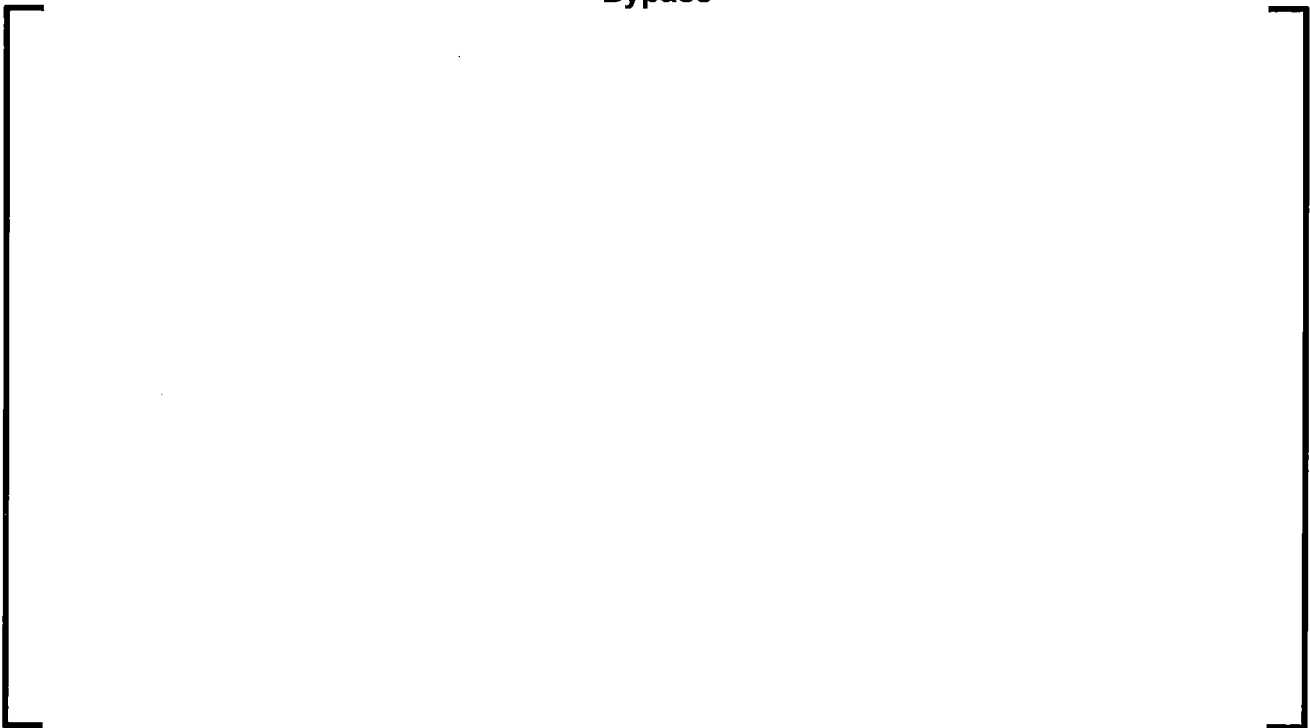


Figure 8.3-195 Semiscale S-07-1 Thermocouple Readings



Figure 8.3-196 Semiscale Test S-07-1: PCT in Hydrodynamic Node 10



Figure 8.3-197 Semiscale Test S-07-1: PCT in Hydrodynamic Node 11



**Figure 8.3-198 Semiscale Test S-07-1: PCT in Hydrodynamic Node 12
(Lower Node)**



**Figure 8.3-199 Semiscale Test S-07-1: PCT in Hydrodynamic Node 12
(Upper Node)**

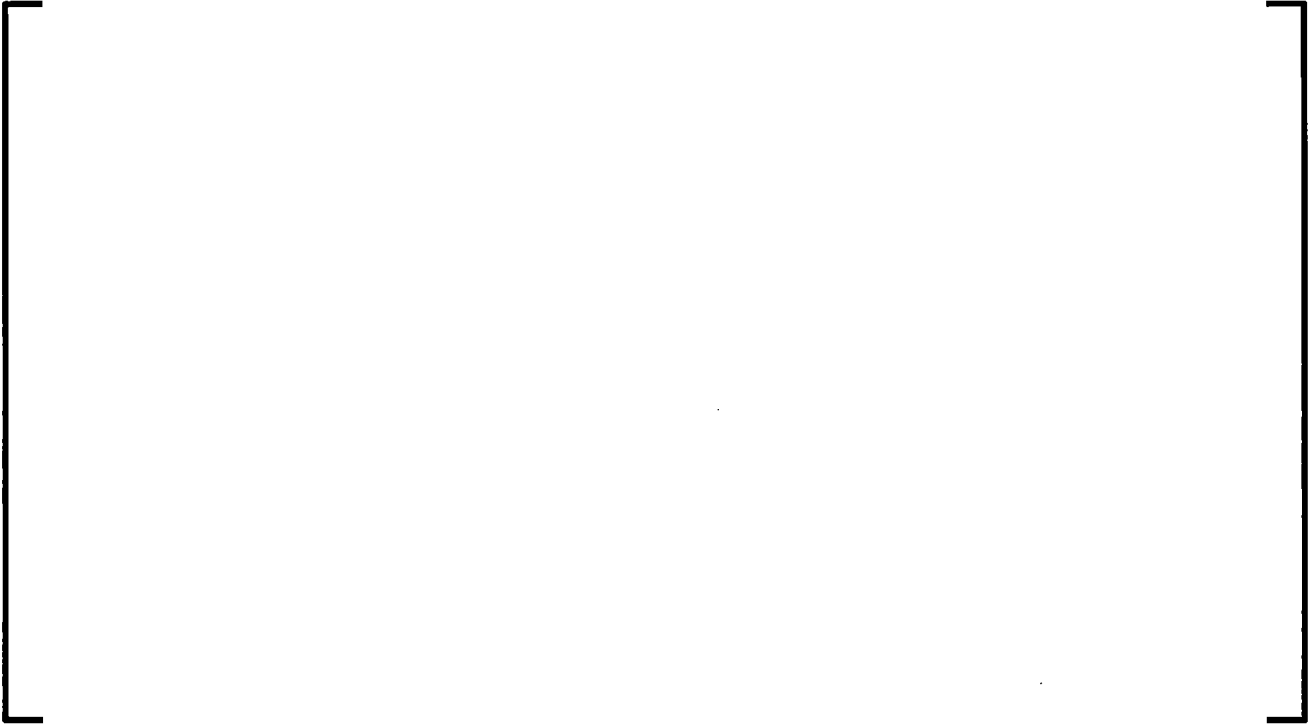


Figure 8.3-200 Semiscale Test S-07-1: PCT in Hydrodynamic Node 13



**Figure 8.3-201 Semiscale Test S-07-1: Comparison of Initial
Temperatures**



**Figure 8.3-202 Semiscale Test S-07-1: Comparison of Peak Clad
Temperatures**



8.4 *Summary of Assessment Uncertainties and Biases*

The separate effects tests (SET) and integral effects tests (IET) presented in Sections 8.2 and 8.3 validate the capabilities of the S-RELAP5 code to predict thermal-hydraulic and heat transfer phenomena associated with light water reactor transients and loss-of-coolant accident (LOCA). In those assessments, code biases were applied to various parameters. Those biases represent the code bias uncertainties that were determined from the code performance applied to phenomena or processes identified in the phenomena identification and ranking table (PIRT) as presented in Section 5.0.

In a CSAU methodology, the code performance is required to be quantified with respect to its predictive capability of all the important phenomena identified in the PIRT. This quantification is usually expressed in terms of a statistical bias, standard deviation, and probability distribution for code calculated phenomena. These are defined as the code uncertainties.

In addition to code uncertainties, the methodology includes the uncertainties associated with the plant operation and plant data, which have to be quantified by the utility and/or vendor. These are termed operational, or plant uncertainties. The methodology to combine uncertainties requires a large number of LOCA calculations in which all the uncertainties are randomly varied according to their initial value, the bias, and the quantified uncertainty and distribution. Table 8.4-1 contains the complete list of code uncertainty parameters that are used in the RLBOCA methodology.

The following sections describe the development of the biases and uncertainties that are given in Table 8.4-1 for the S-RELAP5 code.

**Table 8.4-1: Summary of Evaluated Biases and Uncertainties of
Important Code Related PIRT Parameters**

--	--

8.4.1 Film Boiling Heat Transfer

Film boiling heat transfer is significant to the outcome of the RLBLOCA methodology. The assessment of the film boiling heat transfer and its uncertainty are based on the separate effects experiment: Full-Length Emergency Cooling Heat Transfer, System Effects, and Separate Effects Tests (FLECHT-SEASET) (Section 8.2.3). The FLECHT-SEASET tests were chosen because they exclusively represent low pressure industry-accepted and -evaluated experiments applicable to pressurized water reactor (PWR) post-critical heat flux (CHF) heat transfer. Test results from the Oak Ridge National Laboratory/Thermal Hydraulic Test Facility (ORNL/THTF) (Section 8.2.1) are used for confirmation purposes.

In Reference 8.4-1, the complete process of the calculation of the film boiling heat transfer coefficient bias, and uncertainty associated with the S-RELAP5 determinations of the film boiling heat transfer coefficients, was presented and a condensed version is presented later in this section.

The discussion presented in Section 8.4.1.2 shows the determination of the heat transfer coefficient uncertainties and multipliers for FILMBL and DFFBHTC under low pressure reflood conditions. The multiplier FILMBL is applied to the inverted annular film boiling heat transfer regime, which is considered (in these discussions) as the low void regime. The multiplier DFFBHTC is applied to the dispersed flow film boiling heat transfer regime, which is considered as the high void regime. In the RLBLOCA plant model, the values from the uncertainty determination [

] are applied to the hot assembly, high power region, average power region, and the core periphery.

⁵ [

The discussion presented in Section 8.4.1.3 shows the determination of the heat transfer coefficient uncertainties for FILMBL and DFFBHTC when rod-to-rod radiation is explicitly calculated between the hot rod and its surroundings. In the RLBLOCA plant model, the values of FILMBL and DFFBHTC that are applied to the hot rod are determined from random sampling of their respective distributions described in this section.

8.4.1.1 Multiplier Correlation

The measured and calculated HTC's were compared by computing the ratio

$$M = \frac{h_{meas}}{h_{calc}}$$

Then, statistics are generated to determine the mean of M and the standard deviation, which determines the uncertainty of that mean. This is useful for indicating over or under prediction of the data in a general sense, and gives a relative measure of average accuracy. By this definition, perfect agreement between measured and calculated multipliers exists if $M = 1$, $M < 1$ indicates over-predicted heat transfer, and $M > 1$ indicates under-predicted heat transfer.

In setting up the comparison process, temporal differences between measured and calculated data are removed by aligning the quench fronts to a common location. It is assumed that if the quench front in the data is at the same elevation as the quench front in the S-RELAP5 calculation, then the thermal-hydraulic conditions for all of the downstream volumes are comparable.

The S-RELAP5 quench time versus elevation table was linearly interpolated to find the calculation time for which the quench front in the calculation was at the same elevation as the measured data in Table 8.4-3. A snapshot of the axial profile was taken at this time and the data associated with this time were then filtered. []

• []

]

- [

]

- [

]

8.4.1.2 Film Boiling Multiplier Statistics

8.4.1.2.1 *Defining Data Set*

The multiplier pairs for which calculations were to be performed were based on the outcome of comparing the calculated to the experimental data. When examining the histogram from the comparison, the ratio of measured to calculated HTC shows a large number counts at unrealistically high ratios. Consequently, the distribution was truncated based on frequency criteria. The original and truncated distributions are shown in Figure 8.4-1. Note that there were truncations at low ratios, but this did not significantly affect the outcome of the final HTC [

]

Figure 8.4-2 compares the truncated distribution with a normal distribution, and Figure 8.4-3 compares the cumulative probabilities from the truncated and normal distributions. The truncated distribution does not strictly bound its corresponding normal distribution, however in this case, this behavior is acceptable since the distribution was truncated by removing large value ratios and since these (low and high void) distributions will not be sampled to define the hot rod multipliers for plant LBLOCA calculations.

[] will therefore be applied to all core heat structures that are expected to experience post-CHF heat transfer except for the hot rod(s). The multipliers for the hot rod(s) will be discussed in Section 8.4.1.3.

A linear least squares curve fit of M as a function of void fraction was performed. If it is reasonable to use a single coefficient over the entire range of void fractions (i.e., two correlations and an interpolation region), then the least squares curve fit should give a correlation that is relatively flat with void fraction and a constant close to 1. The curve fit is:

$$[]$$

This curve fit indicates that, from an engineering standpoint, the constant (multiplier) fits the data.

8.4.1.2.2 Validating Data Set

Figure 8.4-4 shows the validating data set compared with a normal distribution [

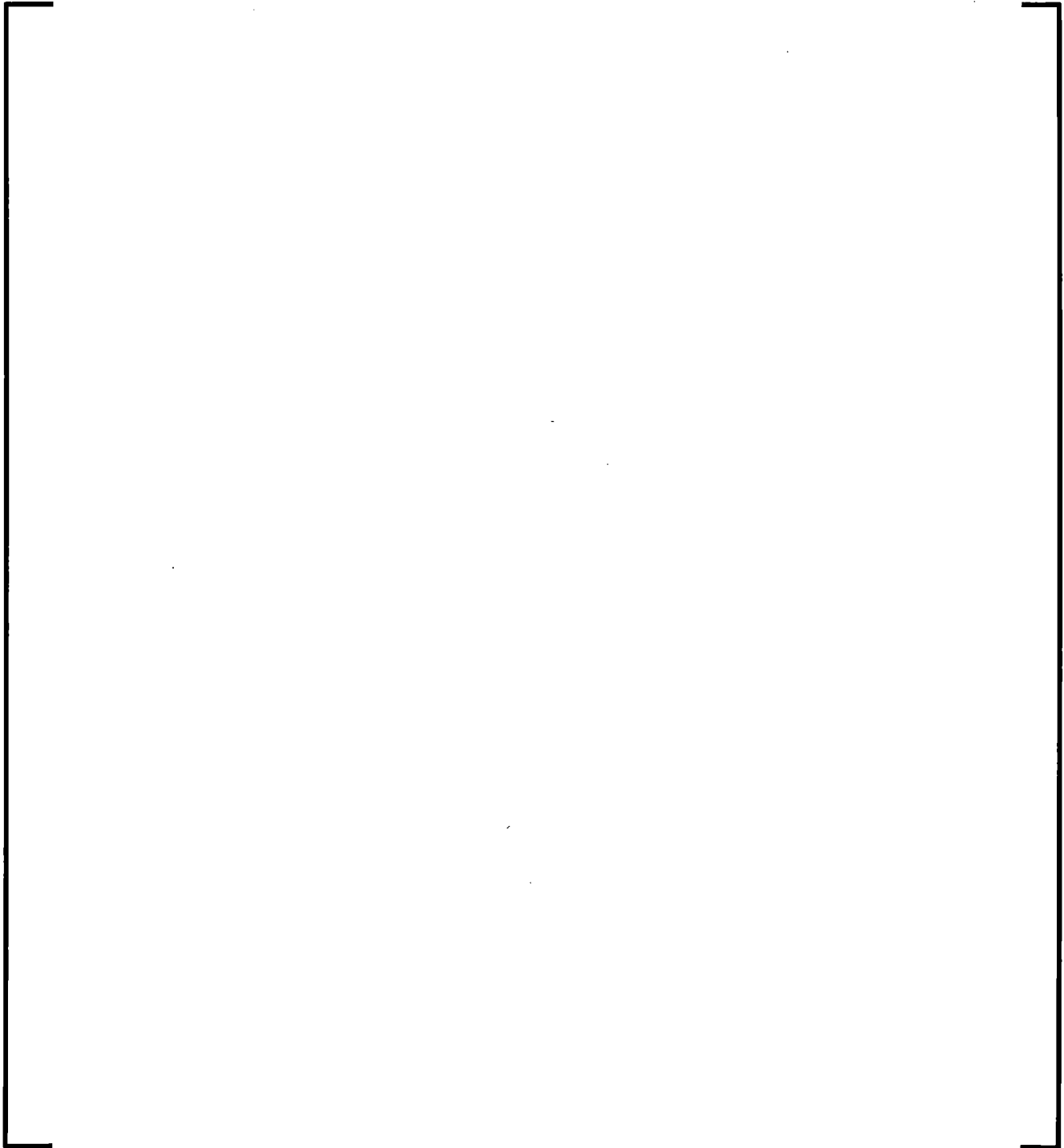
] These results look as good as the correlating set of data, and they fall within the range of the mean and standard deviation. An additional comparison is made by examining the means and 2σ ranges of the defining and validating sets separately and combined, as shown in Table 8.4-3. From this table, it is observed that the use of the defining data set mean and standard deviation bounds both the validating data set and the combined data set.

8.4.1.3 Post-CHF Heat Transfer Probability Distributions for the Hot Rod

In the plant LBLOCA calculations, the hot rod is assumed to have a power level that is somewhat elevated compared to its surrounding rods in the hot assembly. To more accurately assess the hot rod, a rod-to-rod radiation model is included in the post CHF heat transfer evaluation. Because the remainder of the core modeling assesses the average consequences over a rather large set of differing rods (207 for a 15x15 array), this radiation heat transfer is applied only for the hot rod. Rod-to-Rod radiation adds to the previous model which already included thermal radiation from structures to the fluid (rod-to-droplets and rod-to-steam). The development of heat transfer uncertainties for the hot rod is done separately from the rest of the core, because the rod-to-rod radiation model is exclusively applied to the hot rod.

The film boiling HTC multipliers developed in Section 8.4.1.2 [

] were determined without specific calculation of rod-to-rod radiation, and can only be applied where rod-to-rod radiation is not explicitly evaluated (FLECHT-SEASET 31504 Radiation Evaluation).



8.4.1.3.1 *Determination of artificial power for FLECHT SEASET bundle*

To include rod-to-rod radiation in the benchmark of test 31504, additional heat structures were added to the otherwise unchanged (except for numbering) S-RELAP5 input model discussed in Section 8.2.3.5. A new 'hot rod' (donor rod) structure was created, as a supplemental heat structure, [

] A new "auxiliary rod" (receptor rod) structure was created, as a supplemental heat structure, [

] This is the receptor structure for which the power will be varied, reduced iteratively, until the radiation heat transfer between this structure and the hot rod matches that calculated by the FLECHT researchers, Reference 8.4-14. When this occurs, the temperature of the receptor rod should, in combination with the view factor, be representative of the importance weighted temperature of the surrounding rods in the experiment. [

]

[

] The bundle is not affected by the rod-to-rod radiation model (rod-to-rod is applied only to the hot rod which is a supplemental heat structure), and its role is to give a best estimate of the coolant properties. [

]



8.4.1.3.2 Determination of Hot Rod Multipliers

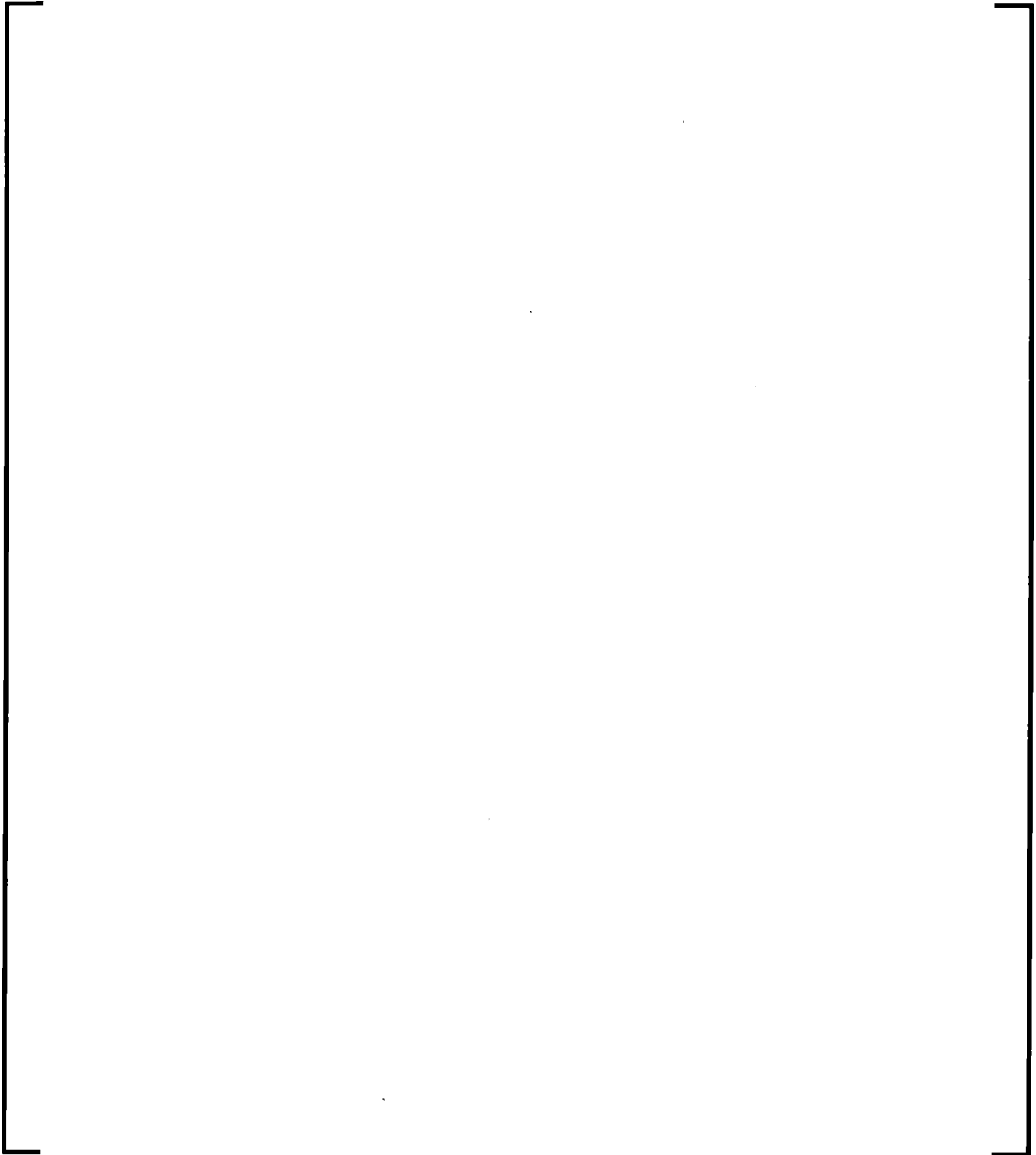
Assessment of this configuration is performed by using the same FLECHT-SEASET reflood tests that were used to determine the heat transfer multipliers FILMBL and DFFBHTC, as discussed in the previous sub-section, Section 8.4.1.2. The revised model for including rod-to-rod radiation treats the 161-rod FLECHT SEASET bundle as a hot assembly, and applies the heat transfer multipliers [

] A hot rod and a reduced power surrounding auxiliary rod are added without multipliers so that the heat transfer uncertainty can be determined on the hot rod which explicitly accounts for rod-to-rod heat transfer. [

]

As before, the multiplier distributions are determined based on the outcome of comparing the calculated heat transfer coefficients to the experimental data with the distributions treated separately for the low and the high void regions. [

]



8.4.1.4 Reevaluation of Film Boiling Multipliers

The FILMBL and DFFBHTC discussed above were developed using Rev. 2 methodology. Modifications to the Rev. 2 methodology were added including the grid cooling model. Therefore, these multipliers were reevaluated following the same methodology. The PDFs for the new FILMBL and DFFBHTC multipliers are given in Appendix A.2.3.6.5.

Table 8.4-2: FLECHT SEASET Time of Quench (seconds)

Test	Elevations			
	36 inch	47 inch	59 inch	71 inch
31203	61.2	101.2	154.5	214.2
31302	38.5	64.9	99.9	138.6
31504	76.8	126.5	195.0	274.4
31701	20.0	30.1	42.6	56.4
31805	74.4	132.2	219.1	324.6
32013	66.9	103.7	154.9	215.4
34209	91.7	152.8	240.5	344.8

Table 8.4-3: Statistical Comparisons Between Data Sets**Table 8.4-4: Defining Distributions for FILMBL**

Table 8.4-5: Defining Distributions for DFFBHTC

--	--

Figure 8.4-1 Histogram Plot of Measured-to-Calculated HTC Ratio



**Figure 8.4-2 Comparison of Measured-to-Calculated HTC Ratio Data
to a Normal Distribution [**

]



Figure 8.4-3 Comparison of Data to Normal Cumulative Distribution

[

]



Figure 8.4-4 Validating Data Set Compared with a Normal Distribution

[

]



**Figure 8.4-5 Histogram of Measured-to-Calculated HTC Ratio for
FILMBL with Probability Density Function Overlay**



**Figure 8.4-6 Histogram Plot of Measured-to-Calculated HTC Ratio for
DFFBHTC with Probability Density Function Overlay**



**Figure 8.4-7 Comparison of Data for FILMBL to Cumulative
Probability Distribution**

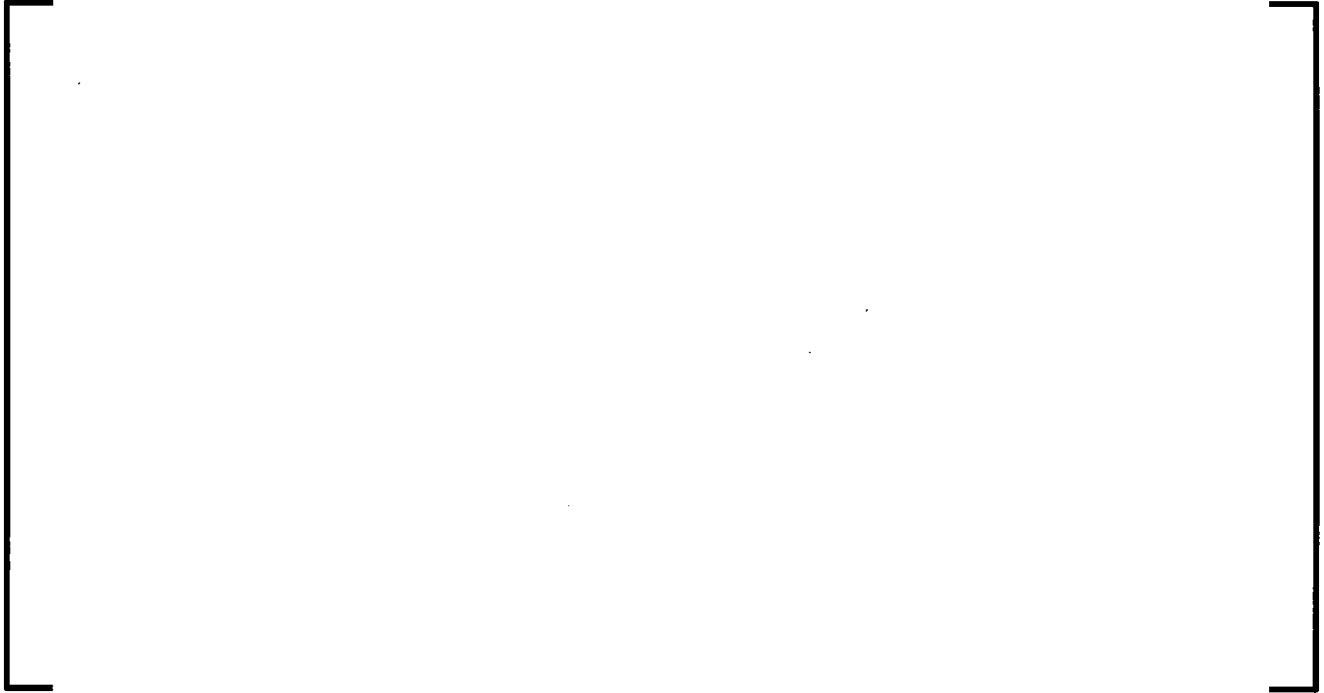


**Figure 8.4-8 Comparison of Data for DFFBHTC to Cumulative
Probability Distribution**



8.4.2 Interfacial Condensation Heat Transfer

Several integral and separate effect tests were conducted to investigate the steam/water flow phenomena in the cold legs during the refill and reflood phase of a LOCA. These include small scale tests, like the Electric Power Research Institute (EPRI) 1/3rd scale tests, and full scale tests such as Upper Plenum Test Facility (UPTF) Test 8 (only Part 1 covering cold-leg ECC injection) and Test 25. These tests generally cover both the accumulator and pump injection period, and were used to develop the S-RELAP5 interphase heat transfer multipliers.

The liquid side (CONMAS) and vapor side (CONMSG) interphase heat transfer multipliers are developed to provide good agreement when predicting the cold-leg condensation using S-RELAP5. [

]

8.4.2.1 Analytical Methodology

The EPRI and UPTF tests were performed to cover both the accumulator and pump injection period. From these tests the following conclusions can be made:

- During the accumulator injection period of the tests, the condensation potential of the ECCS water exceeds the steam flow, (i.e., thermodynamic potential (RT) greater than 1.0), and the flow regime is generally plug flow. The thermodynamic potential is the ratio of the potential condensation rate to the steam flow (Reference 8.4-3).

$$R_T = \frac{W_l \cdot (h_{fsat} - h_l)}{W_g \cdot (h_g - h_{fsat})}$$

- During the pumped injection period, when RT is less than 1.0, the flow is always stratified. This is typical for full-sized plants when only one ECCS train is available. When both the trains are available, the RT is generally greater than one, and plug flow is prevalent. The cold leg condensation model was developed as follows:

- The horizontal stratified flow regime was bypassed in the ECC injection node of the cold leg.

When water is injected into the cold leg, the water does not undergo stratified flow but rather creates a vortex and a liquid film covers the inner wall of the pipe at this section. The stratified flow option was therefore bypassed at this ECC injection branch segment. The normalization factors for interphase heat transfer, CONMAS and CONMSG, were determined by benchmarking EPRI and UPTF tests of varying conditions. Within this set, the void fraction and liquid temperature trended directly with the thermodynamic ratio. [

] The following sections provide details on the justification for these normalization values.

8.4.2.2 Comparison of S-RELAP5 Results to Experimental Data

8.4.2.2.1 EPRI

The W/EPRI one-third scaled tests are appropriate and representative of conditions encountered in the reflood and post-reflood phases of a PWR LBLOCA. The W/EPRI test cases used in this analysis and their test conditions are outlined in Table 8.4-6. The S-RELAP5 nodalization used in this analysis is depicted and discussed in Section 8.2.10. The cold leg test section for the EPRI model is shown in Figure 8.4-10 along with the thermocouple locations. Cold water from the storage tank was allowed to enter the test section through either one of the injection points. Thermocouple 29, in the lower right hand corner of the diagram, was used for liquid temperature evaluations, while thermocouple 13, in the upper right hand corner of the diagram, was used for the vapor temperature evaluation.

Figure 8.4-11 provides both the ECCS subcooling at the cold leg exit and mixing void fraction as a function of the test thermodynamic ratio for most of the series 5 tests published in Reference 8.4-4. Also included in Figure 8.4-11 are the S-RELAP5 test section exit subcooling and void fraction with the normalization factors applied. The S-RELAP5 exit subcooling agrees well with the measure test subcooling for each of these benchmarks. With the normalization factors applied, the condensation rate calculated by S-RELAP5 agrees well with the experimental data. The CONMAS normalization factor functionality with void fraction is therefore sufficient enough to predict the cold leg condensation behavior across a range of thermodynamic ratios from 0.0 to slightly greater than 2.0.

Analysis of Figure 8.4-12 justifies the CONMSG multiplier selected, and displays the measured versus predicted temperature for Thermocouple 13. The temperature value from the experimental data is taken from Thermocouple 13 and compared to the S-RELAP5 calculated temperature in the last node of the cold leg piping (Figure 8.2-314 in Section 8.2.10). Two of the predicted values are slightly off from the experimental data. The negative vapor velocity at junction 180-02 in Run 5-24 and Run 5-52 indicates air returning to the cold leg, which results in lower predicted temperatures than measured by Thermocouple 13. In summary, the remaining S-RELAP5 calculated values have good agreement with the W/EPRI experimental data.

8.4.2.2.2 UPTF Test 8

The purpose of Test 8 was to investigate the thermal hydraulic behavior of ECC water injection during the end-of-blowdown, refill, and reflood phases of a postulated LOCA (Reference 8.4-5). Test 8 was conducted in two phases. The main difference between the phases was that the pump simulator K-factor in Loop 2 was higher for Phase B (Run 112) than for Phase A (Run 111). A description of the test facility, the

S-RELAP5 nodalization, and the test conditions for both Phase A and Phase B of UPTF Test 8 are discussed in Section 8.2.9. Figure 8.4-13 compares the condensation rate from the experimental data with the S-RELAP5 results, with the normalization factors applied, for Phase A (Run 111) of Test 8. The S-RELAP5 void fraction at the injection node and the condensation potential are also shown in Figure 8.4-13. The S-RELAP5 condensation rates agree well with the data. For a thermodynamic ratio less than 1.0, S-RELAP5 predicts highly voided conditions in the cold leg. When the thermodynamic ratio is greater than 1.0, the code predicts around a 60% void fraction in the cold leg. These void distributions match reasonably well with expectations based on experimental observations. For thermodynamic ratios above 1.0, the condensation potential exceeds that actually occurring in the cold leg. The cold leg is no longer in stratified flow but in a plug type flow wherein the surface area for condensation is greatly reduced. This flow pattern is characteristic of the accumulator injection period. Similar results are observed in Figure 8.4-14 for Phase B (Run 112) of Test 8 where the S-RELAP5 condensation rates again agree well with the data.

Figure 8.2-254 and Figure 8.2-266 from Section 8.2.9 respectively display the measured and calculated fluid temperatures in the cold leg for both Phase A (Run 111) and Phase B (Run 112). Figure 8.2-254 illustrates how the liquid temperature agrees well with the data for the accumulator injection period and the pumped injection period.

8.4.2.2.3 UPTF Test 25

The UPTF test facility is described in Section 8.2.9. The purpose of UPTF Test 25 was to obtain full scale data on the thermal-hydraulics related to the interaction of subcooled ECC and steam in the cold leg, and to determine the effects of steam flow rate and steam superheat (Reference 8.4-6). Test 25 consisted of two steady-state phases with varying steam flow rates. Phase A included four runs designed to address downcomer water level and entrainment with superheated downcomer walls. Phase B included a run to address this behavior with no superheated walls. The remaining four runs from Phase B were designed to address cold leg flow regimes, and provide data on downcomer level and entrainment during reflood conditions. Test conditions for UPTF Test 25 are outlined in Table 8.4-7. The S-RELAP5 nodalization diagram in Section 8.2.9 also applies for the predictions provided here.

Figure 8.4-15 contains the condensation rate as a function of thermodynamic ratio for UPTF Test 25 Phase A. The figure shows that the S-RELAP5 model for the UPTF agrees well with the measured data. Similarly in Figure 8.4-16, the S-RELAP5 model for UPTF Test 25 Phase B agrees well with the condensation rate from the experiment. As shown in both figures, it is evident that below a thermodynamic ratio of around 1.3, stratified flow begins to occur in the cold leg and void fraction increases. Above a thermodynamic ratio of 1.3, the void fraction value remains low and approximately constant, which is representative of the plug flow. With thermodynamic ratios above 1.0 in Figure 8.4-16 the condensation potential exceeded the steam injection rate, which is consistent with accumulator injection.

8.4.2.3 Conclusions

These normalization factors applied to the S-RELAP5 correlations will calculate the proper cold leg condensation during the entire LOCA transient. The void dependent CONMAS and constant CONMSG multipliers adequately model the condensation rate in the cold-leg at different thermodynamic ratios for both the EPRI and UPTF experiments. These multiplier values provide a good representation of the condensation in the cold leg model for both the accumulator injection period and pump injection period.

Table 8.4-6: Test Conditions for W/EPRI 1/3 Scale Cold Leg Condensation Model

Run	Pressure (psia)	Steam Temp. (F)	Steam Flow (lbm/hr)	ECC Temp (F)	ECC Velocity (ft/s)	T_{out}^6 (F)	Tsat (F)
5-18	22.2	251	11000	120	12.61	188	233
5-19	22.2	250	11000	122	14.41	181	233
5-20	22.3	254	11000	123	4.24	233	233
5-22	50.0	285	22000	121	8.21	281	281
5-24	49.7	285	22000	121	16.49	219	281
5-25	50.1	504	22000	87	4.08	281	281
5-26	50.2	509	22000	88	8.08	281	281
5-27	34.5	505	22000	85	12.28	227	258
5-34	49.6	506	22000	120	16.51	229	281
5-38	22.0	500	23000	118	4.11	233	233
5-42	21.8	271	23000	116	16.27	220	233
5-50	21.8	236	5000	112	2.03	233	233
5-52	22.5	238	5000	118	4.03	211	233
5-53	22.0	237	5000	120	6.05	183	233
5-55	22.1	271	22000	120	1.99	233	233
5-57	50.2	505	22000	122	2.01	281	281
5-60	21.8	490	11000	117	4.15	233	233
5-65	22.0	491	11000	121	16.0	179	233

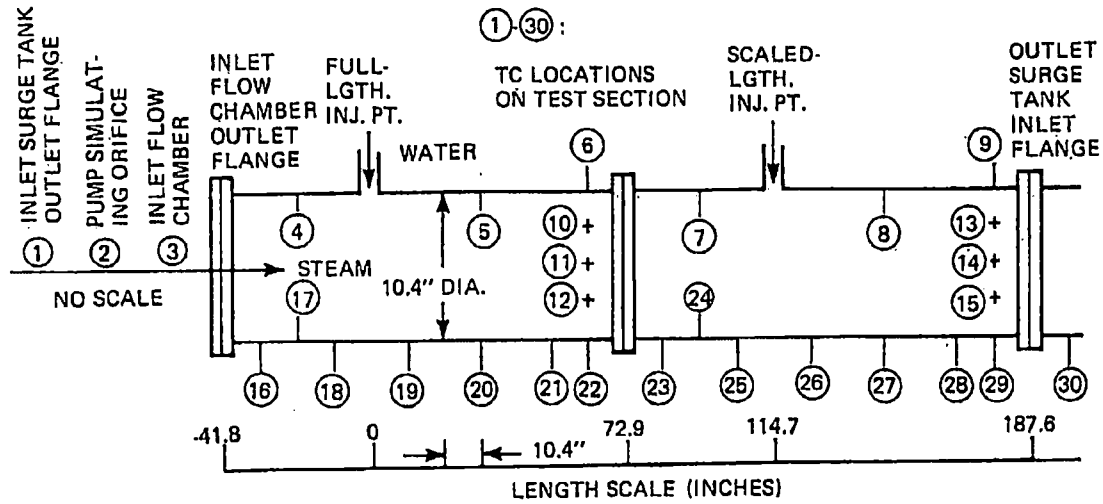
⁶ Specifies the average temperature of the steam and water mixture

Table 8.4-7: Test Conditions for UPTF Test 25

Phase- Part	Loop Pressure (kPa)	W_g (kg/s)	W_l (kg/s)	Steam ΔT_{sup} (C)	Liquid ΔT_{sup} (C)	Containment Pressure (kPa)
25-A-I	310	30	85	34	106	250
25-A-II	270	25	85	35	101	250
25-A-III	260	20	85	35	100	250
25-A-IV	260	15	85	35	100	250
25-B-I	310	29	82	23	106	250
25-B-II	280	29	143	27	102	250
25-B-III	250	23	143	31	98	250
25-B-IV	250	18	143	31	98	250
25-B-V	250	11	143	31	98	250

Figure 8.4-9 CONMAS Multiplier as a Function of Cold Leg Void Fraction



Figure 8.4-10 EPRI 1/3 Scale Test Thermocouple Locations on Test Section**Figure 8.4-11 ECCS Subcooling (or Mixing Region Void Fraction) at Cold Leg Exit vs. Thermodynamic Ratio for EPRI Model**

**Figure 8.4-12 Measured vs. Predicted Tg at TC-13 and Junction
180-02**



**Figure 8.4-13 UPTF Test 8a: Cold Leg Condensation Rate and Mixing
Node Void Fraction**



**Figure 8.4-14 UPTF Test 8b: Cold Leg Condensation Rate and Mixing
Node Void Fraction**



**Figure 8.4-15 UPTF Test 25a: Cold Leg Condensation Rate and
Mixing Node Void Fraction**



**Figure 8.4-16 UPTF Test 25b: Cold Leg Condensation Rate and
Mixing Node Void Fraction**



8.4.3 Blowdown Heat Transfer

Section 8.4.4 presents the uncertainty and bias for post-CHF heat transfer under high pressure conditions developed from the THTF tests. As shown within that section, justification is given for using the low pressure reflood heat transfer biases,

[] during the entire LBLOCA calculation, which includes the blowdown phase. Section 8.2.1 presented assessment results showing the effects of the reflood heat transfer uncertainties applied to transient boil-off and reflood tests from THTF with acceptable results. In conclusion, the integral effects tests from LOFT and Semiscale, discussed in Sections 8.3.1 and 8.3.2, demonstrate the slightly conservative overall performance of the heat transfer model with those same heat transfer biases [] for the entire LOCA.

In particular are, the LOFT tests L2-3 and LP-LB-06, which show the blowdown quench phenomena occurring at the limiting PCT elevation. The S-RELAP5 calculated results from those assessments show that the code did not capture the blowdown quench phenomena (a conservatism), and that the maximum calculated cladding temperatures from the peak power regions were shown to be within the data uncertainty or conservative for each of the experiments simulated.

In summary, all of the assessments that were performed under blowdown conditions used the heat transfer biases [] The results from those assessments show that S-RELAP5 calculates conservative cladding temperatures during the blowdown period. The treatment of the blowdown heat transfer by the aforementioned biases is therefore considered to be acceptable.

8.4.4 THTF Heat Transfer

The heat transfer tests, at the THTF, addressed heat transfer from typical pressurized water reactor (PWR) fuel rods at elevated temperatures and pressures. Of the many tests that were performed at this facility, the 22 steady-state tests (Reference 8.4-7), are the focus of this study. The steady-state tests provide steady-state film-boiling data for rod bundles over a range of flow conditions and pressures, as shown in Table 8.4-8. Because they are at a steady-state, these tests allow the reduction of fluid and rod conditions analytically, which allows a relatively simple comparison to heat transfer models.

If this high pressure scale factor PSTCHF were to be used for blowdown heat transfer, a transition to the low pressure scales factors FILMBL and DFFBHTC for reflood conditions would be required. The overall uncertainty for the low pressure heat transfer, discussed in Section 8.4.1, conservatively bounds the upper and lower limits of the high pressure PSTCHF multiplier. Potentially, the low pressure uncertainties can be applied to all post-CHF heat transfer.

To confirm that the low pressure heat transfer scaling is acceptable for LBLOCA, the temperature traces for the transient blowdown and reflood tests were compared to the S-RELAP5 predictions. For these comparisons, as discussed in Section 8.2.1, the uncertainty in the measurements were included, as were the upper and lower limits of the HTC scaling factors FILMBL and DFFBHTC. For all the tests analyzed, the temperature is generally over-predicted by the S-RELAP5 model. At the peak temperatures, S-RELAP5 generally over-predicts the temperature at the lower elevations. At the higher elevations, the model results trend closer to the test data at the peak temperature, yet still show a general over-prediction of the temperature. The S-RELAP5 results also show adequate prediction of the time of the temperature peak with respect to the test data for the range of elevations.

[

Since the THTF facility approximates a typical AREVA NP LBLOCA plant model hot assembly, the results from this analysis are considered to be applicable to the AREVA NP LBLOCA core models.

In the process of deriving the optimal CHF scale factor, the probability distribution of post-CHF measured/calculated HTC ratios shown in Figure 8.4-18 was developed. This distribution provides a possible means of applying an uncertainty multiplier for high pressure post-CHF HTC values, however it has been concluded that the low pressure post-CHF HTC uncertainty multipliers used for the high pressure THTF transient boil-off and reflood analyses described in Section 8.2.1 will provide a more conservative adjustment to high pressure heat transfer than would the high pressure uncertainty in Figure 8.4-18. Since the high pressure calculations described in Section 8.2.1 yield reasonable comparisons to test data, it has therefore been decided to use the low pressure post-CHF HTC uncertainty multipliers at all pressures.

**Table 8.4-8: Test Conditions for Steady State ORNL/THTF Test
3.07.09**

Run Id.	Nodal Power (W)	Inlet Flow (lb/s)	Inlet Temperature (°F)	Sink Pressure (psia)
B	4101.8	0.1430	590.34	1848.5
C	2576.2	0.0671	558.71	1805.1
D	3154.3	0.1038	573.21	1846.8
E	3229.2	0.1190	579.76	1907.4
F	1747.0	0.0512	561.31	1829.5
G	1488.7	0.0500	563.33	1817.5
H	1901.1	0.0514	507.95	1288.8
I	2521.1	0.0728	507.95	1331.3
J	3482.5	0.1468	582.34	1936.3
K	2030.0	0.0453	409.82	634.7
L	3518.1	0.1057	528.49	1202.0
M	3960.1	0.1317	539.61	1241.3
N	4277.1	0.1618	545.05	1233.0
O	2417.4	0.0616	487.50	866.5
P	3680.6	0.1044	512.60	873.8
Q	2561.9	0.0652	501.82	946.5
R	2895.1	0.0729	499.33	952.2
T	1470.5	0.0481	566.63	1722.9
U	1470.8	0.0484	566.61	1694.3
V	1485.8	0.0500	562.70	1744.5
W	1745.8	0.0513	561.22	1819.4
X	2686.7	0.0691	513.86	871.3

**Figure 8.4-17 Heat Transfer Coefficients from THTF Steady State
Calculations Compared with Data**



**Figure 8.4-18 Cumulative Probability of the PSTCHF Distribution
Compared with a Normal Distribution [**

]



8.4.5 Critical Flow

]

The calculated uncertainties are therefore approximately equal to the measured value indicating excellent agreement.

The Marviken Critical Flow Tests show that the maximum void fraction at the break is approximately 30% (Section 8.2.7). However, during the major portion of the blowdown and the early refill phases in a typical LBLOCA transient, when the flow at the break plane is choked, the void fraction can be as high as 95%. The break flow comparison plots for LOFT and Semiscale benchmarks given in Sections 8.3.1 and 8.3.2, respectively, show that there is no void-dependent bias in the S-RELAP5 calculated break flows. The bias and uncertainty calculated using the Marviken tests in the two-phase regime can therefore be applied to the entire two-phase range, thereby preserving the combined Marviken mean and standard deviation. It is to be noted that the break flow area is a sampled parameter in the RLBLOCA methodology. The break flow uncertainty, which is another sampled parameter, is essentially a multiplier on the sampled break area. Consequently, the break spectrum effectively accounts for the uncertainties in the calculation of break flow. A description of the statistical treatment of the break size is provided further in Section 8.5.2.6.

8.4.6 Interfacial Drag and Liquid Carryover During Reflood

Shown in this section is the approach used to assure that the S-RELAP5 code will calculate realistic to conservative liquid entrainment to the STGR tube region during the reflood phase of LBLOCA. During the reflood phase of a LBLOCA, the steam generated in the core region entrains liquid droplets, which then are carried into the reactor vessel upper plenum. As the steam-droplet mixture flows through the loops, some liquid droplets are de-entrained in the upper plenum, in the hot legs and in the STGR inlet plenums, and the remaining droplets are carried into the STGR tube regions. In the STGR tube regions, the majority of the remaining droplets are vaporized by reverse heat transfer from secondary side to the primary side. Any remaining droplets are carried over by the steam to the cold legs where they may interact with cold ECC water and eventually flow out through the break to the containment. The evaporation of liquid in the steam generator tube region increases the pressure drop through the steam generators, resulting in delayed or reduced reflooding of the core. This effect is the supposed "steam binding" phenomenon in the LBLOCA and affects the cladding thermal response and therefore needs to be realistically calculated by S-RELAP5.

UPTF Tests 10, Run 081 (Test 10B), and 29, Runs 211 and 212 (Test 29B) were analyzed to provide specific S-RELAP5 input modeling guidelines for the hot leg and STGR inlet plenum regions to ensure that S-RELAP5 properly predicts the liquid entrainment to steam generator (STGR) tube region, and to limit countercurrent flow at the upper core tie plate (UTP) of a PWR during the LBLOCA reflood phase. These tests were the separate effect tests specifically designed under the 2D/3D program to investigate water mass distribution in the reactor vessel upper plenum, hot-legs, STGR inlet plenums, and in the STGR tube region during the reflood phase of a LBLOCA transient. UPTF Tests 10B and 29B, the S-RELAP5 input model and simulation results were discussed in Section 8.2.9.6.

The simulation results of Tests 10B and 29B show that S-RELAP5, with the RLBLOCA plant nodalization and the specific guidelines described below, conservatively over-predicts the carryover of liquid to the steam generators.

- [

]

These specific modeling options promote the entrainment of liquid droplets to the STGR tube region and limit liquid down flow from the vessel upper plenum to the core region. The UPTF tests 10B and 29B, S-RELAP5 input model and simulation results were discussed in Section 8.2.9.6.

The specific input modeling options described above are incorporated in the benchmarks of SCTF and CCTF tests. These tests were conducted under the 2D/3D program to evaluate the core thermal hydraulics during the reflood phase of a LOCA. The simulations of these tests are described in Sections 8.2.12 and 8.2.13, respectively. UPTF is scaled to approximate a full scale 4-loop PWR, while the SCTF and CCTF are scaled facilities, these test simulations can be used to evaluate the scaling effect of the modeling adjustment described above.

SCTF hot leg geometry is atypical. It's inside geometry is elliptical with its height (major axis) close to the inside diameter of a typical 4-loop PWR. The width (minor axis) is very narrow to preserve the volume flow area scaling of a 4-loop PWR. In the S-RELAP5 model, the oval geometry is approximated by a circular pipe with same volume flow area. In SCTF there is no active steam generator. A steam water separator is used to simulate the primary side of the steam generator. The inlet chamber represents the inlet plenum of four scaled steam generators. The outlet chamber collects the liquid that is entrained from the inlet chamber. In the tests the liquid level in the outlet chamber is measured. This collected liquid represents the liquid that will be entrained into the tube region during the LOCA in a scaled PWR. Six SCTF Core-II tests were simulated using S-RELAP5, and the results are summarized in Section 8.2.12. The measured and S-RELAP5 calculated liquid levels for the two gravity feed (Tests S2-AC1 and S2-SH1) and four forced feed tests (S2-10, S2-11, S2-17, and S2-18) are shown in Figure 8.2-421 through Figure 8.2-426 in Section 8.2.12. Considering the atypicality of the SCTF hot leg, and the approximation used in modeling the hot leg in the S-RELAP5 input model, S-RELAP5 calculated liquid entrainment to the S/W separator is acceptable.

Four CCTF tests (Tests 54, 62, 67, and 68) were simulated using S-RELAP5. CCTF has active scaled steam generators. The tests realistically simulate the entrainment process and the droplet evaporation in the tube region. However, there is very little information available to make a direct comparison between the measurement and calculation of the liquid entrained to the tube region. In CCTF the pump side break is connected to Containment Tank 2, which has a liquid separator at the top. This separator traps all liquid exiting the broken loop steam generator side of the break. With the assumption that the calculated droplet evaporation in the tube region is comparable to the data, then a comparison between the measured and calculated liquid collected in Tank 2 provides a reasonable comparison between the measured and calculated liquid entrainment to the tube region of the broken loop STGR (experimental acronym for Steam Generator).

S-RELAP5 calculated and measured Containment Tank 2 levels for the four tests are shown in Figure 8.2-470, Figure 8.2-500, Figure 8.2-530, and Figure 8.2-560 in Section 8.2.13. Considering the uncertainty in the broken loop steam generator tube region, the uncertainty in the extent to which the piping is adiabatic (as it is modeled in S-RELAP5), and the uncertainty in the dimensions of Containment Tank 2 (dimensioned drawings were not available at the time of the analysis), the S-RELAP5 calculated entrainment rate to the tube region is acceptable.

UPTF is scaled to approximate a full-scale 4-loop PWR, and SCTF and CCTF are scaled facilities. The S-RELAP5 simulation of the tests conducted in these facilities show that the code calculated entrainment to the tube region is acceptable. From the results discussed above, it can be concluded that S-RELAP5, with the specific input modeling options described earlier will acceptably predict (on conservative side) the liquid entrainment to steam generator tube region of a PWR during the LBLOCA reflood phase.

8.4.7 T_{\min}

The primary objective of this analysis is to quantify the bias (if present) and uncertainty associated with the TMINK parameter of the S-RELAP5 code. The S-RELAP5 heat transfer package does not have an explicit model for the minimum stable film boiling temperature (T_{\min}) to determine the wall surface temperature at which transition from film to nucleate boiling can begin. Instead, for the heat transfer regime to be considered to be in transition boiling, the following criteria have to be met:

- The surface heat flux calculated using the transition boiling correlation must be greater than that calculated for film boiling.
- The wall surface temperature must be less than the parameter TMINK.
- The void fraction must be less than 0.95 in the hydrodynamic volume.

In conclusion, the proposed value for TMINK was shown to contain a considerable degree of conservatism because of its neglect of high pressure and use of stainless steel data to represent zirconium alloys and zirconium oxide effects.

The overall approach used to determine these values is summarized as follows:

- Develop a distribution for the quench temperature using the low-pressure database.
- Assume that the minimum film boiling temperature is essentially equal to the quench temperature.
- Develop a relationship between T_{\min} and the code parameter TMINK.

- Combine the distribution for the quench temperature with the relationship between T_{min} and $TMINK$ to produce the value and uncertainty distribution for $TMINK$.

An S-RELAP5 example calculation for a Westinghouse 3-loop PWR was used to determine the range of parameters that could vary the minimum film boiling temperature. Parameters considered are pressure, subcooling, and reflood rate. The pressure range for reflood is found to be about 30 to 40 psia. The top of the lower plenum is predicted to always be at saturation which corresponds to zero subcooling, and the reflood rate varies from about 6 inch/s to less than 1 inch/s.

A set of seven FLECHT SEASET tests was used to evaluate the trends with these parameters. Table 8.4-9 shows the seven tests and the nominal conditions. Based on the trends, a rationale was developed to use only the data from the 3 inch/s reflood rate tests (Test 31302) to develop the low-pressure distribution for the quench temperature. Figure 8.4-19 plots the quench temperature data for Test 31302, as well as a normal distribution that provides a conservative bounding distribution. [

] Below

this value, the data values have a higher probability of occurrence; however, these low values for the quench temperature probably are unrealistic, but result from the clad being cooled below the quench temperature before the arrival of the two-phase mixture level. This small nonconservatism is felt to be justified by all of the other conservative assumptions that have been applied (e.g., using only the data from the 3 inch/s test). In conclusion, [] is equal to that calculated using the Henry model (Reference 8.4-10) for a pressure of [

] further supporting this value.

As discussed in Reference 8.4-11, this low-pressure bounding distribution is clearly conservative even when compared to the high-pressure data with the lowest values of the quench temperature (ROSA/TPTF), and is highly conservative compared to the data from the ORNL/THTF and the Westinghouse G1/G2 tests. Discussion in Reference 8.4-11 also concludes that a substantial degree of conservatism has been built into the proposed distribution (relative to zirconium alloy including M5[®] clad rods) by basing it on only low pressure data for stainless steel clad rods. These conclusions remain valid for Revision 3.

A relationship between the effective value of T_{\min} and the specified value of the code parameter TMINK was developed. These two not being equal was attributed to the manner in which the boiling curve is evaluated for fine mesh nodes. [

]



Table 8.4-9: Reflood Test Matrix

Run Number	Pressure (psia)	Peak Power (kW/ft)	Flow Rate (in/sec)	Coolant Temp. (°F)
Reflood Rate				
31805	40	0.70	0.81	124
31504	40	0.70	0.97	123
31203	40	0.70	1.51	126
31302	40	0.69	3.01	126
31701	40	0.70	6.10	127
Pressure Variation				
34209	20	0.72	1.07	90
31504	40	0.70	0.97	123
32013	60	0.70	1.04	150

**Figure 8.4-19 Comparison of the Cumulative Probability Distribution
for the Quench Temperatures of FLECHT SEASET Test 31302 and a
Bounding Normal Distribution**



8.4.8 COPENIC Uncertainties

8.4.8.1 Background



8.4.8.2 COPENIC2 Bias Determination

8.4.8.3 COPENIC2 Uncertainty

8.4.8.4 Conclusions

**Figure 8.4-20 COPENIC2 Benchmark Data Set (Fuel Centerline
Temperatures)**



**Figure 8.4-21 COPENIC2 Benchmark Data Set (Fuel Centerline
Temperatures) with IFA 432-3 Removed**



**Figure 8.4-22 COPENIC2 Underprediction Benchmark Data Set (Full
Set of Fuel Centerline Temperatures)**



Figure 8.4-23 COPENIC2 Cumulative Probability Distributions



8.4.9 Metal-Water Reaction

Two LOCA ECCS criteria limit the extent of local and core-wide reaction of the zirconium-based cladding with water; therefore, metal-water reaction is an important parameter to be calculated for LOCA analyses. For realistic calculation of PWR large break LOCA, S-RELAP5 uses the metal-water reaction rate equation from Cathcart and Pawel (Reference 8.4-13). Two constants in this rate equation are derived from experimental data and have uncertainties as determined by the authors, the reaction rate constant and a constant in the temperature dependent exponential term. These uncertainties are shown in Table 8.4-1 and are applied in the realistic LOCA analyses. The Cathcart-Pawel equation is applicable to all zirconium based cladding alloys currently used, including M5[®] cladding.

8.4.10 Hot Wall (CHF Multiplier)

During the LOCA energy is added to the fluid due to sensible heat transfer from hot metal components such as the reactor vessel walls. To assure that the maximum energy is transferred, the hot wall CHF value is sampled from a discrete, binary 50/50 distribution with one possible outcome the nominal calculated value and the other possible outcome a value of 1000.0 times the normal calculated value, as shown in Table 8.4-1. This assures nucleate boiling is calculated for these walls in 50 percent of the cases studied.

8.4.11 Containment Pressure

For some LOCAs, the reflood rate may become limited by the steam binding phenomenon. When this happens, the steam density is determined primarily by the containment pressure and thus the containment pressure is a significant parameter affecting the reflood rate. Low containment pressure reduces the reflood rate and increases PCT. However, for many of the LOCAs calculated with S-RELAP5, reflood rate is not calculated to be limited by steam binding. For these LOCA conditions, the reflood rate is insensitive to changes in containment pressure. To assure that any LOCA reflood calculation affected by containment pressure is bounded; uncertainties affecting a large variation in containment pressure are imposed on the analyses.

The containment pressure is varied by imposing a uniform variation of containment volume between the minimum free volume, potential for maximum containment pressure, and the maximum free volume, potential for minimum containment pressure, of the containment structure, as shown in Table 8.4-1.

8.4.12 References

- 8.4-1 AREVA NP (Framatome ANP), EMF-2102(P) Revision 0. S-RELAP5: Code Verification and Validation. August 2001.
- 8.4-2 Electric Power Research Institute, EPRI NP-2013, NUREG/CR-2256, WCAP-9891. PWR FLECHT SEASET Unblocked Bundle, Forced and Gravity Reflood Task Data Evaluation and Analysis Report. February 1982.
- 8.4-3 MPR Associates, Inc., MPR-1208. Summary of Results from the UPTF Cold Leg Flow Regime Separate Effects Tests, Comparison to Previous Scaled Tests, and Application to U. S. Pressurized Water Reactors. October 1992.
- 8.4-4 Electric Power Research Institute, EPRI-294-2. Mixing of ECC Water with Steam: 1/3 Scale Test and Summary. June 1975.
- 8.4-5 Siemens AG, Erlangen Germany, U9 316/88/11. Upper Plenum Test Facility, Test No. 8 Cold/Hot Leg Flow Pattern Test Quick Look Report. September 1988.
- 8.4-6 Siemens AG UB KWU, U9 314/90/13. UPTF Quick Look Report: Test No. 25, Downcomer/Cold Leg Steam/Water Interaction Test. September 1990.
- 8.4-7 Oak Ridge National Laboratory, NUREG/CR-2435, ORNL-5822. Dispersed Flow Film Boiling in Rod Bundle Geometry - Steady State Heat Transfer Data and Correlation Comparisons. March 1982.
- 8.4-8 Nuclear Regulatory Commission, NUREG-1230. Compendium of ECCS Research for Realistic LOCA Analysis. December 1988.
- 8.4-9 Studsvik Eco & Safety AB, MXC-301, NUREG/CR-2671. The Marviken Full-Scale Critical Flow Tests, Summary Report. May 1982.
- 8.4-10 AIChE, Vol. 70 No. 138. A Correlation For The Minimum Film Boiling Temperature.

- 8.4-11 AREVA NP (Framatome ANP), EMF-2102(P) Revision 0. S-RELAP5: Code Verification and Validation. August 2001.
- 8.4-12 BAW-10231P-A, Revision 1, COPENIC Fuel Rod Design Computer Code, Framatome ANP, January 2004.
- 8.4-13 Oak Ridge National Laboratory, ORNL/NUREG-17. Zirconium Metal-Water Oxidation Kinetics: IV. Reaction Rate Studies. August 1977.
- 8.4-14 Electric Power Research Institute, EPRI NP-2013, NUREG/CR-2256, WCAP-9891, PWR FLECHT SEASET Unblocked Bundle, Forced and Gravity Reflood Task Data Evaluation and Analysis Report, February 1982.

8.5 *Methodology Treatment of PIRT Phenomena*

Sections 8.2 and 8.3 reviewed the extensive assessment of the S-RELAP5 code with regard to its capability to predict the important phenomena identified in the LBLOCA PIRT. In some cases statistical information was determined with regard to the mean values and uncertainties for predicting a specific phenomenon. Most of this information is also discussed in Section 8.4. In other cases, S-RELAP5 was shown to calculate the phenomenon conservatively and no evaluation of a bias or uncertainty was performed. In these situations, the conservatism associated with these phenomena was simply accepted as unquantified conservatism in the methodology. Table 8.5-1 summarizes the important PIRT phenomena and how those phenomena are being addressed in the methodology.

8.5.1 Important PIRT Phenomena Not Treated Statistically

From the comparison of the S-RELAP5 predictions and data for both the SET and IET assessments, a number of important PIRT phenomena were found to be predicted conservatively by the code. The conservative predictions were either because of a conservative model in S-RELAP5, or the use of conservative input. These phenomena are indicated in Table 8.5-1 as being treated in the methodology as an "inherent conservatism" or an "input conservatism." By "inherent conservatism," it is meant that a code model or combination of models was demonstrated to conservatively predict these phenomena. By "input conservatism," it is meant that the input being provided to the code was demonstrated to be conservative and will be used in NPP analyses. These conservatisms are accepted in the methodology as an unquantified conservatism above that indicated by the statistical analysis. These phenomena are discussed individually in the following sections.

8.5.1.1 Core Multi-Dimensional Flow and Void Distributions

The core flow distribution and void distribution are determined by the initial power distributions and [

] While in effect, this will result in a wide variation of calculated flow and void distributions in the core.

The ability of S-RELAP5 to calculate axial void distributions has been demonstrated in the SET assessments performed for the THTF Level Swell (Section 8.2.1), GE Level Swell (Section 8.2.8), FRIGG-2 (Section 8.2.11), FLECHT-SEASET and FLECHT Skewed tests (Section 8.2.3). For these assessments, the agreement between code prediction and measured void fractions was good to excellent (Section 8.2). The THTF and FRIGG-2 tests are high pressure tests. The GE Level Swell test is a transient depressurization test from high pressure. The FLECHT-SEASET and FLECHT Skewed test facilities are instrumented to measure ΔP s in the bundle at 12 inch intervals. At low flow conditions, which typically occur during the reflood phase of a LOCA, the ΔP s directly give the void distribution in the bundle. The assessments of several FLECHT-SEASET and FLECHT Skewed tests, discussed in Section 8.2.3, show that the code calculated ΔP s reasonably agree with the data. These assessments indicate S-RELAP5 is capable of calculating acceptable void distributions in the core at high and low pressure conditions.

The FLECHT-SEASET tests were also used to calculate the heat transfer biases and uncertainties. The prediction of flow and void distributions is an essential part of determining the code heat transfer biases and uncertainties. [

]

The ability of S-RELAP5 to calculate flow distributions in the core was demonstrated in the SET assessments (Section 8.2) performed for the multi-dimensional flow tests, CCTF, and SCTF. The multi-dimensional flow tests demonstrated S-RELAP5 was capable of modeling and predicting the measured flows in these tests. The SCTF tests were conducted specifically to study the two-dimensional flow behavior in the core region during the reflood phase of the LOCA. The overall bundle ΔP s and PCTs are good indications of the core flow distribution. The assessments of several of the SCTF tests show that S-RELAP5 calculated hot bundle ΔP s and PCTs reasonably agree with the data. Additionally, the calculated void fraction in the upper region of the hot bundle is somewhat higher than the data. These assessments demonstrated that the combined code and core nodalization was capable of predicting the effects of changes in radial power distribution and associated flows during the reflood period of a LBLOCA.

The CCTF assessments further demonstrated that the combined code and core nodalization were able to predict the core flows, hot bundle ΔP s, and resulting PCTs in a cylindrical facility. The cylindrical bundle region modeling used is consistent with the input modeling used in the methodology NPP nodalization.

Based on the information listed above, the combination of these assessments clearly demonstrates S-RELAP5 is capable of realistically predicting the core flows and void distributions as the statistical parameters are being varied in the statistical analysis of a LBLOCA.

8.5.1.2 Liquid Entrainment in the Core

The liquid entrainment in the core has been demonstrated to be conservatively calculated by S-RELAP5 and the methodology nodalization, which is shown in the assessments performed for CCTF, UPTF, and FLECHT-SEASET, and reported in Section 8.4.6. In the CCTF tests examined (Tests 54, 62, 67, and 68), the conclusion was that the liquid entrained from the core into the upper plenum was overpredicted by S-RELAP5 during the early part of the test. This overprediction occurred until 400 to 500 seconds into the test. Following the overprediction, the code underpredicted the amount of liquid in the upper plenum. Only after quenching occurred in the test, the data indicated higher levels. Both the measured and calculated time of PCT occurred before the calculation began to underpredict the liquid in the upper plenum.

For the FLECHT-SEASET tests, as shown in Figure 8.2-127 through 8.2-135, the mass of water in the test section is underpredicted by S-RELAP5 and the methodology nodalization. In conclusion, S-RELAP5 predicted liquid carryout from the core to the upper plenum had been examined in three different test facilities. In all three test facilities, the amount of liquid carryout of the core into the upper plenum was overpredicted. Due to these results from three different test facilities, it is concluded that the code and methodology prediction of core entrainment is conservative and no bias or uncertainty was developed to take credit for this conservatism.

8.5.1.3 Core Flow Reversal/Stagnation

The reversal and stagnation of flow in the core is the result of the size of the break and the rate of coolant loss versus the rate of coolant injection from the ECC systems. In general, a combination of other phenomena occur to determine the limiting set of conditions that result in the worse situation, where the flow in the core is essentially stagnant or has a low reflood rate for the longest period of time. This condition is addressed by the random variation of the other dominant phenomena. [

]

8.5.1.4 Upper Plenum Liquid Entrainment/Deentrainment

When liquid droplets are entrained in the core and carried up into the upper plenum, they can remain there, fall back into the core (deentrainment), or be carried out into the hot leg (entrainment). The major modeling concern for an LBLOCA is that allowing too much liquid to fall back into the core would result in a top-down quench and a significant underprediction of the PCT. It would also reduce steam binding. Several SCTF, CCTF, and UPTF tests were used to demonstrate S-RELAP5 will carry over an acceptable amount of liquid to the steam generator tube region, ttherefore limiting the liquid accumulation in the upper plenum to an acceptable amount.

Several input options were developed to make sure S-RELAP5 will entrain an acceptable amount of liquid to the steam generator tube region during the reflood phase of a LOCA in a PWR plant. The simulation of UPTF Test 10, Run 080 and Test 12, Run 014 (Section 8.2.9.5), demonstrate that by using a Kutateladze-type CCFL correlation, S-RELAP5 will conservatively calculate liquid down flow from the upper plenum. A Wallis-type CCFL correlation developed by MPR using UPTF Test 11 is applied at the hot leg-to-steam generator inlet plenum junction to limit the liquid drain back to the upper plenum. UPTF Test 10, Run 081 and Test 29, Runs 211 and 212 (Section 8.2.9.6), were simulated to develop upper plenum, hot leg, and steam generator inlet plenum input options to ensure acceptable liquid entrainment to the tube region. These benchmarks are discussed in Section 8.2.9.

In the simulation of several CCTF and SCTF tests, all the above discussed input options were used. The SCTF hot leg geometry is atypical due to the inside geometry being elliptical. The height (major axis) of the hot leg is close to the inside diameter of a typical 4-loop PWR. In order to preserve the volume flow area scaling of a 4-loop PWR, the width (minor axis) of the hot leg is very narrow. In the S-RELAP5 model, the oval geometry is approximated by a circular pipe while preserving the total volume flow area. In SCTF there is no active steam generator; a steam-water separator is used to simulate the primary side of the steam generator. The inlet chamber represents the inlet plenum of four scaled steam generators. The outlet chamber collects the liquid entrained from the inlet chamber. In the tests, the liquid level in the outlet chamber is measured. This collected liquid represents the liquid entrained into the tube region during a LOCA in a scaled PWR. Six SCTF Core-II tests were simulated using S-RELAP5. The results are summarized in Section 8.2.12. The measured and S-RELAP5 calculated liquid levels for the two gravity feed (Tests S2-AC1 and S2-SH1) and four forced feed tests (S2-10, S2-11, S2-17, and S2-18) are shown in Figure 8.2-421 through Figure 8.2-426. Considering the atypicality of the SCTF hot leg and the approximation used in modeling the hot leg in the S-RELAP5 input model, the calculated liquid entrainment to the steam-water separator is considered acceptable.

Four CCTF tests (Tests 54, 62, 67, and 68) were simulated using S-RELAP5. CCTF has active scaled steam generators. The tests realistically simulate the entrainment process and therefore droplet evaporation in the tube region. However, there is little information available to make a direct comparison between measured and calculated liquid entrained to the tube region. In CCTF, the pump side break is connected to a containment tank (Containment Tank II), which has a liquid separator at the top. This separator traps all liquid exiting the broken loop steam generator side of the break. With the assumption that the calculated droplet evaporation in the tube region is comparable to the data, a comparison between the measured and calculated liquid collected in Containment Tank II provides a reasonable comparison to the measured and calculated liquid entrainment to the tube region of the broken loop steam generator. The results are summarized in Section 8.2.13.

S-RELAP5 calculated and measured Containment Tank II levels for the four tests are shown in Figure 8.2-470, Figure 8.2-500, Figure 8.2-530 and Figure 8.2-560.

Considering the differences in the broken loop steam generator tube region heat transfer between the test and the S-RELAP5 prediction, the uncertainty in the extent to which the piping is adiabatic (as it is modeled in S-RELAP5), and the uncertainty in the dimensions of Containment Tank II (dimensioned drawings were not available at the time of the analysis), the S-RELAP5 calculated entrainment rate to the tube region is considered acceptable.

In summary, several input options are developed to make sure an acceptable amount of liquid is entrained into the upper plenum and carried over to the steam generator tube region during the reflood phase of a LOCA in a PWR. This approach will also limit the liquid accumulation in the upper plenum to an acceptable level during the reflood phase of a LOCA.

8.5.1.5 Countercurrent Flow Limit

The CCFL correlations with specific CCFL parameters are applied [

] These models are applied in all the appropriate benchmarks and are used in the plant models.

Therefore, the conservative set of parameters used in the assessments is also used in the NPP analysis so that the CSAU requirement that the assessments use the same model as the NPP analysis is satisfied.

8.5.1.6 Hot Leg Entrainment/Deentrainment

As discussed in Section 8.5.1.4, several input options are developed to make sure an acceptable amount of liquid is entrained into the upper plenum and carried over to the steam generator tube region during the reflood phase of a LOCA in a PWR. This approach also limits liquid accumulation in the hot leg to an acceptable level during the reflood phase.

8.5.1.7 Two-Phase Pump Degradation

Two-phase pump degradation is addressed in the methodology as a best-estimate input. Based on the sensitivity study described in Reference 8.5-1 for a limiting break on both a 3-loop and a 4-loop plant, it is shown that two-phase pump degradation is not an important phenomenon for the limiting LBLOCA case. The use of the Semiscale two-phase degradation model, instead of the CE/EPRI two-phase degradation model, produced essentially no impact on the 3-loop results and only an 18 °F (10 K) change in PCT for the 4-loop plant. Therefore, the best-estimate CE/EPRI model is used in the RLBLOCA methodology.

8.5.1.8 Pump Differential Pressure Loss

The pump differential pressure loss is addressed in the methodology strictly as a best-estimate model. The S-RELAP5 code has the ability to input the pump-specific homologous curves for the NPP being analyzed, and this option is used. The homologous curves for the specific NPP pumps are obtained from the utility and, if plant data are available, a pump coast down benchmark is performed to ensure the behavior is consistent.

8.5.1.9 Noncondensible Transport

The treatment of noncondensibles in the S-RELAP5 code was demonstrated to be conservative through the assessment of the ACHILLES ISP 25. The rod thermocouples in the test all clearly showed a reduction in temperature following the introduction of nitrogen into the system. The S-RELAP5 code conservatively underpredicted this cooldown, as shown in Figure 8.2-606 through Figure 8.2-611. Figure 8.2-613 shows the calculated increase in system pressure is lower than the data, which also potentially reduces the core cooling because of the effect of system pressure on steam binding. The impact of the nitrogen injection following the accumulator emptying of water will therefore be conservatively predicted in the NPP analysis.

8.5.1.10 Downcomer Entrainment

The S-RELAP5 code prediction of the ECC bypass during the refill phase of a LOCA was demonstrated to be conservative through the assessment of UPTF Tests 6 and 7 (Section 8.2.9.3). Additionally, a CCFL correlation developed by MPR Associates is used in the sample plant cases given in Appendix B to demonstrate S-RELAP5 conservatively calculates the bottom of core recovery (or beginning of core reflood) time. The MPR correlation is described in Section 8.6.2.2.7. Acceptable downcomer entrainment during the reflood phase was demonstrated for the CCTF benchmarks discussed in Section 8.5.1.12.

Based on these results, it is determined that S-RELAP5 will appropriately calculate the ECC bypass, the core recovery time, and will calculate realistic downcomer entrainment during the reflood phase of a LBLOCA in PWRs where the ECCS delivery to the reactor vessel is not limited to locations adjacent to the broken cold leg.

8.5.1.11 Downcomer Liquid Level Oscillations

Downcomer liquid level oscillation is another phenomenon that is controlled primarily by other important phenomena, such as steam-ECC water mixing in the cold legs. A special cold leg condensation model (summarized in Section 8.5.1.14 and discussed in detail in 8.4.2) was developed using UPTF Test 8, UPTF Test 25, and the EPRI 1/3-scaled tests. The cold leg condensation model is used in all the benchmarks discussed in Sections 8.2 and 8.3, where there is ECC injection into the cold legs. The simulation results for UPTF Test 8, discussed in Section 8.2.9, shows S-RELAP5 predicted the observed flow regimes reasonably well, which indicates the code is capable of calculating the appropriate phenomena associated with steam-ECC mixing in the cold leg in the plant. Since the complete UPTF primary system was not modeled using S-RELAP5, the system oscillations were not calculated by the code. The CCTF, SCTF and LOFT benchmarks (Sections 8.2.13, 8.2.12, 8.3.1, respectively) compared the calculated and measured differential pressures. These results show the code calculated acceptable oscillations during the refill and reflood phases of the transients.

In summary, from the simulation of the above tests, it can be determined that S-RELAP5 will calculate the acceptable primary system and downcomer oscillations during a LBLOCA in a PWR.

8.5.1.12 Lower Plenum Sweepout

The conservatism of the S-RELAP5 lower plenum sweepout is demonstrated in the essentially full-scale UPTF Test 6 and 7 assessments. These tests were again performed with a constant ECC injection rate and with various steam flow rates up the downcomer. The measured versus code prediction of the lower plenum level is provided in Figure 8.2-195, Figure 8.2-203, Figure 8.2-211, Figure 8.2-219, and Figure 8.2-227 for Test 6, and Figure 8.2-236, Test 7.

The large sweepout events calculated in the UPTF Test 6 and 7 benchmarks, but not seen in the measured data, are a direct result of the 1-D nodalization used in the lower plenum to simulate a highly multi-dimensional flow phenomenon during the refill phase. The calculated results confirm the conservatism of the S-RELAP5 lower plenum sweepout.

8.5.1.13 Steam Binding

Steam generator liquid entrainment was examined in the code assessments for CCTF (Section 8.2.13) and UPTF (Section 8.2.9). As discussed in Section 8.5.1.4 and Section 8.5.1.6, several input options are developed using UPTF 10B and 29B (Section 8.2.9.6) to assure an acceptable amount of liquid is entrained into the upper plenum, and carried over into the steam generator tube region during the reflood phase of a LBLOCA. One of the input options is the interphase drag bias which is applied at the tube inlet junctions. These input options are used in the SCTF and CCTF tests assessments. From the tests assessments, it can be concluded that S-RELAP5 entrains an acceptable amount of liquid into the steam generator tube region during the reflood phase of a LBLOCA.

8.5.1.14 Cold Leg Condensation

A cold leg condensation model was developed using several Westinghouse/EPRI 1/3-scaled Tests (Section 8.4.2.2.1), UPTF Test 8 (Phase A, Run 111 and Phase B, Run 112) (Section 8.4.2.2.2) and Test 25 (Section 8.4.2.2.3), to calculate a proper cold leg condensation rate during the accumulator and pumped injection period. The tests selected for this development generally cover both periods, and the input models used are similar to those used in the benchmarks discussed in Section 8.2. The condensation model consists of biases (multipliers) on the liquid and vapor side heat transfer coefficients that determine the condensation due to steam–water mixing. The condensation model is described in detail in Section 8.4.2 and a summary of the model is described below.

During cold leg condensation, due to ECC mixing with steam in the cold leg, the vapor side heat transfer primarily affects desuperheating of the steam. It was determined that

[

]. The condensation is primarily determined by the liquid side heat transfer and a void dependent multiplier, CONMAS, as shown in Figure 8.4-9. CONMAS is used to calculate the liquid temperature as it enters the downcomer. The ECC injection node void fraction is used to determine the value of CONMAS. It is applied to the intact cold leg piping, from the pump discharge location to the downcomer, and to the pump discharge side of the broken cold leg. Additionally, since the flow regime in the ECC injection location is highly complex, the non-stratified flow regime option is selected in the ECC injection node. During the accumulator injection period, the flow regime in the cold leg piping downstream from the injection location is generally slug (plug) flow and the void fraction is generally below 50 percent. During the pumped injection period, especially with the possibility of a single failure, the steam energy available will generally exceed the ECC condensation potential, the flow regime in the cold leg will usually be stratified, and the void fraction is high (80 to 95 percent). During this period, the liquid side heat transfer [

] With these input options, S-RELAP5 is found to calculate acceptable cold leg condensation for the selected UPTF and EPRI tests. These results are discussed in detail in Section 8.4.2.

Additional EPRI tests were simulated using S-RELAP5 and the results are discussed in Section 8.2.10. These input modeling options are used in all the benchmarks discussed in Section 8.0, where there is cold leg ECC injection, and are summarized in Table 8.5-4. This option will be used to model cold leg condensation in plant application cases.

In summary, S-RELAP5 calculates acceptable cold leg condensation during both the accumulator and pumped injection periods of a LBLOCA in a PWR.

8.5.1.15 Fuel Rod, Stored Energy, Gap Conductivity

The gap conductivity from the fuel performance code (COPERNIC2) under the fuel and system conditions calculated by S-RELAP5 is used throughout the transient evaluation. The fuel codes are considered best-estimate solutions to the thermal performance of the fuel rods and were benchmarked against experimental data (see Section 8.4.8), to determine any appropriate bias and uncertainty. Uncertainty in the prediction of gap conductivity is accounted for by the adjustment of the thermal conductivity of the fuel pellet. This adjustment is comprised of a burnup dependent bias and a sampled uncertainty, implemented at the beginning of the steady-state initialization for each case calculation and maintained throughout the transient. The adjustment controls the primary factor of the initial energy within the fuel pellet and also responds to the ability to transport energy to the coolant during the transient. The approach is considered acceptable for a best-estimate methodology and no further assessment is required.

8.5.1.16 Fuel Rod, Stored Energy, Axial and Radial Peaking

The axial and radial peaking is set conservatively for each case of the sample set. Radial peaking for the hot assembly and hot rod is set in accordance with plant technical specification maximums. Axial peaking is sampled, with a flat distribution, between that expected at normal operation for the hot rod and that which would provide a peak local heating rate equal to the F_q limit for the plant at the case burnup. The local power peak is a dominant factor in determining cladding temperature and oxidation responses. Off normal values for the local power result from plant maneuvering; they are time wise random occurrences and are rare. A realistic probability distribution would therefore be exponential in nature and the assumed flat distribution used in the RLBLOCA methodology is conservative and no further assessment is required.

8.5.1.17 Fuel Rod, Decay Heat

The RLBLOCA EM decay heat calculations are based on the ANSI/ANS 5.1-1979 standard (Reference 8.5-2). This standard is applicable to all light water reactors containing low enriched uranium as the initial fissile material. The selected approach to simulate fission product decay assures a representative, yet conservative, treatment. The fission product decay heat simulation and the basis for the conservatism of the approach are outlined below.



In order to treat the plutonium buildup effect conservatively and to ensure the finite irradiation curves are conservative, six different sensitivity studies, covering a range of cycle management and enrichment assumptions, were conducted. The six sensitivity studies included variations of spectrum hardness, boron concentrations, moderator temperature coefficient, enrichment, power density (average core versus hot rod), and

Figure 8.5-1 Decay Heat Comparisons, Infinite Operation U235, Finite Operation, All Isotopes



**Figure 8.5-2 Decay Heat Comparisons, Infinite Operation U235, Finite Operation, All
Isotopes**



**Figure 8.5-3 Decay Heat Ratios, Finite Operation Over Infinite Operation U235,
All Isotopes (0 to 10 seconds)**



**Figure 8.5-4 Decay Heat Ratios, Finite Operation Over Infinite Operation U235, All
Isotopes (0 to 600 seconds)**



8.5.1.18 Downcomer, Flow Pattern, CCFL, Slug Flow, and Non-Equilibrium

The downcomer LBLOCA phenomena of multidimensional flow patterns, CCFL and non-equilibrium flow primarily affect the refill period by influencing the duration of ECCS bypass.

UPTF Test 6 (Runs 131, 132, 133, 135, and 136) and Test 7 (Run 203) were designed specifically to examine downcomer countercurrent flow behavior during blowdown, ECC bypass, and lower plenum refill with cold leg ECC injection and they are included in assessment as documented in Section 8.2.9.3. The ECC injection is activated in a PWR during the end-of-blowdown and refill phases of a cold leg break LBLOCA transient. These interactions play a key role in determining the rate at which ECC water is able to refill the lower plenum.

The tests were analyzed to demonstrate the ability of S-RELAP5 to self-limit countercurrent flow in the downcomer and predict reasonable refill behavior, including ECC bypass compared to experimental data. For these runs, the UPTF system was configured to simulate the late blowdown and refill phases of a cold leg break PWR LBLOCA. These tests all were initiated with no water inventory in the lower plenum. Steam injected in the core region traveled downward to the lower plenum, and then exited the vessel via the downcomer and broken cold leg. An identical pattern of ECC injection was used for all the runs analyzed, with a constant injection rate into each of the three intact cold legs. A wide range of steam flow rates was used for the various runs and, depending on the downcomer steam flow rate, the ECC water entering the downcomer either bypassed to the broken cold leg, or penetrated downward to fill the lower plenum.

The following general observations regarding UPTF Tests 6 and 7 were found to be true for both the experiments and their corresponding S-RELAP5 simulations.

- Little water was delivered to the downcomer and lower plenum during the period that the intact cold legs were filling with ECC water. Only after the cold legs were filled did a significant amount of ECC penetration begin to the downcomer and lower plenum.
- When ECC penetration to the lower plenum did occur, the rate of that penetration tended to vary inversely with the rate of steam flow in the downcomer.
- During the period of ECC penetration, ECC water from the two cold legs opposite the broken cold leg tended to penetrate directly downward to the lower plenum. ECC water from the cold leg immediately adjacent to the broken cold leg tended to be bypassed to the broken cold leg.
- Highly unstable flow conditions were observed in the downcomer during the entire period of ECC injection.

The specific LBLOCA refill phenomena addressed by the analyses of Tests 6 and 7 include the following:

- Downcomer multi-dimensional effects: Both calculated steam flow and calculated ECC water flow are shown to distribute themselves azimuthally in multidimensional patterns that were consistent with test results.
- Downcomer countercurrent and slug flow: The various runs were performed with a wide range of downcomer steam flow rates, and with two-phase flow conditions including countercurrent and slug flow. In all cases, the code was demonstrated to conservatively (adequate to reasonable agreement with data) predict downcomer penetration of ECC water with the RLBLOCA lower plenum plant nodalization.
- Downcomer condensation and non-equilibrium flow: The various runs were performed with a wide range of ECC subcoolings (and downcomer condensation rates) and in all cases, the code was demonstrated to conservatively predict downcomer penetration of ECC water with the RLBLOCA plant lower plenum nodalization.

In summary, from the simulation results of UPTF Tests 6 and 7, it can be concluded that S-RELAP5 will conservatively calculate lower plenum sweep-out, lower plenum refill, and ECC bypass rates. This results in a conservative beginning of core recovery time during LBLOCA in a PWR. S-RELAP5 also calculates acceptable downcomer condensation rates due to steam-ECC water interaction.

8.5.1.19 Downcomer, Multi-D Phenomena

As discussed in the previous section, simulations of UPTF Tests 6 and 7 were used in part to verify the refill and ECC bypass flow behavior compared to experimental data. The comparisons showed that the multidimensional flow patterns of both steam and ECC liquid were consistent with test results. This indicates that the multidimensional phenomena in the downcomer are being properly included in the methodology.

8.5.1.20 Downcomer, Downcomer Boiling, Noding

Although boiling in the downcomer occurs during blowdown, the biggest potential for impact on clad temperatures is during late reflood following the end of accumulator injection. The impact of downcomer boiling is primarily dependent on the wall heat release rate and on the ability to slip steam up the downcomer and out of the break. The higher the downcomer wall heat release, the more steam is generated within the downcomer and the larger the impact on core reflooding. Similarly, the quicker the passage of steam up the downcomer, the less resident volume within the downcomer is occupied by steam, and the lower the impact on the downcomer average density. The ability to properly simulate downcomer boiling therefore depends on both the heat release (boiling) model, and on the ability to track steam rising through the downcomer.

The S-RELAP5 heat release modeling was validated by a sensitivity study on wall mesh point spacing and a benchmark against a closed form solution (see Figure 8.5-10). Steam tracking was validated through both an axial and an azimuthal fluid control volume sensitivity study done at low pressures (Reference 8.5-1). The axial nodding study was based on an ice condenser plant that is near atmospheric pressure during reflood. These studies demonstrated that S-RELAP5 delivers energy to the downcomer liquid volumes at an appropriate rate, and that the downcomer nodding detail is sufficient to track the distribution of any steam formed. The results indicated that the modeling accuracy within the RLBLOCA methodology is sufficient enough to resolve the effects of downcomer boiling and, to the extent that boiling occurs, the methodology properly resolves the impact on the cladding temperature and cladding oxidation rates. The required methodology for the prediction of downcomer boiling at system pressures approximating those achieved in plants with pressures as low as ice condenser containments was demonstrated.

8.5.1.21 Loop, Flow Oscillation

Loop flow oscillations arise when steam in the cold leg (post-blowdown) is condensed by cold ECC water and forms a liquid plug. The flow rate decreases and the cold leg flow transitions to the stratified flow regime, allowing the steam flow to increase again. This sweeps the liquid out again.

UPTF Test 8 was used to verify the S-RELAP5 cold leg condensation model. The model is applied to the ECC injection node and all downstream nodes in the intact loop cold legs. This includes the selection of the non-stratified option in the ECC injection nodes. The cold leg condensation model is summarized in Section 8.5.1.14.

The primary results from the comparisons of S-RELAP5 to the UPTF data for Test 8 Run 111 and Run 112 are listed below.

- The primary objective of the test simulation was to validate the adequacy of the prediction of the water temperature entering the downcomer, due to its effect on downcomer boiling during the post-accumulator injection period of a postulated LBLOCA. S-RELAP5 correctly predicted the cold leg liquid temperature for both runs.
- The S-RELAP5 calculated flow regimes are in general agreement with the thermocouple data from the tests.

It can be concluded that the S-RELAP5 cold leg condensation model correctly calculates the temperature of the water entering the downcomer during the reflood phase of a postulated LBLOCA, which will result in realistic calculation of loop flow oscillations.

Table 8.5-1 Methodology Treatment of Important PIRT Phenomena

--

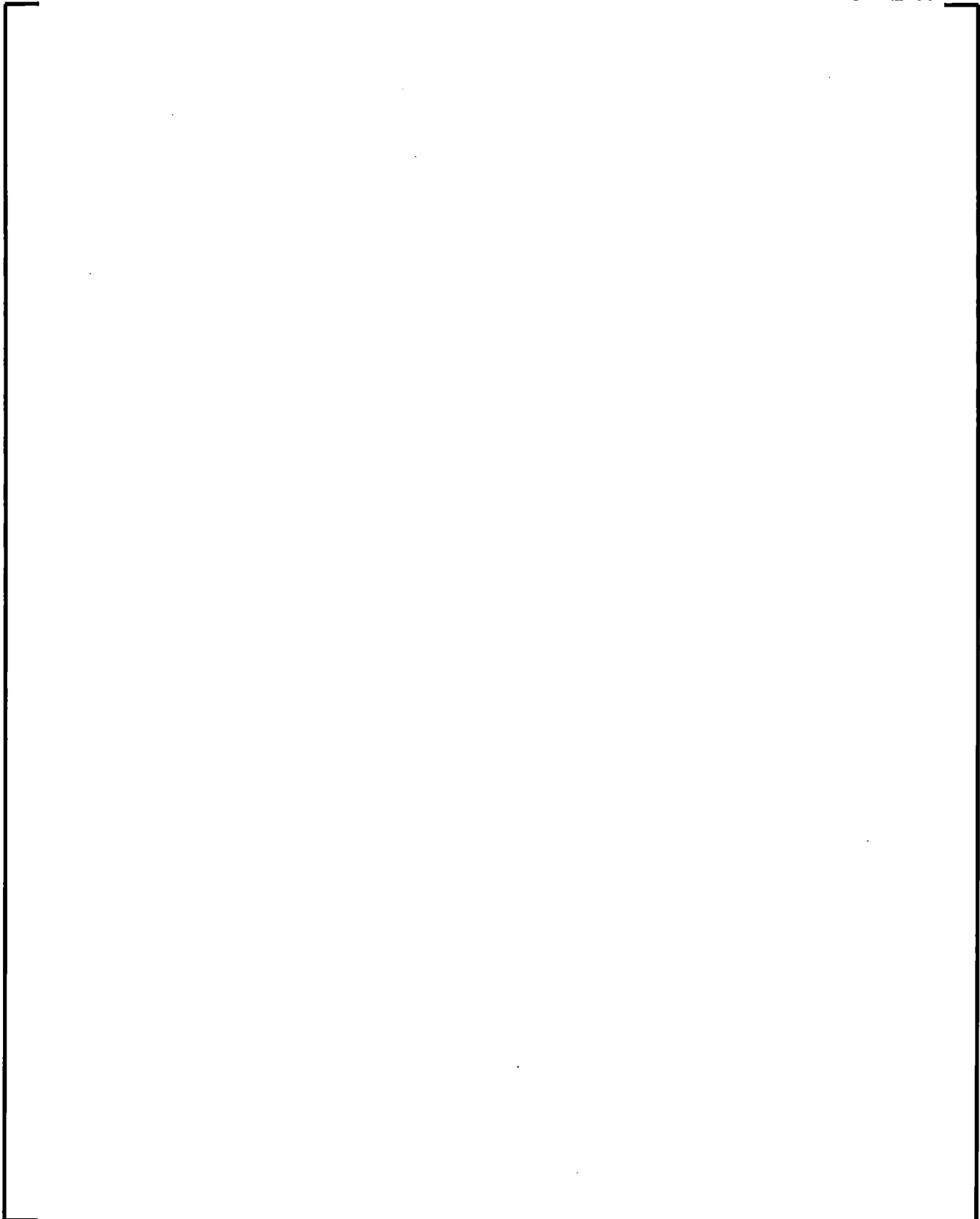




Table 8.5-2 Summary of Evaluated Uncertainties of Important PIRT Parameters

¹ [

]

8.5.2 Important PIRT Phenomena Treated Statistically

A summary, giving the parameter bias and uncertainty, and how they are to be applied in the methodology, is provided in this section. The determination of code or physical phenomena uncertainties is presented in Section 8.4. Other parameters treated statistically are discussed in detail, including background information, justification of the statistical approach and explanation of the objective of the statistical treatment.

Table 8.5-2 presents a summary of the key parameters treated statistically in the AREVA RLBLOCA methodology. The table lists the biases and provides a description of the statistical treatment of uncertainty for each key parameter.

8.5.2.1 Stored Energy

Revision 3 of the RLBLOCA methodology incorporates COPENIC2 (Reference 8.5-12) as the fuel performance code, from which the initial fuel conditions and the fuel thermal mechanical correlations are determined. This code is used for Uranium oxide fuel pellets with and without Gadolinia.

The analysis of stored energy uncertainty was performed in Section 8.4.8 by assessing COPENIC2 predictions for centerline fuel temperature relative to data (see data discussion in Reference 8.5-13). The assessment was established as a bias and an uncertainty in the form of the difference of measured and predicted temperatures ratioed to the predicted temperatures. For the development in Section 8.4.8, the form was:

$$\frac{(T_{Predicted} - T_{Measured})}{T_{Predicted}}$$

This gives an adjustment proportional to the magnitude of the predicted centerline fuel temperature, and is easy to apply within a code structure. The $(T_{Predicted} - T_{Measured})$ means the negative of the adjustment is provided.

COPERNIC2 is an NRC-approved current generation fuel performance code. The assessment database used to develop the bias and uncertainty for the RLBLOCA methodology was incorporated in the code approval. The approval resulted in the assignment of a zero bias and, for deterministic evaluations, a 71 °C increase in the centerline fuel temperature to achieve a 95/95 prediction. This adjustment is an absolute and not dependent on the magnitude of the prediction. For RLBLOCA, it is replaced with a proportional adjustment of the form $(T_{\text{Predicted}} - T_{\text{Measured}})/T_{\text{Predicted}}$. [

]

In line with the realistic treatment of uncertainty, the adjustment is sampled separately for each member analysis of the case set and is sampled as a positive and a negative adjustment. Figure 8.5-9 gives the uncertainty used in the methodology as a cumulative distribution in comparison to the actual cumulative distribution of the benchmarked database. Within the range of negative adjustments to temperature, the adjustment is somewhat less than the data would justify making the methodology slightly conservative.

8.5.2.2 Oxidation

Energy released through the oxidation of cladding is calculated using the Cathcart-Pawel correlation (Reference 8.5-3) for oxide layer growth:

$$\frac{\delta_{\phi}^2}{2} = 0.01126 \cdot e^{\frac{35890}{R \cdot T}}$$

where R is the universal gas constant (1.987 cal/mole-K) and T is clad temperature.

This is given in Section 7.9.3.5 as:

$$\frac{\delta \Delta r_{\phi}}{\delta t} = \left(\frac{0.000002252}{2 \Delta r_{\phi}} \right) e^{\frac{18062}{T}}$$

In Reference 8.5-3, uncertainties are provided for both the constant term and the exponential term. The natural logarithm of the constant term has a normal distribution. The standard deviation for the constant term is determined from its estimated value and the confidence interval given in Reference 8.5-3. The estimated value is -4.48868 with a 90% confidence interval from -4.74691 to -4.23045 (Table A4 of Reference 8.5-3). The one-sided 90% confidence interval corresponds to a critical value $z=1.645$ on the standard normal curve (Reference 8.5-4, page 791); hence, the standard deviation is $(-4.74691+4.48868)/1.645 = 15.698\%$. Similarly, with a normally distributed exponential term, the standard deviation is $2.2\% \div 1.645 = 1.337\%$.

[

]

8.5.2.3 Departure from Nucleate Boiling

Results from the THTF Heat Transfer SETs contributed to identifying a bias in the Biasi CHF correlation (Section 8.4.4). [

] The CHF scaling

is applied for RLBLOCA calculations, and the statistical information on heat transfer is used along with other test data to derive the uncertainty parameters on film boiling and dispersed flow film boiling heat transfer (Section 8.5.2.4).

8.5.2.4 Core Post-CHF Heat Transfer

The post-CHF heat transfer model now includes provisions for thermal radiation between structures (rod-to-rod). This adds to the current model which already includes thermal radiation from structures to the fluid (rod-to-droplets and rod-to-steam). The rod-to-rod radiation model is only applied to the hot rod since its power level is elevated compared to its surroundings. Applying rod-to-rod radiation exclusively to the hot rod logically leads to the development of separate heat transfer uncertainties for the hot rod and the rest of the core.

The core wide heat transfer uncertainty was developed from code comparisons using the FLECHT-SEASET reflood test data as discussed in Section 8.4.1. These comparisons were used to derive the heat transfer multipliers that are applied to film boiling (FILMBL) heat transfer and dispersed flow film boiling heat transfer (DFFBHTC).

[

]

² [

]

[

].

[

]

[

]

[

]

[

] The distribution was integrated to form the cumulative probability, which compared favorably with a [

] However, the uncertainties from the low pressure reflood multipliers FILMBL and DFFBHTC conservatively bound the 2σ interval from the high pressure multiplier. The low pressure reflood multipliers and biases will therefore be applied to the post-CHF heat transfer for the entire LBLOCA event.

The single-phase vapor heat transfer was assessed in Section 8.2.4 and [

] in the FLECHT-SEASET, FLECHT Skewed and THTF assessments. The results from those assessments did not show adverse or unrealistic behavior or temperatures. Based on this analysis, the single-phase vapor heat transfer is unbiased.

The assessments that were used in the bias and uncertainty determinations previously discussed used [

]

8.5.2.5 T_{\min}

A set of seven FLECHT-SEASET tests was used to evaluate the trends in T_{\min} at low pressure. Quench temperatures improve at higher pressures; hence, a T_{\min} uncertainty based on low pressure data was expected to bound high pressure data. This was validated in the Reference 8.5-1 methodology with data from ROSA/TPTF, the ORNL/THTF, and the Westinghouse G1/G2 tests. Examination of FLECHT-SEASET data showed that, based on observable conservatisms, only the 3 inch/s reflood rate test (Test Number 31302) was necessary to evaluate a bounding T_{\min} uncertainty (Section 8.4.7).

From the FLECHT-SEASET data and from an evaluation of code uncertainty with regard to how the LBLOCA multiplier relates to T_{\min} , [

]. The uncertainty

evaluation was demonstrated to be a conservative bounding distribution relative to other datasets.

8.5.2.6 Break Flow

Break flow is a function of break area and critical flow uncertainty. [

] The S-RELAP5 HEM critical flow model applied in this methodology was assessed by comparison to full-scale critical flow tests at the Marviken facility, Sections 8.2.7 and 8.4.5. From these assessments, [

]

8.5.2.7 Accumulator Discharge

Accumulator discharge can be influenced by piping flow resistances and pressure. Most plants provide best-estimate data that may be used to accurately model flow resistance; hence, the largest uncertainty to accumulator discharge is accumulator pressure. To support the technical specification of a plant for accumulator pressure and liquid inventory ranges, these parameters are sampled over the technical specification ranges, using a uniform probability distribution.

8.5.2.8 Reactor Vessel Hot Walls

The heat release from the reactor vessel walls affects the ECC bypass during the early refill phase of a LBLOCA when the primary system is depressurizing. During the reflood phase, the heat release from the downcomer walls affects downcomer boiling. The results from UPTF Tests 6 and 7 (Section 8.2.9.3) demonstrated that S-RELAP5 will overpredict ECC bypass; however, the downcomer wall temperature was much lower than would be expected in an actual operating plant. The hot wall effects can therefore only be partially evaluated using these tests. The hot wall effect can be separated out since it is expected that there is a direct relationship with the degree of nucleate boiling in the downcomer and ECC bypass. To maximize the hot wall effect, heat transfer in the downcomer can be locked into nucleate boiling during the refill phase by raising the CHF point to a high value. In the AREVA NP RLBLOCA methodology, the hot wall effect during the refill phase [

].

During the reflood phase, the downcomer vessel wall heat release is conduction limited and depends on the mesh spacing used in the S-RELAP5 input model. The mesh spacing used to model the downcomer vessel was verified by using a simple benchmark having a closed form solution. The results, shown in Figure 8.5-10, show that S-RELAP5 will adequately calculate the heat release from the downcomer vessel wall during the reflood phase of a LBLOCA in a PWR.

8.5.2.9 Containment Pressure

Containment pressure is reached [

]. A

conservative containment pressure for the post-blowdown portion of a LOCA implies a low containment pressure, which is conservative since it results in an increase in steam binding, and therefore reduces reflood rates to the core. Reduced reflood rates means a longer transient, and therefore, higher cladding temperatures. [

]

8.5.2.10 Upper Head Temperature, Initial Coolant Temperature

This is the initial temperature in the upper head of the reactor vessel. Plant data are examined to determine an average operating temperature, and uncertainty range.

During the case runs, the temperature is adjusted over the uncertainty range by adjusting the flows into and out of the upper head region of the reactor vessel. The value for the upper head temperature corresponds to the expected operating conditions of the plant and requires no further assessment.

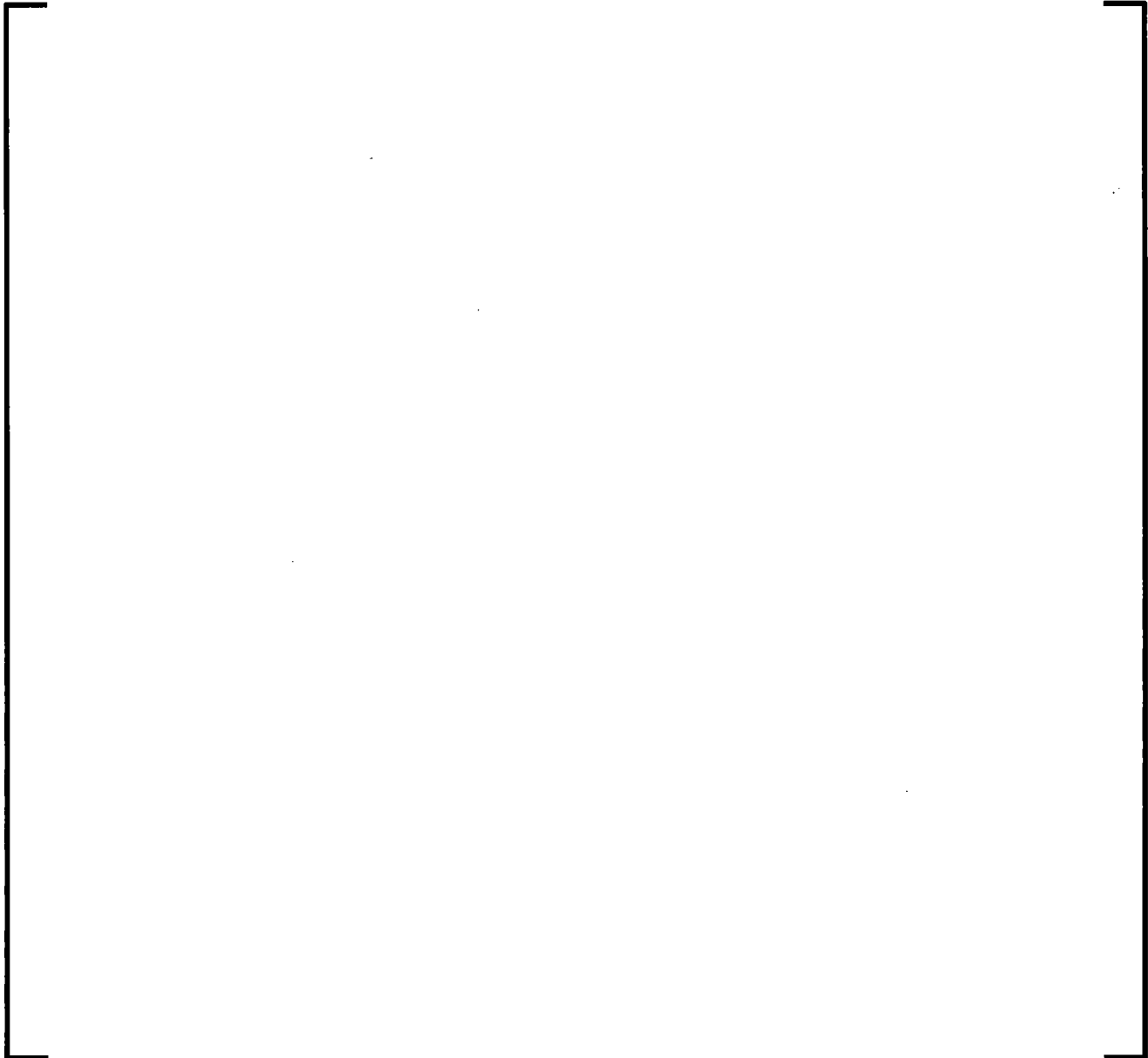
8.5.2.11 Fuel Swelling, Rupture and Relocation

[

]

8.5.2.11.1 [

].



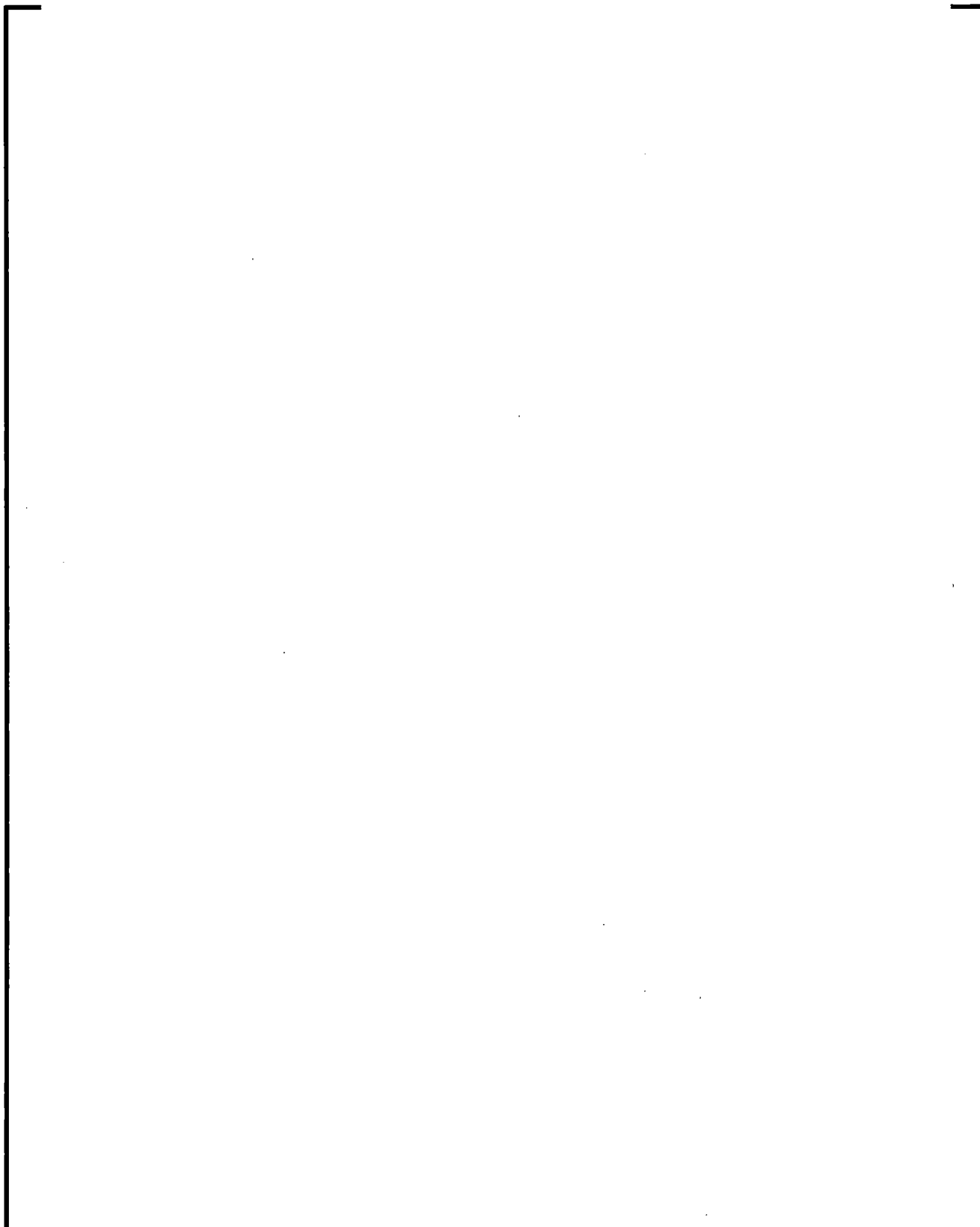


**Figure 8.5-5 Rupture Temperature Data and Dunn's M5
Rupture Temperature Correlation from BAW-10227
(Ref. 8.5-8: p. K-35)**



Cladding Strain Uncertainty

The data for rupture strain indicates that it is a highly stochastic parameter, but boundaries of the expected strain can and have been developed. [

**Figure 8.5-6 M5 Slow Ramp Correlations with
Supporting Rupture Strain Data**

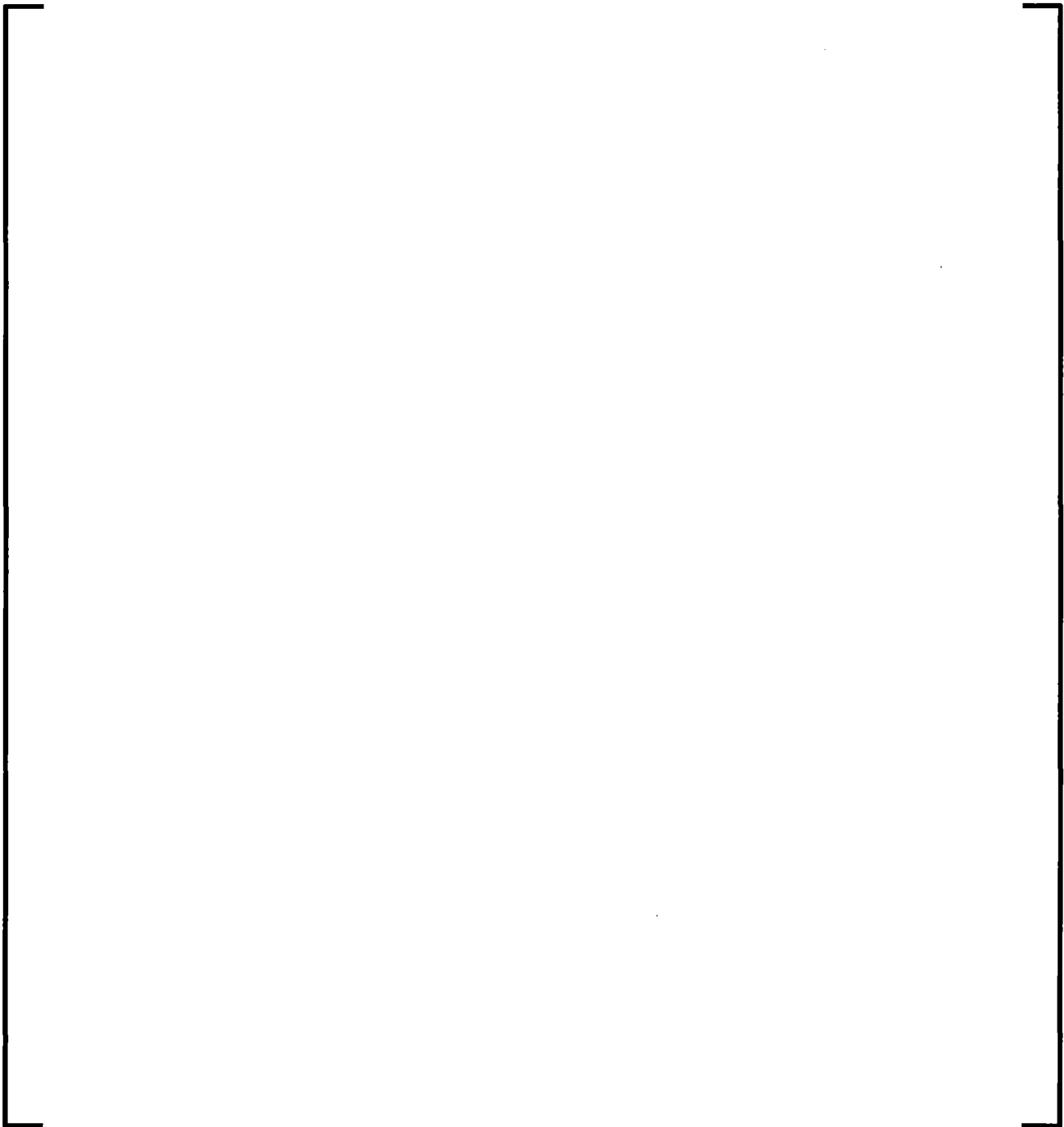




Figure 8.5-8 Packing Factor Data and Fits





Table 8.5-3 Packing Factors and Sources

1

2

3

4

5

6

7

8

9

10

11

12

13

14

15

16

17

18

19

20

21

22

23

24

25

26

27

28

29

30

31

32

33

34

35

36

37

38

39

40

41

42

43

44

45

46

47

48

49

50

51

52

53

54

55

56

57

58

59

60

61

62

63

64

65

66

67

68

69

70

71

72

73

74

75

76

77

78

79

80

81

82

83

84

85

86

87

88

89

90

91

92

93

94

95

96

97

98

99

100

101

102

103

104

105

106

107

108

109

110

111

112

113

114

115

116

117

118

119

120

121

122

123

124

125

126

127

128

129

130

131

132

133

134

135

136

137

138

139

140

141

142

143

144

145

146

147

148

149

150

151

152

153

154

155

156

157

158

159

160

161

162

163

164

165

166

167

168

169

170

171

172

173

174

175

176

177

178

179

180

181

182

183

184

185

186

187

188

189

190

191

192

193

194

195

196

197

198

199

200

201

202

203

204

205

206

207

208

209

210

211

212

213

214

215

216

217

218

219

220

221

222

223

224

225

226

227

228

229

230

231

232

233

234

235

236

237

238

239

240

241

242

243

244

245

246

247

248

249

250

251

252

253

254

255

256

257

258

259

260

261

262

263

264

265

266

267

268

269

270

271

272

273

274

275

276

277

278

279

280

281

282

283

284

285

286

287

288

289

290

291

292

293

294

295

296

297

298

299

300

301

302

303

304

305

306

307

308

309

310

311

312

313

314

315

316

317

318

319

320

321

322

323

324

325

326

327

328

329

330

331

332

333

334

335

336

337

338

339

340

341

342

343

344

345

346

347

348

349

350

351

352

353

354

355

356

357

358

359

360

361

362

363

364

365

366

367

368

369

370

371

372

373

374

375

376

377

378

379

380

381

382

383

384

385

386

387

388

389

390

391

392

393

394

395

396

397

398

399

400

401

402

403

404

405

406

407

408

409

410

411

412

413

414

415

416

417

418

419

420

421

422

423

424

425

426

427

428

429

430

431

432

433

434

435

436

437

438

439

440

441

442

443

444

445

446

447

448

449

450

451

452

453

454

455

456

457

458

459

460

461

462

463

464

465

466

467

468

469

470

471

472

473

474

475

476

477

478

479

480

481

482

483

484

485

486

487

488

489

490

491

492

493

494

495

496

497

498

499

500

501

502

503

504

505

506

507

508

509

510

511

512

513

514

515

516

517

518

519

520

521

522

523

524

525

52

8.5.3 Application of Code Biases

This section summarizes the biases applied to the assessments presented in the previous sections. The biases were developed from uncertainty analyses performed on the SETs. In most instances, each bias developed has an uncertainty associated with it, but the uncertainties were not included in the assessments.

The biases listed below were taken from Table 8.5-2:

--	--

³ [

]

⁴ [

]

⁵ [

]

Listed in Table 8.5-4 are the assessments and the biases used in those assessments.

[

]

Table 8.5-4 Biases Used in Assessments

6 []
7 []
8 []
9 []
10 []

]

]

]

8.5.4 References

- 8.5-1 EMF-2103(P)(A) Revision 0, Realistic Large Break LOCA Methodology, Framatome ANP Richland, Inc., April 2003.
- 8.5-2 ANSI/ANS-5.1-1979, American National Standard for Decay Heat Power in Light Water Reactors, approved August 29, 1979.
- 8.5-3 J. V. Cathcart and R.E. Pawel, Zirconium Metal-Water Oxidation Kinetics: IV. Reaction Rate Studies, ORNL/NUREG-17, August 1977.
- 8.5-4 Kreyszig, E., Advanced Engineering Mathematics, Second Edition, John Wiley & Sons, Inc., 1967.
- 8.5-5 NUREG/CR-2256, EPRI NP-2013, WCAP-8891, FLECHT-SEASET Program, PWR FLECHT SEASET Unblocked Bundle, Forced and Gravity Reflood Task Data Evaluation and Analysis Report, November 1981.
- 8.5-6 EMF-2102(P) Revision 0, S-RELAP5 Code Verification and Validation Document, Framatome ANP Richland, Inc., August 2001.
- 8.5-7 D. A. Powers and R. O. Meyer, NUREG-0630, Cladding Swelling and Rupture Models for LOCA Analysis, US Nuclear Regulatory Commission, Washington D.C., April 1980.
- 8.5-8 D. B. Mitchell and B. M. Dunn, BAW-10227, Evaluation of Advanced Cladding and Structural Material (M5) in PWR Reactor Fuel, AREVA, Lynchburg, Virginia, February 2000.
- 8.5-9 L. J. Siefken, Axial Fuel Relocation in Ballooning Fuel Rods, Transactions of the 7th International Conference on Structural Mechanics in Reactor Technology, Chicago, Illinois, August 1983.

- 8.5-10 NEA/CSNI/R(2010)6, Benchmark Calculations on Halden IFA-650 LOCA Test Results, Organization for Economic Co-Operation and Development (OECD) – Nuclear Energy Agency (NEA), November 2010.
- 8.5-11 B. C. Oberlander, M. Espeland, N. O. Solum, H. K. Jenssen, LOCA IFA650-4: Fuel Relocation Study, LOCA Workshop/HPG Meeting, Prague, September 2007.
- 8.5-12 BAW-10231P-A, Revision 1, COPENIC Fuel Rod Design Computer Code, Framatome ANP, January 2004.
- 8.5-13 EPRI-294-2. Mixing of ECC Water with Steam: 1/3 Scale Test and Summary. June 1975.
- 8.5-14 NUREG-1230. Compendium of ECCS Research for Realistic LOCA Analysis. December 1988.

[illegible]

[REDACTED]

**Figure 8.5-9 COPENIC2 Cumulative Centerline Fuel
Temperature Error Distribution**

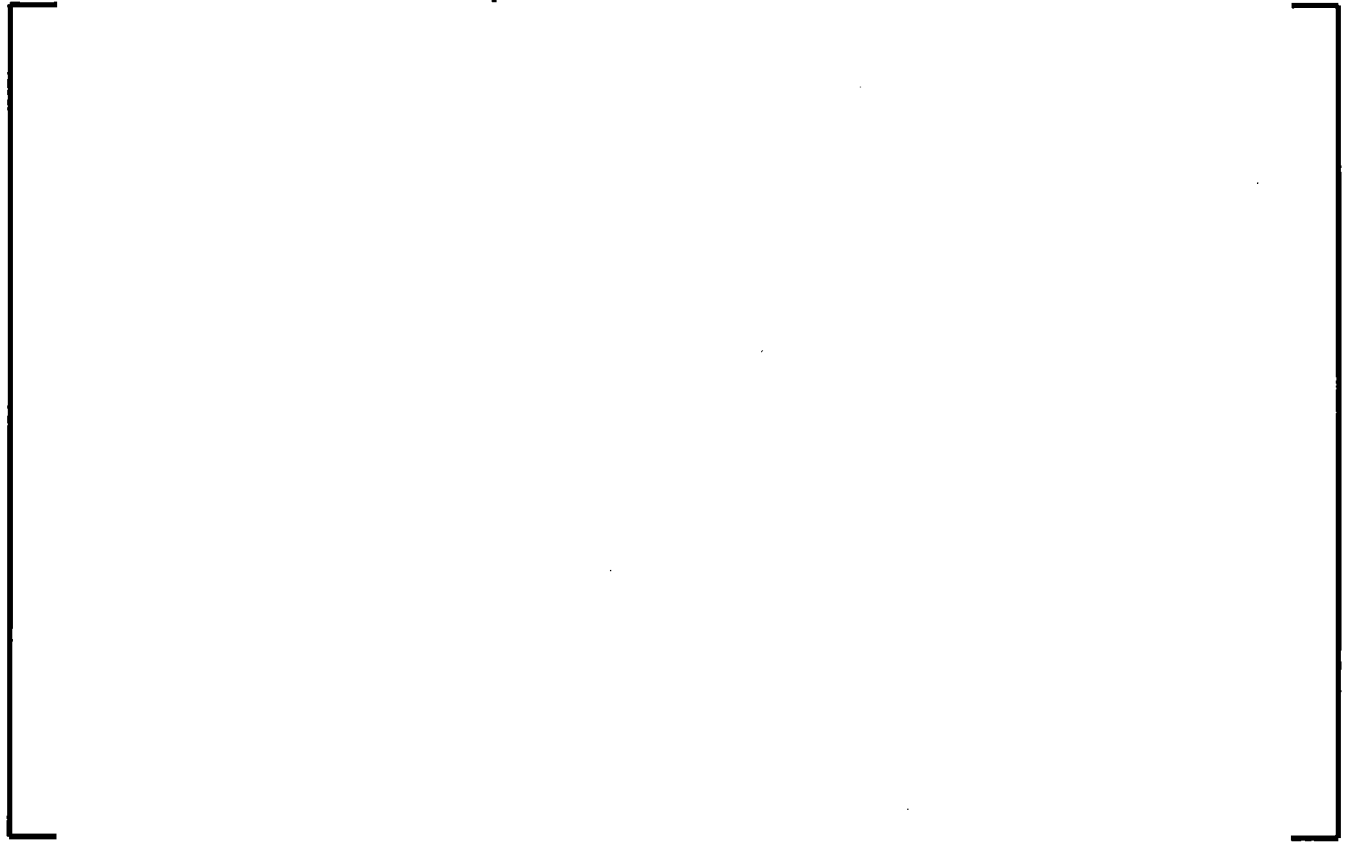
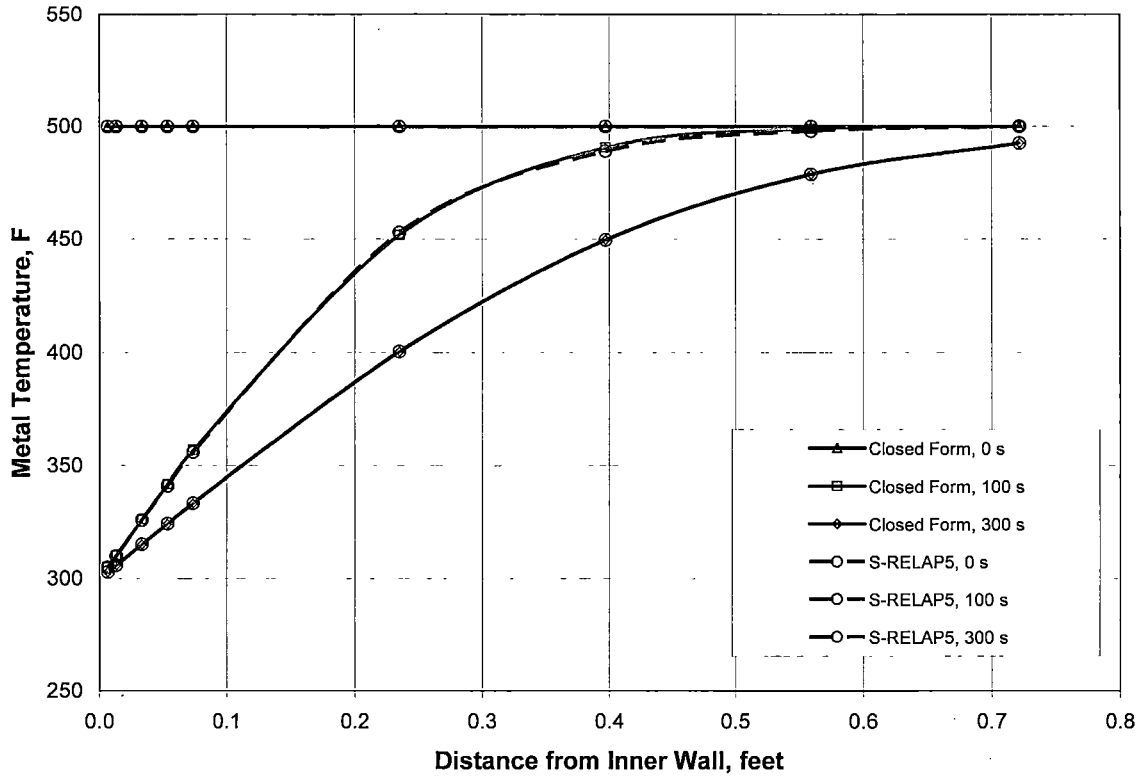


**Figure 8.5-10 Temperature Distribution in the Vessel
Wall – S-RELAP5 versus Exact Solution**



8.6 *Model Scalability Assessment*

The basis for the analysis of a LBLOCA is the entire methodology being used, not just the base code, S-RELAP5. S-RELAP5 is referenced in this section and is defined as the combination of the code and the associated methodology. As noted in Appendix C of Reference 8.61, there are two premises upon which the scalability of the methodology is based. The first premise is that the tests are scalable to an LBLOCA. The second premise is that the models in S-RELAP5 and their implementation result in scalability of the code predictions. In order for the first premise to be true, the selection of tests needs to be so that all of the important phenomena in a PWR LBLOCA are captured by one or more appropriately scaled tests. In order for the second premise to be true, the phenomenological models in S-RELAP5 should apply to both the PWR LBLOCA and the scaled test.

Throughout the assessment program, documented in Section 8.0, S-RELAP5 was used to simulate a variety of tests. These tests are a significant portion of the basis for the RLBLOCA methodology, having been used to demonstrate the ability of S-RELAP5 to predict the test outcomes. There are no tests that exist to fully replicate a LOCA at full-scale because of the cataclysmic nature of a design-basis LBLOCA. All of the IETs and some of the SETs are scaled. One exception is the UPTF, which is full-scale, but has no core and no steam generators. The ability of the scaled tests to capture the phenomena of a LBLOCA is then pivotal to the applicability of the assessments for S-RELAP5.

8.6.1 Test Scaling

Since tests are scaled to preserve certain features of the full-scale phenomena, tests with different scaling are used to address different phases or aspects of an LBLOCA. If a test is considered appropriately scaled for the phenomena of interest, then assessment conclusions to that data is considered applicable to the full-scale NPP. A common scaling approach, power-to-volume ratio, was shown (Reference 8.61) to preserve system response results as considerably similar under most circumstances. Its application and other approaches are discussed in reference to specific portions of the methodology in the following subsections.

8.6.1.1 Blowdown

Power-to-volume scaling for the blowdown period was demonstrated in Reference 8.61. Five system tests, with powers from $1/48^{\text{th}}$ of a typical PWR to $1/30,000^{\text{th}}$, were used as a basis for the comparison. Each of these facilities was scaled so the ratio of power to volume was preserved. The peak temperature during blowdown was plotted as a function of linear power for each of these test facilities. The measured peak temperatures all fell within 350 °F of a linear regression line (temperature versus LHGR). The data scatter for a single facility was as great as, or greater than, any differences between facilities. As a result, it is concluded that tests which preserve the power-to-volume ratio of a PWR will scale properly for the blowdown phase of the LBLOCA.

8.6.1.2 Refill

During refill and early reflood, scale dependent multi-dimensional flow behavior has been observed in the downcomer for facilities using power-to-volume scaling. The Semiscale and LOFT facilities were compared for analogous tests in Reference 8.6-3. Under ideal scaling, the two tests should have shown the same behavior. However, during the refill portion of the simulation, the downcomer flow was observed to be generally upward for the Semiscale test before the pressure increase accompanying the emptying of the accumulator. For the analogous test in the LOFT facility, the flow was asymmetric; downward for the regions near the intact loop and upward for the region near the broken loop. This was attributed to differences in the downcomer gap and the distance between the cold leg penetrations. This allows multi-dimensional flow effects to dominate the flow in the LOFT facility, whereas they do not occur to the same extent in the Semiscale facility. The downcomer gap, volume and surface area-to-fluid volume ratios do not scale between these two facilities in such a way as to preserve the transit time and the heat transfer to the fluid from the walls.

The UPTF facility (see Section 8.2.9) was designed to simulate a four-loop 3900 MWt PWR primary system and to provide a full-scale simulation of thermal-hydraulic behavior in the primary system during the end of blowdown and refill phases of a PWR LBLOCA. The reactor vessel, the core barrel, and the greater part of the vessel internals are full-sized representations of the reference PWR, as well as the four hot and cold legs that simulate three intact loops and one broken loop. The dimensions of the test vessel are those of the reactor pressure vessel of the reference PWR, with the exception that the vessel wall is thinner. The downcomer annulus, which is formed by the vessel wall and the core barrel, has a gap width that varies from 0.25 meters (0.82 feet) in the lower part to 0.21 meters (0.69 feet) in the upper part. The loop geometry and flow areas correspond to the 4-loop PWR.

With the exception of the wall thickness, the UPTF is full-scale. The hot-wall effect should be slightly under-estimated, because of the slight reduction in vessel mass and stored energy. However, there is ample amount of metal in the vessel so that the UPTF tests are applicable to the refill portion of a LBLOCA.

8.6.1.3 Reflood

Scaling issues associated with reflood were addressed in Reference 8.6-1, where the effects of refill scaling were removed from the data by comparing the temperature rise to reflood rates. The temperature rise considered is the change from the beginning of reflood to the PCT. Temperature rise data were collected for eight facilities with volumes scaled from 1/21 to 1/1700. All were power-to-volume scaled. Figure 34 of Reference 8.6-1 compares the temperature rise for all eight facilities to the reflood rate. The data were fit with a regression relation and the tolerance bands added. As with the blowdown data, the spread in the data for a single facility was as great as or greater than the difference between the facilities. Tests which scale by maintaining the power-to-volume are applicable to the reflood phase of a LBLOCA.

8.6.2 Code Scaling

The issue of code scaling is primarily determined by the ability of the correlations and closure relations used to describe complicated thermal-hydraulic phenomena that are not treated from a mechanistic, theoretical approach. Generally, phase transitions, heat transfer, phasic interactions, and CHF fall in this category. The models, correlations, and closure relations used in S-RELAP5 are described in Section 7.0. The numerical implementation may be subject to scaling issues to a lesser extent. Issues of numerics are generally treated by addressing the converged nature of the nodalization and time step criteria. This demonstrates that the computer code can solve the mathematical model correctly over the applicable range for the tests and an LBLOCA. This leaves the issue of scaling of the correlations and the closure relations employed in LBLOCA analysis.

Code scaling evaluation will focus on those items identified by the sensitivity studies of PIRT phenomena as having the greatest impact on LBLOCA. Table 6-1 shows the results of sensitivity studies on the PIRT phenomena in a PWR LBLOCA. The models, related to these phenomena, and the scalability of each of these models, are discussed in the following paragraphs.

Items related to fuel rod performance are not affected by scaling, because the basis for the fuel-stored energy and dynamic response are based on COPENIC2 (Reference 8.6-2), which was benchmarked to data from actual fuel rods.

8.6.2.1 Post-CHF and Reflood Heat Transfer

When heat flux from the fuel rods and any other metal masses exceeds the CHF, the heat transfer is calculated using correlations specific to the heat transfer regimes. The single-phase vapor, transition boiling and film boiling regimes constitute the post-CHF heat transfer regimes. For each of these regimes, the effects of radiation heat transfer also are considered.

Single-phase vapor heat transfer is the maximum of the Wong-Hochreiter correlation for forced flow regimes (turbulent and laminar) and the turbulent natural convection heat transfer recommended by Holman, as described in Sections 7.7.5 and 7.7.8. The Wong-Hochreiter correlation generally determines the heat transfer.

The natural convection heat transfer model is based on data from the flow between vertical plates. If the boundary layer is small compared to the diameter of the rod, then heat transfer through this layer would be very similar to that through the boundary layer on a plate. With the Prandtl number near unity and the rod diameter large compared to the boundary layer, the Holman formulation for natural convection heat transfer used in S-RELAP5 applies as long as

$$\frac{D}{L} \geq 35 \cdot Gr^{-0.25}$$

where D is the rod diameter, L is the length used in calculating the Grashof number, and Gr is the Grashof number. When these conditions are met, the flat plate solution does not differ by more than 5 percent from the solution for the cylinder. In the turbulent flow regime, this implies $0.02 \leq D/L \leq 0.2$. For a 17x17 fuel design, with a pin diameter of 0.376 inches, the length can be as low as 1.9 inches and as large as 19 inches. Within the RLBLOCA methodology, normal heat transfer lengths in the core [

] These fall within the range of applicability of the natural convection heat transfer correlation.

The Wong-Hochreiter correlation was developed from steam cooling tests performed on the FLECHT-SEASET test facility. Consequently it is scaled to the desired geometry. The steam temperature data was taken at low pressure, and temperature for Reynolds numbers ranging from 3,000 to 20,000, with provisions for lower Reynolds numbers. The Reynolds and Prandtl numbers are functions of thermodynamic and transport properties, and scale appropriately with pressure and temperature. Figure 8.6-1 shows the data from Figure 4-10 of Reference 8.6-4 along with the Wong-Hochreiter fit. In this figure, the Dittus-Boelter correlation (Reference 8.6-5) is shown for comparison to demonstrate its inadequacy when applied to tube bundle geometries.

In conclusion, the model for single-phase vapor heat transfer used in S-RELAP5 can be applied to a full-scale PWR LBLOCA.

Transition boiling is not really a heat transfer regime in the sense that it can be characterized by a homogeneous, steady, heat transfer mechanism. It is a combination of dynamically varying heat transfer mechanisms, including nucleate boiling, film boiling and vapor heat transfer. The amount of time a region spends in one of these heat transfer modes determines the effective heat transfer rate. Few measurements are available for transition boiling heat transfer and they do not cover a wide range. Additionally, the unsteady nature of the process makes modeling the process challenging.

Despite the complexity of this regime, exact modeling of the transition boiling heat transfer is not particularly important for an LBLOCA because most volumes in the core move through this heat transfer regime rather quickly, and are not sensitive to the details of the modeling. The main requirement for simulating an LBLOCA is so that the point at which the code predicts the beginning and end of the transition region will be reliable. Additionally, the heat transfer in the transition region should be significantly better than the vapor heat transfer and it should remain below the CHF. The value of CHF in this region is computed using the modified Zuber CHF correlation (Section 7.7.4).

The major assumption in modeling this regime is that it can be modeled by a combination of steady-state boiling heat transfer to liquid and convective heat transfer to vapor. In this model, the heat flux is bounded by the CHF at the lowest wall temperatures, and it approaches the flux based on single-phase vapor heat transfer as the wall temperature rises. The heat transfer is based on a modified Chen correlation for transition heat transfer (Section 7.7.6). This model makes a smooth transition from the CHF to the single-phase vapor heat transfer, with the calculated fraction of liquid heat transfer based on the wall temperature. The Chen correlation was tested against data and behaves adequately, which is sufficient for LBLOCA transition boiling.

Film boiling occurs when the wall temperature exceeds the minimum temperature for stable film boiling and the void fraction lies in the appropriate range. The coolant consists of vapor and water droplets in this mode. The heat transfer mechanisms consist of boiling heat transfer to liquid droplets, convective heat transfer to vapor, and radiative heat transfer to droplets and vapor.

[

]

[

]

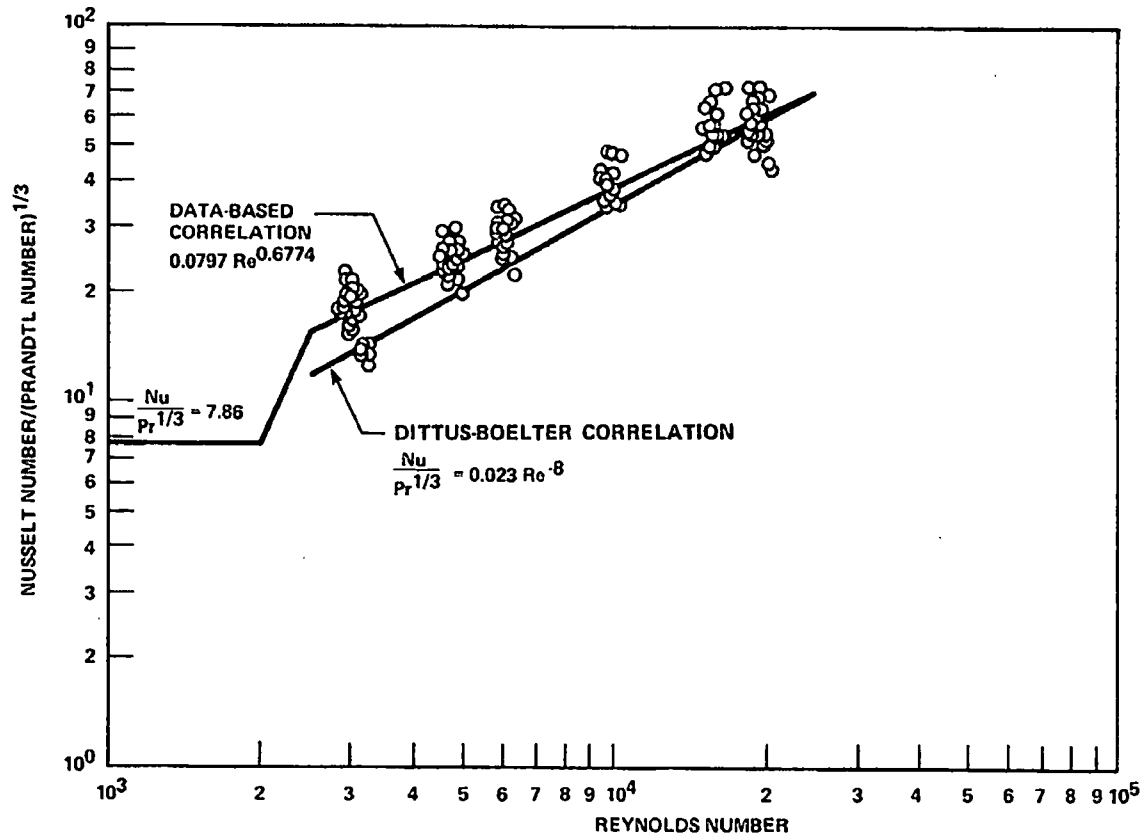
[

]

[

]

**Figure 8.6-1 Data Based Nusselt Number versus Reynolds Number
for FLECHT-SEASET Steam Cooling Tests Compared with
Dittus-Boelter Correlation**



8.6.2.2 Scaling from Tests

While analytical arguments (see prior section) can provide a basis for code scaling for selected cases, frequently the issue of scaling needs to be addressed by a comparison to test data. Code scaling and the tests making up the basis are discussed in the following paragraphs.

8.6.2.2.1 Film Boiling Heat Transfer

A series of tests was performed in the THTF at Oak Ridge National Laboratory to measure heat transfer at higher pressures and flows. These included 22 steady-state dry-out tests (Section 8.4.4), three transient boil-off tests (Section 8.2.1), and two sets of transient reflood tests (also Section 8.2.1). The reactor core was simulated by an 8x8 array of heated rods with dimensions corresponding to those of a Westinghouse 17x17 fuel assembly. The axial power shape was uniform. The FLECHT-SEASET used 161 full-length simulated fuel rods and axially-dependent power shapes (Section 8.2.3). Based on rod count, these two test facilities differ by a scaling factor of 2.5.

These tests were used to evaluate the film boiling heat transfer. Table 8.6-1 compares the ranges for LBLOCA calculations for parameters that affect heat transfer with the ranges covered by the THTF tests and FLECHT-SEASET. Given the near prototypic nature of the fuel rod simulators and the extent to which the tests span the applicable ranges for LBLOCA, it is concluded that the heat transfer models, including correlations and closure relations, in S-RELAP5 are sufficient to allow direct application to a PWR LBLOCA and that the uncertainties obtained from these tests are applicable.

8.6.2.2.2 *Core Entrainment*

Entrainment of water droplets by the steam flow in the core can affect the predicted core cooling flow. The primary determinant of entrainment is the drag exerted on the liquid droplets by the steam flowing up out of the core. This drag, in turn, depends on the vertical flow regime in the core model. The determinants of the model applicability to a PWR LBLOCA are primarily local and, in the core, principally related to the conditions within the flow channel between the fuel rods. The axial effects predominate in this phenomenon. Radial redistribution is a second-order effect, in that it makes fluid available in a channel or removes it. The RLBLOCA methodology makes use of the TWODEE component in S-RELAP5 to model the radial behavior in the core.

The tests used in the assessments, CCTF (Section 8.2.13), FLECHT-SEASET (Section 8.2.3), and THTF (Sections 8.2.1 and 8.4.4), use bundles of full-length fuel rods. ACHILLES (Section 8.2.15) also used full-length rods, but the gaps between the rods and the piping containing the rods caused some radial flow redistributions which made it less suitable for confirming scaling of core entrainment. The LOFT (Section 8.3.1 and Semiscale Test S-06-03 (Section 8.3.2) cores were too short for entrainment scaling. Based on the comparisons to CCTF, FLECHT-SEASET and THTF, the core entrainment model in S-RELAP5 is conservative and will scale suitably to a full-scale PWR LBLOCA.

8.6.2.2.3 *Critical Flow at Break*

The choked flow model used for AREVA NP RLBLOCA analyses is the homogeneous equilibrium model (HEM). Choking for break flow occurs when the flow velocity reaches the speed of sound at the break. The critical flow model is not scale dependent; however, the Marviken Full-Scale Critical Flow Test data were used to determine the S-RELAP5 critical flow multipliers and uncertainties as discussed in Sections 8.4.5. The Marviken test facility and S-RELAP5 results are discussed in Section 8.2.7.

The test facility consists of four major components: a full-scale BWR vessel, a discharge pipe attached to the bottom of the vessel, a test nozzle connecting to the downstream end of the discharge pipe, and a rupture disk assembly attached to the downstream end of the nozzle. Nozzles of various length-to-diameter ratios are used in the tests. The Marviken test data are widely used in assessing critical flow models of various system codes over a range of flows to confirm the scalability. The Marviken tests provide a suitable basis for code scaling verification and the determination of uncertainties.

8.6.2.2.4 Carry-over to Steam Generator

Steam binding during the reflood phase of an LBLOCA in a PWR occurs as a result of steam production in the steam generator. This steam production occurs when water carried over from the core enters the hot steam generator. The resulting vaporization expansion increases the pressure drop through the steam generator, and produces steam binding that reduces the core reflood rate.

Several UPTF (Section 8.2.9), SCTF (Section 8.2.12) and CCTF (Section 8.2.13) tests were used to benchmark and verify the RLBLOCA methodology, and S-RELAP5. The UPTF is a full-scale simulation of a German PWR. The geometry of UPTF is also close to a Westinghouse 4-loop PWR. In UPTF, the steam generators are replaced with steam separators and the pumps are simulated with mechanical resistance. The CCTF and SCTF are scaled such that they are prototypic of a Westinghouse PWR, in the dimension parallel to flow and scaled down (~ 0.2) in the orthogonal directions.

The UPTF has no core as such, and reflood is simulated with steam and water injection in the core simulator region. The CCTF and SCTF have electrically heated rods in the core. The upper plenum region was tested at full-scale in the UPTF, as were the hot legs and the steam generator inlet plenum. The steam generator tubing geometry is prototypical in the CCTF (although the number of tubes is smaller). In SCTF, a steam-water separator is used instead of an active steam generator. As discussed in Section 8.5.1.4 and 8.5.1.6, several input options are developed to make sure that an acceptable amount of liquid that is entrained to the upper plenum during the reflood phase of a large break LOCA is carried over to the steam generator tube region. One of the input options is the [

] These input options are used in the UPTF, SCTF, and CCTF tests assessments. In all of the assessments, S-RELAP5 entrained an acceptable amount of liquid into the steam generator tube (or tube simulator) region. While each test by itself has some deficiencies in terms of simulating a PWR and in terms of scale, the combination of the simulation of tests from these three different test facilities provides a substantial basis to justify the ability of the code to calculate an acceptable amount of liquid entrainment into the steam generator tube region during the reflood phase of a large break LOCA in a PWR.

¹ [

8.6.2.2.5 *Pump Scaling*

The S-RELAP5 code uses normalized single-phase homologous curves for a full-scale reactor coolant pump (RCP) as code input. The use of full-scale data for the pump makes code scaling moot. These homologous curves are set to applicable values by entering plant-specific values for rated head, torque, moment of inertia, etc. The coastdown of the pump is driven by the torque and moment of inertia of the rotating mass. The torque includes the effects of friction and back EMF (pump torque), and of the loop pressure losses (hydraulic torque). Although the two-phase degradation of RCP performance is not considered a phenomenon of significance (Table 5-1), the single-phase pump head and torque curves are adjusted for two-phase effects based on the EPRI two-phase degradation data (Section 7.9.2.3). The pumps in the EPRI test program are similar to PWR coolant pumps and the data represents a best estimate approximation of both the single phase and two phase performance.

8.6.2.2.6 *Cold Leg Condensation*

As discussed in Section 8.4.2, several EPRI 1/3 scale tests, in combination with UPTF Test 8 Phase A (Run 111), and Phase B (Run 112), and Test 25, were simulated using S-RELAP5. The simulation results were used to develop the biases (multipliers) on the liquid-side (CONMAS) and vapor-side (CONMSG) interphase heat transfer coefficients. The tests selected generally cover both the accumulator and pumped injection period of the LOCA transient. Additionally, further EPRI tests were simulated using S-RELAP5, and the results are discussed in Section 8.2.10. The UPTF is close to a full-scale facility and the EPRI test facility is a 1/3 scaled facility.

Correlations based on the Stanton numbers are used to calculate the interphase condensation. These correlations are generally insensitive to geometry as demonstrated by the EPRI and UPTF benchmark results. The interphase heat transfer correlations used in S-RELAP5 are discussed in detail in Section 7.6.4.

In summary, with the biases determined from the tests conducted in these facilities, S-RELAP5 will calculate acceptable condensation in the cold legs during a large break LOCA in a PWR.

8.6.2.2.7 ECC Water Bypass of Downcomer during Refill and Lower Plenum Sweep-Out

The S-RELAP5 code prediction of the ECC bypass during the refill phase of a LOCA was demonstrated to be conservative through the assessment of UPTF Tests 6 and 7 (Section 8.2.9.3). Additionally, a CCFL correlation developed by MPR Associates is used in the sample plant cases given in Appendix B to demonstrate S-RELAP5 conservatively calculates the bottom of core recovery (or beginning of core reflood) time.

As discussed in Section 8.2.9.3, UPTF Tests 6 and 7 were steady-state downcomer counter current flow tests. UPTF Tests 6 and 7 were specifically designed under the 2D/3D program to examine downcomer countercurrent flow behavior, ECC bypass, and lower plenum refill during the refill phase in plants with cold leg ECC injection. In these tests, the lower plenum fill rate was measured as a function of time. The comparison of the lower plenum liquid level for UPTF Test 6 is provided in Figure 8.2-203, Figure 8.2-211, Figure 8.2-219, and Figure 8.2-227, and for UPTF Test 7 in Figure 8.2-236. The liquid level comparisons show S-RELAP5 underpredicts the lower plenum level which indicates the code is overpredicting ECC bypass. Since UPTF is a full scale test facility, results from the Tests 6 and 7 simulations demonstrate S-RELAP5 will conservatively calculate ECC bypass, lower plenum fill, and the core recovery time during the LOCA in a PWR.

Under the 2D/3D program, MPR Associates developed a Wallis-type CCFL correlation using UPTF data from the steady-state countercurrent flow tests (which included UPTF Test 5, Phase B, and UPTF Tests 6 and 7) to calculate the liquid downflow into the lower plenum during the refill phase:



The details of this CCFL correlation are given in Reference 8.6-6. In this correlation, $J_{g,eff}^*$ is the net steam flow rate available to entrain the ECC liquid to the break and its value determines the potential for ECC bypass. If $J_{g,eff}^*$ is zero or negative, the steam flow is insufficient to entrain liquid, and bypass will not occur (complete end-of-bypass). If $J_{g,eff}^*$ is positive, then partial or full bypass occurs.

Since the correlation is normalized using the downcomer flow area and circumference, it is directly applicable to calculate the ECC bypass in the plant during the refill phase. This correlation has already been approved by the NRC to calculate the complete end-of-bypass time ($J_{g,eff}^* < 0.0$) as part of AREVA NP's Appendix K-based Recirculating Steam Generator LOCA Evaluation Model (Reference 8.6-7).

The correlation is used in the sample plant cases discussed in Appendix B to estimate the beginning of core reflood time in order to demonstrate S-RELAP5 will appropriately calculate the beginning of core reflood time. To estimate the beginning of core reflood time, the correlation is used to calculate the complete end-of-bypass time. At this time, the liquid volume in the lower head, lower plenum, and downcomer below the active core region is determined. Knowing this time, the beginning of core reflood time can be estimated by the ECC injection rates in the intact cold legs and the remaining fluid volume below the active core region that need to be filled with water. The results for the sample cases (Figure B-18, Figure B-36 and Figure B-54) demonstrate S-RELAP5 calculates the beginning of core reflood time appropriately.

The highly separated flow behavior observed in the full-scale UPTF tests (see Figure 4.1-3 in Reference 8.6-8) were not observed in scaled facilities like LOFT and Semiscale. The tests conducted in these scaled facilities therefore cannot be used to determine code scalability of ECC bypass, and the multi-dimensional flow phenomena that will occur in the downcomer and lower plenum during the refill phase.

In summary, it is demonstrated that S-RELAP5 will appropriately calculate the ECC bypass during refill and the beginning of core reflood time during the large break LOCA in a PWR.

8.6.2.2.8 Loop Oscillations

UPTF Test 8 (Section 8.2.9.4) investigated the behavior during the end-of-blowdown, refill, and reflood phases of a postulated LOCA with cold leg ECC injection. The focus of the test was the pressure and fluid oscillations in the cold legs. These oscillations arise when the steam is condensed by the ECC water and forms a liquid plug in the cold leg. The ECC flow rate was varied from typical accumulator flows down to pumped injection flows. The test results show the flow regimes switching from the slug (plug) flow during the accumulator injection period to stratified flow during the pumped injection period. Test 8, Runs 111 and 112, were performed by isolating one intact loop at the pump simulator, opening a second intact loop to stabilize the pressure drop between the upper plenum and the downcomer, opening the break valves on the broken loop, injecting steam into the test vessel, and varying ECC water injection into the third intact loop cold leg downstream from the pump simulator. The S-RELAP5 simulation of the Test 8 modeled the cold leg piping for the third loop from the steam generator simulator to the pump simulator (including loop seal), the pump simulator, and the cold leg piping from the pump simulator to the vessel downcomer; which are all full-scale.

The simulation is discussed in Section 8.2.9.4. S-RELAP5 predicted the observed flow regimes reasonably well, which indicate the code is capable of calculating the appropriate phenomena associated with steam-ECC mixing in the cold leg in the plant. However, since the complete UPTF primary system was not modeled using S-RELAP5, the system oscillations were not calculated by the code.

The CCTF, SCTF and LOFT benchmarks (Sections 8.2.13, 8.2.12, and 8.3.1, respectively) compared the calculated and measured differential pressures. The results show the code calculated acceptable oscillations during the refill and reflood phases.

In summary, from the simulation of the above tests, it can be concluded that S-RELAP5 will calculate the acceptable loop oscillations during a large break LOCA in a PWR.

Table 8.6-1: Test Ranges for Film Boiling Heat Transfer Test Comparison

Parameter	Maximum		Minimum	
	Tests	LBLOCA	Tests	LBLOCA
Pressure (MPa)	8.2	10.8	0.13	0.22
Mass Flux Vapor (kg/s-m ²)	907	367	0	0
Mass Flux Liquid (kg/s-m ²)	4254	945	0	0
Void Fraction	1	1	0.13	0.13
Saturation Temperature (K)	570	589	381	390
Vapor Temperature (K)	1294	1160	384	391
Wall Temperature (K)	1525	1400	390	396
Quality	1	1	-0.11	0

8.6.3 References

- 8.6-1 NUREG/CR-5249, Quantifying Reactor Safety Margins, Application of Code Scaling, Applicability, and Uncertainty Evaluation Methodology to a Large Break, Loss-of-Coolant Accident, December 1989.
- 8.6-2 BAW-10231P-A, Revision 1, COPENIC Fuel Rod Design Computer Code, Framatome ANP, January 2004.
- 8.6-3 NUREG/CR-0410, Comparisons of Thermal-Hydraulic Phenomena During Isothermal Loss-Of-Coolant Experiments and Effect of Scale in LOFT and SEMISCALE MOD-1, December 1978.
- 8.6-4 NUREG/CR-1533, Analysis of the FLECHT-SEASET Unblocked Bundle Steam Cooling and Boil-off Tests, January 1981.
- 8.6-5 Dittus, F. W. and L. M. K. Boelter, Heat Transfer in Automobile Radiators of the Tubular Type, Publications in Engineering, Volume 2, pp. 443-461. University of California, Berkeley, 1930.

8.6-6 MPR Report, Summary of Results from the UPTF Downcomer Separate Effects Tests, Comparisons to Previous Scaled Tests, and Application to U.S. Pressurized Water Reactors, MPR-1163, July 1190.

8.6-7 BAW-10168-A, Revision 3, RSG LOCA – BWNT Loss-of-Coolant Accident Evaluation Model for Recirculating Steam Generator Plants, Volume I – Large Break, December 1996.

8.6-8 Damerell, P. S., Simsons, J. W., Reactor Safety Issues Resolved by the 2D/3D Program, NUREG/IA-0127, July 1993.

9.0 EVALUATION MODEL DESCRIPTION

The AREVA NP Realistic Large Break LOCA evaluation model is based on the application of nonparametric statistics to characterize the population of possible LB LOCAs. In this endeavor, the LOCA predictions of S-RELAP5 are accepted, based on the qualifying efforts and benchmarks presented in this topical. The first step in the evaluation is to establish the limits of the population to be characterized. This was done by determining the scenario for the LOCAs, and by selecting and qualifying S-RELAP5 as sufficient to assess individual members of the population (called events). The population is considered to be all LOCAs from breaks in high pressure pipes, [

] The steps in the evaluation of a plant are:

1. To establish base S-RELAP5, including the containment, model for the plant (described in Section 9.1),
2. Based on a random selection, execute as many LOCA cases, each an event from the population of LOCAs, as required to produce 95% confidence that 95% of the population meets the criteria of 10 CFR 50.46. A single uncertainty analysis case is depicted in Figure 9-1. For a single case, the required computational order is to calculate fuel rod properties with COPENIC, followed by an S-RELAP5 steady-state initialization calculation at the sampled conditions, and finally, an S-RELAP5 LBLOCA transient calculation is performed restarting from the sampled steady-state conditions. The details of the parameter sampling are found in Appendix A (the analysis guideline).
3. To extract the calculated values for each of the three parameters limited by 10 CFR 50.46, [

] which are then compared to the regulatory 10 CFR 50.46 limits.

The plant base model is fixed for the evaluation and serves as the model to which each of individual cases makes modification before case execution. The cases differ from the base model by the values of the sampled parameters assigned for each case. These parameters comprise the set of highly important parameters identified within the PIRT and selected plant operational parameters, which may be identified as beneficial to include. The PIRT identified parameters are listed in Table 5-1.

A representative sample of plant parameters is shown in Table B-9, Table B-16, and Table B-23 for each of the sample problem calculations in Appendix B, respectively.

9.1 *Base Model*

The base model establishes the special discretization, noding, with which the components of the reactor system are modeled, and associated modeling of flow paths and heat structures, including the subparts of each of these, and initial conditions. After some general guidance discussion, each of these is described, in turn, in the following subsections.

9.1.1 Nodalization Methodology

Reference 9-1 ("Quantifying Reactor Safety Margins") makes the following statements regarding nodalization:

The plant model must be nodalized finely enough to represent both the important phenomena and design characteristics of the NPP but coarsely enough to remain economical.

Thus, the preferred path is to establish a standard NPP nodalization for the subsequent analysis. This minimizes or removes nodalization, and the freedom to manipulate noding, as a contributor to uncertainty.

Therefore, a nodalization selection procedure defines the minimum noding needed to capture the important phenomena. This procedure starts with analyst experience in previous code assessment and application studies and any documented nodalization studies. Next, nodalization studies are performed during the simulation of separate- and integral-effects code data comparisons. Finally, an iterative process using the NPP model is employed to determine sufficiency of the NPP model nodalization.

Given these general recommendations, the goal of a nodalization methodology is to optimize priorities that are incompletely independent. These include preserving dominant phenomena, minimizing code uncertainty, conforming to design characteristics, and minimizing computational expense. As a convenience and a slight conservatism, the AREVA NP RLBLOCA minimizes the initial coolant volume by sizing the RCS volumes at their cold condition as a convenience and a slight conservatism, the AREVA RLBLOCA evaluation model is quantitatively explicit wherever possible to remove nodalization as a contributor to uncertainty. Because not all plants of the same type are identical, the modeling guidelines provide guidance for deriving the appropriate nodalization. This strategy serves to both remove nodalization as a contributor to uncertainty, and to define a method for automating the generation of input for a RLBLOCA analysis.

As described by Step 8 of the CSAU process, this task is iterative, and was so during development of Revision 0 (Reference 9-2) of the methodology. Revision 3 of the methodology initiates the basic nodalization with the Revision 0 model, and improves it, in selected areas, based on studies described later in this section.

The derived input prescription defines the standardized nodalization scheme, specifies a logical numbering system, and recommends key parameter inputs for the S-RELAP5 input model. Noding details were determined from experience with simulation of integral- and separate-effects tests (Sections 8.2 and 8.3) that result in a technically and economically sound nodalization scheme for simulating LBLOCA in a PWR.

Assessment calculations of the FLECHT-SEASET reflood experiments provide data for the axial nodalization of the core region. Studies of the Cylindrical Core Test Facility (CCTF) and Slab Core Test Facility (SCTF) were used to identify two-dimensional modeling techniques for the downcomer and core. Analyses of the LOFT and Semiscale experiments gave information describing the primary coolant loops, reactor coolant pumps, reactor vessel, and steam generators. Assessments of UPTF tests also were used to identify two-dimensional modeling techniques and provide useful plant information, including experimental data on full-scale downcomer fluid behavior during all phases of a LBLOCA.

Column 1 of Table 9-1 defines a particular NPP component or coolant system region, and the S-RELAP5 components generally used for its simulation. Column 2 lists the important phenomena associated with the component as evaluated through the PIRT process (Section 5.0). Column 3 defines the number of control volumes required, based on user experience and assessment calculations, to provide adequate detail.

Experience indicates that S-RELAP5 plant models of Westinghouse/AREVA 3- and 4-loop PWRs and CE 2x4 loop PWRs require between 200 and 500 control volumes, junction flow paths, and heat structures. The AREVA 3- and 4- loop plants closely pattern the Westinghouse 3- and 4- loop plants and do not require separate nodalization schemes. The following figures show the modeling techniques.

- Figure 9-2: Sample Loop Nodalization for NPP
- Figure 9-3: Sample Steam Generator Secondary Nodalization for NPP
- Figure 9-4: Double-Ended Guillotine and Split Break Nodalization
- Figure 9-5: Sample Reactor Vessel Nodalization for NPP

- Figure 9-6: Westinghouse/AREVA 3- and 4-Loop and CE 2x4 Plant Vessel Downcomer

Configurations:

- Figure 9-7: NPP Core Nodalization
- Figure 9-8: Sample NPP Upper Plenum Nodalization – Axial Plane
- Figure 9-9: Sample NPP Upper Plenum Nodalization – Cross-Sectional Plane

9.1.2 Numerical Considerations

The nodalization of a particular model translates into a computational array used to solve the mass, momentum, and energy equations. Numerical constraints also must therefore be considered in the the sizing and the configuration of component volumes. The primary numerical issues are accuracy, numerical stability, and code variability. While optimizing these three issues, it is necessary to have useable results. Some code variability can be tolerated provided it is reasonably defined. However, numerical stability must be ensured before performing production calculations to assess accuracy through code/data comparisons.

In general, the RELAP5 series of codes have a solid foundation regarding numerical stability (this is further detailed in Section 7.0). Both nodalization and time step decisions can, however, influence numerical stability. It is generally understood that numerical solutions are well behaved if the number of mesh points is small enough. Such small nodes necessitate equally small time steps to satisfy the Courant stability requirement, leading to long uneconomical code execution times. Conversely, it was shown that modeling interfacial drag contributes to the stability of coarser mesh models for two-phase flow codes, such as RELAP5 (Reference 9-7). While modeling interfacial drag works to destabilize the solution for small mesh sizes, it supports the coarser mesh models required for economical code execution times. As a result, considering hydraulic phenomena exclusively, spatial mesh configuration is not a high concern for numerical stability.

For code accuracy, mesh sizing becomes more important for heated surfaces. Steep temperature gradients influence the adjacent fluid conditions. For this reason, small mesh sizes are used on heated surfaces to capture expected phenomena.

The final figure-of-merit for quantifying code variability comes from the calculation of the hot rod PCT. For a set of equivalent input models, differing only in time step (constrained to be less than the Courant limit), comparisons of PCT traces can be used to evaluate expected code variability. By using this approach, nodalization decisions can be made in an effort to minimize the impact of code variability.

In summary, the iteration process for defining a nodalization methodology included decisions to change a component nodalization based on the analysis of either assessments (integral- and separate-effects) or plant sensitivity studies. These calculative results, documented in Section 8 and in Appendix B, were generally used to confirm the adequacy of a chosen nodalization scheme.

9.1.3 Reactor Coolant System Loop Model

The RCS loop includes those components outside the reactor vessel, including the pressurizer and ECCS. All loops are modeled individually (i.e., the unbroken loops are not lumped into a single combined loop). Each loop models the hot leg piping, steam generator primary and secondary fluid volume, pump suction piping, pump, and pump discharge cold leg piping. The pressurizer and surge line are attached to the hot leg piping of one of the loops. Each loop also contains modeling of the accumulator, and high- and low-pressure injection ECCSs. The nodalization scheme is presented in Figure 9-1 for a sample loop with the pressurizer. Heat transfer within each of the components and piping section is modeled as appropriate.

The following are key features and assumptions for the reactor coolant loops.

- The nodalization detail for the coolant loops, pressurizer, and primary and secondary sides of the steam generators was selected to give consistent results without increasing running time because of excessive nodalization. The nodalization is consistent with that used in years of experience with LOCA and non-LOCA event analysis, and is supported by various assessment calculations.

Assessment of loop nodalization comes from various facility test programs, including SCTF, CCTF, LOFT, Semiscale, and UPTF. In addition, the Westinghouse/EPRI 1/3 Scale Steam/Water tests, a separate-effects test examining ECC mixing in the cold leg, is also a useful assessment. Acceptance of nodalization schemes was based on the general agreement in code/data comparisons for pressures, differential pressures, mass flow rates, and heat structure temperatures.

9.1.3.1 Hot Leg

The hot leg connects the reactor vessel to the steam generator inlet plenum. [

]

[

] The entrainment of droplets from

the reactor vessel will enhance the effect of steam binding, which inhibits reflood.

Code-to-data comparisons of tests performed at the CCTF and the UPTF

(Sections 8.2.13 and 8.2.9, respectively) show that S-RELAP5 predicts entrainment between the reactor vessel and the steam generator inlet plenum accurately or with a slight overprediction. This is acceptable because the result will be a reasonable to slightly conservative simulation of steam binding and its impact on cladding temperature.

Heat transfer between the pipe to the coolant is modeled with heat structures that preserve the mass of the pipe metal and the inside surface area.

9.1.3.2 Steam Generator

The steam generator nodalization scheme is essentially identical to the traditional approach used by other large thermal-hydraulic codes such as TRAC and RELAP5 (References 9-1 and 9-8, respectively). [

]

The dominant phenomena of importance are the steady-state heat balance and steam binding during reflood. Heat balance is ensured by the use of control systems controlling feed water and steam flow depending on steam generator inventory to obtain an acceptable comparison to plant data at steady-state conditions. [

] In

general, LBLOCA is statistically insensitive to steam generator secondary nodalization. Benchmark simulations of the CCTF tests (Section 8.2.13) showed S-RELAP5 conservatively estimates the steam binding effect in the steam generator tubes. Therefore, the nodalization scheme is acceptable.

9.1.3.3 Pump Suction

[

]

9.1.3.4 Reactor Coolant Pump

The pump is a component model, meaning that the pump physics is independent of nodalization; hence, the primary objective of the nodalization scheme is to ensure consistency with the structural characteristics. [

]

9.1.3.5 Cold Leg and Break

The cold leg extends from the RCS pump discharge to, and including, the reactor vessel inlet nozzle. [

] The break model is either a double-ended guillotine with discharge from both cold leg volumes or a split with discharge from both cold leg volumes. The difference between the guillotine and the split is that the flow path between the two cold leg volumes at the break plane is preserved for a split break, and closed for a guillotine break. The noding configuration for the two break types is shown in Figure 9-4. [

]

[

]

- [

]

Heat structures are used to model the cold leg piping wall, preserving metal mass and heat transfer surface area.

9.1.3.6 ECCS

The ECCS includes models for the accumulator and the piping connecting it to the RCS with sufficient detail to allow the code to accurately predict coolant flow splits for low-pressure injection flows. Figure 9-1 includes a typical nodalization for the ECCS of a three-loop plant. The accumulators are the dominant component in the ECCS.

[

]

The dominant phenomena of importance are the accumulator liquid discharge, the pumped injection rate, and the noncondensable gas transport following accumulator liquid discharge. Activity in the accumulator lines can be characterized as a period of single-phase incompressible flow (accumulator water discharge), followed by a two-phase mixture; nitrogen from the accumulator and water from the low pressure injection system. Noncondensable gas transport to the cold leg can continue for several seconds after the end of liquid discharge and may, for some events, be limited by critical flow. The nitrogen in the accumulator will transport from the accumulator to the RCS by gas expansion and pressure forces. Dissolved nitrogen will come out of solution as the system pressure decreases. Heat structures are used to model the accumulator discharge piping walls, primarily to prevent numerical difficulties with rapidly decreasing temperatures as the pressure falls during discharge.

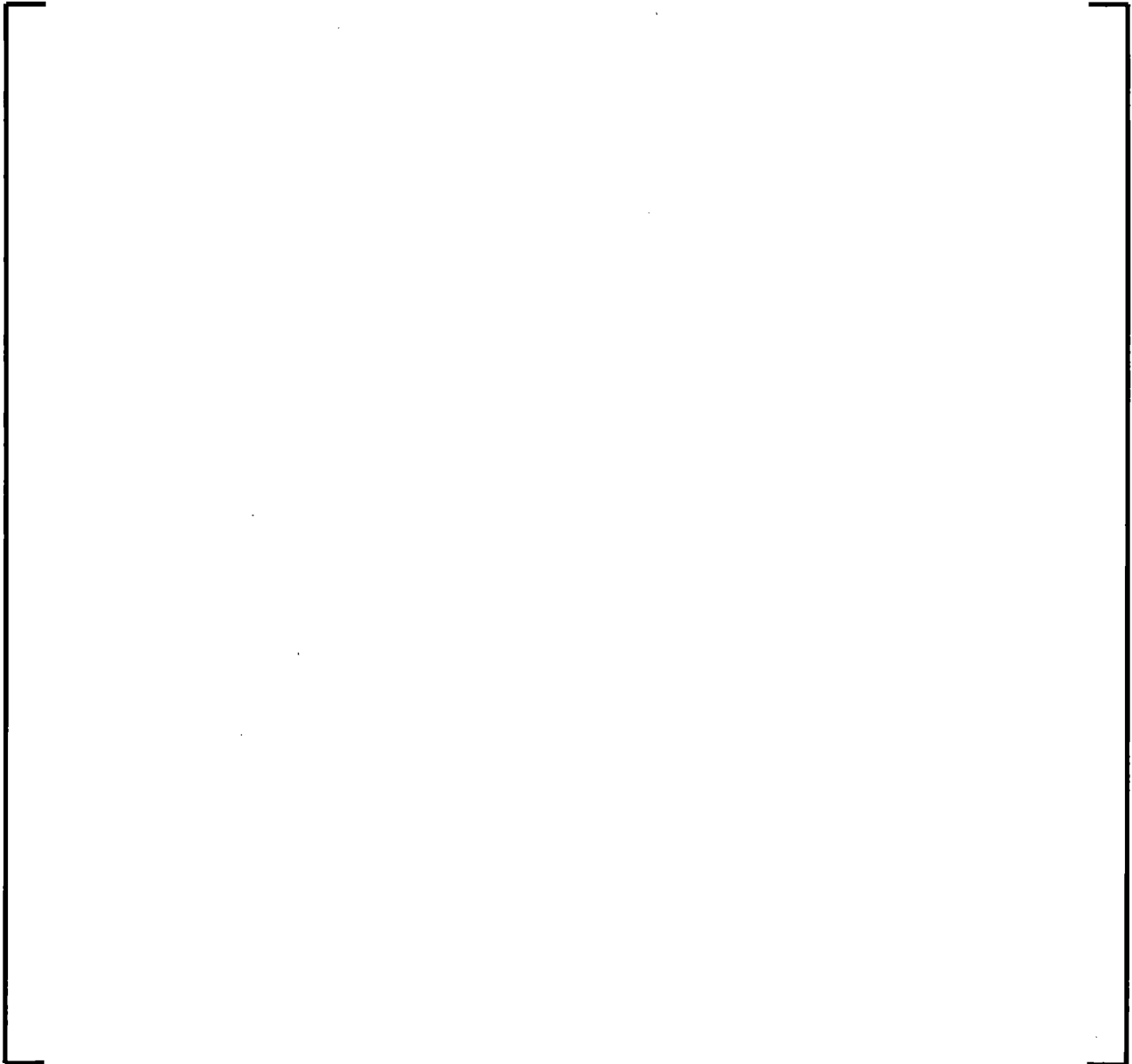
9.1.3.7 Pressurizer

The pressurizer vessel is modeled with [

] The dominant phenomena of interest are early lower core quench and critical flow in the surge line. Neither phenomenon shows much sensitivity to nodalization because the surge line remains choked during the period in which these concerns are important (blowdown).

9.1.4 Reactor Vessel Model

The key components of the reactor vessel are the downcomer, lower head and plenum, core, and upper head and plenum. The nodalization is presented in Figure 9-5. The key features and assumptions for the reactor vessel are:



9.1.4.1 Downcomer

The reactor downcomer is modeled using [

]

For asymmetric cold and hot leg connections to the reactor vessel, the only practical nodalization option is [

]

The dominant downcomer LBLOCA phenomena (condensation, hot wall effects, multi-dimensional flow, CCFL, and entrainment) affect the refill period. These phenomena primarily influence the duration of ECCS bypass. The hot wall effect is conservatively treated by forcing nucleate boiling for any portion of the downcomer in contact with water.

The UPTF Test 6 (Section 8.2.9) experiments investigated the countercurrent flow of steam, reactor coolant and ECC water in the downcomer during the refill phase for a 4-loop PWR LOCA and were used to validate the downcomer nodalization.

A downcomer nodding sensitivity study was also done on a 4-loop plant model. The base modeling comprises [

] The conclusion from the study was that the lower plenum refill is relatively insensitive to downcomer nodalization for uniform ECC water injection into all intact loops.

[

] This improvement to the axial and azimuthal nodding density gives a well converged model of the downcomer, which captures relevant geometric features.

Heat structures are used to model the vessel wall and the core barrel, preserving the mass of the metal. The structures are segmented so that each volume in the two-dimensional downcomer component is connected to a separate heat structure representing the portion of the total wetted surface area corresponding to each volume. Thermal shield or neutron pads, if present in the vessel, are also modeled with multi-node heat structures.

Bypass flow paths from the downcomer around the hot leg sleeve penetrations to the hot leg nozzles is not modeled. The fraction of design bypass flow associated with this leakage is added to the guide tube bypass flow from lower plenum to upper plenum to preserve both the design bypass flow rate and the active core flow rate.

[

]

9.1.4.2 Lower Vessel

The lower vessel includes all volumes [

]

- [

]

- [

]

- [

]

[

]

Heat structures are used to model both the vessel wall and lower hemispherical head in this region, as well as any internal structure present such as a flow skirt, snubbers, flanges, support columns, or support plates.

The dominant nodalization-influenced LBLOCA phenomena of importance are liquid sweep-out and steam water mixture content as the plant approaches the bottom of core recovery. The nodalization of the lower vessel region is shown in Figure 9-5. As demonstrated in the UPTF Tests 6 and 7 assessment (Section 8.2.9), the calculation of the sweep-out phenomenon is conservatively overpredicted.

9.1.4.3 Core, Core Bypass, and Fuel

The core region extends from the bottom of the active core to the top of the upper core support plate. [

]

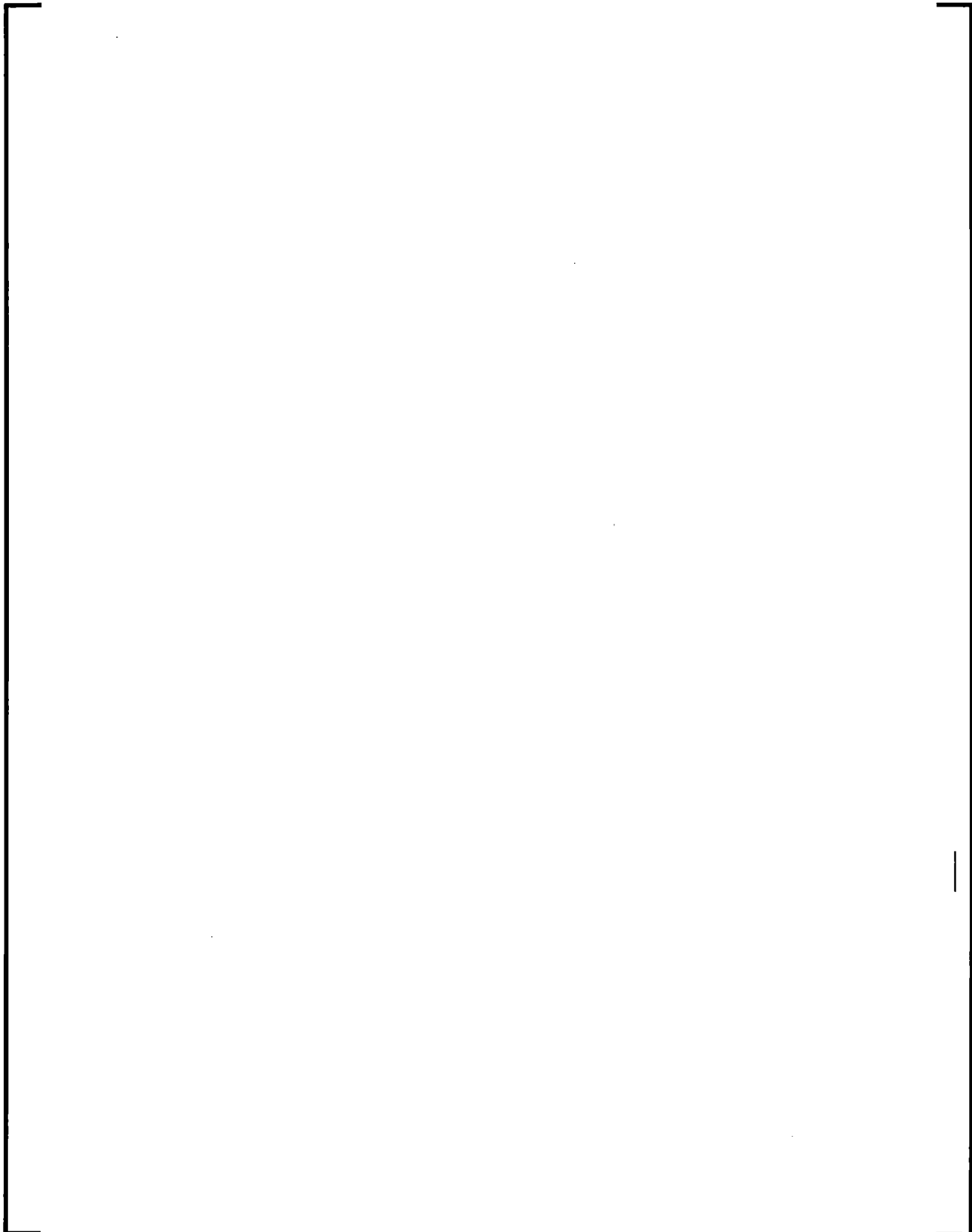
The most important contributor to nodalization sensitivity is expected to be core nodalization because it directly affects the liquid distribution in the core. The key phenomena of importance influenced by nodalization are the heat transfer modes, entrainment/de-entrainment, multi-dimensional flow, stored energy, oxidation, core power distribution, and decay heat. Since the heat transfer modes, entrainment/de-entrainment, hot region power, and stored energy are treated statistically; adequate representation of multi-dimensional flow phenomenon is of prime relevance for nodalization.

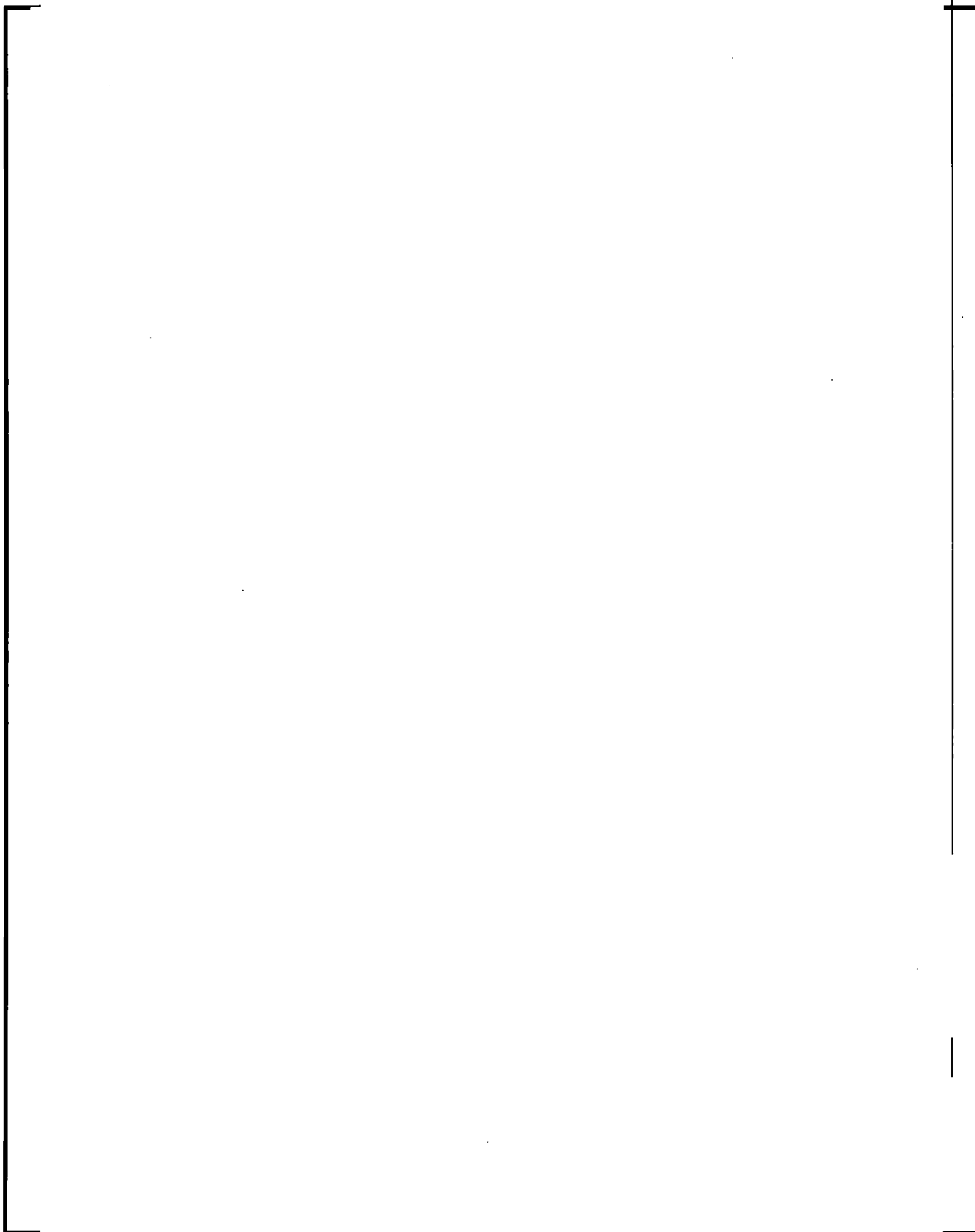
Given the expense of moving to a finer nodalization, the axial nodalization was defined in the range of [

] The node lengths are the smallest defined for the S-RELAP5 plant model; hence, they will define the Courant limit.

[

]





9.1.4.4 Upper Plenum/Upper Head

The upper plenum region extends from the top of the upper core plate to the top of the upper support plate. [

]

The dominant phenomena of importance are entrainment/de-entrainment, fallback (CCFL), and upper head temperature. The entrainment phenomenon is considered in the same manner as it was for the hot legs. The entrainment of droplets from the reactor vessel will enhance the effect of steam binding, which inhibits reflood. Code-to-data comparisons of tests performed at the CCTF and the UPTF (Sections 8.2.13 and 8.2.9, respectively) show that S-RELAP5 predicts entrainment between the reactor vessel and the steam generator tube inlet accurately to a slight overprediction. This is acceptable because the result will be a reasonable to slightly conservative simulation of steam binding and its impact on cladding temperature.

The upper head temperature is treated statistically. [

] This

configuration captures the preference for fallback to colder assemblies as demonstrated in the plant sample problems (Appendix B), showing a general conservatism in the treatment of liquid fallback.

In many plants, flow asymmetry into the upper plenum can exist. Flow can either travel directly into the upper plenum or be forced through a support column or mixer vane nozzle and then deposited in the middle of the upper plenum. [

]

9.1.5 Containment Model

Nodalization of the containment for the RLBLOCA is defined in a separate input file from the normal S-RELAP5 input. The containment model input is equivalent to the input used for the ICECON code (Reference 9-3), which is the AREVA proprietary version of the CONTEMPT code (Reference 9-6). ICECON was incorporated as a routine in S-RELAP5. The S-RELAP5 input file contains a link between the S-RELAP5 input and the ICECON input. [

] S-RELAP5 drives the containment calculations with mass flow and enthalpy, and the ICECON subroutines return containment pressure and temperature to update the S-RELAP5 time-dependent volumes.

[

]

The dominant parameter of interest related to the containment model is containment pressure. The goal of the modeling is to provide a reasonable prediction that remains responsive to the industry-held perception that lower containment pressures increase steam binding, which restricts the reflooding process by imposing higher steam specific volumes. Three modeling concepts ensure this:

1. The heat structure modeling is in line with the recommendations of NUREG-0800 Branch Technical Position 6.2 (Reference 9-5). This ensures that the interior heat absorbing structures are modeled with recognition of the probable best-estimate characterization.
2. The containment condensing heat transfer is a practical bound of benchmark data for ten experiments. Although the benchmarks were conducted using GOTHIC (Reference 9-12, Figure 5-42, page 5-48), the result was the establishment of a benchmark data set for the condensing heat transfer coefficient to the Uchida correlation. [

]

3. The containment volume [

]

The combination of these three factors provides assurance that the containment pressure applied in the RLBLOCA calculation is conservative, but not enough to seriously bias the results.

9.1.6 Plant Model Summary

The nodalization described in this section was developed by applying the approach described in Reference 9-1. This nodalization development methodology was an iterative approach. The base nodalization originated through experience gained by RELAP5 users at the Idaho National Engineering Laboratory, and by ANF-RELAP and S-RELAP5 users at AREVA. The nodalization was refined from both plant and code assessment tests, which used the same nodalization and modeling choices as in the full NPP model for those portions of the assessment model that would affect the phenomena being examined.

The uncertainty associated with the nodalization is considered minimal and is subsumed in the uncertainties determined for key LBLOCA parameters because, to the extent possible, the NPP nodalization was used in determining those uncertainties.

Table 9-1 Large Break LOCA Nodalization

Figure 9-1 Uncertainty Analysis Case Description

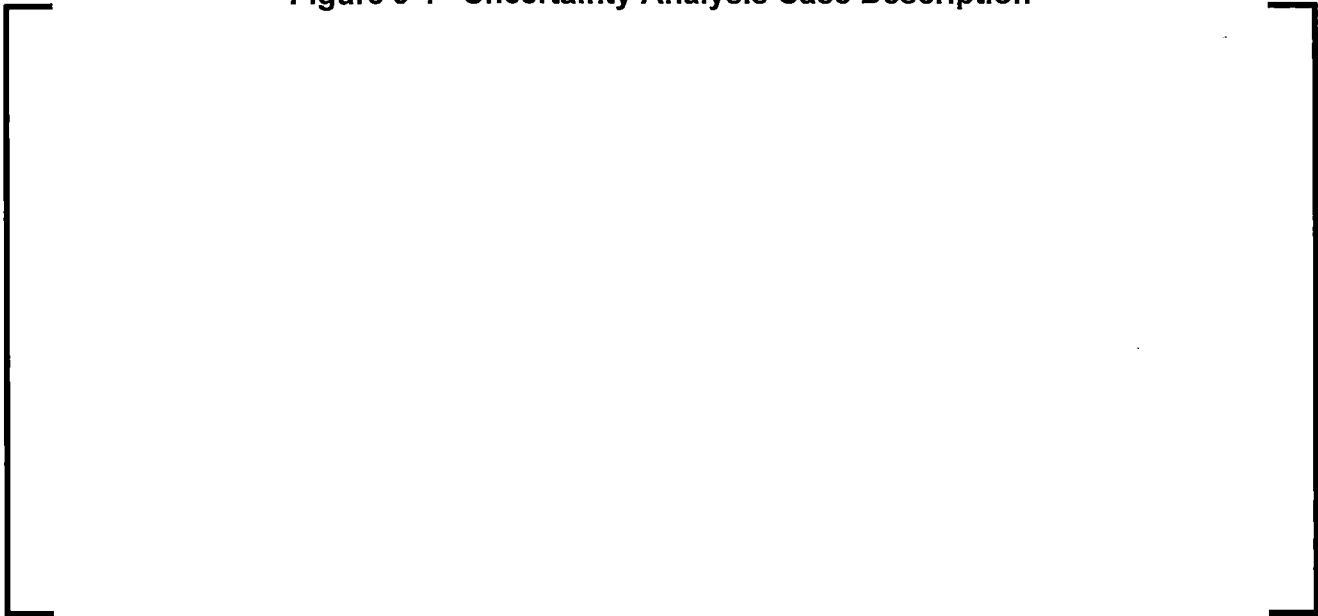
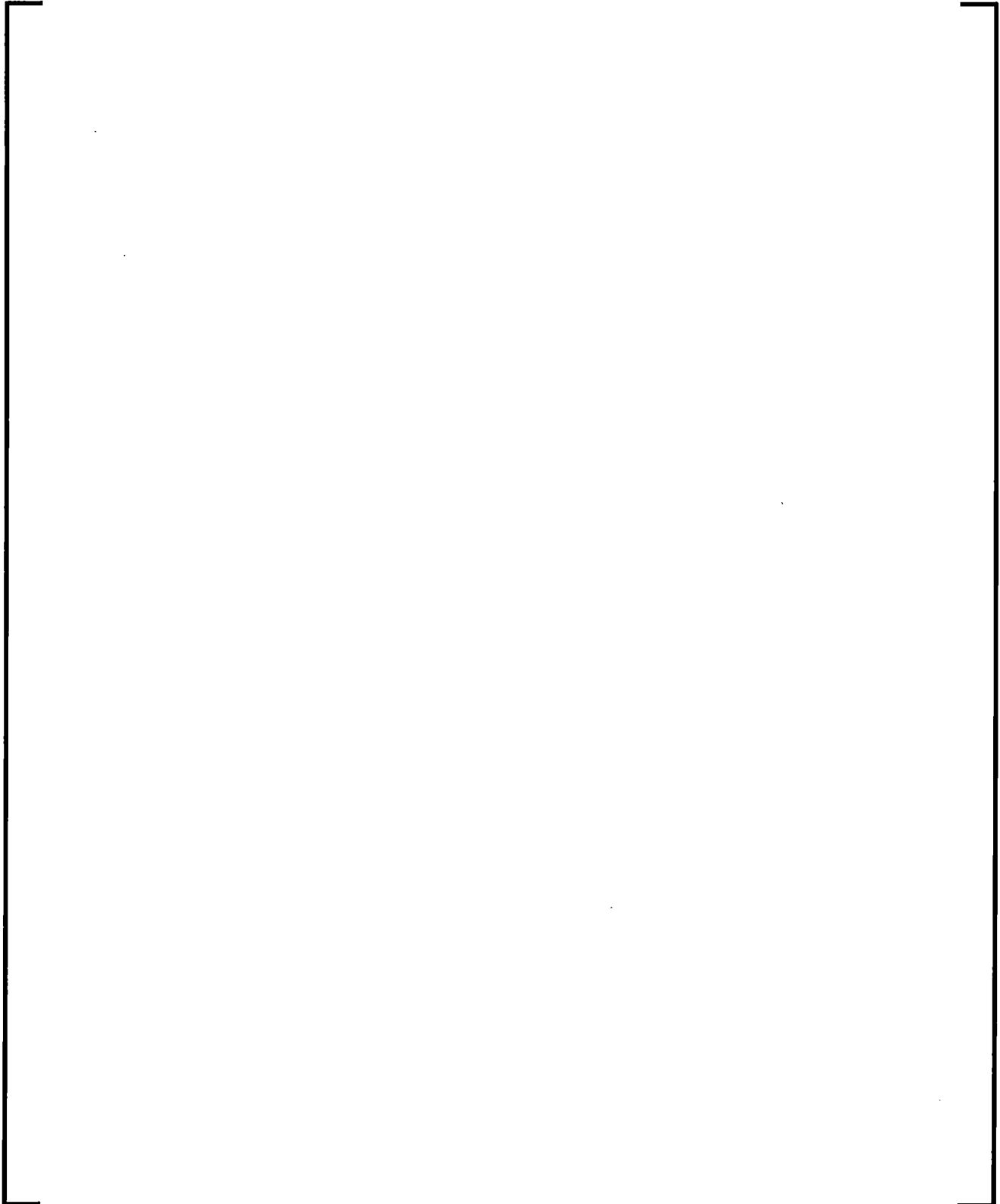


Figure 9-2 Sample Loop Nodalization for NPP



**Figure 9-3 Sample Steam Generator Secondary Nodalization for
NPP**

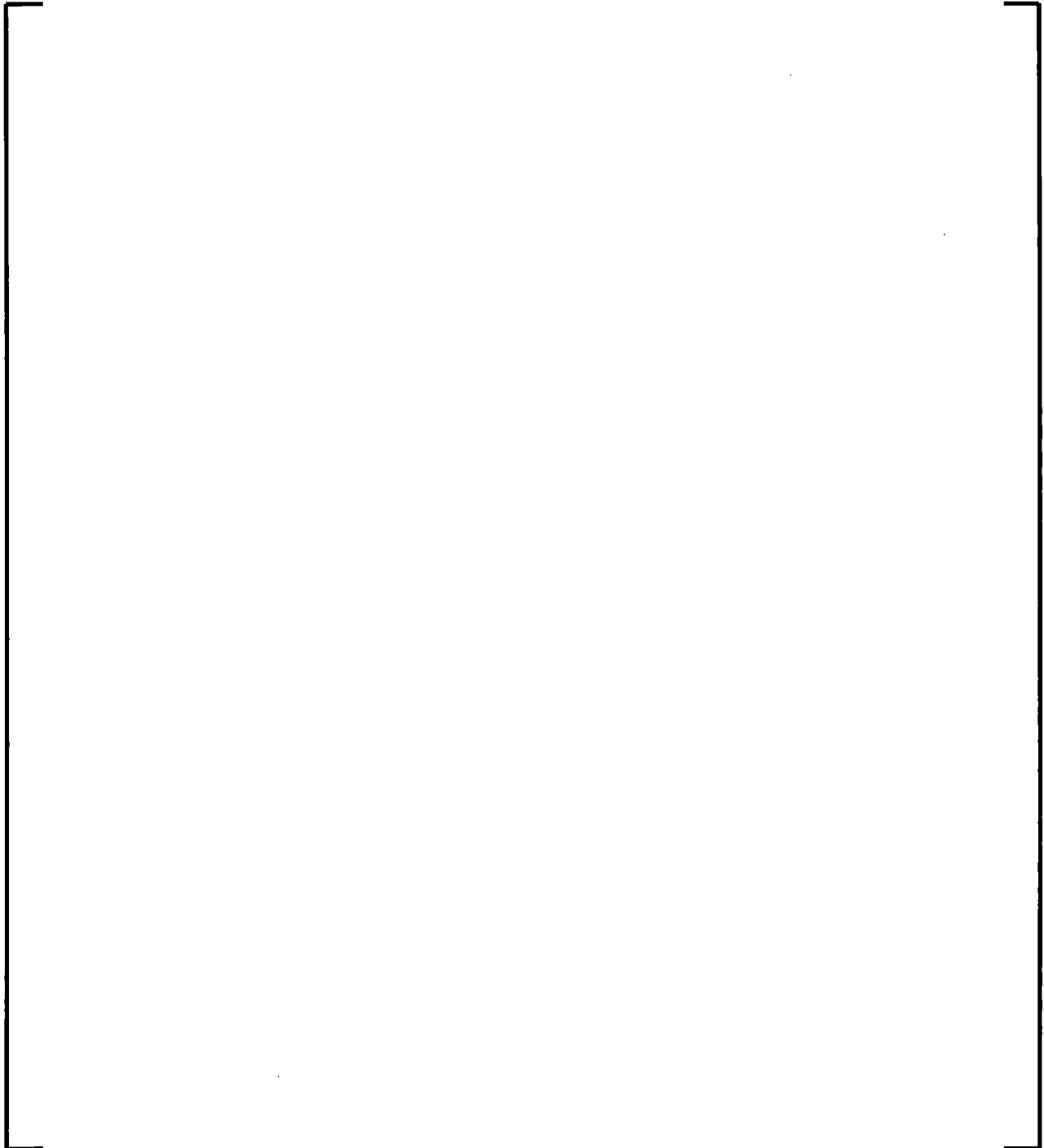


Figure 9-4 Double-Ended Guillotine and Split Break Nodalization

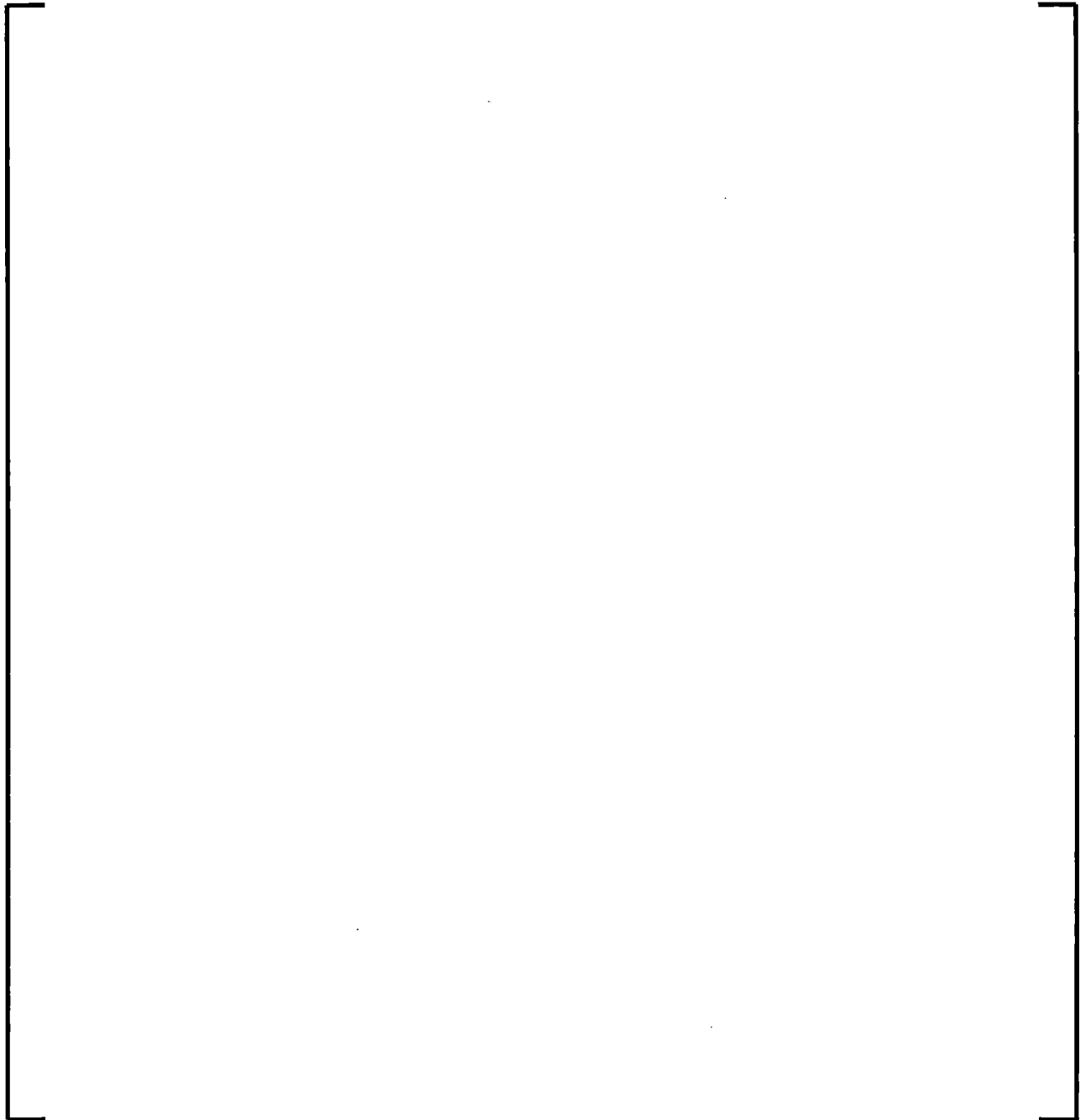
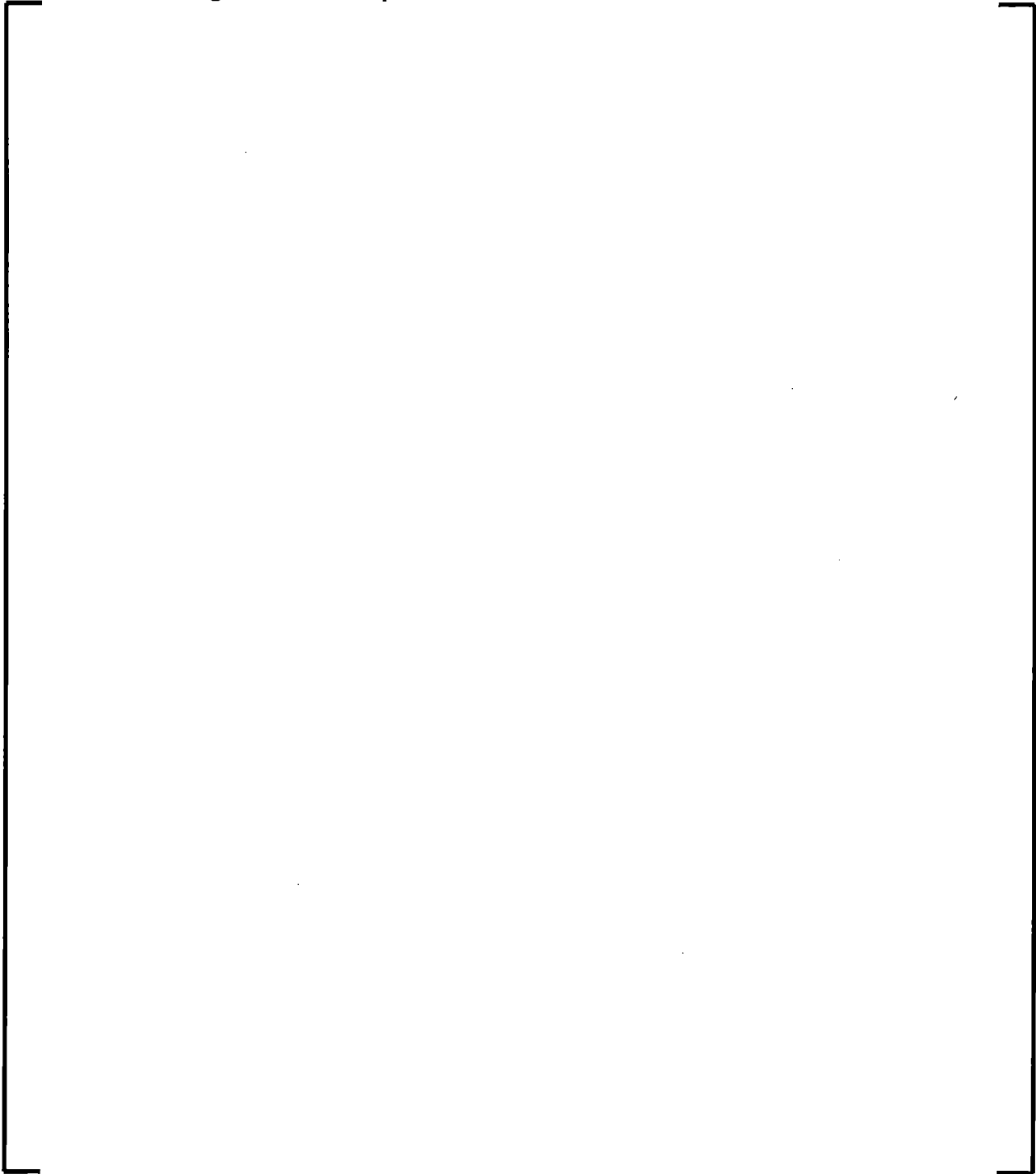


Figure 9-5 Sample Reactor Vessel Nodalization for NPP



**Figure 9-6 Westinghouse/AREVA 3- and 4-Loop and CE 2x4 Plant
Vessel Downcomer Configurations**

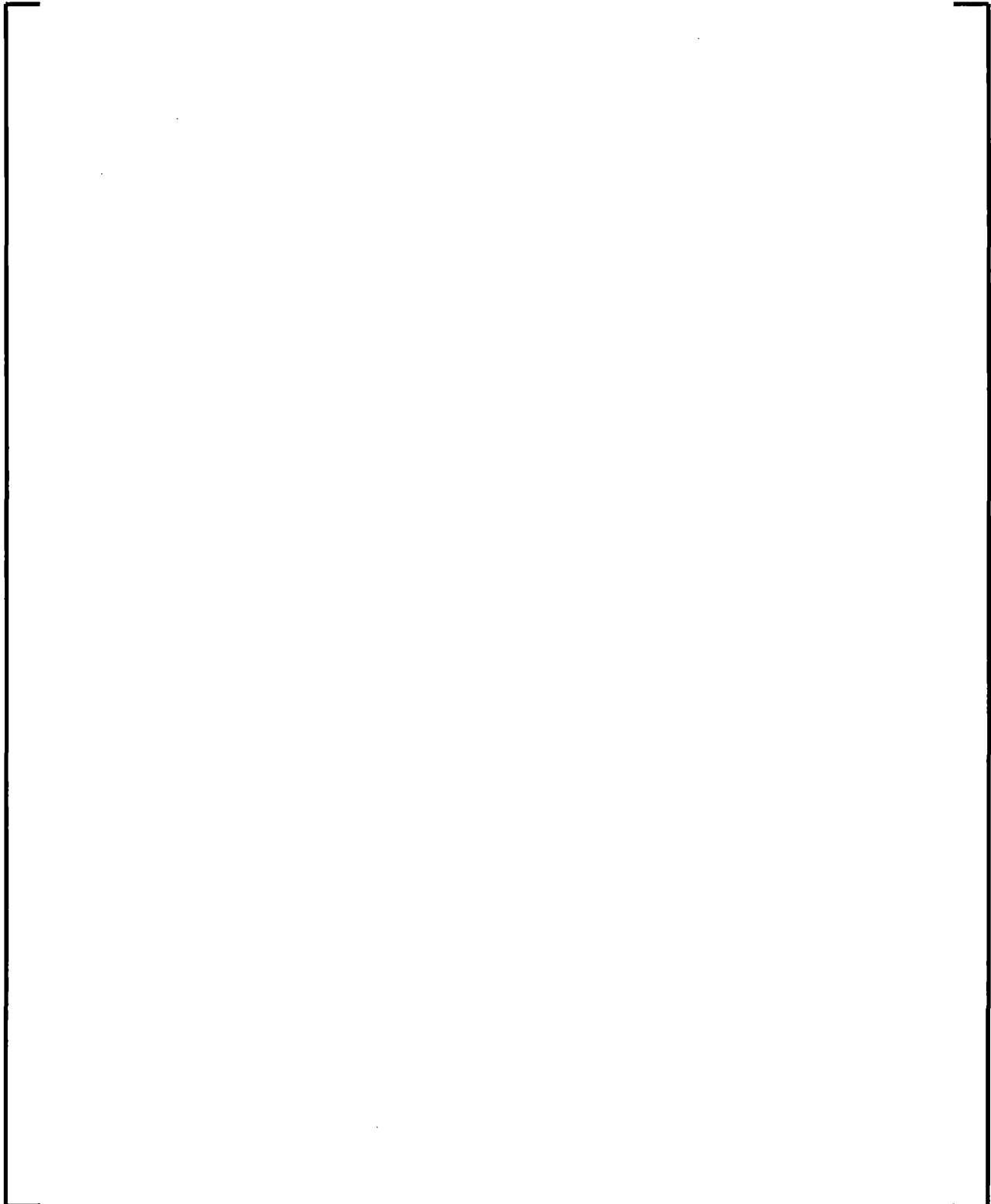


Figure 9-7 NPP Core Nodalization

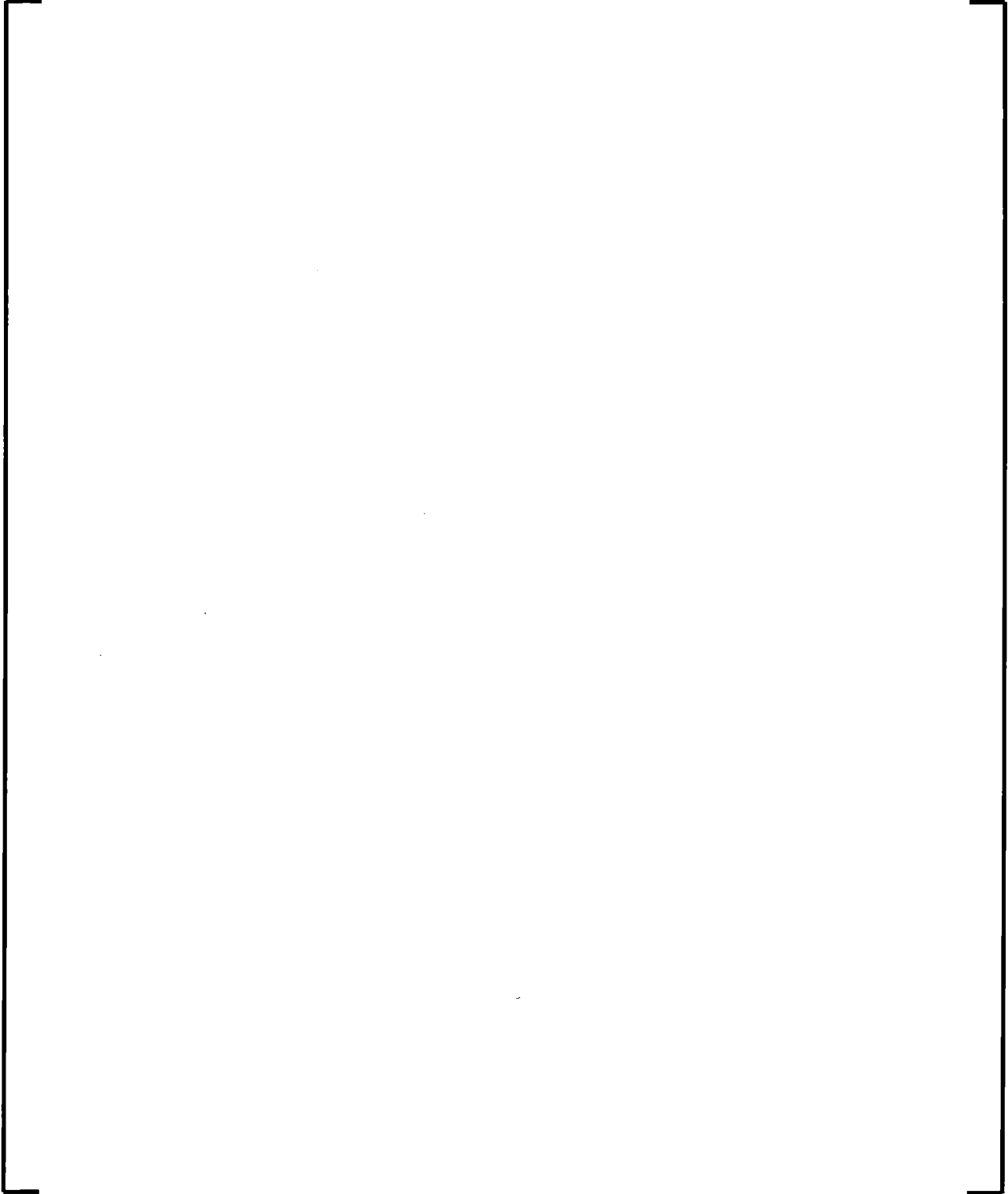
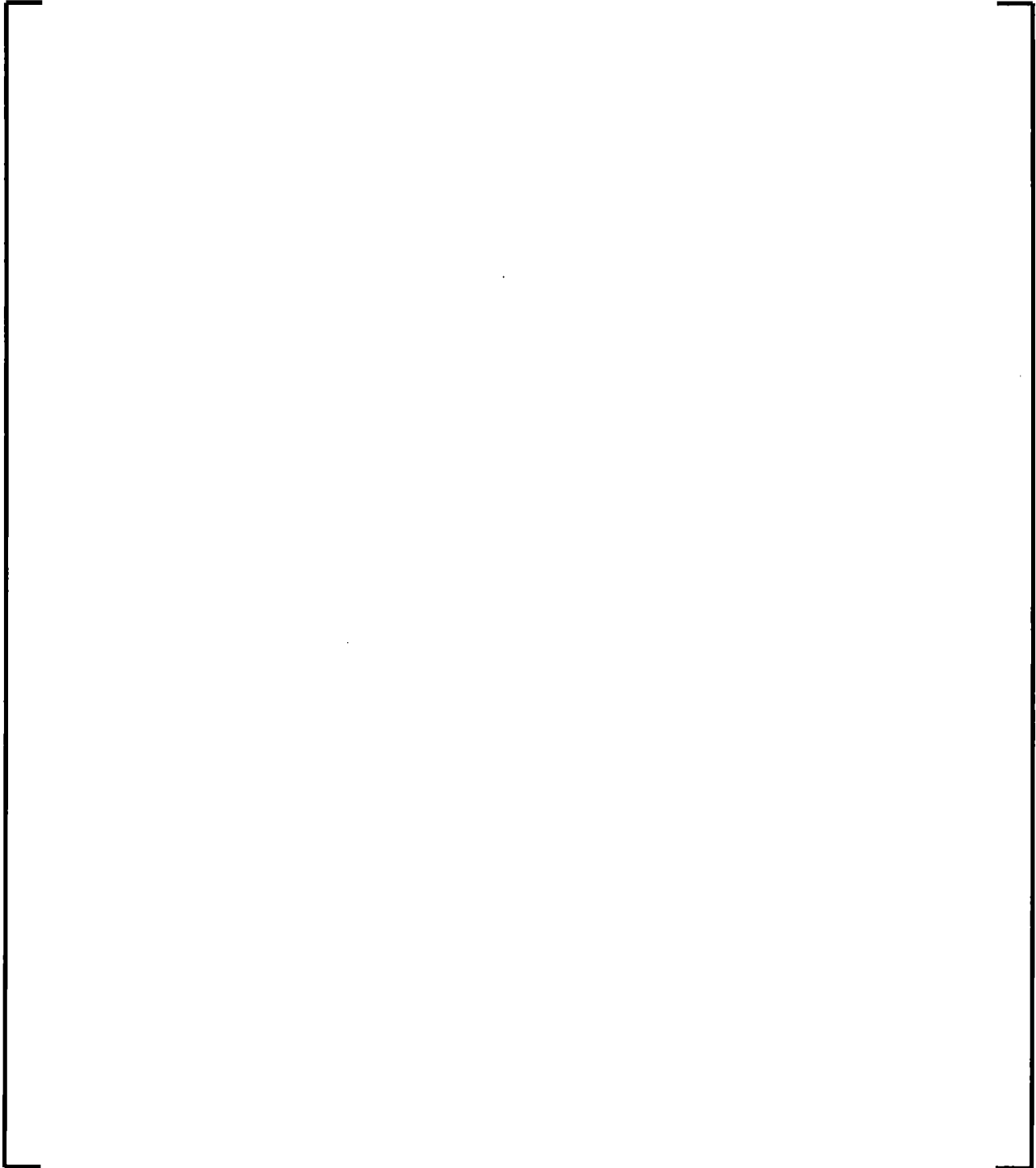


Figure 9-8 Sample NPP Upper Plenum Nodalization - Axial Plane



**Figure 9-9 Sample NPP Upper Plenum Nodalization - Cross-
Sectional Plane**

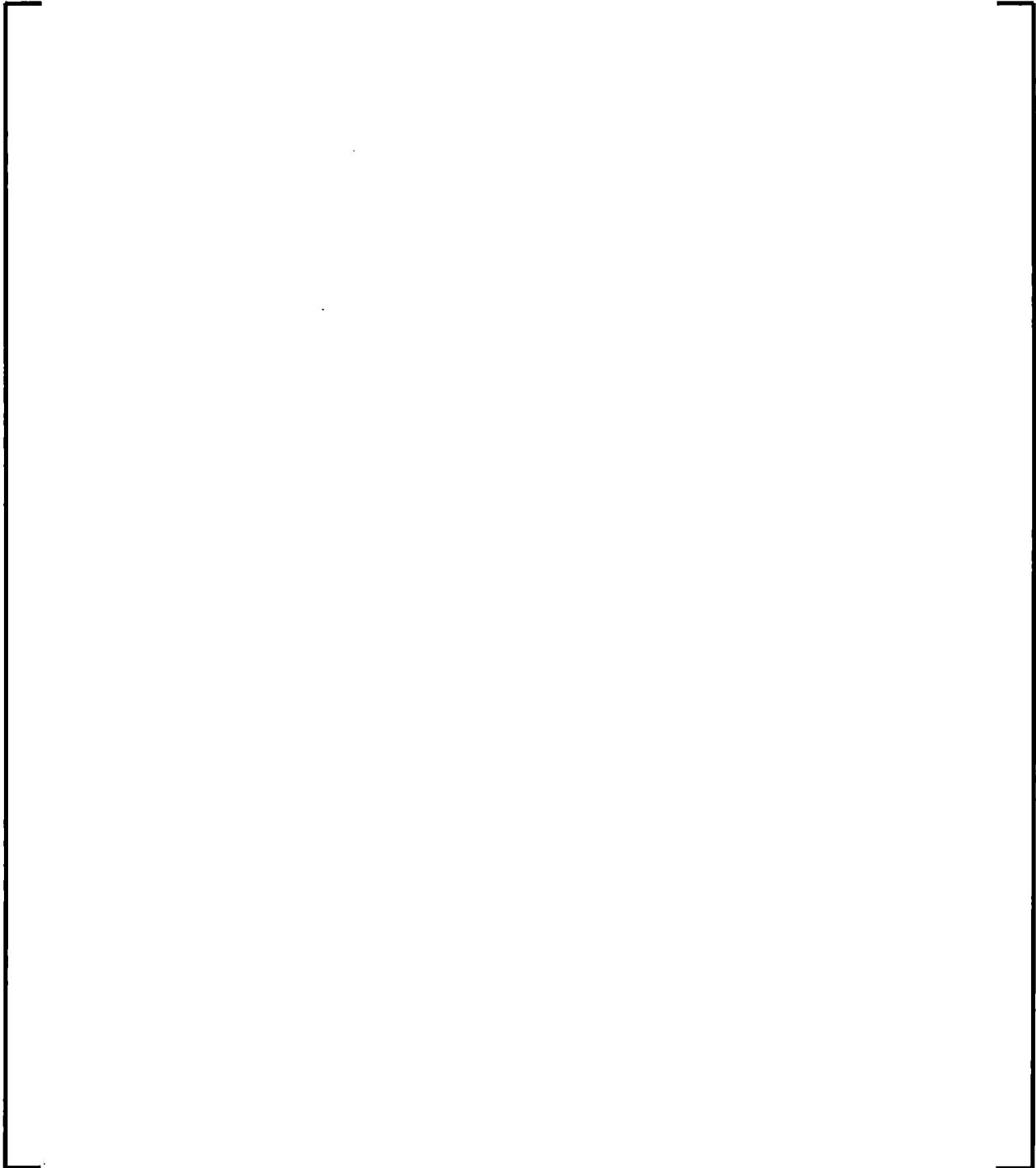
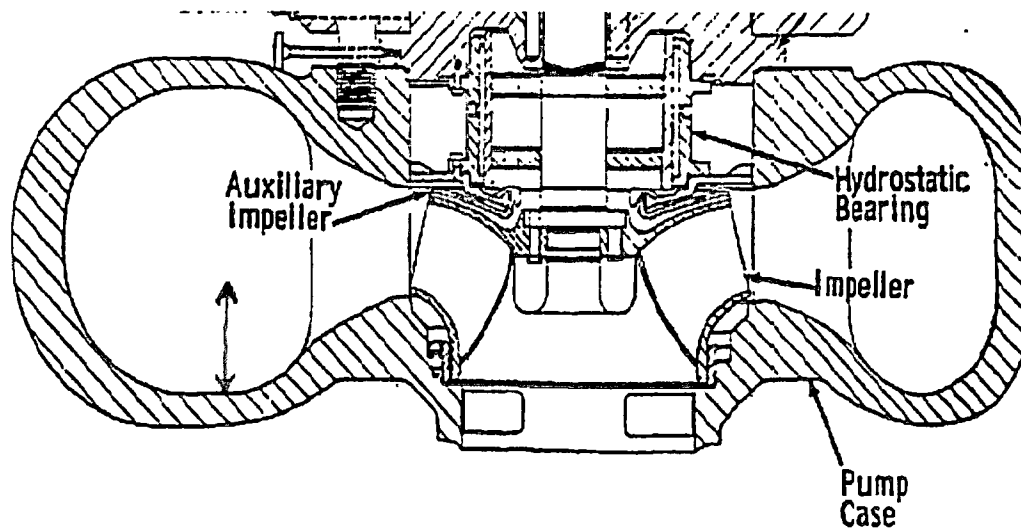


Figure 9-10 Reactor Coolant Pump Showing Impeller Spill Height

9.2 *Sensitivity and Uncertainty Analysis*

This section demonstrates plant compliance with high probability to the following criteria of 10 CFR 50.46(b) :

1. Peak cladding temperature. The calculated maximum fuel element cladding temperature shall not exceed 2200 °F.
2. Maximum cladding oxidation. The calculated total oxidation of the cladding shall not exceed 0.17 times the total cladding thickness before oxidation. As used in this subparagraph total oxidation means the total thickness of cladding metal that would be locally converted to oxide if all the oxygen absorbed by, and reacted with, the cladding locally were converted to stoichiometric zirconium dioxide. If cladding rupture is calculated to occur, the inside surfaces of the cladding shall be included in the oxidation, beginning at the calculated time of rupture. Cladding thickness before oxidation means the radial distance from inside to outside the cladding, after any calculated rupture or swelling has occurred but before significant oxidation. Where the calculated conditions of transient pressure and temperature lead to a prediction of cladding swelling, with or without cladding rupture, the unoxidized cladding thickness shall be defined as the cladding cross-sectional area, taken at a horizontal plane at the elevation of the rupture, if it occurs, or at the elevation of the highest cladding temperature if no rupture is calculated to occur, divided by the average circumference at that elevation. For ruptured cladding the circumference does not include the rupture opening.
3. Maximum hydrogen generation. The calculated total amount of hydrogen generated from the chemical reaction of the cladding with water or steam shall not exceed 0.01 times the hypothetical amount that would be generated if all of the metal in the cladding cylinders surrounding the fuel, excluding the cladding surrounding the plenum volume, were to react.
4. Coolable geometry. Calculated changes in core geometry shall be made in such a way that the core remains amenable to cooling.

5. Long-term cooling. After any calculated successful initial operation of the ECCS, the calculated core temperature shall be maintained at an acceptably low value and decay heat shall be removed for the extended period of time required by the long-lived radioactivity remaining in the core.

The first three of these criteria are addressed by the RLBLOCA methodology. The remaining two require evaluations beyond the applicability of the methodology, and are treated separately during plant evaluations.

For the AREVA RLBLOCA evaluation model, high probability was defined as having 95 percent confidence that 95 percent of LBLOCAs will meet the acceptance criteria of 10 CFR 50.46(b). This is accomplished by applying non-parametric statistical techniques to the calculation results of the evaluation. The key premise is that the RLBLOCA evaluation tool, S-RELAP5 and the attendant codes, is accurate in representing the possible LBLOCAs and the frequency with which specific LBLOCA results will occur. Thus, S-RELAP5 contains the domain of all possible LBLOCA results within the scenario defined in Section 3.1. Extracting information about this domain is done by random sampling (running individual LOCA calculations referred to as cases or events) with random values for the initial conditions and the parameter values, including those that alter the simulation of important phenomena and deducing from those samples the content of the domain. To accomplish this entails two requirements: 1) the calculation evaluation tool, S-RELAP5 and COPENIC, must be established as sufficiently accurate or conservatively biased so that any calculation provides a result that is accurate or conservative for the sampled choices and 2) a method of evaluating the results sampled from the domain be established to provide accurate probability and confidence. Section 9.3 presents the establishment and evaluation of the first requirement, and Sections 9.4 and 9.5 present the second. Sample RLBLOCA evaluations illustrating the analysis steps described below are provided for representative Westinghouse 3- and 4-loop and CE 2x4 plants in Appendix B.

The next step in the evaluation is the generation of a set of results of LOCA evaluations for which the inputs of the selected sample parameters are randomly determined. Recall that the sampled parameters have been selected through the PIRT as having the dominant influences on the LOCA results or have been requested arbitrarily to ensure that the ranges allowed in the technical specification are appropriate for LOCA. The sampling of the PIRT identified dominant parameters is required. Because the remaining sampled parameters are not dominant, their inclusion as sampled parameters is optional. The listing in Appendix A provides the dominant parameters and a representative selection of the optional parameters.

In either case, a normalized probability density function (PDF), is determined for each of the sampled parameters. The function is then integrated to provide a cumulative density function (CDF) and then it is inverted. Feeding random numbers, between 0 and 1, into the inverted CDF provides a set of results that match the original normalized PDF, and can be used within a series of LOCA evaluations to generate a set of LOCA cases for which the values of the sampled parameters distribute according to the PDFs for each parameter. This set of cases can then be evaluated by statistical inference techniques to determine the probability and confidence of the outcome of a LOCA calculation. To the extent that the calculational technique predicts the real world LOCA, the resultant probability and confidence is characteristic, for the plant studie, of what can be expected of a LOCA. As with any calculational technique completely comprehensive treatment is not possible. Compromises must be made to make the evaluation a practicality. For important but not dominant phenomena, these compromises are selected to be conservative. For items of little importance, the values may be selected as nominal or best estimate. Thus, the probability and confidence have imbedded conservatism beyond their determined values.

9.3 *Determination of the Effect of Reactor Input Parameters and State (CSAU Step 11)*

The uncertainties associated with the prediction of LOCA results can be categorized into three groups:

1. Fixed design factors (e.g., system geometry) that do not change, but that can still only be rendered in approximation.
2. Operational processes (e.g., core power peaking), which do not change during the transient, but vary across the spectrum of conditions at which a LOCA may occur.
3. Phenomena that evolve during the transient (e.g., core heat transfer coefficients), and may take on differing normalized performance across the spectrum of LOCAs within the domain.

The treatment of fixed design factors and operational processes are discussed in Section 9.1 and Section 9.3.1, respectively. The treatment and development of uncertainty distributions for phenomena is presented in Section 8.4 and Section 8.5.

9.3.1 Operational Process

In contrast to phenomenological or fixed design factors, process parameters characterize the state of operation of the plant and are, to various degrees, controllable by plant operators in such a way that realistic variations can be expected. The importance of these parameters must be established and, for those of significance, the ability of the model to predict appropriate results must be validated, and an appropriate uncertainty distribution established.

9.3.1.1 Determining Important Process Parameters

From an operational standpoint, the NPP operating state is a function of the time in cycle (burnup and power distribution), and the actual conditions present in the various NPP components. Treating these process parameters statistically accounts for higher order behavior by including all possible combinations in the domain of possible LOCAs.

As part of the AREVA RLBLOCA methodology development, a review was performed to identify the NPP parameters that are to be addressed in the performance of an LBLOCA analysis. The identified parameters are provided in Table 9-9. The basis for inclusion in this list comes from three sources: PIRT, plant-specific technical specifications, and utility requests.

Determination of which process parameters to treat statistically begins with identifying the relationship a particular parameter has to any PIRT phenomenon. Table 9-3 lists process parameters determined to be important based on their potential influence to the moderate-to-high ranked phenomena given in the PIRT, Table 5-1.

A refinement of the conclusions presented in Table 9-2, based on sensitivity studies, is within the precepts of the methodology. Such studies can be used to adopt a bias over an uncertainty distribution for process parameters or to assist in the quantification of an uncertainty range or distribution.

Other process parameters are considered to be of lower importance, and are generally treated on a nominal basis. As with any parameter, there is no prohibition to treating these parameters on a statistical basis.

9.3.1.2 Quantifying Uncertainty for Process Parameters

To treat a parameter statistically, the parameter uncertainty must be quantified in terms of biases and distributions. Quantifying this uncertainty with plant data is the best approach. At most plants, histories of parameters values, such as RCS flow rate, core inlet temperature, pressurizer condition, accumulator parameters, and containment temperature are maintained and useable for quantifying RLBLOCA analysis uncertainties. Operational uncertainty is defined as the true fluctuation of a parameter during normal operation. Setting the uncertainty distribution for a process parameter requires addressing the impact of measurement uncertainty for the parameter.

The choice of distribution may be influenced by how a utility manages a given process parameter. For example, using a uniform distribution may properly reflect the control provided for a parameter, if that control is random within a range. A uniform distribution is also considered a conservative approach in that equal likelihood is given for values at the limits of the distribution where the strongest influence is expected. However, if there is an expectation that the true distribution is substantially non-uniform, the actual distribution can be used.

As shown in Table 9-9, some parameters lack explicit definition (technical specifications or data). For parameters for which no plant data are available, ranges may be established based on physical constraints or by analytical methods. [

] It may also be demonstrated that a particular parameter has a limited range of influence based on a set of sensitivity studies.

9.3.1.3 Treatment of Time in Cycle

The time in cycle establishes the fuel rod properties and the lower bound for the global power peaking factor, F_q . Power history calculations are performed using an NRC-approved methodology (References 9-9 and 9-10). [

]

In contrast to a traditional safety analysis, which assumes conservative fuel rod models consistent with Appendix K requirements, [

]

1. [

]

2. [

]

3. [

]

4. [

]

The data produced by this method are used primarily to develop input for the
COPERNIC fuel rod sub-code within S-RELAP5. [

]

9.3.1.4 Treatment of Axial and Radial Power Shapes

Once the fuel rod histories for the fuel rod sub-code are found to be as described, the axial and radial power shapes for the S-RELAP5 core model are selected as follows. To support plant Technical Specification for the core peaking factor, F_q , the axial power shape must be adjusted from the nominal axial power shape extracted for the limiting fuel rod. During normal operation, F_q will likely occur relatively near the nominal F_q represented in the power history files. [

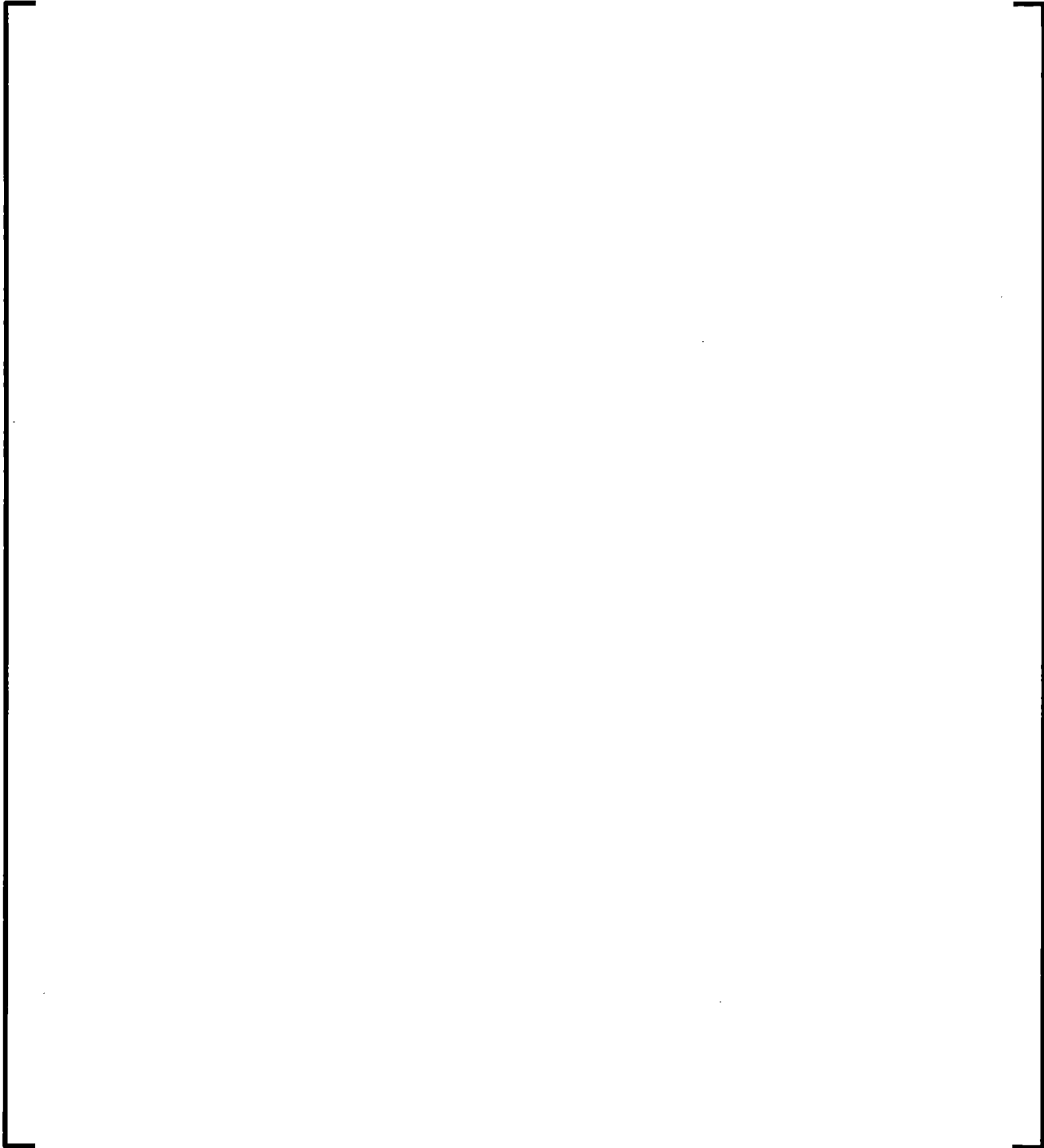
]

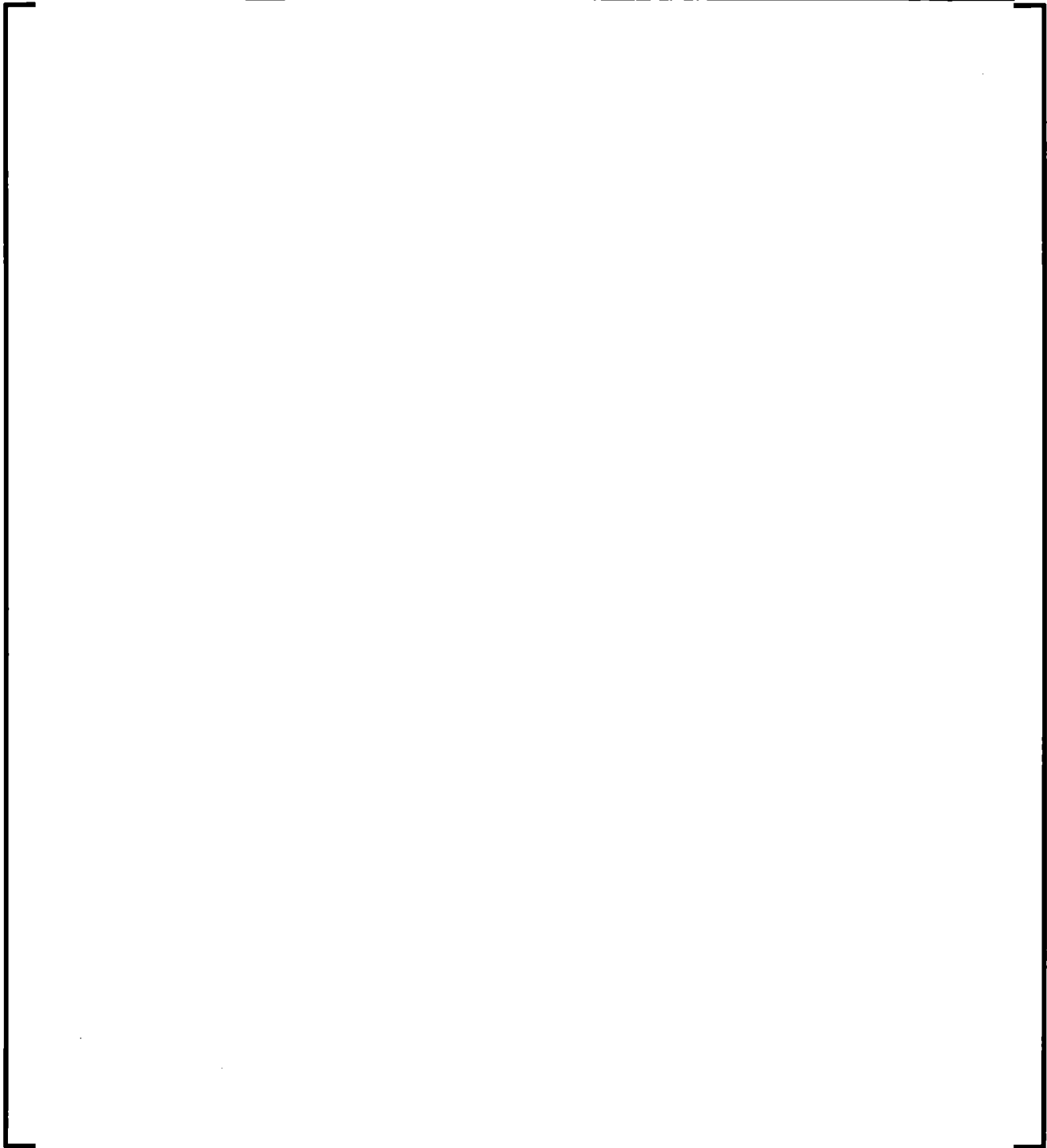
9.3.1.5 Treatment of GDC-35 Criteria

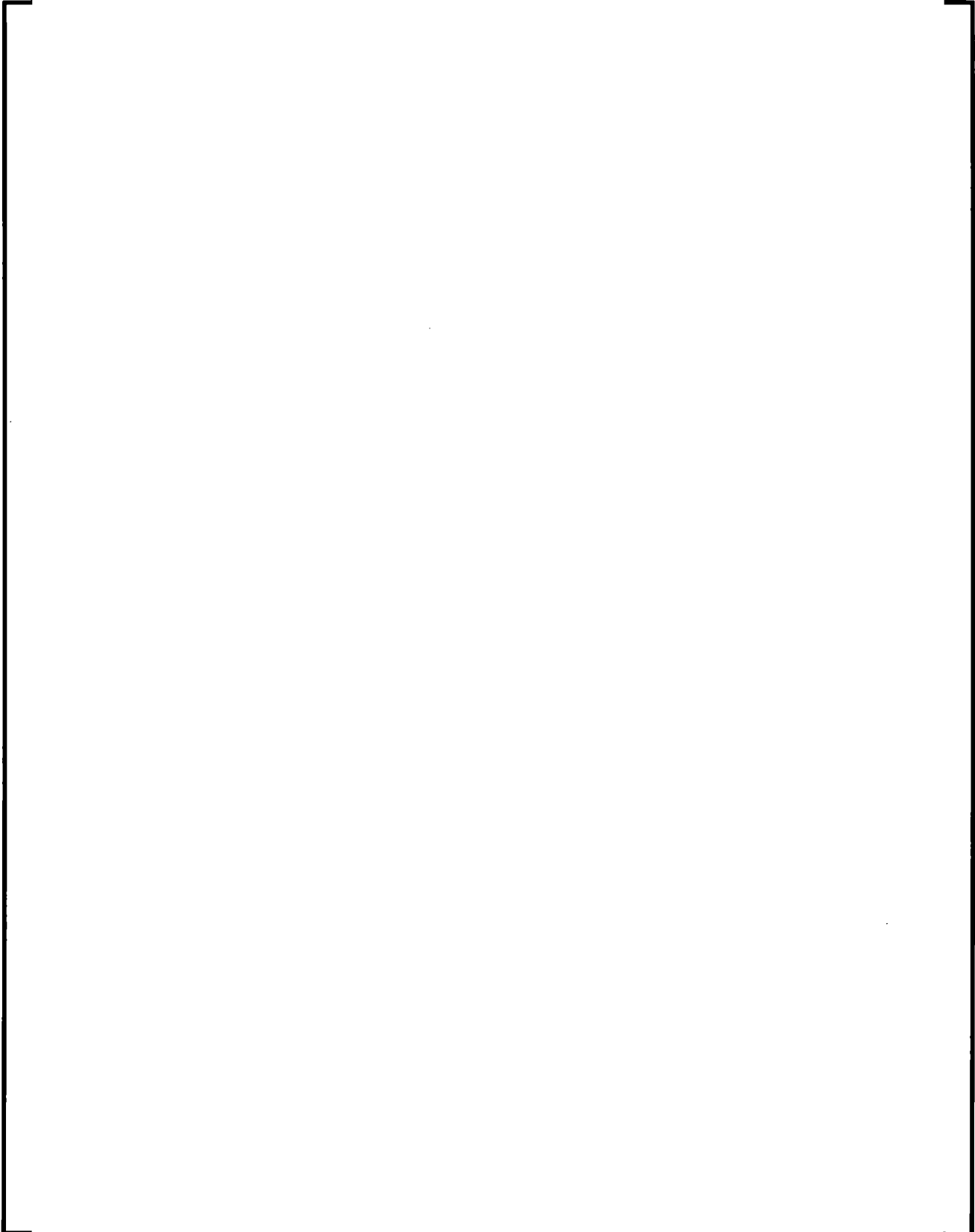
GDC-35 states that the plant shall be able to mitigate design basis accidents, with or without offsite power available. [

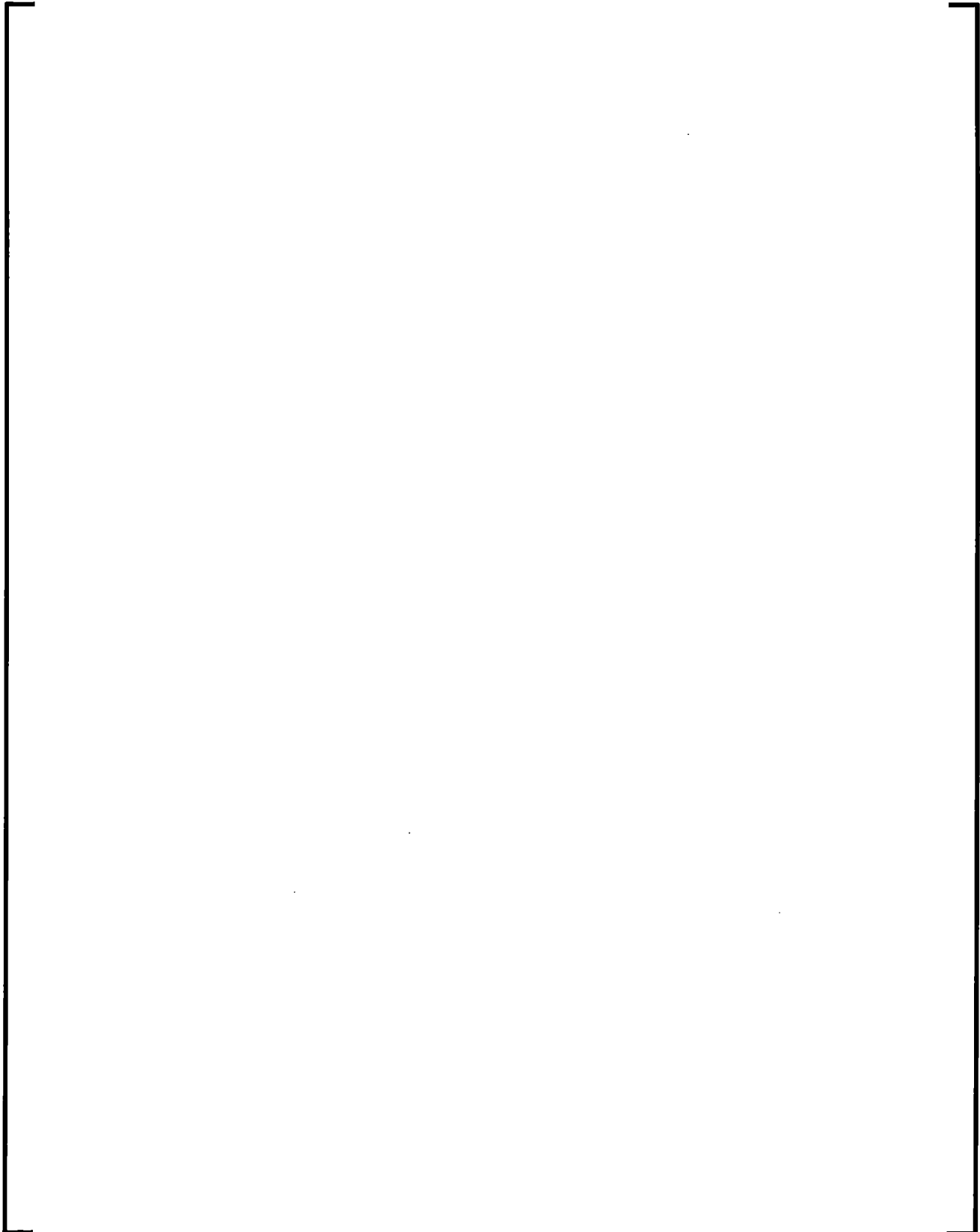
] Further details are provided in Appendix B, Section B.1.3.

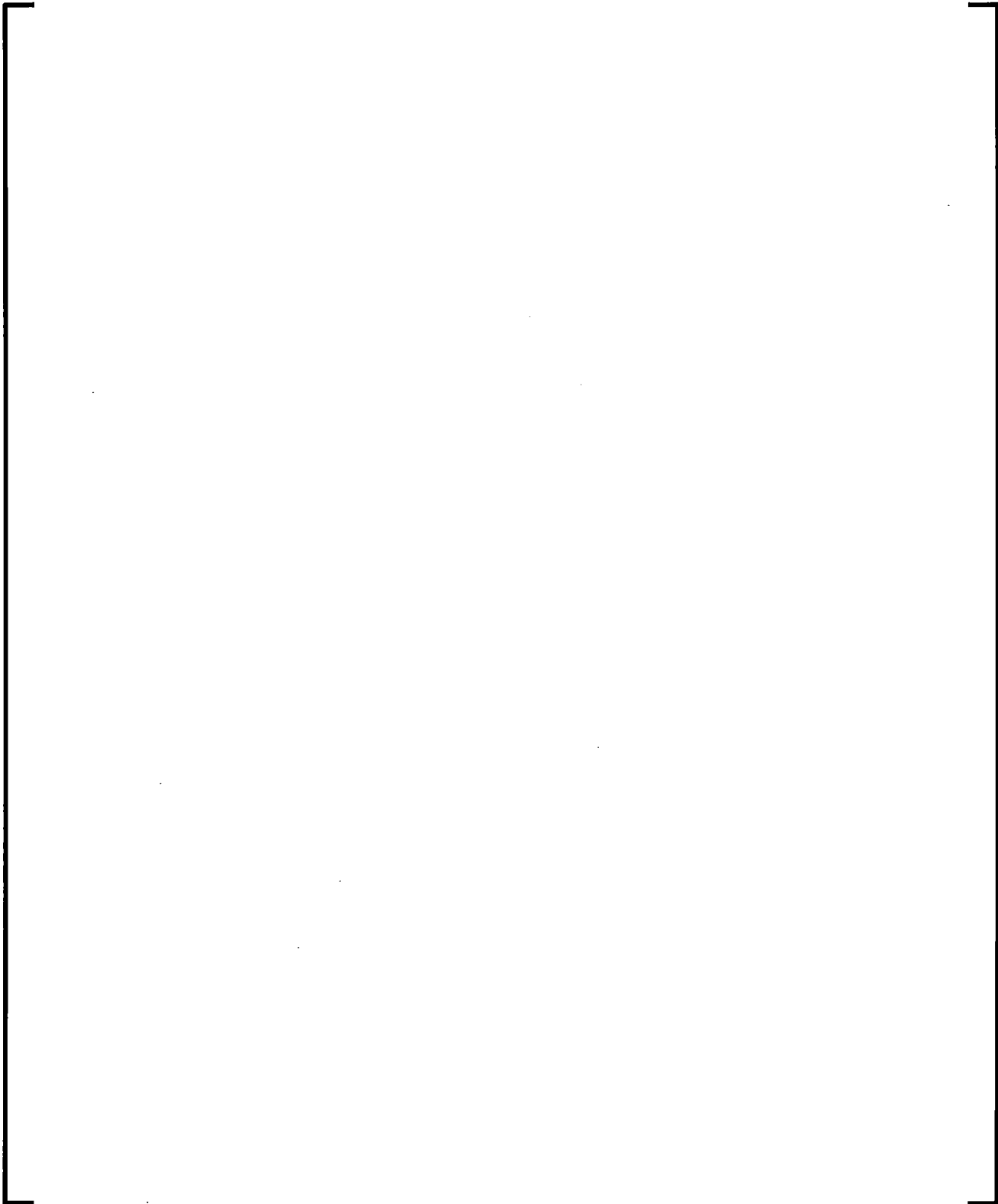
9.4 Performance of NPP Sensitivity Calculations and Determination of Combined Bias and Uncertainty (CSAU Steps 12 and 13)

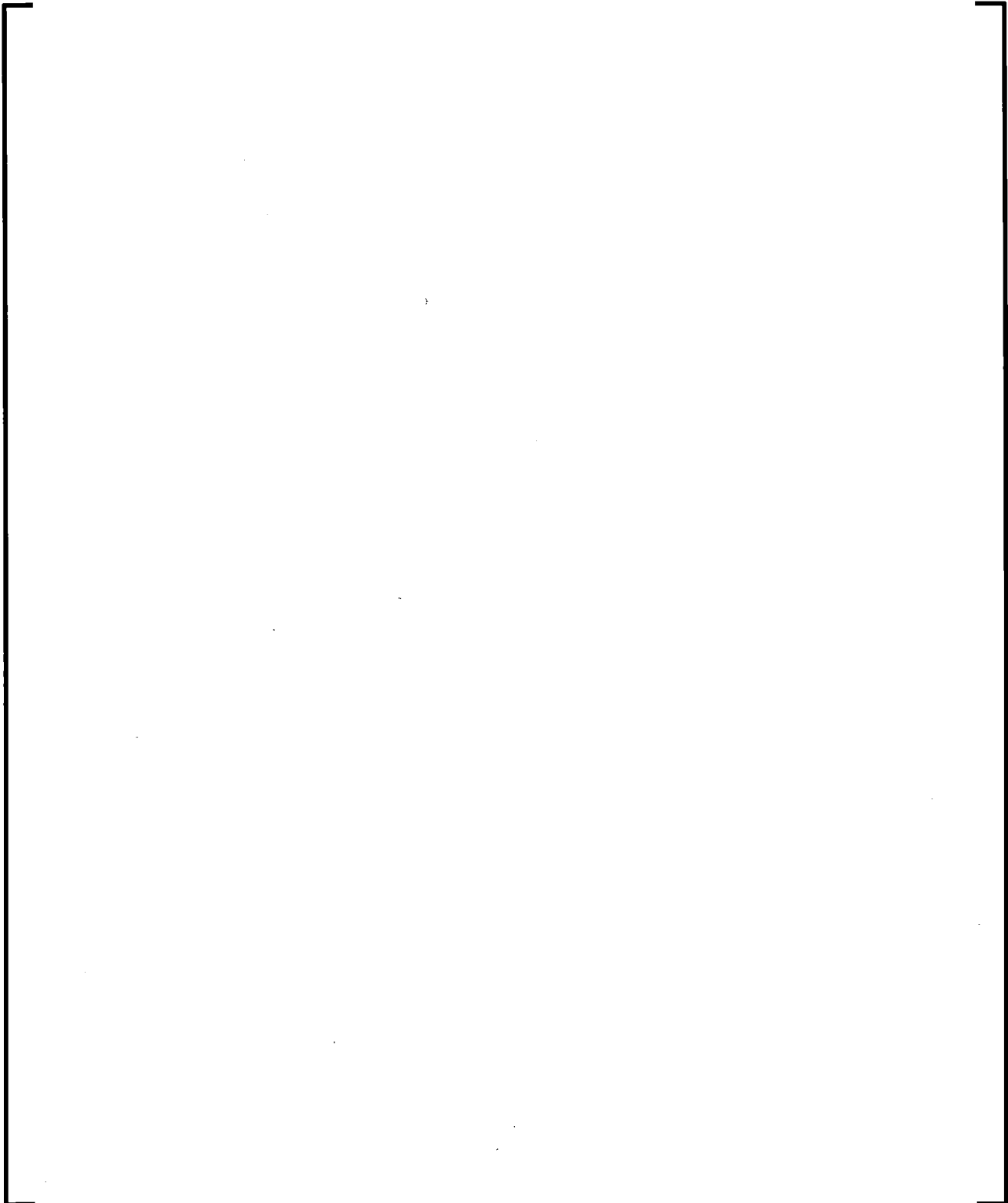












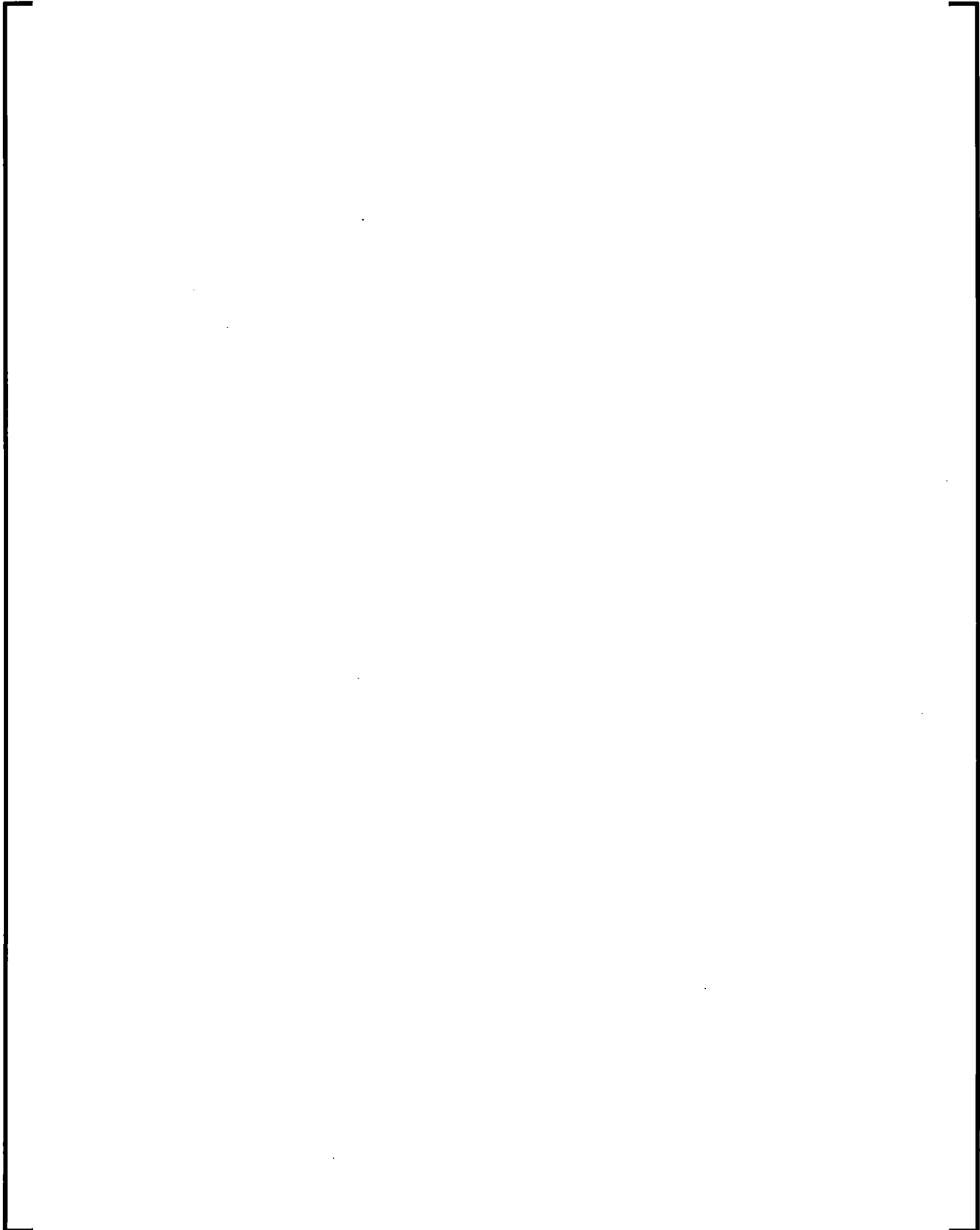
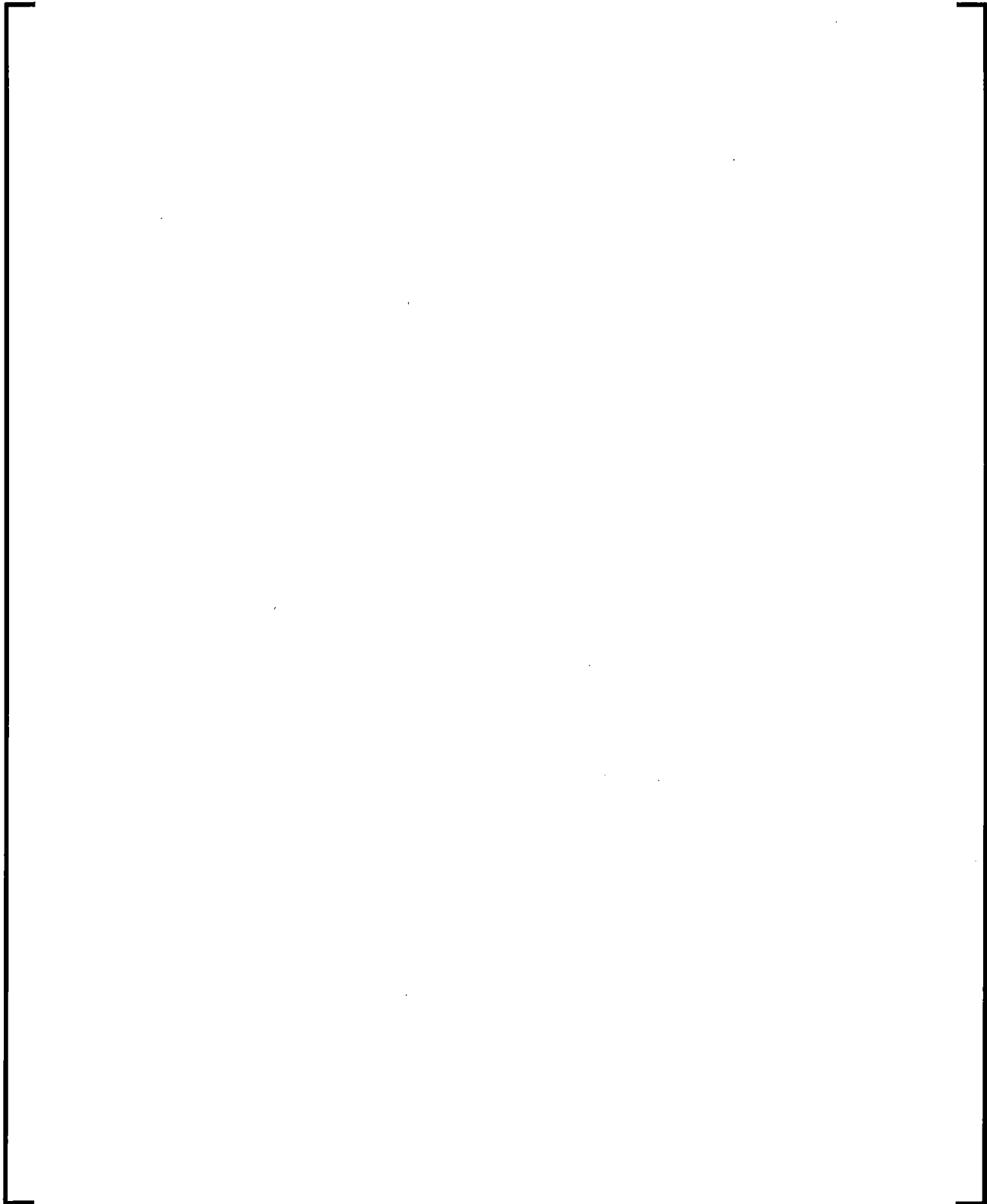


Table 9-2 [

]

--



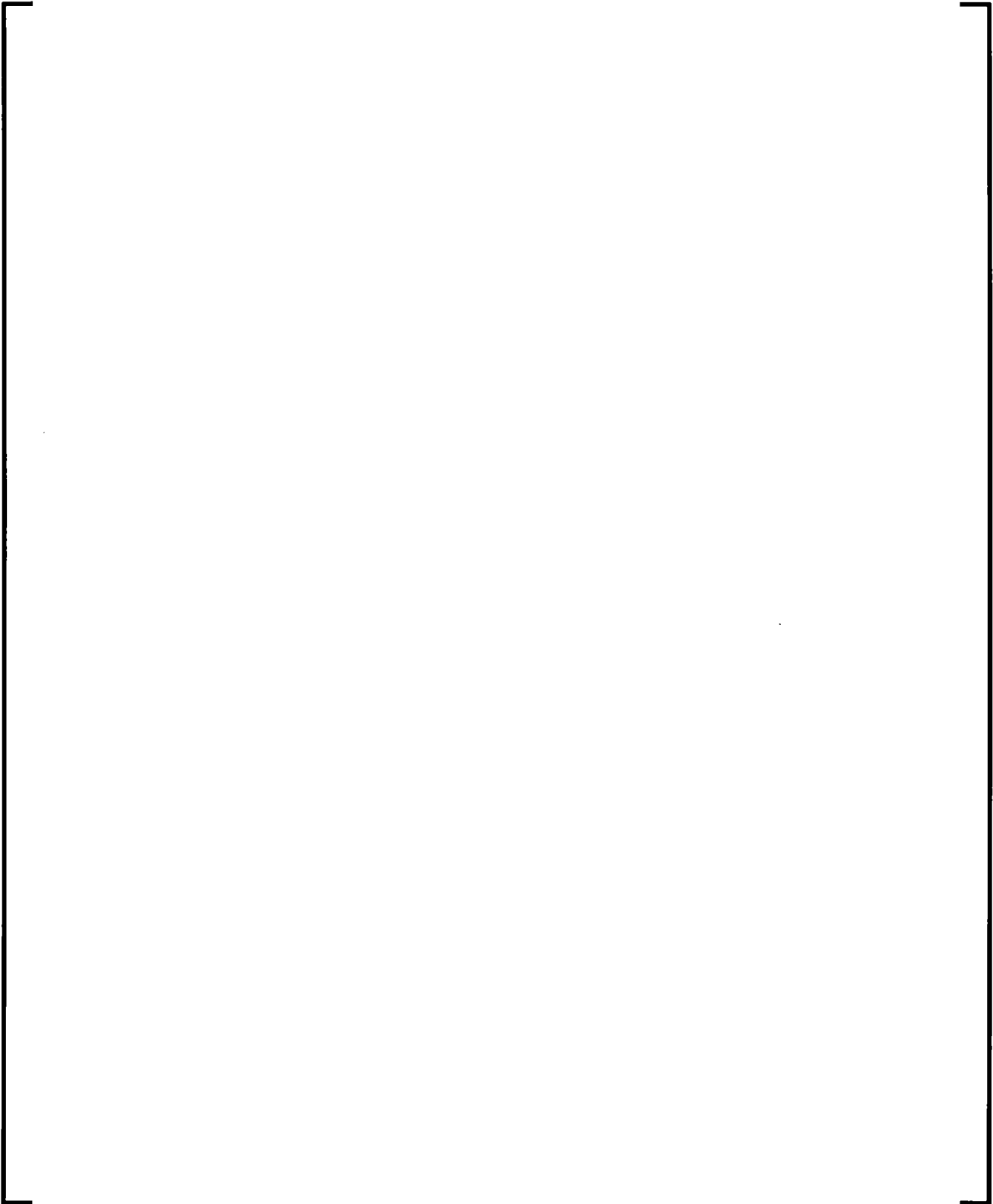




Table 9-3 [

]

--

Table 9-4 [

]

[

]


Table 9-5 [

Table 9-6 [

]

--	--

Table 9-7 [

]

--	--

Table 9-8 [

1

--

9.5 *Determination of Combined Bias and Uncertainty and Determination of Total Uncertainty (CSAU Steps 13 and 14)*

CSAU Step 13 provides for the determination of the combined bias and uncertainty for the NPP. This is basically the application of the process described in Section 9.4. The procedure is executed for each of three sample problems in Appendix B.

The total uncertainty for the evaluation is determined by comparing the bounding parameter value for the limiting parameter to the mean probability value of the sampled case set, for that parameter within the domain defining the high probability of compliance. Examples of this value are also reported for each of the sample problem in Appendix B.

Table 9-9 NPP Parameters for Consideration in the Performance of a RLBLOCA Analysis

This image shows a completely blank white rectangular area enclosed within a thick black frame. There are no markings, text, or illustrations present on the page.

Table 9-10 Relationship of PIRT to Operational Parameters

Process Parameter	Influenced Phenomenon (PIRT subset)
Fuel State (Burnup and Power Peaking)	Stored energy
Core Power	Stored energy
Power Peaking, Axial Shape	Stored energy
Loop Flow Rate	Flow split, DNB
Core Inlet Temperature	DNB
Upper Head Temperature	Flow reversal, stagnation
Pressurizer Pressure, Level	Critical flow in surge line
Accumulator Pressure, Temperature, Level	Accumulator discharge, condensation, noncondensable gas
Containment Volume, Heat Transfer, Sprays	Backpressure, critical flow
Offsite Power and Diesel Start Delay	Core heat transfer via pumped ECC

9.6 References

- 9-1. NUREG/CR-5249, "Quantifying Reactor Safety Margins, Application of Code Scaling, Applicability, and Uncertainty Evaluation Methodology to a Large Break, Loss-of-Coolant Accident," December 1989.
- 9-2. EMF-2103(P)(A) Revision 0, "Realistic Large Break LOCA Methodology," Framatome ANP Richland, Inc., April 2003.
- 9-3. AREVA NP Document FS1-0011182, Revision 2.0, "FSQA-08 S-RELAP5 Models and Correlations Code Manual (Theory)," August 2013.
- 9-4. EMF-CC-039(P) Revision 4, "ICECON Code User's Manual: A Computer Program Used to Calculate Containment Back Pressure for LOCA Analysis (Including Ice Condenser Plants)," December 2007.
- 9-5. NUREG-0800, "U.S. Nuclear Regulatory Commission Standard Review Plan," U.S. Nuclear Regulatory Commission.

- 9-6. TID-4500, ANCR-1219, "CONTEMPT-LT – A computer Program for Predicting Containment Pressure-Temperature Response to a Loss-Of-Coolant Accident," June 1975.
- 9-7. NUREG/CR-5535, S. Shieh, V. H. Ransom, R. Krishnamurthy, "RELAP5/MOD3 Code Manual, Validation of Numerical Techniques in RELAP5/MOD3," Volume 6, August 1994.
- 9-8. R. R. Schultz, "RELAP5-3D Code Manual, User's Guidelines," INEEL-EXT-98-00834, February 2001.
- 9-9. XN-75-27(A), "Exxon Nuclear Neutronic Design Methods for Pressurized Water Reactors," Exxon Nuclear Company, April 1977.
- 9-10. EMF-96-029(P)(A), *Reactor Analysis System for PWRs*, January 1997.
- 9-11. K. Krishnamoorthy and Thomas Mathew, *Statistical Tolerance Regions: Theory, Applications and Computation*, 2009 John Wiley & Sons, Inc.
- 9-12. NAI 8907-09, Revision 10, Version 7.2b(QA), "GOTHIC Containment Analysis Package Qualification Report," EPRI, Palo Alto, California, March 2009.

10.0 QUALITY ASSURANCE PLAN

The quality assurance plan is not discussed within the topical report. The AREVA NP quality assurance plan is contained in Reference 10.1.

10.1 *References*

- 10.1 Fuel Management Manual, Revision 3, "AREVA Front End Business Group Fuel Business Unit Management Manual," AREVA NP Inc., May 2012.